UNIVERSITY of TASMANIA | AMC Australian Maritime College

Wing-In-Ground Effect Oscillating Foils for Marine Propulsion

by

Jiadong Wang

B.Eng. and M.Eng. (Naval Architecture and Ocean Engineering)

National Centre for Maritime Engineering and Hydrodynamics

Australian Maritime College

Submitted in fulfilment of the requirements for the degree of

Doctor of Philosophy

University of Tasmania

October 2021

Statements and Declarations

Declaration of Originality

This thesis contains no material which has been accepted for a degree or diploma by the University or any other institution, except by way of background information and duly acknowledged in the thesis, and to the best of my knowledge and belief no material previously published or written by another person except where due acknowledgement is made in the text of the thesis, nor does the thesis contain any material that infringes copyright.

Authority of Access Statement

This thesis may be made available for loan and limited copying and communication in accordance with the Copyright Act 1968.

Statement Regarding Published Work

The publishers of the papers comprising Chapters 3 to 6 hold the copyright for that content and access to the material should be sought from the respective journals/publishers. The remaining nonpublished content of the thesis may be made available for loan and limited copying and communication in accordance with the Statement of Access and the Copyright Act 1968.

Signed: _____ Date: 26/10/2021

Jiadong Wang

National Centre for Maritime Engineering and Hydrodynamics

Australian Maritime College

University of Tasmania

Statement of Co-Authorship

The following people and institutions contributed to the publication of work undertaken as part of this thesis:

Candidate:	Mr. Jiadong Wang	University of Tasmania
Author 1:	Dr. Christopher Chin	University of Tasmania
Author 2:	Prof. Pengfei Liu	Newcastle University
Author 3:	Prof. Guanghua He	Harbin Institute of Technology
Author 4:	Mr. Weizhen Song	University of Tasmania
Author 5:	Mr. Weijie Mo	Harbin Institute of Technology

Contribution of work by co-authors for each paper:

PAPER 1: Located in Chapter 3

WANG, J., LIU, P., CHIN, C. & HE, G. 2019. Numerical investigation of auto-pitch wing-in-ground effect oscillating foil propulsor. ***Applied Ocean Research,*** **89, 71-84.**

Author contributions:

Conceived and designed simulation: Candidate & Author 2

Performed the simulations: Candidate

Analyzed the data: Candidate, Author 1 & Author 2

Manuscript preparation: Candidate

Manuscript revision: Candidate, Author 1, Author 2 & Author 3

PAPER 2: Located in Chapter 4

WANG, J., LIU, P., CHIN, C., HE, G. & SONG, W. 2020. Parametric study on hydro-elasticity characteristics of auto-pitch wing-in-ground effect oscillating foil propulsors. ***Ocean Engineering,*** **201, 107115.**

Author contributions:

Conceived and designed simulation: Candidate & Author 2

Performed the simulations: Candidate

Analyzed the data: Candidate, Author 1 & Author 2

Manuscript preparation: Candidate

Manuscript revision: Candidate, Author 1, Author 2, Author 3 & Author 4

PAPER 3: Located in Chapter 5

WANG, J., LIU, P., CHIN, C. & HE, G. 2020. Auto-pitch wing-in-ground effect oscillating foils for marine propulsion. ***The 30th International Ocean and Polar Engineering Conference, ISOPE-2020*****. International Society of Offshore and Polar Engineers.**

Author contributions:

Conceived and designed simulation: Candidate & Author 2

Performed the simulations: Candidate

Analyzed the data: Candidate, Author 1 & Author 2

Manuscript preparation: Candidate

Manuscript revision: Candidate, Author 1, Author 2 & Author 3

PAPER 4: Located in Chapter 6

WANG, J., LIU, P., CHIN, C., HE, G. & Mo, W. 2021. Three-dimensional propulsion characteristics of counter-phase oscillating dual-foil propulsor. ***Ocean Engineering,*** **238, 109761.**

Author contributions:

Conceived and designed simulation: Candidate & Author 2

Performed the simulations: Candidate

Analyzed the data: Candidate, Author 1 & Author 2

Manuscript preparation: Candidate

Manuscript revision: Candidate, Author 1, Author 2, Author 3 & Author 5

We, the undersigned, endorse the above stated contribution of work undertaken for each of the published (or submitted) peer-reviewed manuscripts contributing to this thesis:

Signed: _____ Date: 26/10/2021

Jiadong Wang – Candidate

National Centre for Maritime Engineering and Hydrodynamics

Australian Maritime College

University of Tasmania

Signed: _____ Date: 26/10/2021

Dr. Christopher Chin – Primary Supervisor

National Centre for Maritime Engineering and Hydrodynamics

Australian Maritime College

University of Tasmania

Signed: _____ Date: 27/10/2021

Dr. Vikram Garaniya – Director

National Centre for Maritime Engineering and Hydrodynamics

Australian Maritime College

University of Tasmania

Acknowledgements

As the wonderful trip comes to an end, I wish to deeply and genuinely acknowledge many generous individuals who contribute to the completion of this thesis.

I would like to express my sincere gratitude to my supervisory team for their continuous support. I am always touched by endless enthusiasm and professional attitude of Professor Pengfei Liu who offered me the valuable opportunity to pursue a doctorate. His guidance, inspiration and immense expertise remarkably facilitate my PhD study and moreover sharpen my research skills in the future career. It has been a great pleasure to work together with him over the past few years. As my primary supervisor in the latter half of PhD project, Dr Christopher Chin gave me great assistance and support in my research work. His significant supervision with patience and encouragement helped me get through a struggling period and made me complete this thesis timely. I am especially grateful to my co-supervisor, Professor Guanghua He who kindly provided me with the work place and computing facilities in Harbin Institute of Technology to continue my study during the pandemic of coronavirus. His advice, instructions and wealth of knowledge greatly benefit my graduate study and enable me to have a rewarding experience. It was a privilege to have his guidance along the way.

I want to thank Dr Bryce Pearce and Dr James Venning for the valuable comments and suggestions, which improve this research work in many aspects. Thankfulness is extended to Professor Jonathan Binns for sharing the knowledge in data processing and analysis. The research scholarship from University of Tasmania is gratefully acknowledged. Many thanks to all the staff at Australian Maritime College for their help and support in the course of my PhD study.

I wish to appreciate my colleagues in the Connell Building for their encouragement and support in a variety of ways. I highly value our meaningful and fruitful conversations that provide insights for my research. I would like to express deep gratitude to my peers in Harbin Institute of Technology for their generous help and assistance during my stay in their lab. They provided me with the warm hospitality, various resources and comfortable environment that make my study proceed smoothly. My genuine appreciation also goes to all my friends in both Tasmania and homeland of China. This venture was filled with enjoyment owing to their constant companion. A special acknowledgement to Dr Ray who has an extraordinary passion in fluid mechanics. Our academic discussions have always been a source of inspiration for my research work.

Last but not least, I will be eternally indebted to my dear parents. None of this would have been possible without their endless love, unconditional trust and selfless dedication. I am so lucky to be born in such a lovely family. Their support has allowed me to pursue my dream fearlessly over all these years.

Table of Contents

List of Figures

List of Tables

Nomenclature

Symbol	Definition	Unit
A	Characteristic width of created jet flow	m
B	Additive constant	-
c	Chord length	m
C	Cell of interest	-
C_k	Correction factor	-
C_l	Time-varying lift coefficient	-
C_t	Time-varying thrust coefficient	-
C_P	Time-averaged power coefficient	-
C_T	Time-averaged thrust coefficient	-
$\mathbf{d}$	Length vector	-
D_{foil}	Equivalent diameter of foil	m
D_{pitch}	Pitching damping coefficient	-
f	Oscillating frequency	Hz
$\mathbf{f}$	Arbitrary body force	N
F	Time-averaged thrust	N
F_m	Mass flux	$kg \cdot s^{-1} \cdot m^{-2}$
Fs	Flat faces between different cells	-
f_n	Natural frequency	Hz
h_0	Heaving amplitude	m
$h(t)$	Time-varying vertical position of elastic pitching axis	m
$\mathbf{I}$	Identity matrix	-
I_{axis}	Moment of inertia about pivot axis	$kg \cdot m^2$
J	Advance coefficient	-
k	Reduced frequency	-
k_t	Turbulent kinetic energy	$m^2 \cdot s^{-2}$
K	Torsional spring stiffness	$N \cdot m \cdot rad^{-1}$

K^*	Non-dimensional torsional spring stiffness	-
K_{pitch}	Torsional stiffness coefficient	-
K_Q	Torque coefficient of screw propeller	-
K_T	Thrust coefficient of screw propeller	-
M_{axis}	Hydrodynamic moment about elastic axis	N·m
$\mathbf{n}$	Unit vector normal to surface element	-
N	Neighboring cell	-
p	Pressure	Pa
p_k	Order of accuracy	-
p_{kest}	Estimate for limiting order of accuracy	-
P	Time-averaged input power	W
$Q(t)$	Time-varying torque about pivot axis	N·m
r_k	Refinement ratio of k-th input parameter	-
Re	Reynolds number	-
R_k	Convergence ratio of k-th input parameter	-
s	Span length	m
S	Area of bounding surface	m^2
S_i	i-th numerical solution	-
S_ϕ	Source term	-
St	Strouhal number	-
t	Time	s
T	Oscillatory cycle	s
u^+	Non-dimensional velocity	-
u_τ	Friction velocity	$m·s^{-1}$
$\bar{u}$	Time-averaged wake velocity	$m·s^{-1}$
U	Freestream velocity	$m·s^{-1}$
U_k	Numerical uncertainty of k-th input parameter	-
U_{kc}	Corrected numerical uncertainty of k-th input parameter	-
U_{max}	Maximum mean velocity	$m·s^{-1}$

$\mathbf{v}$	Fluid velocity	$m \cdot s^{-1}$
$\mathbf{v}_b$	Boundary velocity of control volume	$m \cdot s^{-1}$
V	Volume of fluid element	m^3
x	Coordinate position along horizontal direction	m
$X(t)$	Time-varying force in forward direction	N
y	Coordinate position along vertical direction	m
y^+	Non-dimensional distance from the wall	-
y_w	Distance from the wall	m
$Y(t)$	Time-varying force in lift direction	N
z	Coordinate position along spanwise direction	m
$\alpha(t)$	Time-varying effective angle of attack	°
δ	Boundary layer thickness	m
δ_k^*	Numerical error of k-th input parameter	-
$\delta_{RE_{k1}}^*$	One-term numerical error	-
ε_k	Variation between two solutions for k-th input parameter	-
η	Propulsive efficiency	-
η_o	Open-water efficiency of screw propeller	-
θ_0	Pitching amplitude	°
$\theta(t)$	Time-varying pitching angle	°
κ	von Kármán's constant	-
λ_D	Density ratio between structure and fluid	-
λ_F	Frequency ratio between natural and oscillating frequency	-
ρ	Fluid density	$kg \cdot m^{-3}$
ρ_s	Structure density	$kg \cdot m^{-3}$
μ	Dynamic viscosity	$N \cdot s \cdot m^{-2}$
μ_t	Dynamic turbulent viscosity	$N \cdot s \cdot m^{-2}$
ν	Kinematic viscosity	$m^2 \cdot s^{-1}$
ν_t	Kinematic eddy viscosity	$m^2 \cdot s^{-1}$
$\boldsymbol{\tau}$	Turbulent stresses	Pa

$\boldsymbol{\tau}_R$	Reynolds stresses	Pa
τ_ω	Wall shear stress	Pa
ϕ	Arbitrary variable	-
φ	Phase angle between pitch and heave	°
ω	Angular frequency	$rad \cdot s^{-1}$
ω_t	Turbulence frequency	s^{-1}
Δt	Size of time step	s
Δy	Mesh height of first cell layer	m
Γ	Diffusion coefficient	-

Abbreviations

Notation	Description
ALE	Arbitrary Lagrangian Eulerian
AMC	Australian Maritime College
AMI	Arbitrary Mesh Interface
AoA	Angle of Attack
AR	Aspect Ratio
ARC	Australian Research Council
APWIGs	Auto-Pitch Wing-In-Ground Effect Oscillating Foil Propulsors
AUV	Autonomous Underwater Vehicle
CFD	Computational Fluid Dynamics
CFL	Courant-Friedrichs-Lewy
DES	Detached Eddy Simulation
DNS	Direct Numerical Simulation
FDM	Finite Difference Method
FEM	Finite Element Method
FVM	Finite Volume Method
GAMG	Geometric-Algebraic Multi-Grid
GGI	Generalized Grid Interface
ISE	International Submarine Engineering
LES	Large Eddy Simulation
LDV	Laser Doppler Velocimetry
MARIN	Maritime Research Institute of the Netherlands
MAV	Micro Air Vehicle
OSFBEM	Oscillating Foil Boundary Element Method
PBiCG	Preconditioned Bi-Conjugate Gradient
PISO	Pressure Implicit with Splitting of Operators
PIV	Particle Image Velocimetry

RANS	Reynolds-Averaged Navier-Stokes
RBF	Radial Basis Function
SIMPLE	Semi-Implicit Method for Pressure-Linked Equations
Slerp	Spherical linear interpolation
SST	Shear Stress Transport
URANS	Unsteady Reynolds-Averaged Navier-Stokes
UTAS	University of Tasmania
WIG	Wing-In-Ground
6-DOF	Six Degrees of Freedom

“inventas aut qui vitam excoluere per artes”

– Virgil

Abstract

Development of propulsion systems for both marine vehicles and aircrafts experienced a magnificent evolution in the past and will not slow the pace in the future. Remarkable performance with respect to thrust generation and maneuverability from the natural world using high-aspect-ratio appendages had inspired human beings to pursue more novel techniques for propulsion community. Owing to superior advantages in various aspects, the oscillating foil propulsor with optimized geometry and locomotion is considered as an alternative technology to conventional screw propellers. The configuration of interest in the current study is the auto-pitch wing-in-ground effect oscillating foil propulsors (APWIGs) which is characterized as a combination of biplane arrangement and flow-induced pitching motion. The biplane configuration with imposed counter-phase heaving motion can produce a beneficial dynamic wing-in-ground (WIG) effect. The lumped flexibility modelled by torsional spring attached to pitching axis is capable of improving the surrounding flow and simplifying the control mechanism. Based on the established and well-validated unsteady Reynolds-Averaged Navier-Stokes (URANS) model, a numerical study was undertaken to quantitatively evaluate and systematically analyze the propulsive characteristics of current concerned oscillating foil propulsor.

The initial focus was the effect of individual parameters on the hydrodynamic behaviors of APWIGs. The torsional spring stiffness is a dominant parameter that determines both dynamic responses and propulsive performance. Hence, the hydro-elasticity characteristics of APWIGs with the variation of torsional flexibility was firstly investigated. It was found that there exists an optimum spring stiffness for APWIGs that produces the highest propulsive efficiency under certain conditions. As an indication of non-dimensional spring stiffness, the frequency ratio was employed to distinguish the locomotion states and depict the performance metrics. Simulations showed that the forward-motion regime and stable locomotion state with periodic dynamical behaviors can only be obtained by a specific range of frequency ratio. Especially, the optimal propulsive efficiency is achieved at a frequency ratio in the range of 1.1 to 1.4. In addition, a parametric study with the consideration of various kinematic and geometry parameters was conducted. It was noted that the oscillating frequency highly affects the vortex shedding along both leading and trailing edges of each foil. The parameters including heaving amplitude, equilibrium distance between two foils and position of pitching axis have a strong effect on the pitch-leading phase difference and maximum pitching angle. Based on an appropriate parameter combination, the APWIGs can produce a high efficiency of over 70% within the considered parametric space.

A comparative study between the current configuration of interest and the widely examined oscillating foil systems was performed to demonstrate the advantages of APWIGs in both thrust production and efficiency enhancement. The contrasted propulsion systems consist of the single auto-pitch oscillating foil, biplane heave-only configuration and biplane fully-prescribed configuration. The maximum increase of propulsive efficiency of over 10% was obtained as a result of favorable WIG effect. It was revealed that the flow-adapted pitching motion can substantially reduce the flow separation, resulting

in a significant improvement of propulsive performance. The efficiency of APWIGs was found to be independent of advance speed compared with a fully-prescribed configuration that is dramatically sensitive to the inflow velocity.

To completely understand the physical mechanisms of oscillating foil propulsors, a series of three-dimensional simulations on the hydrodynamic characteristics of biplane configuration were carried out. The effect of aspect ratio (*AR*) on the propulsive performance and wake topology of WIG effect oscillating foil propulsors with fully-prescribed kinematics was firstly investigated by covering an adequately large range of *AR* from 1 to 10. Three-dimensional effect was found to be dominant for the flow behaviors of oscillating foils with an *AR* of below 2. Considering the compromise among multiple factors including efficiency deterioration, manufacturing cost, navigation and maneuvering of target vehicle, an *AR* range of 3-5 is recommended for the practical application of biplane oscillating foil propulsors. Furthermore, the preceding two-dimensional studies on the APWIGs were extended to the real three-dimensional flow. The hydro-elasticity characteristics of finite-span APWIGs was found to be analogical to two-dimensional predictions with an averaged efficiency loss of around 10% due to low-aspect-ratio effect. Numerical visualization of wake topologies showed that the flow pattern of finite-span oscillating foil is characterized as two sets of intertwined vortex rings, which largely differ from the wake structure of reverse Kármán vortex street in the two-dimensional flow.

Based on the framework of comprehensive computations and analyses, a design procedure for APWIGs was proposed to guide parameter selection regarding both kinematic aspect and geometric consideration. In order to satisfy specific requirements of target vehicles, several approaches were developed to perform the parameter optimization that aims to maximize propulsive performance. A case study on the application of APWIGs to an autonomous underwater vehicle (AUV) was conducted to demonstrate detailed process of the design procedure. In general, the presented research in this thesis makes original contributions to the development of novel propulsors and the understanding of fundamental flow physics. The highlighted findings provide significant insights into hydrodynamics of oscillating foils with biplane arrangement and flow-adapted pitch. The outcomes of the current study are regarded as an essential reference for the design, optimization and prototyping of WIG effect propulsors and a considerable supplement to the engineering solutions of unconventional marine propulsion.

CHAPTER 1

Introduction

1.1 Background and Significance

Historical evolution of propulsion systems for both aircrafts and water vehicles is an exploration process to find optimum technical solutions. The remarkable propulsive performance on animals with ability to fly and swim has fascinated human curiosity for a long time. Observations on the thrust-producing appendages from natural world inspire researchers to enhance and supplement the existing propulsion community by the high-aspect-ratio wings with appropriate locomotion. Tremendous efforts by a number of pioneers have been enriching and sharpening the tools to study these problems. More importantly, extensive endeavors into the pursuit of efficient cruise and swift maneuverability by oscillating foils have facilitated the understanding of fundamental physics and the development of engineering technologies.

For the last few decades, there is a growing interest in oscillating foil propulsors due to widespread application of autonomous underwater vehicle (AUV) and micro air vehicle (MAV). These man-made vehicles operating in special and complex environment might have a high requirement for scale and performance of thrusters, which cannot be satisfied by traditional propulsive systems in the most cases. Compared with conventional screw propellers, the oscillating foil propulsion system shows superior advantages in many aspects. It is well-established that the oscillating foil propulsor using rational kinematics presents a significant potential in efficiency maximization. From the view of engineering practice, high maneuverability can be achieved by the appropriate installation of oscillating foils for different flight regimes. Propulsive characteristics of oscillating foils show a remarkable independence on advance speeds compared to screw propellers. Blade-based propellers generally experience the challenge of cavitation issue, which can be prevented by oscillating foil configuration to a large extent. A typical oscillating foil thruster has a simple geometry consisting of one or multiple wings. The corresponding loading distribution along the surface of these wings are less nonuniform, suggesting a lower possibility of noise, vibration and structural damage over propeller blades with concentrated loading and high velocity in the tip regions. Owing to these structural and kinematic features, the oscillating foil propulsion system is an environment-friendly technique with the low impact on surrounding creatures.

General methods for the studies on hydrodynamics and aerodynamics of oscillating foils include mathematical analysis, computational fluid dynamics (CFD) and experimental measurements. Due to the significant reliability and high accuracy of numerical simulations, computational models based on the linear theory, lifting surface theory, quasi-vortex-lattice method, panel method and Navier-Stokes solver were frequently employed (Rozhdestvensky and Ryzhov, 2003; Fish and Lauder, 2006). A basic timeline of status regarding this problem is firstly presented here. Exploration of oscillating foils for propulsion can be traced back to the era of Leonardo da Vinci, who proposed a mechanical design of flapping wing machine based on the observation of birds (Shyy et al., 2013). The first demonstration for the thrust-producing mechanism by a flapping wing was provided by Knoller (1909) and Betz (1912),

respectively. They found the effective angle of attack (AoA) can be created for a flapping wing indicating that the generated aerodynamic force can be decomposed into thrust and lift components. By testing the averaged thrust of a stationary wing in sinusoidally oscillating wind stream, Katzmayr (1922) is the first to verify the Knoller-Betz effect. Birnbaum (1924) conducted the first analysis on an oscillating airfoil in the incompressible flow using linearized potential flow theory. He developed a non-dimensional parameter, namely reduced frequency, to characterize the ratio of flapping velocity to flight speed. Another commonly used non-dimensional parameter to measure the flight performance of flapping wings is the Strouhal number (Strouhal, 1878), which is an indication of oscillatory flow mechanisms. Taylor et al. (2003) investigated 42 species of flying animals by analyzing their oscillating frequencies and flapping amplitudes. He found that the operating Strouhal number of these animals mainly concentrate on the range between 0.2 and 0.4, suggesting that the Strouhal number is a significant similarity parameter to characterize the flight behaviors of flapping wings. The first theoretical explanation for the thrust production of a flapping airfoil based on the observed wake structures was presented by von Kármán and Burgers (1934). It was shown that the induced velocity deficit by vortex shedding can be identified in the wake profile of a drag-producing oscillating foil, while the wake pattern for a thrust-producing case is characterized as a reverse Kármán vortex street. Theodorsen (1935) and Küssner (1935) developed the linear theory in different forms to solve the aeroelasticity problems for airplane wing-fuselage system in turbulent and gusty air. This approach was extended to predict the propulsive performance for harmonically heaving and pitching airfoils by Garrick (1936). At about the same time, Gray (1936) performed a biochemical analysis on dolphin swimming and reported that its muscle power cannot overcome the experienced drag in water which is referred as the Gray's paradox. This claim raised the keen interests for researchers in the studies of fish swimming at that time although it is considered to be resolved now. Other noteworthy works include the studies by Taylor (1952) and Wu (1961) on the locomotion of long and waving aquatic animals.

The pioneering study on the propulsion performance of large-amplitude oscillating airfoil was carried out by Scherer (1968) using early linear theory. Significant contributions to the fundamental understanding of fish propulsion were given by Lighthill (1969; 1970; 1971), who introduced the nonlinear theory to investigate the large-amplitude oscillations with the consideration of undulation and three dimensions. He also provided the first explanation of lunate-tail wing theory for the aquatic-animal studies. Wu (1971a; 1971b; 1971c) further developed the linearized inviscid flow theory and applied it to the studies of undulatory swimming propulsion, which revealed several significant physical mechanisms with respect to the thrust optimization of flexible oscillating plate. Newman (1973) and Newman and Wu (1973) developed a consistent slender-body theory to involve the body thickness effect, kinematic and dynamic interactions, and vortex shedding from caudal fins in the fish locomotion. Such a generalized mathematical demonstration covering various relevant factors is more representative for the modelling of oscillating fin propulsion. Cheng and Murillo (1984) conducted an asymptotic analysis on the high-aspect-ratio lunate tail by taking into account the influence of wake vorticity using classical lifting line theory. His study provided great insights into flow mechanisms of swimming propulsion

regarding three-dimensional and unsteady effects. Pioneering investigations into the effect of planform shape and deforming flexibility on the propulsive metrics of three-dimensional oscillating foil propulsors were performed by Liu (1991; 1996) using quasi-vortex-lattice method and time-domain panel method, respectively. Under certain assumptions, these works contributed an accurate and reliable numerical solution to the evaluation of hydrodynamic performance of oscillating foils. With the rapid development of measuring techniques and computational facilities over the past decades, the systematic force presentations by experimental measurements (Anderson et al., 1998) and comprehensive CFD simulations by Navier-Stokes solver (Tuncer and Platzer, 2000) were achieved for unsteady flow around the oscillating foils. Owing to that, it becomes feasible to take into account the complicated physical mechanisms including viscous effect, turbulent effect, flow separation, dynamic stall and vortices evolution for the performance analysis of oscillating foil propulsors.

Tremendous efforts have been devoted to enhance our understanding in flow physics of oscillating foils so far. A number of issues related to aerodynamics and hydrodynamics, fluid-structure interaction and unsteady flow characteristics were indicated comprehensively (Triantafyllou et al., 2000; Platzer et al., 2008; Dabiri, 2009; Shyy et al., 2010; Wu, 2011; Shelley and Zhang, 2011). In summary, the past and ongoing concerned aspects regarding oscillating foil researches include the physical mechanisms of thrust production, development of powerful tools (theoretical methods, CFD models and experimental techniques), performance optimization based on kinematic parameter study, complete understanding of vortex behaviors and flow patterns, effect of flexibility in different forms, multiple-wing arrangement and wing-vortex interactions, and oscillatory locomotion in support of various flight modes (forward flight, fast-start, take-off, hovering and gliding). In the foreseeable future, the major interests and potential challenges for oscillating foil propulsion are expected to remain in several fields. Efficiency or thrust maximization by optimizing foil geometry and kinematic parameters is still the primary objective for relevant studies. Further implications of oscillatory locomotion for high maneuverability are needed to promote the engineering applications. Understanding of dynamics and stability for the oscillating foils with both chordwise and spanwise flexibility remains highly insufficient. Active control systems using actuator or adaptive control techniques based on flow feedback are essential to achieve specified wing locomotion and resulting propulsion performance which are still fairly limited in existing studies. The ultimate aim of oscillating foil studies is to generate thrust for different vehicles to attain the required flight or swimming mode. To this end, the interaction of oscillating foils with vehicle body and the influence of vehicle wake on the propulsor characteristics need to be fully explored.

1.2 Literature Review

The state of the art regarding hydrodynamics and aerodynamics of oscillating foils was reviewed in this section. Several aspects that attract past and recent attention were discussed to highlight the development and progress in this field. The focus of the current review was mainly on the oscillating

foil propulsion in which concerned metrics are characterized as thrust generation and propulsive efficiency. A brief summary in research status of oscillating foils for energy harvesters was also provided for the sake of completeness. The presentation of pioneering studies covers a wide range from the fundamental physical insights to the systematic performance evaluations.

1.2.1 Single-foil configuration

Early understanding of thrust-producing physics for the oscillating foil propulsion was mainly indicated by studies on a single-foil configuration. The corresponding locomotion commonly has two degrees of freedom with fully prescribed heaving and pitching motion. Chopra (1976) developed a large-amplitude theory to analyze the lunate-tail hydrodynamics, suggesting that the optimal propulsive performance of an oscillating lunate tail can be achieved by a reduced frequency of around 0.8 and a large amplitude of twice the central chord length. DeLaurier and Harris (1982) performed an experimental study on the propulsive characteristics of a heaving and pitching oscillating wing. In their measurements, the kinematic parameters were set to avoid the flow separation. It was found that the thrust approximately shows a linear dependence on the reduced frequency. They also claimed that the phase angle of 90-120 degrees of pitch lagging heave tends to produce the best propulsive performance. Koochesfahani (1989) examined the vortical wake structures induced by a flapping airfoil with small-amplitude pitching motion. A significant finding of this study is that the cores of wake vortices have an axial flow suggesting a linear dependence on the oscillating frequency and amplitude.

Liu and Bose (1993) performed a numerical study on the propulsive performance of cetacean flukes using lifting surface theory. The planform geometries mimicking flukes of white-sided dolphin, fin whale and white whale were examined to maximize the thrust generation and propulsive efficiency. It was found that for various planform shapes, the propulsive performance shows different sensitivities to the change of heaving amplitude, pitching amplitude and position of pitching axis. Streitlien et al. (1996) conducted a two-dimensional analysis on the influence of vortex structures on propulsive efficiency of a heaving and pitching hydrofoil. It was highlighted that an appropriate manipulation of vorticity can promote the propulsive performance of oscillating foils. They indicated that the phase difference between foil motion and incidence of inflow vortices show a significant effect on the propulsive efficiency. It was also found that the maximum efficiency appears when the oscillating foil approaches the oncoming vortices. Hall and Hall (1996) numerically predicted the minimum requirements of induced power for the flapping wing flight. They employed the Betz criterion to develop two flapping models including a small-amplitude motion and a large-amplitude oscillation. It was proved that the induced power for thrust production shows a decreasing trend when the flapping frequency and amplitude becomes larger. Results also indicated that an optimum flapping amplitude can be found when both thrust and lift generations are required.

Massachusetts Institute of Technology seems to build the first robotic fish called RoboTuna which is propelled by an oscillating tail foil (Barrett, 1996). The propulsive potential of this biological

configuration was experimentally explored suggesting that a man-made system can achieve a significant swimming performance. Jones et al. (1998) performed a series of measurements and computations on the Knoller-Betz effect generated by a sinusoidally heaving airfoil. It was suggested that the vortex behaviors in wake indicating thrust production are mainly inviscid phenomena. The nonsymmetric and deflected wake patterns were identified both experimentally and numerically at the Strouhal numbers of exceeding 1.0 in this study. Harper et al. (1998) modelled the dynamics of an oscillating foil propulsor, in which the forces of actuators were transmitted to the foil by a spring. It was found that the energy costs of one actuator can be reduced by 33% using this mechanism although it might introduce the issue of instability.

Anderson et al. (1998) conducted a comprehensive experimental study on the force generation and flow visualization of thrust-producing oscillating foils undergoing harmonically heaving and pitching motion. Multiple combinations of varying kinematic parameters were tested to find high performance, including the Strouhal number, heaving amplitude, AoA and phase angle between heave and pitch. Significant propulsive efficiency of 87% was reported in this study obtained by the Strouhal number in the range between 0.25 and 0.4, a large heaving amplitude with a motion-to-chord ratio of order one, the maximum AoA in the range of 15-25 degrees, and a phase difference between pitching and heaving motion of about 75 degrees. Observation of flow fields indicated that high propulsive efficiency corresponds to the formation of leading-edge vortex around the alternating sides of oscillating foil and the resulting interactions between the leading-edge and trailing-edge vortices. These vortex structures eventually evolve into a reverse Kármán vortex street in the downstream wake. The same experimental apparatus was employed by Read et al. (2003) to investigate the propulsion and maneuvering of oscillating foils. It was reported a planform area thrust coefficient of 2.4 at the maximum AoA of 35 degrees and the propulsive efficiency of up to 71.5% at the maximum AoA of 15 degrees. A plateau of satisfactory efficiency in the range of 50-60% was obtained under certain conditions. Especially, it was reported that the best propulsion performance was achieved by a phase angle in the range of 90-100 degrees between pitch and heave. Hover et al. (2004) examined the effect of AoA profiles on the propulsive performance of this flapping foil model. It was found that a significant improvement of performance can be attained by a cosine profile of AoA, while the maximum thrust coefficients tend to be obtained by a sawtooth profile of AoA.

Isogai et al. (1999) presented a series of simulations on the dynamic-stall behaviors of an oscillating foil in combined heaving and pitching motion. The considered kinematic parameters include the reduced frequency, phase difference and amplitude ratio. They observed the maximum efficiency at the pitch-leading phase angle of 90 degrees coupled with an optimum reduced frequency without apparent flow separation. Lai and Platzer (1999) and Lai et al. (2002) examined the wake flow of a pure heaving airfoil in the water tunnel using a single-component laser Doppler velocimetry (LDV). The dye flow visualizations indicated that the vortex structures produced by a heaving airfoil tend to change from a drag-producing wake pattern to a thrust-producing jet profile when the non-dimensional heaving velocity is larger than about 0.4.

The aerodynamics of a combined pitching and heaving airfoil was numerically simulated by Tuncer and Platzer (2000). Both thrust-producing wake structures and flow separation characteristics were presented in this computation. It was suggested that the highly attached flow around the airfoil surface tends to produce the maximum propulsive efficiency. The aerodynamic force measurements on a dynamically scaled flapping wing model mimicking insect flight were performed by Sane and Dickinson (2001). This study examined 191 sets of kinematic patterns based on the variation of stroke amplitude, stroke deviation, flip timing, flip duration and AoA. Several implications with respect to the role of kinematics on the force performance of flapping wings were presented. Jones et al. (2002b) conducted a collaborative study to evaluate the capability of various methods in predicting the propulsion performance of flapping wings. Comprehensive comparisons between experimental measurements and numerical computations using flat-plate theory, panel method, Euler solver and Navier-Stokes model were performed to indicate the merits and limitations of each tool. Murray and Howle (2003) examined the flapping wing system with a spring-based heaving motion. It was suggested that the passively heaving mechanism tends to reduce the critical frequency at which the positive thrust is generated. The dynamic-stall characteristics of a pitching airfoil were numerically simulated by Akbari and Price (2003) using a vortex method. Compared with static-stall scenario, the delayed flow separation with higher incidences for an oscillating airfoil was identified in this study. Guglielmini and Blondeaux (2004) numerically confirmed that the introduce of pitching motion is the only means for the thrust generation in hovering mode. It was also indicated that the combination of heaving and pitching motion tends to produce a higher thrust and efficiency compared to the oscillating foils in a pure heaving motion.

Experimental measurements by Schouveiler et al. (2005) on the propulsion performance of a harmonic heaving and pitching flapping foil reported a high efficiency of more than 70% under the optimum combination of kinematic parameters. It was also observed that nonsymmetrical flapping motion can improve the maneuvering capability of flapping foil system. The optimization of thrust performance for a combined heaving and pitching airfoil was performed by Tuncer and Kaya (2005). The involved parameters include the heaving amplitude, pitching amplitude and phase difference between them. Computational results showed that the high thrust production is achieved at the cost of propulsion efficiency. A satisfactory efficiency might require a small effective AoA and low leading-edge vortex formation. After that, they numerically tested the propulsion performance of a flapping airfoil following a non-sinusoidal oscillatory path (Kaya and Tuncer, 2007). It was reported that there is a significant increase of thrust production using a non-sinusoidal oscillating mode compared to a sinusoidal flapping airfoil. The hydrodynamic features of an oscillating foil under the free surface were computationally investigated by Zhu et al. (2006). This study modelled two types of foil configuration including a heaving foil in horizontal layout and a swaying foil in vertical arrangement. It was found that the free-surface effect on the propulsive performance of oscillating foils depends on an unsteady parameter.

A comprehensive comparison of efficiency performance by a flapping wing between the experimental measurements, simulations of Navier-Stokes solver, predictions by inviscid analytical method and

computations using unsteady panel method was conducted by Young and Lai (2007), suggesting that the maximum propulsive efficiency and corresponding Strouhal number are affected by plenty of physical mechanisms. von Ellenrieder et al. (2008) developed a hypothesis with respect to the fluid mechanism of flapping wing, which considers the selection of Strouhal number in flapping flight as a limit cycle process. They believed that the steady-state efficiency of a propulsion system should be designed-in instead of actively controlled. Tang et al. (2008) numerically studied the effect of the Reynolds number, kinematics and reduced frequency on the unsteady flow around an elliptic airfoil using a Navier-Stokes solver. Within the considered parametric space, it was found that the delayed-stall behavior is the main cause for the generation of maximum lift peaks in hovering motion. Pesavento and Wang (2009) claimed that the flapping flight can be more efficient than the optimal steady motion with respect to aerodynamic performance. Their two-dimensional computations suggested that the aerodynamic power of up to 27% for the optimal steady flight can be saved by the optimized flapping motion. This aerodynamic behavior can be achieved by the manipulation of interactions between flapping wing and wake structures. The fluid dynamics of a fish-tail model experiencing a transient motion were numerically computed by Guglielmini and Blondeaux (2009), who indicated that the kinematic details of foil significantly affect the time series of propulsive forces. The mechanism of start-up control by fishes and the parametric range for an optimal propulsion were explored in this work.

The vortex wakes of a pitching foil were experimentally visualized by Schnipper et al. (2009), which identified different wake patterns and corresponding transition between them with the variation of oscillating frequency and pitching amplitude. A similar flapping foil model undergoing either pure heaving motion or pure pitching motion was studied by Andersen et al. (2017). They plotted the wake maps as a function of oscillating frequency and amplitude for two motion modes, which were found to be qualitatively similar between heaving and pitching regime. In this investigation, the relationship between the drag-thrust transition and vortical structures for both heaving and pitching modes was numerically presented. Xiao and Liao (2010) numerically studied the effect of AoA profile on the propulsion performance of an oscillating foil. Both heaving and pitching laws are modified to achieve a harmonic cosine function for the effective AoA. Results showed that a poor thrust performance of sinusoidal oscillating mechanism can be significantly improved by an imposed cosine profile of effective AoA. It was found that a stronger reversed Kármán vortex street in wake was numerically identified implying the performance increase. Hu et al. (2011) performed an experimental study on the unsteady flow of a root-fixed flapping wing, which considers several parameters including the flapping frequency, stroke amplitude and wing size. In this work, the evolution of wake vortex structures was identified using the digital particle image velocimetry (PIV) system. By comparing the efficiency performance of oscillating foil to the corresponding wake patterns, Deng et al. (2016) reported that the efficiency tends to constantly increase with the Strouhal number until the wake transition of two-dimensional state to three-dimensional state occurs. Numerical visualization on the flow fields of harmonically oscillating airfoil identified various wake patterns with respect to the induced vortex street, which was found to be highly correlated to the corresponding force behaviors (Zheng et al., 2019).

In addition to general oscillating laws, the effect of adding in-line motion on propulsive characteristics of oscillating foils was experimentally studied by Licht et al. (2010) and Izraelevitz and Triantafyllou (2014). A power downstroke and a feathering upstroke were employed in the motion trajectory of oscillating foils, which can perform both backwards in-line motion and forwards in-line motion depending on the ratio of thrust to lift. It was found that the in-line motion can significantly increase the mean lift, augment thrust and improve efficiency. The force production and wake patterns of a pitching foil in non-sinusoidal profile were numerically investigated by Chao et al. (2019). The non-sinusoidal trajectories of pitching motion were tested from the sawtooth profile to the square profile by an adjustable parameter. It was found that the timing of drag-thrust transition for a pitching foil was significantly influenced by the motion profile.

The flight velocity and propulsive efficiency of an auto-propelled flapping airfoil were computed by Benkherouf et al. (2011) using a Navier-Stokes model. In this simulation, the self-propulsion forces of a heave-only flapping foil were observed by testing different flapping frequency and heaving amplitudes. Numerical computations on the flapping airfoil propulsion with varying thickness and camber were performed by Ashraf et al. (2011). Under the thrust-producing scenario with a low Reynolds number, a thin airfoil was found to produce a better performance than a thick shape. For a relatively high Reynolds number, the flapping airfoil with a thick section tends to generate satisfactory propulsion performance. Their results showed a low influence of camber on the propulsive characteristics. Experimental observations by Jones and Babinsky (2011) on the flow field of insect-like flapping wing identified a low sensitivity of vortex structures to Reynolds numbers within the tested parametric range.

A comparison of efficiency performance between the flapping foil and a conventional propeller was performed by Floc'h et al. (2012) using a potential-flow solver to gain credibility for the oscillating foil propulsors. It was found that the role of Strouhal number for flapping foils is analogous to that of advance parameter for a propeller. A similar trend of hydrodynamic performance between the flapping foils and conventional propellers was indicated. Belibassakis and Politis (2013) presented an analysis on the contribution of flapping wings to ship propulsion in the random waves. The flapping wing system consists of a horizontal wing and a vertical wing. The locomotion of horizontal wing is characterized as the imposed pitching motion and ship-induced heaving motion. The dynamics of vertical wing are provided by the rolling and swaying of ship. Hydrodynamic computations by non-linear panel method suggested a significant performance of this flapping wing propulsor in thrust production, reduction of dynamic responses and shipping stabilization.

The ground effect is commonly considered as a beneficial mechanism for the thrust production of oscillating foils. The unsteady flow around a heaving airfoil above the ground was numerically investigated by Molina and Zhang (2011). They classified the flow into three regimes depending on the reduced frequency. It was indicated that the ground effect is apparent at the low frequencies, while the incidence effect and added mass effect become dominant with the medium frequencies and high frequencies, respectively. Wu et al. (2014) performed a numerical study on the unsteady flow over a

heaving and pitching wing undergoing the ground effect. The influence of distance between wing and ground was examined with the variation of flapping frequency. It was indicated the ground effect tends to affect both force characteristics and flow behaviors. They numerically identified the vortex structures with an oblate shape and obliquely propagating wake due to the presence of ground. Quinn et al. (2014) performed a series of experimental measurements and numerical computations on the propulsion capabilities of a pitching foil near a solid ground. By examining various distances between foil and ground, it was indicated that the ground effect can enhance thrust generation, while the propulsive efficiency is independent to the mean position of foil. Unlike the typical vortex street behind a flapping wing far from the ground, the wake pattern of near-ground pitching foil is identified as the vortex pairs. Mivehchi et al. (2016) conducted a series of experimental measurements on the force generation of heaving and pitching foil near a solid boundary. By testing the different distances of foil from the solid wall, it was suggested that this distance plays a significant role in both lift and thrust production. The strength of ground effect was found to be adjustable such that a certain level of thrust can be achieved by selecting appropriate kinematic parameters.

More recently, the unsteady thrust and lift forces acting on a flapping airfoil with a pure pitching motion was experimentally studied by Mackowski and Williamson (2015). A series of direct measurements were performed to avoid the issues by the deriving-force measurements of local flow region. It was suggested that the early linear theory tends to substantially overpredict the mean thrust, but presents a good performance in the prediction of phase and amplitude of time-varying component. The vortex structures in wake with varying kinematic parameters were also examined using PIV system which indicates that the effect of vortex behaviors on the thrust production of flapping airfoil is highly localized. The kinematics of a pitching and heaving airfoil was computationally modelled by Hoeijmakers and Mulder (2016) to explore the flapping wing propulsion for a robotic bird. It was found that the highest propulsive efficiency appears at the maximum effective AoA of near 11 degrees. Numerical analysis and experimental measurements on the propulsive performance of an undulatory caudal-fin model were carried out by Mannam and Krishnankutty (2018). The capability and potential of this flapping wing system for the propulsion of marine vehicles in both surface and underwater modes were evaluated. Oscillatory foil propulsion with a relatively high heaving amplitude was simulated by Dave et al. (2020). It was suggested that the transition from the high-efficiency regime to the high-thrust regime at a high Reynolds number are dependent on the kinematics of oscillating foil. Satisfactory propulsive efficiencies of exceeding 75% under certain conditions were reported in this study.

Further details with respect to the investigations into single oscillating foil propulsion can be found in comprehensive overviews by Rozhdestvensky and Ryzhov, (2003) and Triantafyllou et al. (2004) in both computational predictions and experimental measurements.

1.2.2 Dual-foil configuration

It has been revealed that the vortex shedding from both leading and trailing edge has a significant

influence on the force behaviors of oscillating foils. Compared to a single-foil configuration, the dual-foil arrangement with close proximity to each other tends to introduce much more complex wing-vortex interactions. The superior advantages of dual-foil configuration over a single oscillating foil have been widely confirmed and highlighted. The favorable wing-vortex interactions achieved by appropriate control of kinematic and geometry parameters have been found to be applicable for different flight modes (Platzer et al., 2008; Lian et al., 2014).

The dual-foil systems with two closely coupled foils are normally arranged either in tandem or biplane configuration. A limited number of studies on tandem configuration were found since the improvement of overall propulsive performance by such an layout is less prominent. He et al. (2007) utilized a potential-flow model to simulate the body-vortex interaction induced by an oscillating foil system in tandem, which has a front pitching foil and a rear static foil. Multiple parameters were tested in this study including the oscillating frequency, distance between two foils, pitching angle and vertical position of rear foil. The propulsion properties of a tandem flapping wing configuration were numerically investigated by Xu et al. (2017) using the panel method. Especially, the interactions of hind foil with wake structures of fore foil were simulated based on the global phase shift. It was indicated that an appropriate distance between two foils can significantly improve the propulsive efficiency. The dynamic responses of a semi-free flexible filament behind a pitching rigid foil were numerically simulated by Lin et al. (2018). The fore pitching foil can produce different wake profiles by adjusting the kinematic parameters. In this study, three dynamic states for the flexible filament were identified including the flapping in a Kármán vortex street, flapping outside a reversed Kármán vortex street, and static in a compact Kármán vortex street. Moreira et al. (2020) conducted a numerical investigation into the hydrodynamic characteristics of a dual-foil configuration in tandem, which can be applied to both ship propulsion and energy extraction. This system has two unaligned oscillating foils along the heaving direction. A two-dimensional parametric computation indicated that the unaligned arrangement presents a better performance over the aligned configuration.

The biplane configuration is considered as a more promising arrangement to improve both thrust production and propulsive efficiency of oscillating foils due to the generated wing-in-ground (WIG) effect by counter-phase heaving motion of two coupled wings. The concept of WIG effect oscillating foil thruster seems to be first proposed by Jones et al. (1997), which is characterized as a biplane configuration with a pure heaving motion or combined heaving and pitching motion. The prescribed heaving motion of two foils is set as counter-phase profile indicating that the upper foil approaches close to lower foil during the downstroke while it moves far away from another one during the upstroke. This oscillatory mechanism can induce a symmetrical plane between two foils and the resulting WIG effect that resembles a single foil in proximity to a solid boundary. Jones and Platzer (1999) and Jones et al. (2001; 2002a) conducted a series of experimental measurements and numerical computations on the propulsive performance of WIG effect oscillating foil propulsors. A typical prototype of biplane oscillating foil propulsion system can be found in Jones et al. (2002a). Results suggested a substantial improvement in both thrust generation and propulsive efficiency for biplane configuration with counter-

phase oscillation compared to a single oscillating foil. It was believed that such a biplane arrangement can take advantage of favorable wake interference. They also reported a strong Reynolds-number dependency for this configuration that might reduce or eliminate the wake-interference benefits at a certain order of Reynolds number. Based on the research insights, a prototype of MAV using the biplane oscillating foil arrangement was designed by Jones and Platzer (2010). In this flapping-wing MAV, a fixed fore wing is utilized to generate the required lift and two counter-phase oscillating wings are employed for the thrust production. It was reported that this MAV can achieve a flying duration of about 15 minutes in the speed range of 2-5m/s using a rechargeable lithium-polymer battery. More details with respect to this flapping wing propulsion system can be referred to Jones and Platzer (2010).

Tuncer and Kaya (2003) evaluated the propulsion performance of two flapping airfoils in biplane configuration by a series of computations. Results indicated that the biplane system can produce 20%-40% more thrust than a single-foil configuration. Recorded flow patterns using particle traces suggested that the maximum thrust production can be obtained by preventing the formation of large-scale vortices. Another implication of this study is that multiple kinematic parameters and distance between two foils need to be optimized for the highest thrust production. Liu (2005a) proposed a biplane oscillating foil propulsion system using a semi-active motion mechanism. This novel oscillating foil propulsor employs an imposed heaving motion while the pitching motion is constrained by the damping means. The hydrodynamic loads acting on the foil members will be offset by the damping torque during the operation. It is expected that a thrust can be generated for the rigid foils at zero forward speed as the pitching angle is controlled by the damping means. The propulsive performance of WIG effect propulsor with a pure heaving motion was also evaluated by Liu (2005b) using the time-domain panel method. Computational results showed that each foil of biplane configuration produces the higher thrust and efficiency than a single oscillating foil due to the generated WIG effect. Another merit for the biplane arrangement is the balance of side hydrodynamic loading so that the vehicle can perform a straight movement without yaw motion. A comparative analysis of propulsive characteristics between the WIG effect thruster and traditional screw propeller was performed by Liu et al. (2010). A similitude system based on the geometry and kinematic parameters was built to directly compare the propulsive performance between WIG effect thruster and screw propeller, indicating an independence of advance speed for WIG effect propulsor under the assumption of ideal fluid. Unlike the screw propellers with an operating-speed limitation, the results revealed that the WIG effect propulsor has a potential in applications to a high-speed regime.

An attempt with respect to the application of multiple flapping wings to aircraft propulsion can be found in the study by Zdunich et al. (2007), who utilized two pair of clap-fling wings as the propulsor of a MAV. More details regarding the prototype of this oscillating foil propulsion system can be found in their study. Based on a series of experimental measurements, it was indicated that the clap-fling phenomenon can produce an increase of 40% in thrust-to-power ratio. Miao et al. (2009) conducted a numerical study on the propulsive performance of a biplane counter-oscillating airfoil configuration with chordwise flexibility. By examining various curvature deformations and kinematic parameters, it

was found that the flexible airfoils using the counter-plunge flapping mechanism can increase both thrust generation and efficiency. The open-water characteristics of WIG effect propulsor with combined heaving and pitching motion was investigated by Politis and Tsarsitalidis (2013) using the boundary element method. Systematic computations with various kinematics were performed in this study, which reported a thrust coefficient order of 0.77 that is higher than the value obtained by traditional propellers. It was also indicated that this configuration has no cavitation issues when operates in the regime of optimal propulsive efficiency.

1.2.3 Flexibility and elastic support

The evident bending of flexible wings and fins in nature inspires researchers to consider the flexibility of oscillating foils as a significant factor for the improvement of propulsive performance. It has been widely confirmed that either the chordwise or spanwise flexibility can dramatically affect the dynamics and hydrodynamics of oscillating foils. The propulsion characteristics of flexible foils with a large-amplitude oscillation were analyzed by Katz and Weihs (1978) based on the assumption of inviscid flow. This parametric study reported a maximum efficiency increase of 20% due to the chordwise flexibility at the cost of small thrust loss. Vest and Katz (1996) developed an unsteady potential flow model to simulate the aerodynamic behaviors of a flapping wing with time-dependent deformation, which can provide the acceptable force predictions but limited flow information. Liu and Bose (1997) evaluated the influence of spanwise flexibility on the propulsion performance of oscillating foil propulsors by a series of numerical computations. It was found that the passive flexibility tends to degrade propulsive efficiency. But they also highlighted that an appropriate control of phase difference between spanwise flexibility and other motion parameters can increase the efficiency to a level exceeding the value of an equivalent rigid foil.

Heathcote et al. (2004) carried out a series of measurements on the thrust performance and flow features of a flexible heaving airfoil at zero freestream velocity. Three different bending stiffness were tested in this study to explore the effect of airfoil flexibility. It was found that the wake structures present different vortical patterns with the variation of airfoil stiffness due to the difference of induced trailing-edge displacement lag. Force measurements suggested that an optimum airfoil stiffness that produces the maximum thrust can be found under some conditions. Heathcote and Gursul (2007) experimentally examined the influence of chordwise flexibility on the propulsion performance of a heaving airfoil. Measurements indicated that the flexibility along chordwise direction can improve both thrust production and propulsive efficiency. Visualization of flow fields revealed that the stronger trailing-edge vortex behaviors tend to produce the higher thrust coefficients, while the weaker leading-edge vortex structures correspond to a higher efficiency.

Bergou et al. (2007) conducted a calculation in the required power for the insect-wing pitching motion suggesting that the fluid forces tend to assist passive wing during hovering flight. The locomotion of a flapping foil with either spanwise or chordwise flexibility was numerically modelled by Zhu (2007).

Two different types of surrounding fluid were considered in this study including a low-density fluid with inertia-dominated foil deformation and a high-density fluid with hydrodynamic-dominated foil deformation. For the low-density fluid, it was indicated that the chordwise flexibility tends to decrease both thrust and efficiency, while the spanwise flexibility improves the thrust without degradation of efficiency under certain conditions. For the high-density fluid, results suggested that the chordwise flexibility improves the efficiency, while the spanwise flexibility tends to decrease the propulsive performance. Connell and Yue (2007) conducted a numerical study on the stability and responses of a thin flapping flag with the high extensional rigidity and low bending rigidity. The related parameters that determine the flag locomotion and force behaviors are structure-fluid mass ratio, Reynolds number and bending rigidity. Three distinct regimes of dynamic responses depending on the variation of mass ratio were identified in this study.

The effect of spanwise flexibility on the performance of a heaving foil was experimentally studied by Heathcote et al. (2008) in the water tunnel. It was found that a certain spanwise flexibility can improve both thrust production and propulsive efficiency, while a relatively large flexibility tends to be detrimental to the propulsive performance due to the phase delay of wing-tip displacement. A potential-flow analysis on the resonance of a flexible flapping wing was conducted by Michelin and Llewellyn Smith (2009), who found that the resonance between forcing frequency and system natural frequency tends to induce the maximum trailing-edge flapping amplitude. The aerodynamics of a flexible flapping wing with a pure heaving motion were computed by Chimakurthi et al. (2009) using a computational aeroelastic framework, suggesting that the spanwise flexibility is beneficial to the thrust production. Whitney and Wood (2010) conducted an experimental study on a flapping wing with the passive rotation to mimic the dynamics of flying insects. Both real-time force predictions and flow visualizations were provided in their measurements. Yang et al. (2010) numerically simulated the interaction between a highly flexible flapping wing and the surrounding flow using a strong-coupling method. For the actively heaving and passively pitching wing, results suggested that the thrust-producing regime can only be achieved as the pitching angle and nominal AoA exceed a certain value.

Alben et al. (2012) both experimentally and numerically examined the dynamics of a heaving foil with chordwise flexibility, and found the resonant-like peaks for advance speed as a function of length and rigidity of foil. Barannyk et al. (2012) studied the propulsive performance of an underwater oscillating plate with chordwise flexibility in the water tunnel. By testing different Strouhal numbers, submergence depths and chordwise stiffness, a high propulsive efficiency of about 80% was reported in this study. Effect of submergence depth is characterized as an increasing trend of thrust coefficient with the proximity of plate to the bottom of water channel. Passive deforming compliance can be beneficial to the lift generation of insect wings. An efficient mechanism is to mitigate the effect of negative wing-wake interactions by streamlining the foil shape (Kang and Shyy, 2012).

Hua et al. (2013) performed a computational investigation into the locomotion of a flapping plate with the chordwise flexibility using the immersed boundary-lattice Boltzmann method. The leading-edge

flapping plate is allowed to freely move along the horizontal direction. Results divided the dynamics of plate into three motion regimes including the forward, backward and irregular depending on the bending flexibility of plate and heaving amplitude of leading edge. It was found that the appropriate chordwise flexibility is beneficial to the propulsive performance for the forward motion regime, in which the corresponding flow structures were characterized as two kinds of vortex wake including normal pattern and deflected profile. Tian et al. (2013) conducted a two-dimensional numerical study to explore the effect of flexibility on the force performance of a flapping wing. The flexible wing has a translating trajectory of inclined stroke and a pitching motion around the leading edge. In this study, the effects of flight speed, stroke plane angle, mass ratio and wing stiffness were examined, indicating that the passive pitch due to wing flexibility can promote thrust production. They also observed an asymmetric behavior with respect to wing deformation under the symmetric conditions of geometry and kinematics.

Richards and Oshkai (2015) experimentally examined the effects of kinematics, stiffness and inertia on the propulsive characteristics of an oscillating foil, which reported an optimum range of frequency ratio from 0.7 to 0.9 that can produce relatively large propulsive efficiency. It was also indicated that the combination of heave and pitch tends to present a higher efficiency at the expense of thrust production compared with the heave-only motion. Experimental observations by Feilich and Lauder (2015) on the hydrodynamics of an undulatory flapping foil suggested a complicated interacting mechanism between foil shape, flexural stiffness and swimming performance. Lucas et al. (2015) examined the effect of nonuniform flexibility on the swimming locomotion of an oscillating foil to reproduce dynamics of fish body with real material properties. They considered four foil models including two configurations using the uniform bending stiffness and two foils with the nonuniform distribution of flexural stiffness. It was found that the nonuniform foils have a higher swimming performance over the configurations with uniform bending flexibility under the non-self-propelling conditions. Stowers and Lentink (2015) developed a new mechanism with respect to the wing morphing of passively flapping configuration. They performed a series of experimental measurements on the dynamics of an unactuated hand wing connected with an arm wing by a wrist joint. Hoke et al. (2015) numerically modelled a flexible flapping foil with the time-varying camber deformation for the purpose of both energy extraction and propulsion. They suggested that the performance improvement can be achieved by an appropriate manipulation of foil shape deformation with the beneficial vortex interactions.

The interaction between vortex structures and elastic-dynamic behaviors was numerically analyzed by Mysa and Venkatraman (2016). Based on the spatial and temporal evolution of foil slope and curvature, the significance of foil deflection topology and corresponding effect on vorticity characteristics were presented in this study. Olivier and Dumas (2016) numerically modelled a self-propelled flexible flapping wing with both pitching and heaving motion. The effects of inertia and flexibility on the performance metrics of freely moving foil were analyzed by a series of two-dimensional computations. They reported that an optimum chordwise flexibility can be found to generate the maximum efficiency with a high pressure-to-inertia ratio, while the flexibility tends to reduce the efficiency when this parameter is low. Fernandez-Prats (2017) performed a series of measurements on the propulsion

features and flow profiles of a heaving flapping foil with chordwise flexural stiffness. It was suggested that the propulsive efficiency of 69% can be achieved by employing an optimum flexural stiffness. Force measurements and flow visualizations were conducted by Iverson et al. (2019) to investigate the influence of chordwise flexibility on the propulsive characteristics of oscillating foils. Three foils with different distribution of inertia and stiffness were examined. They highlighted that the angle of trailing edge relative to the direction of advance speed has a maximum effect on the thrust generation regardless of whether it is produced by the passive flexion or prescribed pitch. Luo et al. (2020) numerically studied the dynamic interaction between a flexible caudal fin and surrounding fluid. The surface of considered fin has a nonuniform flexibility distribution characterizing as five stiffness distribution patterns. It was found that the deformed fin with a cupping stiffness profile produces the highest propulsive efficiency and the heterocercal flexible fin generates the best maneuverability.

For a general wing structure, the flexibility tends to decrease sharply from the leading edge to trailing edge and from the root to tip. Thus, it is reasonable to introduce a torsional spring to model the chordwise flexibility. The assumption of lumped torsional flexibility has been widely applied to the studies of flexible oscillating foils regarding both hydrodynamic behaviors and flow structures. Experimental observations revealed that a passively flapping foil based on a spring-mass-damper model can extract the energy from the wake of upstream body and produce a self-propelled thrust (Beal et al., 2006). This behavior suggests that a passive moving structure has the capability to follow or even catch up another upstream body without any power input. The experimental measurements and numerical simulations on the fluid dynamics of a spring-hinged flapping wing were carried out by Toomey and Eldredge (2008). The two-component configuration consists of an actively heaving wing and a flow-induced part. Based on the analysis of multiple kinematic parameters, it was found that the lift generation mainly depends on the rate and timing of airfoil rotation, while it has a low sensitivity to the translational acceleration. A multi-fidelity study on a semi-active configuration was carried out by Willis et al. (2007), in which a torsional spring is attached to the leading edge of an oscillating foil. The main focus of this research lies in the construction of computational frame. The detailed demonstration for the propulsive performance of oscillating foil with a passive pitch was not presented in their work. Eldredge et al. (2010) conducted a computational study on the aerodynamic characteristics of multi-component flapping wing system. A torsional spring is employed to connect the actively prescribed leading foil and passively oscillating counterpart. Different dynamic mechanisms and propulsive performance with respect to this flapping wing configuration were explored.

Several unexpected behaviors regarding the dynamics of flapping foil with spring-based passive pitch were numerically identified by Spagnolie et al. (2010). The maximum advance velocity was observed when the resonance between flapping frequency and natural frequency of system occurs. The simulation reported a dynamic transition of flapping motion from coherence to chaos, and then back to coherent motion with the variation of cross-section aspect ratio. The locomotion of a passively flapping flat plate was numerically studied by Zhang et al. (2010) using a multiblock lattice Boltzmann method, indicating that there are two dynamic responses for the passively pitching plate depending on the ratio of natural

frequency over heaving frequency. Especially, it was found that the corresponding performance at the forward-movement regime was remarkably improved by the torsional flexibility. A similar flapping-wing configuration with the lumped rotational flexibility was numerically investigated by Xiao et al. (2014), who suggest that either a forward motion or a backward motion can be generated by the symmetry breakdown of flapping wing. The frequency of passive pitch was found to be identical to that of prescribed heave when the flapping wing reaches a stable periodic state. The propulsive performance of such a semi-active flapping wing configuration presents a high dependence on the spring stiffness and position of pitching axis. Liu et al. (2012) performed a numerical investigation into the unsteady flow around a traveling wavy foil hinged by the rigid flat plate. The fore foil has a prescribed undulation and the flat plate experiences a passive motion determined by combination of surrounding fluid and torsional spring. It was found that half of the forward thrust is provided by the passively oscillating flat plate. They reported a significant influence of flexibility characterizing as the non-dimensional natural frequency on both locomotion and force generation of the whole structure.

The dynamic responses of a passively flapping foil in a dense fluid were computationally modelled by Chae et al. (2013) using a Navier-Stokes solver. The effect of added mass, hydrodynamic damping and nonlinear fluid-structure-interaction response on the stability of flapping foil were analyzed in this study. The distributed flexibility of insect-scale flapping wing was approximated as the lumped torsional spring model by Ishihara et al. (2014), who provided an indication in the understanding of aerodynamic behaviors of insect flapping wings with the passively pitching motion. Moore (2014) employed a small-amplitude theory to model the kinematics of a thin flapping wing with the spring-based pitching motion. This study provides several insights into the effects of wing flexibility and fluid inertia on the characteristics of thrust and efficiency. The caudal fin model was simulated by Kancharala and Philen (2014) using a flapping wing configuration consisting of a flexible foil and a spring joint. It was found that a proper thin stiffness can promote the propulsive efficiency, while a further increase of flexibility will lead to a drag generation. Results also indicated that the optimum combination of fin flexibility and joint stiffness that maximizes the performance tends to be varying for different operating conditions. The comparison of propulsive performance between actively pitch-controlled foil and spring-loaded foil was experimentally demonstrated by Bøckmann and Steen (2014). A harmonic heaving foil was considered in this study to explore the capability of oscillating foil as auxiliary propulsor for ships in the waves. The experimental results indicated that the spring-loaded oscillating foil can produce the higher thrust and efficiency than an actively pitch-controlled system.

The aerodynamic forces by a heaving plate with passive flexion was numerically studied by Arora et al. (2015; 2018). By utilizing the lumped flexibility, they developed a multi-component model linked by the torsional springs. It was indicated that the system dynamics are determined by the combination of aerodynamic forces, spring stiffness and structural inertia. The motion phase of passive pitch was found to agree with heaving motion in the flow that structural inertia dominates, while the phase difference between pitch and heave tends to be around 90 degrees with the aerodynamics-dominant flow. Chen et al. (2016) conducted a series of measurements on the dynamics and aerodynamic performance of an

insect-scale flapper, which has an imposed heaving motion and a passively pitching motion. In this system, the hinge rotation is determined by the combination of aerodynamic torques with the hinge compliance. A systematic computation with respect to the effect of torsional stiffness on the propulsive performance of semi-active oscillating foil propulsor was conducted by Thaweewat et al. (2018) using the boundary element method. Results showed that the torsional spring stiffness has a significant influence on both passive pitching angle and effective AoA. The satisfactory efficiency was obtained in a wide range of advance speed for this configuration, which was considered to have an analogical open-water characteristics with a variable-pitch propeller. The passively pitching mechanism of insect wings not only affect the aerodynamics but also has a considerable influence on the maneuverability. It was noted that the aerial maneuverability of flapping wing system can be improved by the introduce of torsional flexibility with a simple control mechanism of kinematics (Zeyghami et al., 2019).

More details relevant to the studies on flexible or elastic-support oscillating foils can be referred to the comprehensive overviews by Ho et al. (2003) who provided a summary of early works regarding the unsteady aerodynamics, aeroelastic coupling and flow control strategies of flapping wing flight in the bird or insect scale, and Shyy et al. (2010) who presented a general review on the progress of flapping-wing aerodynamics and aeroelasticity in both research and application areas.

1.2.4 Three-dimensional effect

The preceding discussions are mostly limited to the two-dimensional cases. Natural observations indicate that plenty of animals employ the low-aspect-ratio wings to achieve an agile locomotion (Shyy et al., 2007). In addition, extensive studies have both numerically and experimentally shown that the wake patterns of real three-dimensional oscillating foils have an apparent discrepancy with the infinite-span foil due to the wing-tip vortex shedding and spanwise vortices distortion. Therefore, it is essential to consider the finite-span effect for the complete understanding of thrust-producing mechanism and flow physics of oscillating foils.

The influence of platform shape on the propulsive performance of three-dimensional oscillating wings mimicking the lunate tails of aquatic animals was investigated by Chopra (1974) and Chopra and Kambe (1977). By testing various geometry and kinematic parameters, it was indicated that compared with the rectangular wing the lunate tail using a curved leading edge decreases the thrust contribution of leading-edge suction. The leading edge with a sweep angle of over 30 degrees was found to decrease the propulsive efficiency significantly. The leading-edge vortices tend to be detached for a two-dimensional flapping wing, while attached vortex structures from the leading edge of a finite-span wing are commonly identified. A hypothesis for this mechanism is that the tip-vortex induced flow can limit the evolution of leading-edge vortex for a three-dimensional flapping wing (Birch and Dickinson, 2001). The evolution of three-dimensional flow structures induced by a heaving and pitching finite-span wing was measured by von Ellenrieder et al. (2003) using the dye flow visualization. The effects of pitching amplitude, heave-pitch phase difference and Strouhal number on the wake patterns were highlighted in

this study. It was noted that the flow structures behind a finite-span flapping wing are characterized as a chain of interconnected vortex loops, showing a high dependence on the Strouhal number.

Three-dimensional dynamic stall of an oscillating airfoil was numerically modelled by Spentzos et al. (2005) using a Navier-Stokes solver. The interaction of dynamic-stall vortex with tip vortex was identified in this study, suggesting that these two vortices tend to originate from the same region when they are formed around the oscillating airfoil. Blondeaux et al. (2005) numerically modelled the vortical patterns around a finite-span flapping foil to mimic the fish-like locomotion. The flow visualization identified the evolution of vortex rings with an apparent dependance on the Strouhal number. Numerical results of this study reinforced the previous experimental observations with respect to three-dimensional vorticity features. Flow visualization by Buchholz and Smits (2006) for a low-aspect-ratio pitching flat panel revealed that the streamwise vorticity tends to dominate the wake pattern, in which the three-dimensional Kármán vortex street is characterized as the horseshoe vortices with alternating sign.

Dong et al. (2006) performed a series of three-dimensional numerical simulations on the wake topology and hydrodynamic performance for a thin ellipsoidal flapping foil. Results indicated that the thrust-producing wake for a finite-span flapping foil is characterized as two sets of interconnected vortex loops, which eventually evolve to the distinct vortex rings with further convection in the downstream. Two oblique jets relating to corresponding hydrodynamic characteristics were identified in the flow wake of these flapping foils. The morphology of unsteady flow over a finite-span oscillating wing was experimentally visualized by Parker et al. (2007). Comparison of vortical pattern between two-dimensional and three-dimensional flow indicated a high complexity with respect to the oscillating wings using a finite aspect ratio. It was found that the morphological behaviors of spanwise vorticity are phase correlated with the kinematics of oscillating wings. Lu and Shen (2008) performed a series of experimental measurements to demonstrate the three-dimensional leading-edge vortex behaviors for a flapping dragonfly wing model during the hovering motion. They claimed that the leading-edge vortex system is characterized as the collection of a primary vortex structure and three minor vortex structures that are highly time-dependent in structure. Green and Smits (2008) conducted a series of measurements on the pressure distributions and unsteady flow structures of a pitching rectangular panel. By testing different parameters, it was found that the three-dimensionality of oscillating foils tends to be more dominant with either a lower aspect ratio or a larger pitching amplitude.

A computational study on the aerodynamics of a low aspect-ratio flapping wing by Shyy et al. (2009) revealed that the tip vortices can promote the lift generation by creating a low-pressure region around the wing tip and preventing the shedding of leading-edge vortex. Numerical simulations on the unsteady flow around a finite-span flapping wing were performed by Guerrero (2010) based on a Navier-Stokes model. It was reported that the three-dimensional wake patterns of rigid wing experiencing a root flapping motion are similar to the vortex structures induced by the flapping wing undergoing a pure heaving motion. The three-dimensional boundary element method was employed by La Mantia and Dabnichki (2011) to investigate the effect of wing shape on the force characteristics of oscillating wings.

Results suggested that the thrust generation tends to increase with the decreasing wing thickness when wing mass remains constant. In contrast, the generated thrust was found to be insensitive to the sweep angle of wing spanwise shape. Three-dimensional wake flow patterns behind an asymmetrical shark-tail model were experimentally recorded by Flammang et al. (2011) using the volumetric imaging technique, which identified a different vortex wake compared with previous two-dimensional flow visualization. Results showed that the hydrodynamic wake of finite-span shark tail is characterized as a row of dual-linked vortex rings appeared per half foil beat. Further comparison between passive tail model and active tail model revealed that the tail flexibility and kinematics have a significant influence on the behaviors of three-dimensional wake patterns.

Yilmaz and Rockwell (2012) employed PIV technique to identify the onset and evolution of vortex structures produced by the low-aspect-ratio pitching wings. Both the rectangular and elliptical wing shape were tested to investigate the effect of wing planform on the flow behaviors. Experimental measurements suggested that the flow structures tend to evolve to a strongly three-dimensional pattern at a relatively high AoA. An experimental study on the flow over a finite-span flexible oscillating fin was carried out by Dewey et al. (2012). In this study, a batoid-like fin was employed to reproduce the locomotion of undulatory propulsion. A series of intertwined vortex rings were observed in the wake of oscillating fin, which is highly influenced by the Strouhal number and wavelength. It was believed that the incorporation of leading-edge vortices with trailing-edge vortices at spanwise location tends to produce the efficient propulsion corresponding to the concentrated fluid momentum along streamwise direction in wake. Yu et al. (2013) demonstrated a bifurcated wake topology by the numerical simulation on the root-fixed heaving wing. It was found that the interaction of trailing-edge vortices with wing-tip vortices is responsible for such a wake behavior behind a finite-span flapping wing.

Van Truong et al. (2013) conducted a series of experimental measurements on the aerodynamic performance of a flapping wing model with the consideration of ground effect, which aims to replicate the initial flight of insects. The three-dimensional flow visualization identified the evolution of leading-edge vortex and the formation of leading-edge spiral vortex. They claimed that the ground effect can substantially benefit the lift generation during takeoff stage of insects. Perkins et al. (2017) noted that the ground effect induced by a high-aspect-ratio harmonically oscillating foil near a solid boundary is a fully three-dimensional phenomenon. The magnitude of ground effect was found to have a nonlinear dependence on the distance between the oscillating foil and solid boundary. It was also indicated that the ground effect tends to be evident within three chord lengths from the solid wall.

A three-dimensional parametric study on the parameter optimization of flapping wing propulsors was conducted by Politis and Tsarsitalidis (2014) using the unsteady boundary element modelling. Multiple geometry and kinematic parameters were considered for the systematic computations of a heaving and pitching flapping wing. In this study, they developed a design methodology for the application of flapping wings as ship thrusters. Results suggested that the flapping wings present several superiorities compared with conventional propellers. The performance optimization of three-dimensional flapping

wing in hover with respect to the wing shape and kinematic parameters was performed by Jones and Yamaleev (2015) using a time-dependent adjoint-based scheme to achieve the maximum lift-to-drag ratio. The deformation effect of three-dimensional flapping wing on the aerodynamic performance was numerically investigated by Medina et al. (2015). It was found that the efficiency increases of 19.5% and 19.0% are achieved by the introduce of root and tip deflection, respectively. Flow visualization of this study reported a low sensitivity of leading-edge vortices to the wing deformation. A three-dimensional numerical simulation on the wake behaviors of a pitching foil was conducted by Deng et al. (2015), who identified the dynamical features of the wake transition between two-dimensional and three-dimensional vortical structures.

The effect of aspect ratio on the vortex structures and circulation for a flat-plate rotating wing was experimentally investigated by Carr et al. (2015). The range of aspect ratio from 1 to 4 was considered in the acquirement of flow quantities and lift measurements. Based on the combination of flow behaviors with force characteristics, the different contributions of flow structures by varying aspect ratios to the lift performance were identified in this study. The flow pattern characterizing as the double-loop vortices with alternating signs from the trailing edge of a low-aspect-ratio pitching-rolling plate was numerically captured by Li and Dong (2016). The further behavior of these vortical structures was identified as interconnected vortex rings, which eventually evolved to a downstream bifurcating wake pattern. Three-dimensional flow evolution of a low-aspect-ratio flat plate wing was experimentally studied by Ehlers et al. (2016) using the tomographic PIV measurements. The vortex dynamics were analyzed by highly resolved flow visualization which identifies multiple leading-edge vortex formations during downstroke. It was found that the small-scale turbulent vortices tend to dominate the flow separation around the leading edge of finite-span flapping wing. Gonzalo et al. (2018) conducted a series of three-dimensional numerical simulations on the unsteady flow over a pair of flapping wings in side-by-side arrangement. A low aspect ratio of 2 was considered in this study in which a parameter for the radius of flapping motion is defined. The transition from the heaving motion to flapping motion can be identified by the variation of radius of flapping motion. It was found that the maximum aerodynamic force shows a decreasing trend with the increase of radius when the vertical displacement of outboard wing tip remains constant. Corresponding flow visualization numerically captured the ring-like vortex structures in wake, showing a certain dependence on the radius of flapping motion.

The correlation of propulsive performance with the flow patterns for a three-dimensional oscillating wing was numerically investigated by Han et al. (2018). It was indicated that the vortex behaviors have a high dependence on the variation of kinematic parameters that significantly affect the propulsive characteristics of oscillating foils. After that, Han et al. (2019) performed a series of three-dimensional computations on the unsteady flow mechanisms and propulsion behaviors of multiple flapping wings, which aims to mimic the biological schooling phenomenon. They simulated three different schooling configurations including the flapping wings in tandem, triangle and diamond arrangement. The major focus of this study is the effect of individual distance along the horizontal direction, which was found to have a significant influence on the thrust production. Zhang et al. (2019) numerically examined the

effect of flapping frequency on the aerodynamic behaviors of multi-wing configuration in a diamond schooling. They found that the thrust performance of last downstream wing shows a maximum sensitivity to frequency difference when the schooling configuration employs different individual flapping frequencies. Li et al. (2019) performed a three-dimensional computation on the propulsive performance of a pair of flapping wings applied to a bionic autonomous underwater glider. The range of aspect ratio from 0.36 to 5 was tested in this study, which recommend an optimum aspect ratio of around 0.6 for the considered vehicle. Arranz et al. (2020) performed a series of numerical simulations on the aerodynamic performance of a tandem flapping wing configuration with finite span. By examining the aspect ratio of 2 and 4, it was found that the finite-span interactions between fore-wing wake structures and hind wing are analogous to a two-dimensional scenario.

The hydrodynamic characteristics of a flexible flapping plate with finite span were numerically analyzed by Ryu et al. (2019). The dynamics of the considered wing are characterized as the prescribed leading-edge heaving motion with chordwise flexibility, which can freely move along the horizontal direction. Different trapezoidal plates with the variation of shape ratio were tested to explore the resulting propulsive performance and three-dimensional vortex behaviors. Ayancik et al. (2019; 2020) developed a novel scaling law for the predictions in thrust production and power consumption of flapping bio-propulsors. Multiple factors were considered in both experimental measurements and numerical simulations, including the three-dimensionality, added mass, upwash and downwash effects. They revealed an intertwined mechanism for the foil shape and kinematics of flapping wing propulsors, indicating that the specific kinematics of flapping wing should correspond to a given foil shape for the purpose of maximum propulsion performance.

1.2.5 Energy harvester

The turbines using oscillating foils to extract energy from an inflow stream or current have been explored over the past several decades. It has been indicated that the oscillating foil energy converters show significant advantages over conventional rotary turbines in many aspects (Young et al., 2014). Although it is still far away from extensively industrial application, there is an increasing interest in the studies on the oscillating foil turbines in recent years. According to activating mechanism of the device, oscillating foil energy harvesters can be classified into three categories including the fully-constrained configuration, semi-activated configuration and fully-passive configuration (Xiao and Zhu, 2014).

The locomotion of fully-constrained configuration is characterized as the forced pitching and heaving motions. Zhu (2011) numerically explored the optimal performance of oscillating foils operating in the energy extraction regime. The focus of this study is the relationship between energy harvesting efficiency and wake stability. It was suggested that the energy extraction characteristics have a close correlation with the efficient wake evolution. Kinsey and Dumas (2012a; 2012b) developed a conceptual tidal turbine using oscillating hydrofoils in a tandem arrangement. Both two-dimensional and three-dimensional computations were carried out to predict performance of this energy harvester.

Results showed that the efficiency of power extraction has a low sensitivity to the perturbations of hydrofoil kinematics and flow conditions. The interaction between downstream foil and wake of upstream was considered as a critical factor that affects the power extraction. It was suggested that a favorable interaction may lead to a power extraction efficiency up to 64%. They also numerically evaluated the performance loss due to three-dimensional effect for a sinusoidally heaving and pitching foil (Kinsey and Dumas, 2012c). It was shown that for such a hydrokinetic turbine, the relative drop of power extracted performance due to finite-span influence can be limited to 10% of two-dimensional prediction by employing the endplates. Liu and Xiao (2013) numerically investigated the performance of energy extraction by a dual-foil configuration in parallel. In this study, each oscillating hydrofoil has a combined heaving and pitching motion with the consideration of chordwise flexibility. Results suggested that the flexible foils present a better performance over the rigid foils, especially for the relatively high oscillating frequencies. Deng et al. (2014) numerically examined the relationship between energy extraction performance and aspect ratio of flapping foil. The three-dimensional effect was found to dominate the flow field for a pitching foil when the aspect ratio is smaller than four which is recommended for the practical application of flapping foil energy harvesting system in this study. Liu (2015) proposed a dual-foil WIG effect turbine to eliminate several disadvantages of traditional horizontal-axis and vertical-axis turbines. The renewable energy performance of this WIG effect turbine was assessed by a series of numerical computations. Based on the same swept area, the extracted annual energy by WIG effect turbine is 1.73 times that of horizontal axis turbines. Results indicated that dual-foil turbine can produce 1.42 times as much energy compared to a single oscillating foil configuration. The oscillating foil turbine with a large heaving amplitude was considered by Picard-Deland et al. (2019). In this model, the sinusoidal profile for AoA was used by adjusting the time-varying pitching motion. Based on a series of two-dimensional computations, a power extraction efficiency of 49% was reported by introducing a constantly high AoA.

A semi-activated system is featured as either combination of prescribed pitching motion and flow-induced heaving motion or combined heaving motion imposed by an actuator and pitching motion generated by fluid forces. The numerical simulations on a semi-active flapping foil were conducted by Zhu and Peng (2009) using a Navier-Stokes solver. This energy harvesting system has an active heaving motion and passively pitching motion based on a viscous damper. The major focus of this study was the vortex-control mechanism, which suggested that the energy harvesting performance can be improved by the manipulation of vortex-body interactions. The performance of energy extraction by a dual-foil system in parallel was numerically studied by Ma et al. (2018). The self-sustained motion of two oscillating foils is governed by a hydraulic coupling system, indicating that the damping coefficient shows a dominant effect on the dynamic responses and hydrodynamic characteristics of oscillating foils. Boudreau et al. (2019) proposed an innovative turbine model with the semi-activated flapping motion to reduce the inherent complexity of controlling mechanism. This flapping foil configuration has an actively prescribed heaving motion and passively flow-induced pitching motion. The pitching angle is determined by the combination of hydrodynamic forces and spring-based elastic supports. They

performed a series of two-dimensional simulations with variation of kinematic parameters to study the corresponding dynamic responses, in which an energy extraction regime characterizing as periodic limit-cycle oscillations was found in their computations. Under appropriate conditions, a maximum energy extraction efficiency of 45.4% was achieved in this study indicating a significant potential of semi-passive flapping-foil turbine.

The oscillatory motion of flapping foil energy harvester using the fully-passive mechanism is generated by flow-induced instabilities. The dynamic responses of a fully-passive flapping foil energy harvester operating in a linear shear flow was numerically analyzed by Zhu (2012). Simulations suggested that the periodic responses that is necessary for reliable energy harvesting can be achieved in a small shear rate, while such dynamical behaviors tend to disappear for the relatively large shear rate. The power extraction capability of this system in a shear flow is believed to be comparable to that of uniform-flow scenario. Young et al. (2013) performed a numerical computation on the performance of power generation by a fully-passive flapping wing. They examined two control mechanisms including the profile of pitching angle and law of AoA. Results suggested that the non-sinusoidal pitching motion produces a higher performance than sinusoidal pitching profile. Energy extraction efficiency of over 41% was obtained by AoA control mechanism, in which the non-sinusoidal law is considered as a better choice for power generation. A self-sustained hydrokinetic energy flow harvester with fully passive dynamics was numerically modelled by Veilleux and Dumas (2017). The energy extraction efficiency of 34% was obtained based on a gradient-like optimization for this configuration. Two beneficial mechanisms were highlighted in this study to enhance the turbine performance, including the adequate synchronization of two degrees of freedom and non-sinusoidal profile of pitching motion. The energy extraction performance of a fully-passive flapping foil was experimentally investigated by Qadri et al. (2020). Based on the measurements of various flow and operating parameters, a power conversion efficiency of 32.5% was achieved. It was found that both heaving and pitching motions can contribute to the energy extraction. A parametric study with respect to the dynamics of a fully-passive flapping-foil turbine was numerically conducted by Boudreau et al. (2020). It was indicated that the performance of the fully-passive flapping foil can match the fully-constrained configuration with the efficiency of over 50% by appropriately setting the structural parameters.

Although the topic of energy harvester is beyond the scope of current study, some similarities in hydrodynamic aspects and flow behaviors can be identified between oscillating foil propulsors and turbines. Hence, a brief review with respect to the progress and development of oscillating foils for energy extraction was provided for the sake of a complete picture.

1.3 Research Objectives and Novelty

It has been confirmed that both biplane arrangement and lumped torsional flexibility are capable of

enhancing the propulsive performance of oscillating foils significantly. The former with counter-phase heave can generate the beneficial WIG effect, while a flow-adapted pitching motion can be introduced by the latter using the torsional spring. Thus, it is reasonable to expect a more satisfactory propulsion performance by the oscillating foil propulsors with combination of these two mechanisms.

Liu (2005a) is the first to propose the concept of auto-pitch wing-in-ground effect oscillating foil propulsors (APWIGs) in the form of a technical patent. His original intention is to generate an initial effective AoA by flow forces such that the oscillating foils can produce a start-up thrust. So far, both computations and measurements regarding the propulsive characteristics of APWIGs have not been found as per the author's knowledge. Available discussions for this configuration are restricted to the hypotheses and expectations. Therefore, it is necessary to conduct a comprehensive investigation to evaluate the performance of APWIGs and explore its perspective potential as the marine propulsor. That is the primary motivation of this work.

To this end, current study mainly concentrates on addressing four research questions: 1) Is the numerical model based on CFD capable of providing reliable and accurate predictions on propulsive performance of oscillating foil propulsors? 2) What are the advantages of APWIGs compared with other oscillating foil configurations? 3) How do relevant geometry and kinematic parameters affect the thrust production and propulsive efficiency of APWIGs? 4) How to design a APWIGs system for marine vehicles?

The principal objective of this work is to numerically assess the performance metrics of APWIGs. A certain parametric space was considered by examining multiple geometry and kinematic parameters. The current study aims to find out the influence of related parameters and provide a propulsive database which can be utilized to perform the thrust maximation and efficiency optimization for APWIGs. The second objective of this research is to highlight the superior advantages of APWIGs compared to other oscillating foil configurations. The major interest is to figure out whether APWIGs has a higher propulsive performance over either the actively prescribed configuration or single oscillating foil. The third objective of this thesis is to provide physical implications for the flow patterns induced by biplane configuration and auto-pitch locomotion. In particular, the major concern is the correlation between vortex behaviors and hydrodynamic characteristics. It is expected that the current research findings can offer significant insights into the manipulation of vortex structures for optimal performance of oscillating foils. At last, it is intended to develop a feasible and efficient design procedure for the practical application of APWIGs since available reports and discussions in design process of oscillating foil propulsors are highly insufficient until now. The ultimate aim of this work is to provide a systematic guideline for the parameter selection, mechanical manufacture and engineering practice of APWIGs based on the established outcomes.

The current study provides original contributions to the propulsion community in both performance analysis and mechanism understanding. Significant novelty is highlighted as follows:

- To fill the void in performance evaluation of APWIGs with lumped torsional flexibility and WIG

effect, the current study performed a systematic computation on propulsive characteristics of this novel configuration. It is believed to be the first comprehensive and quantitative analysis on the thrust generation and efficiency performance of APWIGs. Simulations of flow-induced locomotion based on the framework of biplane arrangement are regarded as highly original in the field of oscillating foil propulsion.

- A comparative study with respect to the hydrodynamic performance between various oscillating foil configurations was carried out. Such a direct and general comparison is rare in existing studies. To enhance the insights into the oscillating foil characteristics, it is essential to distinguish the propulsive metrics and operating features for different configurations. Especially, the remarkable advantages of APWIGs over other systems were highlighted.

- The vortex structures and wake patterns generated by different oscillating foil configurations were numerically visualized in this study. The flow phenomena for dual-foil arrangement and passive pitching mechanism are extremely complicated due to the wing-vortex interactions. The physical understanding for these problems remains unclear in existing literature. This study can provide a wealth of novel insights into the relationship between flow behaviors and propulsive properties.

- The effect of aspect ratio on the propulsive characteristics of APWIGs was investigated in the current study. Most existing numerical computations on oscillating foils were limited to the two-dimensional cases, which is insufficient to identify the real hydrodynamics due to the absence of wing-tip vortices. Current demonstrations on the three-dimensional vortex evolution for biplane configuration are capable of promoting complete understanding of finite-span flow mechanisms.

- The current thesis proposed a general design procedure for APWIGs based on the established numerical database. Although oscillating foils were extensively studied as either aircraft thruster or marine propulsor, the design process in purpose of engineering application was rarely found in the referred works. The developed procedure is expected to provide essential guidance for the parameter selection such that the designed APWIGs can satisfy specific requirements.

1.4 Thesis Outline

This thesis consists of eight chapters in which major results and corresponding discussions are presented in Chapters 3 to 7. Significant findings and achievements of the current study are highlighted in the form of scientific journal and conference articles that have been published. The details of publications were demonstrated in the preceding part. The individual chapters presented in this thesis are organized as follows:

Chapter 2 presented general demonstrations on the problem description and employed methodology. A numerical model aiming to simulate unsteady flow around the oscillating foils was established. The

reliability and accuracy of this model were ensured by systematic verifications and validations, which include the analysis of numerical uncertainties and comparisons with available experimental data.

Chapter 3 performed an investigation into the hydro-elasticity characteristics of APWIGs based on the variation of lumped flexibility. The torsional spring stiffness is considered as a dominant parameter determining the propulsive performance of auto-pitch configuration. Hence, the effect of both non-dimensional stiffness and frequency ratio on the propulsion characteristics of APWIGs was extensively explored to enhance the understanding with respect to classification of locomotion state, hydrodynamic behaviors and wake flow patterns.

Chapter 4 reported a two-dimensional parametric study on the propulsive metrics of APWIGs. The primary aim is to demonstrate the influence of individual parameters on the dynamical behaviors and hydrodynamic performance for the configuration of interest. Various parameters including the oscillating frequency, heaving amplitude, advance speed, position of pitching axis and distance between two foils were taken into account to perform the propulsion analysis. General correlation between wake structures and propulsion properties for APWIGs was indicated to guide the vortices manipulation.

Chapter 5 provided a direct comparison of performance metrics between APWIGs and other oscillating foil configurations. The superior advantages of APWIGs were highlighted with respect to both thrust generation and efficiency enhancement. Physical insights into this performance augment were indicated based on the mechanisms of biplane arrangement and flow-adapted pitching motion. Vortex structures and wake patterns for each oscillating foil configuration were numerically identified.

Chapter 6 investigated the influence of three-dimensionality on the propulsion performance of WIG effect configurations. A series of numerical simulations covering a wide range of aspect ratio were performed to explore in which scenario the three-dimensional effect tends to dominate the flow hydrodynamics. The previous two-dimensional studies on the hydro-elasticity characteristics of APWIGs were extended to the real three-dimensional flow. Wake topologies characterized as intertwined vortex rings generated by finite-span oscillating foils were numerically demonstrated.

Chapter 7 proposed a design procedure for the parameter selection of APWIGs in both kinematic aspect and geometric consideration. Several approaches were developed to deal with different optimization scenarios, such that the operating requirements regarding either thrust production or propulsive efficiency for target vehicles can be satisfied by designed APWIGs. A case study on the application of APWIGs to an AUV was performed to demonstrate detailed process of proposed design procedure.

Chapter 8 concluded this thesis by briefly summarizing the key findings, highlighting the research implications, emphasizing the study significance and indicating the existing limitations. Furthermore, recommendations were provided for the future work in terms of both expectations and challenges.

CHAPTER 2

Theory and Methodology

2.1 Physical Description

General problem illustration and kinematic demonstration are provided in this section. With respect to the configuration of interest in the current study, APWIGs undergoes the active harmonic heaving motion in counter phase and flow-induced pitching motion, as shown in the left schematic of Figure 2-1. The foil structure is assumed as the rigid body. The heaving motion along the *y*-axis is defined as a simple sinusoidal profile. A torsional spring is attached to the pivot axis to restore foils towards the equilibrium position, such that the time-varying pitching motion around *z*-axis is determined by the combination of hydrodynamic moments and restoring torque. In addition, it does not have any other degree of freedom. Figure 2-1 also presents the global coordinate system throughout the study, in which *z*-axis is defined as outward positive direction perpendicular to *xy*-plane. It should be noted that the gravity is not involved in the foil dynamics by current numerical simulations since its direction is assumed to be along the *z*-axis.

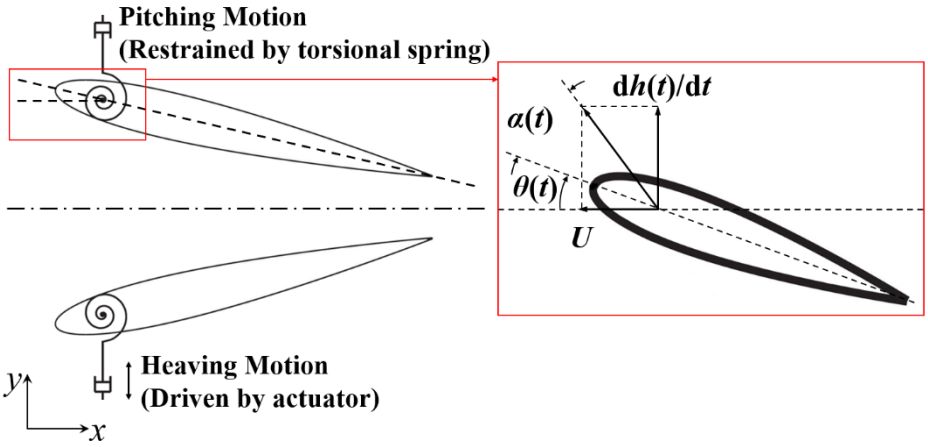

Figure 2-1 Schematic of APWIGs and definition of effective AoA.

The time history of oscillatory position for APWIGs over one cycle is illustrated in Figure 2-2. Based on the generated ground plane by two counter-phase oscillating foils, one foil can be considered as the mirror image of another foil during the oscillation. The generated WIG effect on the hydrodynamic behaviors tends to be prominent when two foils approach close to each other, since such a biplane arrangement with the counter-phase oscillating mechanism has the resemblance with a single oscillating foil in proximity to a solid boundary.

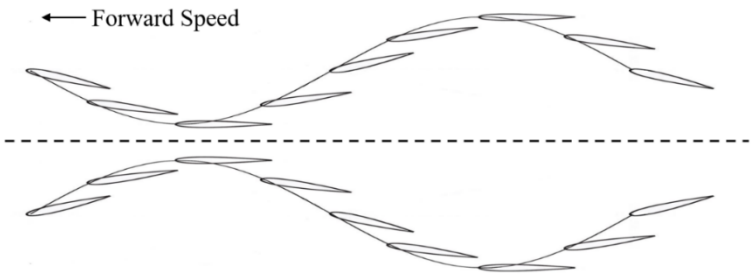

Figure 2-2 Time-varying position evolution of APWIGs over one oscillatory cycle.

A variety of geometry and kinematic parameters are involved in the problem of oscillating foil propulsion. For the current study on APWIGs, several principal parameters are taken into account to investigate the corresponding influence. The considered parameters include the heaving amplitude, equilibrium distance between two foils, position of elastic pitching axis, forward speed characterizing as freestream velocity, oscillating frequency, torsional spring stiffness and aspect ratio. In addition to these actively input parameters, there are three passively derivative parameters that are essential to elucidate the hydrodynamic characteristics of APWIGs, including the maximum pitching angle, maximum effective AoA, phase angle between pitch and heave.

The maximum effective AoA is one of most important parameters that affect the propulsive performance of oscillating foils. The definition of effective AoA at an arbitrary instant is presented in the right schematic of Figure 2-1. Considering the APWIGs with a constant forward speed of U, the instantaneous effective AoA can be defined as follows:

$$\alpha(t) = \tan^{-1}(\frac{1}{U}\frac{dh(t)}{dt}) - \theta(t) \tag{2.1}$$

where $\theta(t)$ and $h(t)$ denote the time-varying pitching angle and vertical position of elastic pitching axis, respectively. For the cases of passively pitching motion, the time-varying pitching angle can only be obtained after each simulation. Thus, the maximum effective AoA can be given by substituting the time series of pitching angle into the equation 2.1 for further analysis.

For clarity and convenience, the relevant parameters can be written as non-dimensional form. The ratio of length variables to chord length is used to characterize the heaving amplitude, distance between two foils and position of elastic pitching axis. The oscillating frequency is represented by either the Strouhal number (St) or reduced frequency (k), which are widely employed to analyze the inherent flow physics of oscillating foils. In this study, the Strouhal number and reduced frequency are given as follows:

$$St = \frac{fA}{U} \tag{2.2}$$

$$k = \frac{\omega c}{2U} \tag{2.3}$$

where f denotes the oscillating frequency in Hz, A is characteristic width of the created jet flow which is usually determined by total excursion of trailing edge of the foil, ω and c denote the angular frequency ($\omega = 2\pi f$) and chord length, respectively. Since the maximum displacement of the trailing edge remains unknown before the simulation, current study mainly uses the reduced frequency to represent the non-dimensional oscillating frequency of APWIGs.

A non-dimensional advance parameter for oscillating foils can be introduced to represent the forward speed by imitating the advance coefficient of screw propeller. Current study follows the nomenclature of Floc'h et al. (2012) to define the oscillating foil advance parameter. Referring to the propeller diameter, an equivalent reference length D_{foil} for foil geometry is first provided by equation 2.4. The

advance parameter for the oscillating foil configuration is then defined as equation 2.5.

$$D_{foil} = \sqrt{\frac{8h_0 s}{\pi}} \tag{2.4}$$

$$J = \frac{U}{fD_{foil}} \tag{2.5}$$

where h_0 and s denote the heaving amplitude and spanwise length, respectively. Thus, the hydrodynamic performance of oscillating foils can be demonstrated as a function of advance number that is analogical to the open-water characteristics of screw propellers in terms of advance coefficient.

There are two key parameters that dominate the dynamics of oscillating foils with spring-based passive pitch, namely density ratio and torsional flexibility. The density ratio of structure and fluid indicating the foil system inertia is directly given as follows:

$$\lambda_D = \frac{\rho_S}{\rho} \tag{2.6}$$

where ρ_s and ρ are the structure density and fluid density, respectively. The torsional flexibility represented by the spring stiffness can be characterized as the frequency ratio of natural frequency f_n and flapping frequency f as follows:

$$\lambda_F = \frac{f_n}{f} \tag{2.7}$$

$$f_n = \frac{1}{2\pi}\sqrt{\frac{K}{I_{axis}}} \tag{2.8}$$

where K and I_{axis} denote the spring stiffness of system and foil moment of inertia about the elastic axis, respectively. Alternatively, the non-dimensional torsional spring stiffness can be defined as follows:

$$K^* = \frac{K}{\rho U^2 s c^2} \tag{2.9}$$

Both the λ_F and K^* are employed to characterize the torsional flexibility of APWIGs by the current study, in which the frequency ratio is used to indicate the dynamic responses and non-dimensional spring coefficient is utilized to plot the performance metrics.

The performance of APWIGs is characterized as the time-averaged thrust and propulsive efficiency. For an auto-pitch oscillating foil that experiences the streamwise force $X(t)$ and vertical force $Y(t)$, the non-dimensional form of time-varying thrust and lift coefficients are given as follows:

$$C_t = \frac{X(t)}{0.5\rho U^2 cs} \tag{2.10}$$

$$C_l = \frac{Y(t)}{0.5\rho U^2 cs} \tag{2.11}$$

For the torsional flexible foil, the actuator only provides power that make the system perform heaving motion. Hence, the time-averaged thrust F and input power P over one oscillatory cycle T for APWIGs are defined as follows:

$$F = \frac{1}{T}\int_t^{t+T} X(t)dt \tag{2.12}$$

$$P = \frac{1}{T}\int_t^{t+T} Y(t)\frac{dh(t)}{dt}dt \tag{2.13}$$

The non-dimensional coefficients of time-averaged thrust and input power are given as follows:

$$C_T = \frac{F}{0.5\rho U^2 cs} \tag{2.14}$$

$$C_P = \frac{P}{0.5\rho U^3 cs} \tag{2.15}$$

The propulsive efficiency can be defined as either the ratio of useful power over input power or the ratio of thrust coefficient over input power coefficient:

$$\eta = \frac{FU}{P} = \frac{C_T}{C_P} \tag{2.16}$$

Note that the relevant torque $Q(t)$ should also be taken into account for the calculation of required power when the pitching motion of oscillating foil is actively imposed. Thus, the corresponding time-averaged input power P per cycle can be defined as follows:

$$P = \frac{1}{T}\left(\int_t^{t+T} Y(t)\frac{dh(t)}{dt}dt + \int_t^{t+T} Q(t)\frac{d\theta(t)}{dt}dt\right) \tag{2.17}$$

where $\theta(t)$ is the imposed time-varying pitching angle. Equation 2.17 is used to calculate the required power of fully prescribed oscillating foil configuration in which both heaving and pitching motions are driven by actuators.

2.2 Flow Solver and Implementation

A numerical model was established to simulate the unsteady flow around oscillating foils based on the open-source CFD code *OpenFOAM*. The demonstration of various aspects with respect to the flow equations, mathematical approaches and numerical setups is performed. Instead of drawing a complete picture of fluid dynamics and CFD in every detail, this section mainly presents the framework of solver implementation with essential interpretations here, which aims to provide instructions for the numerical

modelling of relevant problems.

2.2.1 Governing equations

The fluid is regarded as a continuum in which the corresponding flow behaviors are described in terms of macroscopic properties. Newtonian fluid based on the approximation of Newton's law of viscosity is used for the most cases of interest. According to the conservation laws of physics with respect to mass and momentum, the fluid motion for the incompressible and viscous flow with constant and uniform properties is governed by the continuity and the Navier-Stokes equations as follows:

$$\nabla \cdot \mathbf{v} = 0 \tag{2.18}$$

$$\frac{\partial \mathbf{v}}{\partial t} + (\mathbf{v} \cdot \nabla)\mathbf{v} = \upsilon \nabla^2 \mathbf{v} - \frac{1}{\rho}\nabla p + \mathbf{f} \tag{2.19}$$

where $\mathbf{v}$ is the fluid velocity, υ is the kinematic viscosity, p is the pressure field, and $\mathbf{f}$ denotes the arbitrary body force. Momentum equations can be considered as the Newton's second law for the fluid. The left-hand side of equation 2.19 describes the rate of change of momentum. For the right-hand side of equation 2.19, the terms represent the sum of forces that are applied to the fluid including the viscous forces, pressure and external forces.

The conservative form of fluid equations can be introduced to indicate the commonalities between the various conservation laws of physics. It is referred to as the transport equation for a general variable ϕ which is defined as follows:

$$\frac{\partial(\rho\phi)}{\partial t} + \nabla \cdot (\rho\phi\mathbf{v}) = \nabla \cdot (\Gamma \nabla \phi) + S_\phi \tag{2.20}$$

where Γ denotes the diffusion coefficient, and S_ϕ is the source term for the property ϕ. Equation 2.20 demonstrates the various transport processes for both vector and scalar quantities, in which convective term and diffusive term can be found on two sides of the equation. The partial differential equations for mass and momentum conservation can be obtained by setting ϕ equal to 1 and $\mathbf{v}$ with the appropriate diffusion coefficients and source terms.

In order to use the finite volume method, equation 2.20 needs to be integrated over a three-dimensional control volume. Applying the Gauss's divergence theorem, the integral form of transport equation for a general property ϕ is given as follows:

$$\frac{\partial}{\partial t}\left(\int_V \rho\phi \mathrm{d}V\right) + \int_S \mathbf{n} \cdot (\rho\phi\mathbf{v})\mathrm{d}S = \int_S \mathbf{n} \cdot (\Gamma\nabla\phi)\mathrm{d}S + \int_V S_\phi \mathrm{d}V \tag{2.21}$$

where S represents the bounding surface, $\mathbf{n}$ is the unit vector normal to surface element, and V denotes the volume of fluid element. The physical meaning for each term can be clearly identified in this equation. The first term on the left-hand side of equation 2.21 indicates the change rate of total fluid

property inside the control volume. The convective term on the left-hand side of equation 2.21 signifies the net decrease rate of fluid property due to convection. On the right-hand side of equation 2.21, the diffusive term shows the net increase rate of fluid property due to diffusion and the last term represents the increase rate of property as a result of sources in the fluid element. More details regarding above governing equations can be found in Versteeg and Malalasekera (2007).

2.2.2 Turbulence modelling

Unsteady flows around the oscillating foils tend to be unstable when the Reynolds number is larger than a certain value, which is characterized as the turbulent regime. A random and chaotic state can be identified for the fluid motion of turbulence which shows continuous change of velocity and pressure with time around extensive flow regions. Satisfactory predictions on the effect of turbulence have a high significance since most flows of engineering interest are turbulent.

The wall bounded turbulent flow is the major concern of the current study. For the flows along solid boundaries, the inertia tends to dominate the substantial region of flow far away from the wall, while the viscous effects are significant within a thin layer.

The mean velocity U of flow regime close to the wall is determined by parameters of distance to the wall y_w, fluid density ρ, dynamic viscosity μ and wall shear stress τ_ω. The law of the wall can be given by the dimensional analysis as follows:

$$u^+ = \frac{U}{u_\tau} = f\left(\frac{\rho u_\tau y_w}{\mu}\right) = f(y^+) \tag{2.22}$$

where u_τ denotes the friction velocity that is defined as:

$$u_\tau = \sqrt{\frac{\tau_\omega}{\rho}} \tag{2.23}$$

Within the flow region far away from the wall, the velocity is expected to be affected by the retarding effect of solid boundary through the wall shear stress. The boundary layer thickness δ characterizes the length scale of this region. It gives rise to the following equation by the dimensional analysis.

$$u^+ = \frac{U}{u_\tau} = g\left(\frac{y_w}{\delta}\right) \tag{2.24}$$

The velocity-defect law can be obtained by considering that the velocity deficit (U_{max} - U) is due to the wall shear stress:

$$\frac{U_{\max} - U}{u_\tau} = g\left(\frac{y_w}{\delta}\right) \tag{2.25}$$

The boundary layer around the solid wall can be divided into several regimes that present different flow properties based on the non-dimensional distance to the wall. A general classification of flow regions in wall-bounded boundary layer is demonstrated as follows:

- Viscous sub-layer ($y+ < 5$): The fluid behaviors are dominated by viscous effects. The shear stress is assumed to be equal to the wall shear stress and remain constant. The linear velocity law can be given as following relationship.

$$u^+ = y^+ \tag{2.26}$$

- Log-law layer ($30 < y+ < 500$): Both viscous and turbulent effects are significant in this region. The shear stress is assumed to be constant and changes slowly with the distance to the wall. The velocity profile can be given as following equation with the von Kármán's constant κ of 0.41 and the additive constant B of 5.2.

$$u^+ = \frac{1}{\kappa}\ln(y^+) + B \tag{2.27}$$

- Buffer layer ($5 < y+ < 30$): The transition region between viscous sub-layer and log-law layer. Turbulent and viscous stresses are of similar importance. The velocity profile is not well defined in this region such that the wall functions should set the first cell center outside buffer layer.

The velocity distribution near the wall is presented in Figure 2-3, in which theoretical predictions and experimental data are represented by the lines and points, respectively. Close agreement of two results can be identified in this figure indicating that the validity of relationship between $u+$ and $y+$ is lied in different flow regions.

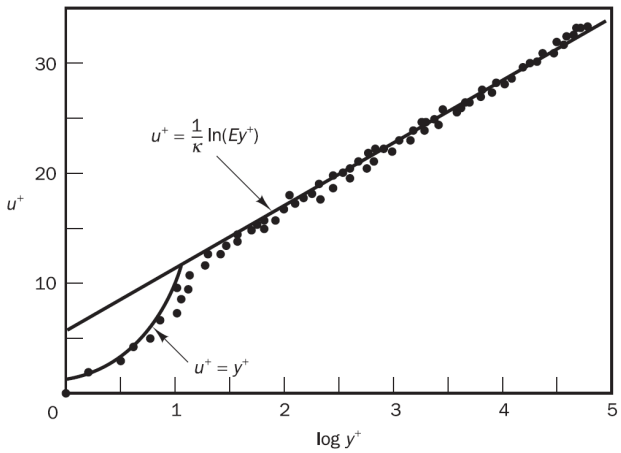

Figure 2-3 Velocity distribution near the solid boundary (Versteeg and Malalasekera, 2007).

Numerical methods for the modelling of turbulence can be generally classified to three groups with different level of results accuracy and computational cost, including the Direct Numerical Simulation (DNS), Large Eddy Simulation (LES) and Reynolds-Averaged Navier-Stokes (RANS) approach.

DNS directly resolve the mean flow and turbulent velocity fluctuations without empirical assumptions. The sufficiently fine spatial grids are required for the calculation of unsteady Navier-Stokes equations. The computational expenses for DNS are extremely high such that this method is not applicable for the engineering computations. LES is an intermediate form for the turbulence modelling, which only capture the behaviors of larger eddies. A space filtering is employed to pass the larger eddies and exclude the smaller eddies before the computations. LES technique directly resolves the larger eddies and models the smaller scales of turbulent motion. This approach shows a good performance for problems with the complex geometry. Although computational costs of LES are significantly reduced compared with DNS, its demands on computing resources are considerably large for many flow cases. RANS approach focuses on the mean flow and the turbulent effects on corresponding properties. The Reynolds averaging is applied to the Navier-Stokes equations which leads to the extra terms that need to be modelled using various turbulence models. The requirement of computing resources for the RANS computations with reasonable accuracy is modest, and hence this method is widely applied to a large variety of engineering flow calculations. For the flows with time-varying properties, unsteady Reynolds-Averaged Navier-Stokes (URANS) method is employed to involve the time derivative term in momentum equations.

In addition to above three methods, a hybrid turbulence model called Detached Eddy Simulation (DES) is developed to balance the simulation accuracy and computational expenses. The basic principle of DES method is to combine the RANS and LES approaches to a single model, in which the RANS approach is employed to compute the regions where the turbulent length scale is below the maximum grid dimension and the LES approach is used to solve the regions where the turbulent length scale is larger than the grid dimension. Therefore, the demands on both modelling accuracy and computing resources can be satisfied by the DES method since the attached boundary layers and separated flows are modelled by RANS and LES, respectively.

The current study considers a relatively simple geometry and aims to perform a parametric investigation with extensive computations. Thus, the URANS approach with reasonable accuracy and modest computational expenses is applicable for the modelling of boundary layer around oscillating foils. A brief description for the implementation of URANS method and the basic concepts of employed turbulence model are provided here. More details with respect to the turbulence modelling and involved equations can be referred to Versteeg and Malalasekera (2007).

According to the Reynolds decomposition, the properties of turbulent flow can be decomposed into a steady mean value and a fluctuating component. Hence, the fields of velocity and pressure can be decomposed as follows:

$$\mathbf{v} = \overline{\mathbf{v}} + \mathbf{v}' \tag{2.28}$$

$$p = \overline{p} + p' \tag{2.29}$$

The Reynolds-averaged Navier-Stokes equations can be obtained by substituting the $\mathbf{v}$ and p to the

continuity and momentum equations, and taking the time average as follows:

$$\nabla \cdot (\rho \overline{\mathbf{v}}) = 0 \tag{2.30}$$

$$\frac{\partial(\rho \overline{\mathbf{v}})}{\partial t} + \nabla \cdot (\rho \overline{\mathbf{v}}\overline{\mathbf{v}}) = -\nabla \overline{p} + \left(\nabla \cdot (\overline{\boldsymbol{\tau}} - \rho \overline{\mathbf{v}'\mathbf{v}'})\right) + \overline{\mathbf{f}} \tag{2.31}$$

Equation 2.31 introduces the Reynolds stresses on the second term of right-hand side, which leads to six additional unknowns for the time-averaged momentum equations. The turbulence models are needed to close the system of flow equations and predict the Reynolds stresses. Based on the Boussinesq Hypothesis, the Reynolds stresses for incompressible flows can be given as follows:

$$\boldsymbol{\tau}_R = -\rho \overline{\mathbf{v}'\mathbf{v}'} = \mu_t \left(\nabla \mathbf{v} + (\nabla \mathbf{v})^{\mathrm{T}}\right) - \frac{2}{3}\rho k_t \mathbf{I} \tag{2.32}$$

$$k_t = \frac{1}{2}\overline{\mathbf{v}' \cdot \mathbf{v}'} \tag{2.33}$$

where $\mathbf{I}$ is the identity matrix, μ_t denotes the turbulent viscosity, and k_t represents the turbulent kinetic energy. Based on this approximation, the calculation of Reynolds stress components can be transformed into calculating the turbulent viscosity and turbulent kinetic energy.

To this end, many turbulence models were developed with different number of additional transport equations to describe the turbulent viscosity μ_t. The classical turbulence models that are widely applied to engineering flow problems include the Spalart-Allmaras model (Spalart and Allmaras, 1992) using one transport equation and the two-equation turbulence models of the k - ε model (Jones and Launder, 1972) and k - ω model (Wilcox, 1988), which have been extensively validated and continually improved over past several decades. However, the weaknesses of these two-equation turbulence models are also prominent. The k - ε model has an unsatisfactory performance in near-wall regions where there exist the adverse pressure gradients, although it is good at addressing the attached flows. The k - ω model has a remarkable performance in calculations of the separated flows but shows a severe sensitivity to the freestream values outside boundary and shear layers.

In order to overcome these deficiencies, Menter (1994) developed the Shear Stress Transport (SST) model which combines the best parts of k - ε model and k - ω model. It is achieved by introducing the blending functions to merge the different elements into a single formulation. Therefore, the SST k - ω turbulence model will act as the k - ε model in the freestream regions and perform as the k - ω model in the near-wall regions. Due to its robust capability in dealing with the complex flow behaviors, current study employs the SST k - ω turbulence model to simulate the turbulent effect of oscillating foils. The mathematical details of additional transport equations and numerical implementation for the SST k - ω turbulence model can be found in the latest modifications (Menter et al., 2003).

With respect to the solution of near-wall regions, these exist two approaches to deal with boundary layer in the RANS models. The first approach is to integrate the turbulence flow to the solid wall using low-

Reynolds models. Such that the viscosity-affected region including the viscous sublayer is resolved by highly dense mesh near the wall which requires substantial computing resources. The recommendation of first cell center position for this case is $y+ = O(1)$. The second approach is to employ the wall functions of high-Reynolds models to simulate the near-wall regions. Basically, the wall functions are a set of empirical equations from the law of the wall that is used to describe the physics in the near-wall regions. The first cell center should be placed in the log-law region to ensure the validity of model, which leads to $30 < y+ <300$. Thus, the mesh requirement and computational expenses are significantly reduced for the turbulence models using wall functions.

2.2.3 Dynamic mesh

The unsteady oscillatory motion of foil boundary suggests that the solution domain will change with time. Therefore, the mesh is required to move to accommodate the movement of foil boundary. Since the coordinate system remains fixed during the simulations, the substitution of relative velocity in convective terms is the only modification for the conservation equations with the moving mesh. In the current numerical model, the flow equations of a moving control volume with the boundary velocity $\mathbf{v}_b$ are described by the Arbitrary Lagrangian Eulerian (ALE) method to involve dynamic mesh into the computations (Ferziger et al., 2002).

$$\frac{\partial}{\partial t}\left(\int_V \rho\phi \mathrm{d}V\right) + \int_S \mathbf{n}\cdot(\rho\phi(\mathbf{v}-\mathbf{v}_b))\mathrm{d}S = \int_S \mathbf{n}\cdot(\Gamma\nabla\phi)\mathrm{d}S + \int_V S_\phi \mathrm{d}V \tag{2.34}$$

According to the space conservation law, the following equation gives the relationship between the rate of change of the control volume and the velocity of the bounding surface as:

$$\frac{\partial}{\partial t}\int_V \mathrm{d}V - \int_S \mathbf{n}\cdot\mathbf{v}_b \mathrm{d}S = 0 \tag{2.35}$$

The CFD toolbox of *OpenFOAM* implements a variety of algorithms to deal with the mesh motion. The widely validated and applied approaches include the sliding interface technique, algorithms based on interpolation function and solution of differential equations. The sliding interface technique such as the Arbitrary Mesh Interface (AMI) and Generalized Grid Interface (GGI), divides the computational domain into multiple zones that are adjacent and disconnected to each other. During the simulation, the moving zone with the fixed mesh around the solid boundary can perform the extreme rotation or translation relative to other regions. The interpolation techniques conduct the calculation of mesh movement by the interpolation of rotation and displacement based on the distance to the moving surface. The spherical linear interpolation (Slerp) and Radial Basis Function interpolation (RBF) are two well developed interpolation algorithms that show a satisfactory performance in preserving the mesh quality near the moving boundary.

For the mesh deformation based on the differential equations, the time-varying spatial nodes are calculated by solving the mesh motion equations, which generally involve the spring analogy equation, elliptic equation (Laplace equation or solid-body rotation stress equation) and linear pseudo-solid equation. The motion of solid body is regarded as the boundary condition of mesh motion equations, and hence determines the changing position of mesh points. In terms of numerical implementation, a diffusivity parameter needs to be introduced to describe the rigidity of the mesh, which controls the corresponding mesh spacing and points with the change of time. Available diffusivity models in *OpenFOAM* toolbox include the uniform, directional, inverse distance, linear, quadratic and exponential methods. Due to its good performance in preserving mesh quality around the oscillating foils with modest rotation and significantly high computing efficiency, current numerical model employs dynamic mesh approach that solves the solid-body rotation stress equations to address the mesh motion. The diffusivity model is selected as the inverse distance method, which calculates the domain diffusivity based on the inverse of the distance from the specified boundaries.

A typical mesh deformation in the computational domain with biplane oscillating foil configuration is shown in Figure 2-4. Owing to the implemented model of mesh motion, the slight distortion is identified near the foil surface, while the stretching and squeezing tend to be more severe with the increasing distance from the mesh cell center to foil boundary.

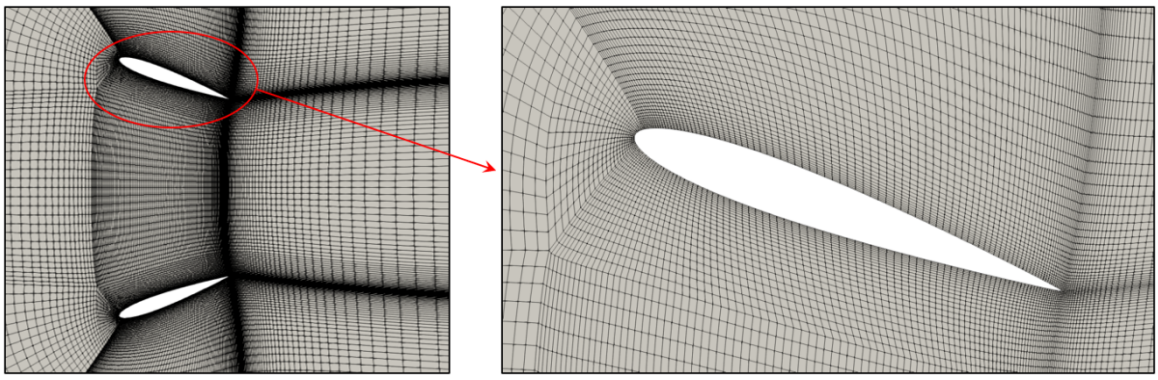

(a) During first-half oscillatory cycle

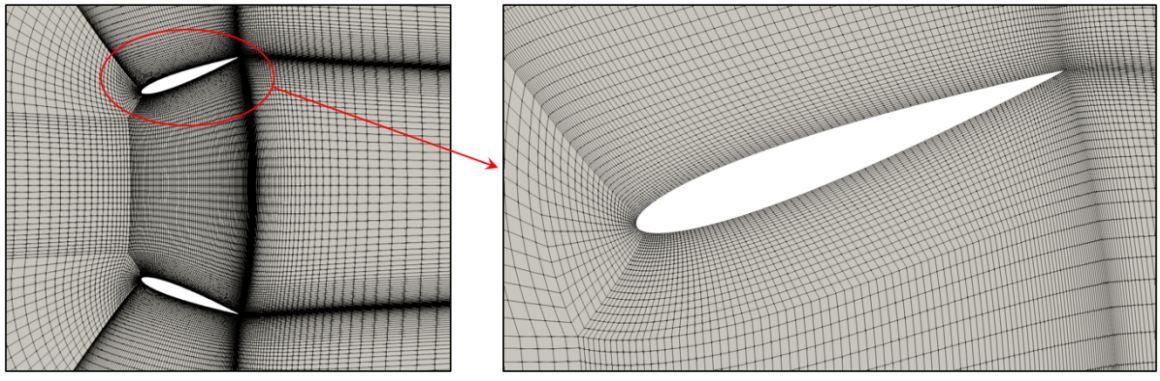

(b) During second-half oscillatory cycle

Figure 2-4 The dynamic mesh around the biplane oscillating foil configuration.

2.2.4 Numerical schemes and iterative methods

After the modelling of physical phenomena and geometric domain, the discretization needs to be conducted to obtain the numerical solution for the flow problems of interest. The discretization process consists of two steps, which are characterized as the discretization of geometric domain into the computational mesh and transformation of conservation governing equations into the equivalent system of algebraic equations, respectively. Then, the resulting set of algebraic equations are solved by the iterative methods which provides the discrete property values over each mesh element of computational domain. The ultimate objective is to replace the continuous exact solution of flow governing equations with the numerical solutions characterizing as the discrete values. In general, the discretization approaches for the conservation flow equations involve the Finite Difference Method (FDM), Finite Volume Method (FVM) and Finite Element Method (FEM).

The *OpenFOAM* code employs the FVM to discretize the conservation equations, which divides the computational domain into a finite number of control volumes and takes the integral form of flow governing equations as a starting point. The discretization of individual terms for the integral form of transport equation with a general property ϕ can be performed as following equations.

- Convective term:

$$\int_V \nabla \cdot (\rho \mathbf{v}\phi) \mathrm{d}V = \int_S \mathrm{d}\mathbf{S} \cdot (\rho \mathbf{v}\phi) = \sum_{Fs} \mathbf{S}_{Fs} \cdot (\rho \mathbf{v})_{Fs} \phi_{Fs} = \sum_{Fs} F_m \phi_{Fs} \tag{2.36}$$

where Fs indicates the flat faces that connects different cells, $\mathbf{S}_{Fs}$ denotes the face area vector, ϕ_{Fs} represents the face field which can be evaluated by a variety of schemes, and F_m is the mass flux that is defined as:

$$F_m = \mathbf{S}_{Fs} \cdot (\rho \mathbf{v})_{Fs} \tag{2.37}$$

- Diffusive term:

$$\int_V \nabla \cdot (\Gamma \nabla \phi) \mathrm{d}V = \int_S \mathrm{d}\mathbf{S} \cdot (\Gamma \nabla \phi) = \sum_{Fs} \Gamma_{Fs} \mathbf{S}_{Fs} \cdot (\nabla \phi)_{Fs} \tag{2.38}$$

The surface normal gradient can be evaluated using the central difference scheme when the mesh is orthogonal, which gives the following expression:

$$\mathbf{S}_{Fs} \cdot (\nabla \phi)_{Fs} = |\mathbf{S}_{Fs}| \frac{\phi_N - \phi_C}{|\mathbf{d}|} \tag{2.39}$$

where N and C denote the neighboring cell and the cell of interest, respectively. $\mathbf{d}$ is the length vector between the center of these two cells.

- Source term:

All terms that are not included in the spatial differentiation belong to the source terms. For an implicit source term, it can be linearized and evaluated by the one-point Gauss quadrature.

$$\int_V \rho\phi \mathrm{d}V = \rho_C V_C \phi_C \tag{2.40}$$

- Temporal term:

The first-time derivative can be integrated over a control volume as following expression.

$$\frac{\partial}{\partial t}\int_V \rho\phi \mathrm{d}V \tag{2.41}$$

The discretization of temporal term is performed using a straightforward approach. The process needs the values from three different time levels including the new values at the current time step, old values at the previous time step and the old-old values at the time step previous to the last. The widely used discretization schemes for the temporal term are Euler implicit scheme, backward differencing scheme and Crank-Nicolson scheme.

The convection of a general scalar variable ϕ depends on the local velocity field. Normally, the velocity field is unknown and hence needs to be solved along with all other variables by the set of governing equations. Considering the incompressible flows, the problem becomes highly complicated due to the strong coupling between pressure and velocity. A popular approach to address this issue is the iterative solution strategy. The SIMPLE and PISO algorithms which stands for Semi-Implicit Method for Pressure-Linked Equations and Pressure Implicit with Splitting of Operators are two most widely used methods to solve the pressure-velocity coupling. Over past several decades, SIMPLE and PISO algorithms along with their variations have been implemented into numerous fluid solver to handle a large variety of flow problems with satisfactory accuracy.

The SIMPLE algorithm employs a guess-and-correct procedure to calculate the pressure, which is performed on the staggered grid. Its procedure starts with the guessed field of pressure and velocity. Then, the guessed pressure field is used to solve the discretized momentum equations to yield a new velocity field. Based on the updated mass flow rates, the pressure correction field p' can be obtained by solving the pressure correction equation. After that, the pressure and velocity fields are updated to satisfy the continuity equation. The above steps are repeated along with setup of $p^* = p$ and $\mathbf{v}^* = \mathbf{v}$ until convergence. The general implementation procedure of SIMPLE algorithm for the steady flow is shown in Figure 2-5.

The PISO algorithm consists of one predictor step and two corrector steps. In the predictor step, the new velocity field is obtained by solving the discretized momentum equations with the guessed pressure field as the method of SIMPLE algorithm. In the corrector step one, the corrected velocity field is

provided by the first corrector step of SIMPLE. Thus, the first pressure correction equation of PISO method can be obtained by substituting the corrected velocity field in the discretized continuity equation, which is used to produce the first pressure correction field. In the corrector step two, the second pressure correction equation can be obtained by substituting the twice-corrected velocity field in the discretized continuity equation, which is solved to yield the second pressure correction field and hence the twice-corrected pressure field. Figure 2-6 presents the general procedure of steady-state PISO algorithm. With respect to the calculation of unsteady flows, the transient terms need to be included in the discretized momentum equations, which may lead to the additional terms in momentum and pressure correction equations. One may refer to Versteeg and Malalasekera (2007) for more details of transient SIMPLE and PISO algorithms.

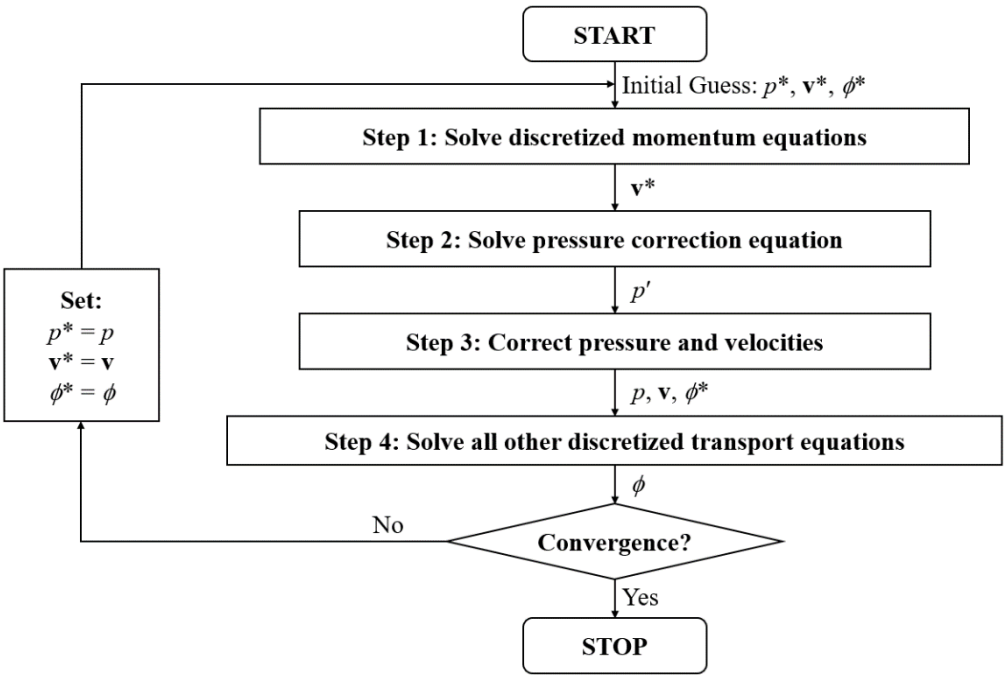

Figure 2-5 The general procedure of SIMPLE algorithm.

In the current numerical model, the pressure-velocity coupling of incompressible transient flow is solved by the PIMPLE algorithm, which is essentially the combination of PISO and SIMPLE algorithm. One key advantage for PIMPLE algorithm is that it enables the usage of large time step with satisfactory numerical stability. The principal of this algorithm can be briefly described as: It performs as the SIMPLE algorithm to find the steady-state solution within every single time step which accompanied with an under-relaxation strategy. In order to obtain this solution within each time step, the outer correction loops are required to ensure the convergence of explicit components of the equations. Once the input tolerance criterion is reached, the calculation is moved on to the next time step until the simulation is complete.

In addition, the time discretization is conducted by the first-order implicit Euler scheme. For the space discretization, a second-order linear upwind scheme and a second-order linear interpolation scheme are

used to discretize the convective term and diffusive term, respectively. With respect to the resulting set of algebraic equations, the generalized Geometric-Algebraic Multi-Grid (GAMG) method is employed to solve the pressure equations. The calculation of velocity and turbulence equations is conducted by the Preconditioned Bi-Conjugate Gradient (PBiCG) method.

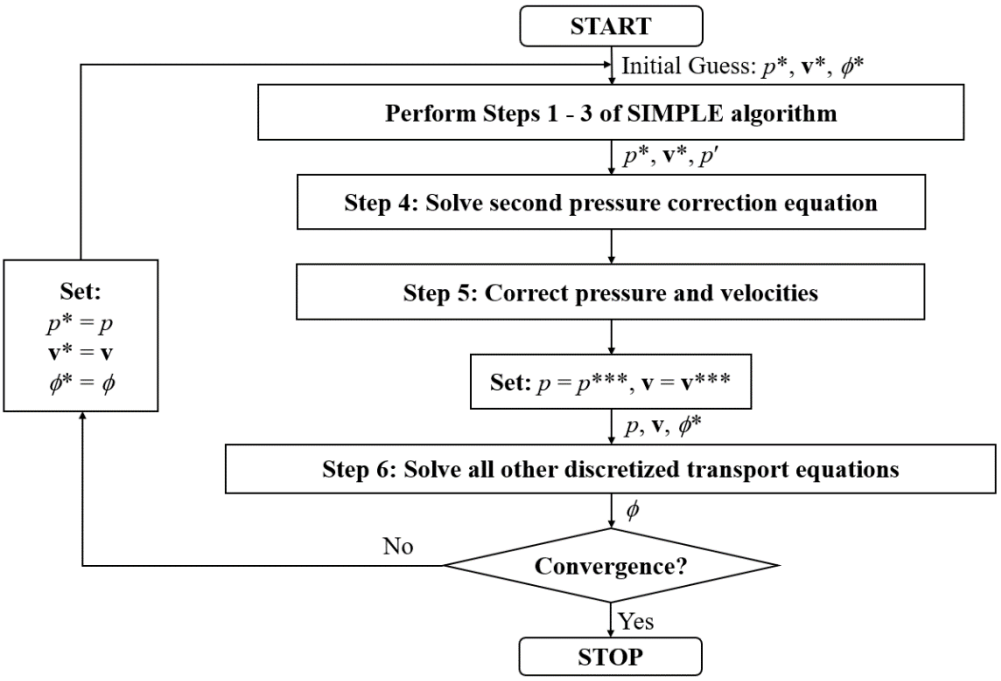

Figure 2-6 The general procedure of PISO algorithm.

2.2.5 Computational domain and boundary conditions

The schematic of a two-dimensional computational domain for the current model is presented in Figure 2-7. It has a horizontal length of 50*c* and a vertical height of 40*c*. An adequately large domain is used to ensure that the minimum distance from the outer boundaries to moving foils significantly exceeds five characteristic lengths (chord length in the current case).

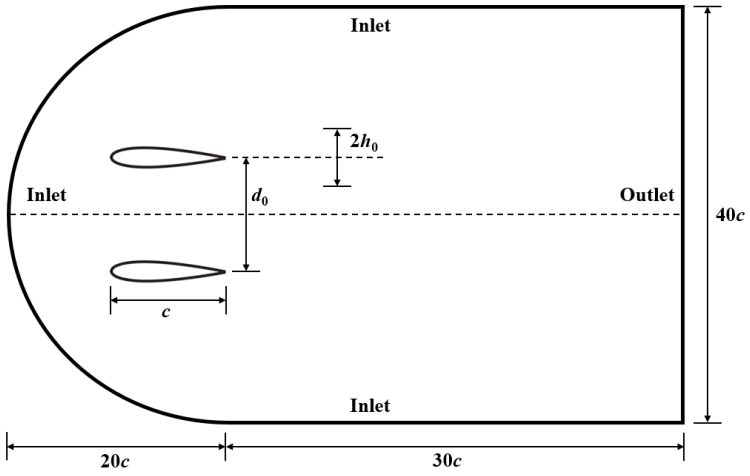

Figure 2-7 Schematic of a two-dimensional computational domain.

The mesh resolution and division details around each foil for the biplane configuration is shown in Figure 2-8, which is generated by the software package of *ICEM CFD*. The boundary layer around the oscillating foils is simulated by the turbulence model with the wall functions. Hence, the minimum $y+$ at near-wall regions is set as around 45 to ensure that the first cell center is placed in the log-law region, indicating the flow behaviors in the viscous sub-layer are modelled by the law of the wall.

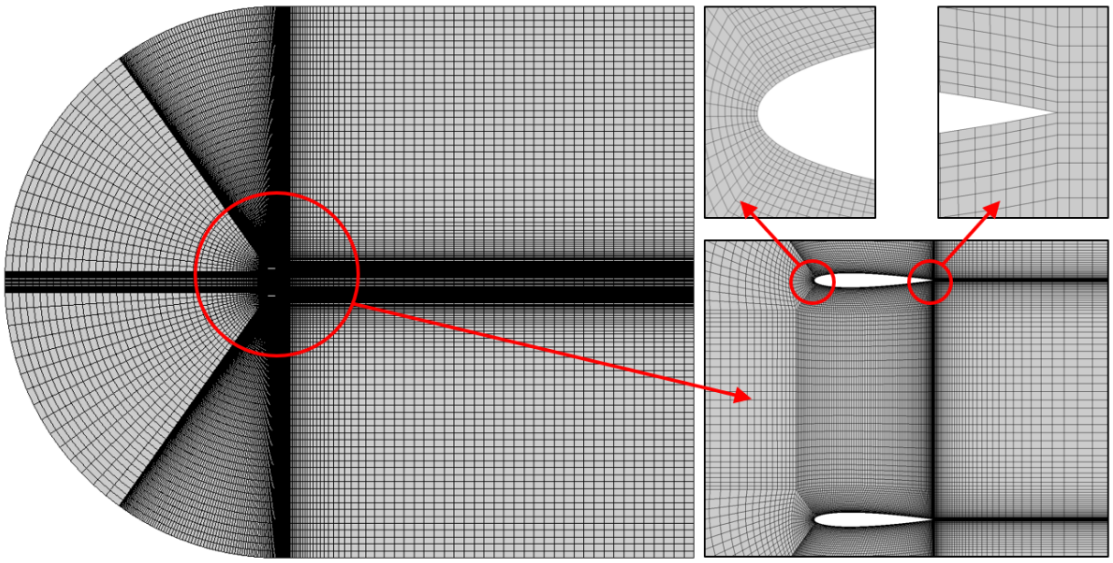

Figure 2-8 Two-dimensional mesh resolution around the foil of biplane configuration.

There are a number of boundary conditions for the solution of partial differential equations. The Dirichlet and the Neumann boundary conditions are most extensively used ones among them for the general scalars. In terms of mathematical aspect, the Dirichlet boundary condition (or first type) specifies the values of the solution function at the boundary, while the Neumann boundary condition (or second type) prescribes the values of the derivative at the boundary.

Four types of boundary conditions need to be addressed for the current model, including the inlet, outlet, foils and lateral planes. The constant and uniform velocity is imposed at the upstream inlet. The boundary condition of downstream outlet is set as the constant static pressure. The foil boundary is implemented as the moving wall with no flux normal to the body surface. The lateral boundaries for the three-dimensional domain are set to the symmetry planes. The detailed implementation of boundary conditions is presented in Table 2-1, in which the value and derivative of a given parameter with the mark of N_0 and T_0 denote the component along the normal and tangential direction, respectively.

Symmetry boundary condition is characterized as no flow and no scalar flux across the boundary. The implementation of a scalar variable is performed by setting its normal gradient to zero. For the velocity vector in the viscous flows, its numerical setup is similar to a slip wall boundary condition, which has the zero normal component and the zero tangential gradient. The further demonstration of boundary conditions, computational domain and mesh division for the three-dimensional cases are presented in the subsequent chapter.

Table 2-1 Implementation of boundary conditions for the current numerical model.

Boundary	Parameter	Condition
Inlet	**v** (Velocity)	$\mathbf{v} = (U_\infty, 0, 0)$
	p (Pressure)	$\partial p/\partial N_0 = 0$
	k_t (Turbulent kinetic energy)	Fixed Value (depend on flow conditions)
	ω_t (Turbulence frequency)	Fixed Value (depend on flow conditions)
	v_t (Kinematic eddy viscosity)	Calculated
Outlet	**v** (Velocity)	$\partial \mathbf{v}/\partial N_0 = 0$
	p (Pressure)	$p = 0$
	k_t (Turbulent kinetic energy)	$\partial k_t/\partial N_0 = 0$
	ω_t (Turbulence frequency)	$\partial \omega_t/\partial N_0 = 0$
	v_t (Kinematic eddy viscosity)	Calculated
Foils	**v** (Velocity)	$\mathbf{v} = (0, 0, 0)$
	p (Pressure)	$\partial p/\partial N_0 = 0$
	k_t (Turbulent kinetic energy)	Wall Function
	ω_t (Turbulence frequency)	Wall Function
	v_t (Kinematic eddy viscosity)	Wall Function
Symmetry	**v** (Velocity)	$\mathbf{v}\ (N_0) = 0$, $\partial \mathbf{v}/\partial T_0 = 0$
	ϕ (Scalar Properties)	$\partial \phi/\partial N_0 = 0$

2.3 Fluid-Structure Coupling

For a fully prescribed oscillating foil configuration, the straightforward interaction between the moving body and surrounding flow is taken into account by implementing an imposed boundary condition of structure. The dynamics of foil are directly defined as following sinusoidal profiles, which provide the position and velocity of solid boundary at each time step. Thus, the updated flow field in time has no influence on the locomotion of foils.

$$h(t) = h_0 \sin(\omega t) \tag{2.42}$$

$$\theta(t) = \theta_0 \sin(\omega t + \varphi) \tag{2.43}$$

where θ_0 denotes the pitching amplitude, and φ represents the phase angle between pitching motion and

heaving motion.

With respect to the configuration of interest in the current study, the APWIGs has a semi-active motion mechanism which is characterized as the combination of actively imposed heaving motion and flow-induced pitching motion restrained by the attached torsional springs. A fluid-structure coupling can be identified for the hydrodynamic behaviors of APWIGs since that the pitching motion of each foil arises from the flow forces and the resulting position of foil boundary alters the flow fields in turn. The monolithic strategy is believed to be the most accurate and robust approach to address the issue of fluid-structure coupling at the expense of computing efficiency. Both flow equations and structure equations are implemented into one single solver by this approach, which solve the system of equations by the iterative manner. The partitioned strategy is another approach to deal with the problem of fluid-structure coupling, which individually solves the flow equations and the structure equations using a sequential manner. Although partitioned strategy requires relatively low computing resources, the fidelity of numerical model using this approach is significantly reduced since the physical essence of strong coupling for flow-induced motion is not fully involved.

In this study, the monolithic approach is employed to solve the complicated coupling between flow fluid and oscillating foils. For the APWIGs, the motion of each foil can be modelled as a linear mass-spring-damping system which is subject to the external forces consisting of the hydrodynamic moment and restoring moment of torsional spring. In addition, multiple constraints are implemented to limit all other degree of freedom. Hence, the corresponding dynamic responses are governed by following equation.

$$M_{axis} = I_{axis}\ddot{\theta} + D_{pitch}\dot{\theta} + K_{pitch}\theta \tag{2.44}$$

where M_{axis} is the hydrodynamic moment about the elastic axis, D_{pitch} and K_{pitch} denotes the pitching damping coefficient and torsional stiffness coefficient, respectively. It should be noted that the damping effect is not considered in the current simulations although damping term is involved in this equation for generalization.

The locomotion of each foil for APWIGs is determined by the set of equations 2.42 and 2.44. A six degrees of freedom (6-DOF) solver in *OpenFOAM* toolbox is modified to simulate the kinematics of APWIGs. The solution of equation 2.44 is performed by a second-order explicit scheme named Symplectic Splitting Method (Dullweber et al., 1997), which has a robust performance in the simulation of 6-DOF solid-body motion and is readily available within the *OpenFOAM* code.

The interaction loop for the fluid-structure coupling within each time step is shown in Figure 2-9. Based on the initial conditions of structure, the velocity and pressure fields of computational domain are first calculated by the flow solver. The hydrodynamic forces and moments acting on each foil are then calculated by the pressure integral along the body surface. After that, the new positions and velocities of foils can be provided by the solution of equations 2.42 and 2.44. The obtained boundary conditions of solid body are transferred back to the flow solver to update the boundary conditions of fluid field and

perform corresponding mesh deformation. Once the convergence criterion is satisfied, the iteration loop will move on to the next time step.

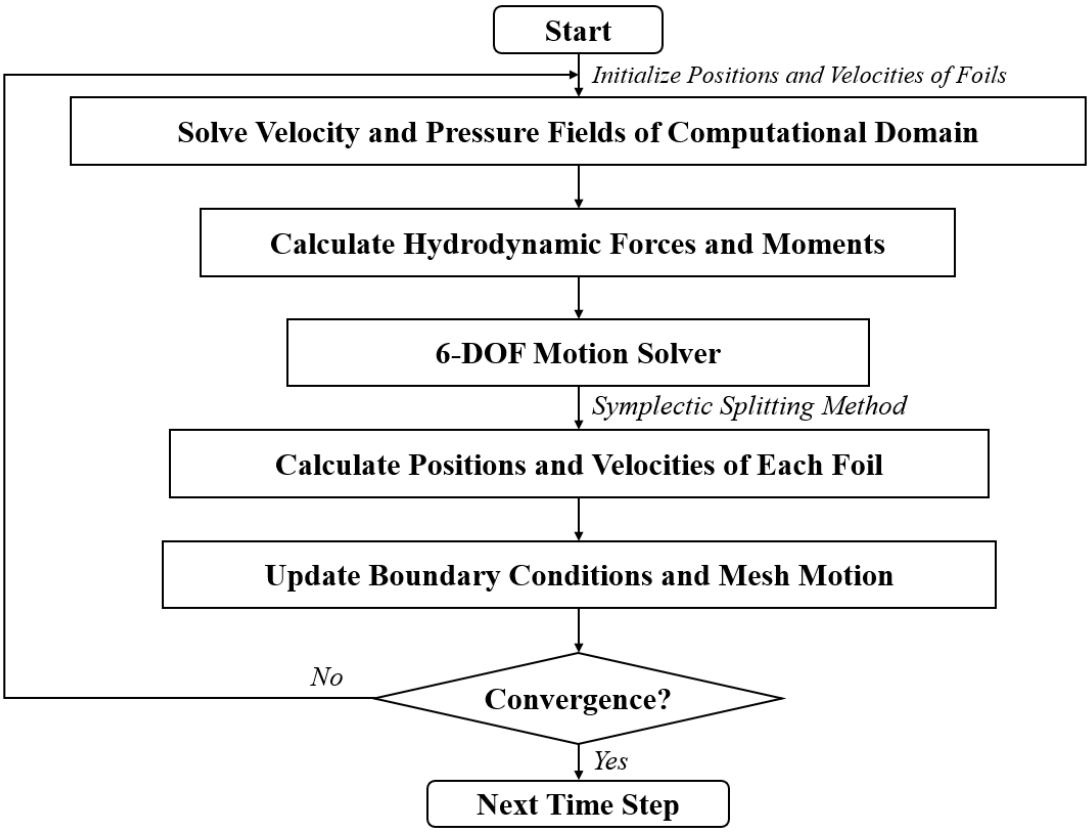

Figure 2-9 Numerical implementation of fluid-structure coupling within each time step.

2.4 Verification and Validation

The established numerical model is comprehensively verified and validated in this section. A convergence study with respect to both grid size and time step is first performed. The numerical uncertainties are then estimated and analyzed by following the specific procedure. The convergence study and uncertainty analysis are carried out by the concerned APWIGs. The available experimental data relevant to the unsteady flow around prescribed oscillating foils in literature are selected as the benchmark to validate the accuracy and reliability of developed model. In the current study, the foil section is taken as NACA0012 with a chord length of 0.1m. The density ratio of structure over fluid is set as 15 to ensure the numerical stability. The kinematic and geometry parameters of APWIGs for this section is set as following description. The heaving amplitude and mean distance between two foils are 0.5c and 2c, respectively. The elastic pitching axis is fixed at 0.25 chord position from the leading edge. The oscillating frequency of each foil is set as 4Hz resulting in an oscillatory cycle of 0.25s. The Reynolds number based on chord length is 200000. The torsional spring stiffness is taken as a value that produces stable motion and satisfactory propulsive performance.

2.4.1 Convergence study

The typical time histories of flow-induced pitching angle and force coefficients for APWIGs are presented in Figure 2-10. Numerical results show that both the pitching angle of two foils and force coefficients of each foil tend to present the periodic characteristics after the fourth oscillatory cycle. Especially, the pitching angle of the upper foil has the same value and opposite direction with that of the lower foil, indicating that the dynamic responses of the two foils are symmetric with respect to the generated ground plane. If not particularly noted, the rest of the numerical simulations are monitored with five oscillatory cycles to ensure that each case reaches a periodic state. Moreover, all time-averaged results are obtained based on the calculation of the last oscillatory cycle.

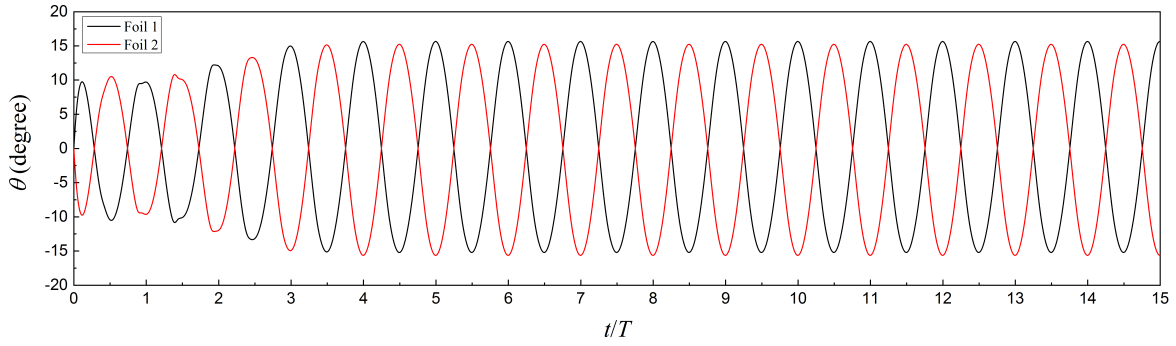

(a) Pitching angle

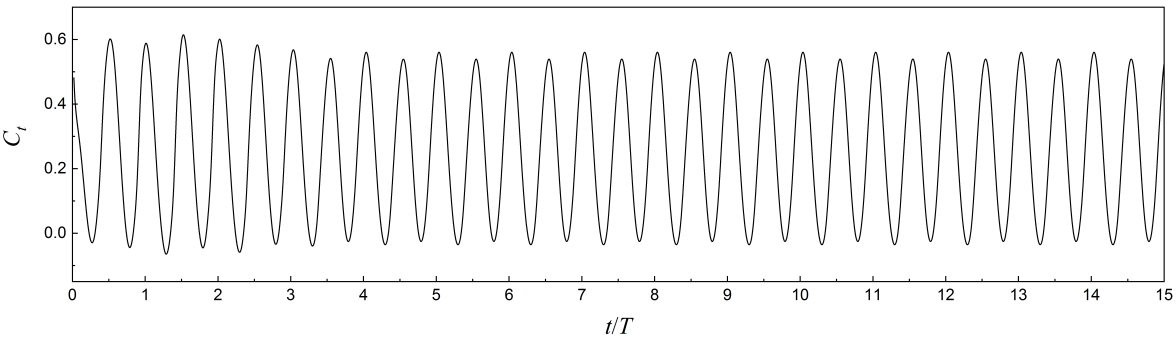

(b) Thrust coefficient

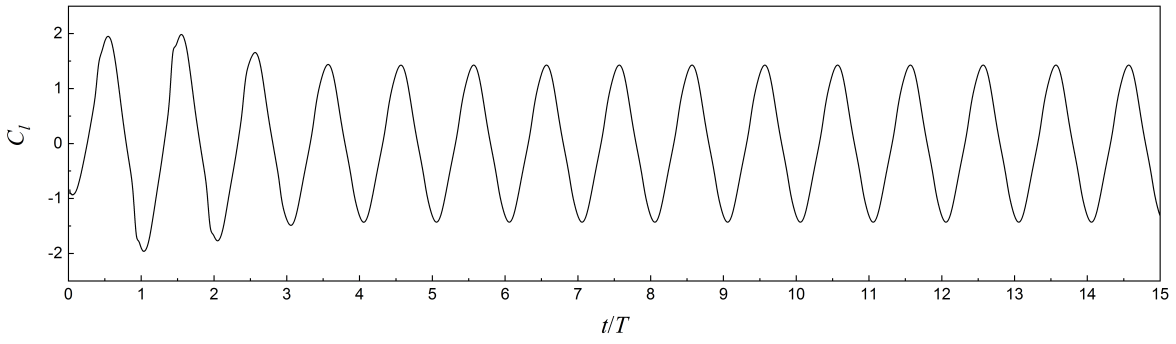

(c) Lift coefficient

Figure 2-10 Typical time history of flow-induced pitching angle and force coefficients for APWIGs within 15 oscillatory cycles.

There exists two ways in the numerical model that control the time step during the simulation. The first method is to adjust the time step by implementing a maximum Courant number. Hence, the adaptive time step during the simulation is determined by the Courant-Friedrichs-Lewy (CFL) condition. The second method is to directly set a constant time step during the simulation. In this case, the local Courant number needs to be monitored for computational stability. Herein, the convergence study is conducted by considering both time-step controlling methods. The stability and accuracy of numerical solutions are the priority in this section since the two-dimensional computations are highly efficient.

In the first part, a maximum Courant number of 0.9 for all simulations was implemented leading to the value of maximum time step less than 0.0001s (T/2500). Such a temporal size is sufficient to guarantee the numerical accuracy in time. For the spatial convergence, there are two dominant parameters that determine the accuracy in space, including the height of the first cell layer and the number of nodes distributed on the foil surface. Figure 2-11 presents the time-averaged thrust coefficient with six different heights of the first cell layer. Results show that thrust coefficient tends to converge towards value of 0.25, indicating that the first cell height of 0.0003m is sufficient for the current simulations.

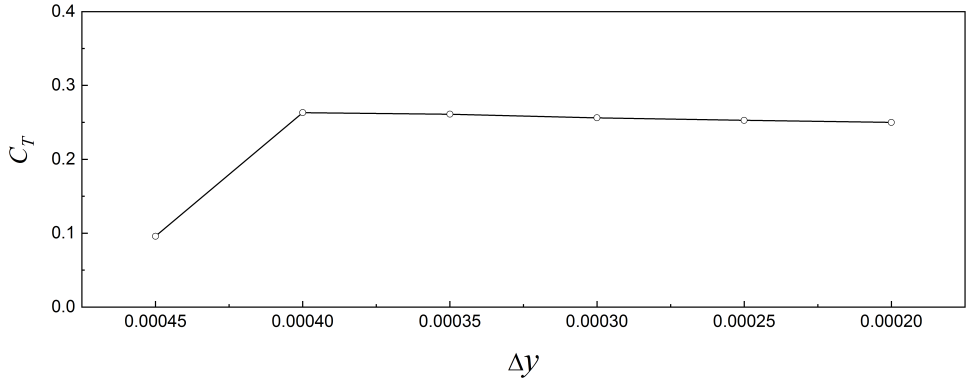

Figure 2-11 Time-averaged thrust coefficient with different first cell heights.

With the fixed first cell height of 0.0003m, five grid resolutions were considered by adjusting the number of nodes distributed on the foil surface, as shown in Table 2-2. The time variation of thrust and lift coefficient with different grid resolutions are presented in Figure 2-12. Note that the caption is shared by a same set of figures throughout whole thesis if not particularly indicated. As the results show, the satisfactory convergence in space was obtained with five grid resolutions. The maximum variation of instantaneous force coefficient between results of Grid 3 and 5 is less than 1%.

Table 2-2 Grid-size setup for the first part of convergence study.

Grid	**1**	**2**	**3**	**4**	**5**
Δy (m)	0.0003	0.0003	0.0003	0.0003	0.0003
Num of nodes	140	160	180	200	220
Num of cells	28466	31652	34050	38088	50930

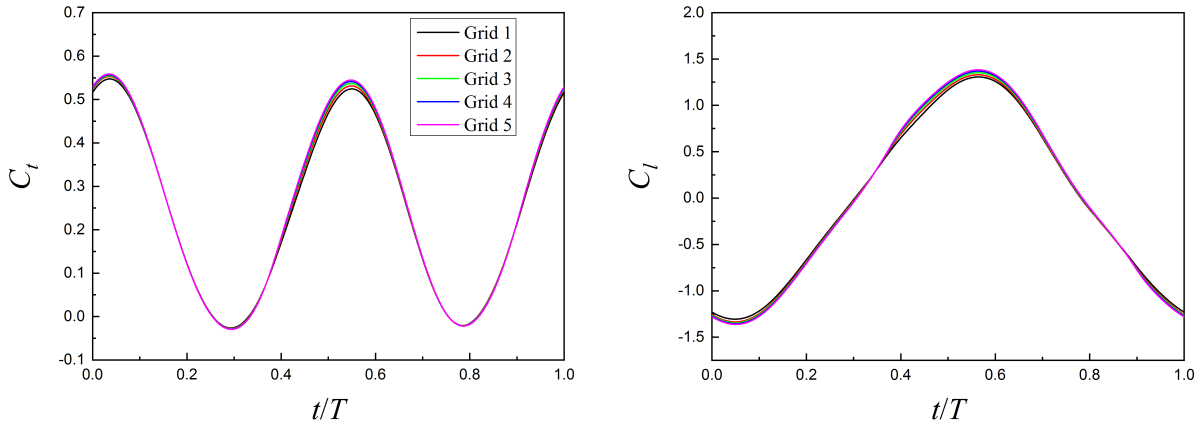

(a) Thrust coefficient (b) Lift coefficient

Figure 2-12 Time-varying force coefficients over one oscillatory cycle with different grids (Time step is determined by the maximum Courant number during the simulation).

In the second part, a fixed time step during the simulation was implemented. The convergence study with respect to both time and grid was carried out to ensure that the current numerical model has the satisfactory temporal and spatial independence. This part of computations considers five time-step sizes and four grid resolutions, as shown in Table 2-3.

Table 2-3 Time-step and grid-size setup for the second part of convergence study.

Setup	**1**	**2**	**3**	**4**	**5**
Δt	1.5×10^{-4}	1×10^{-4}	8×10^{-5}	5×10^{-5}	3×10^{-5}
Grid	22730	32676	48186	70836	-

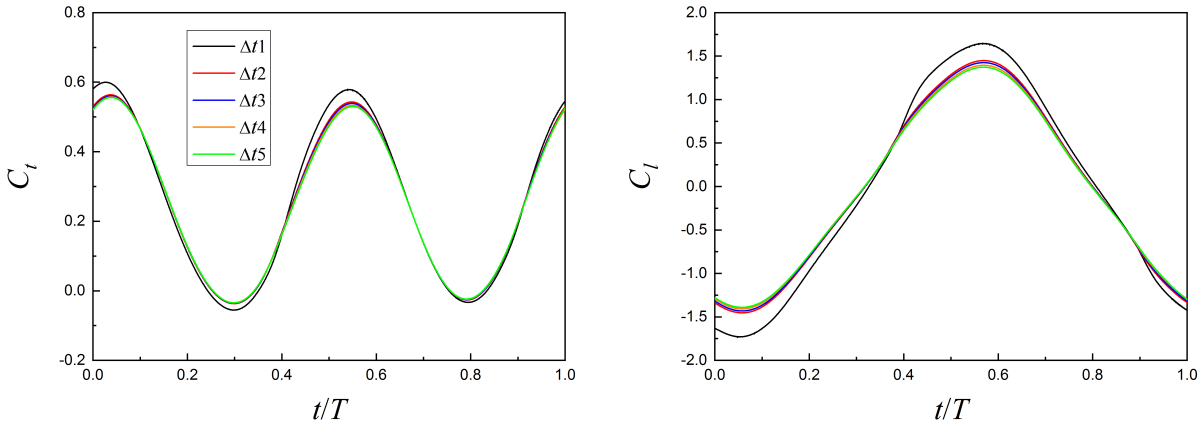

(a) Thrust coefficient (b) Lift coefficient

Figure 2-13 Time-varying force coefficients over one oscillatory cycle with different time steps (Time step is fixed as a constant value during the simulation).

The time variation of force coefficients over one oscillatory cycle using different time steps are presented in Figure 2-13, which suggests that the time step below 1×10^{-4}s (T/2500) provide a

satisfactory accuracy in time. Such a behavior agrees well with the indication in the first part of convergence study. Therefore, the time step size of 8×10^{-5} is used to perform the following convergence computations with respect to grid size. As shown in Figure 2-14, the satisfactory convergence in space was obtained for the time-varying force coefficients by a medium mesh resolution with the cell number of 48186. The maximum difference of instantaneous peak force coefficients between results by Grid 3 and results by Grid 4 is also less than 1%.

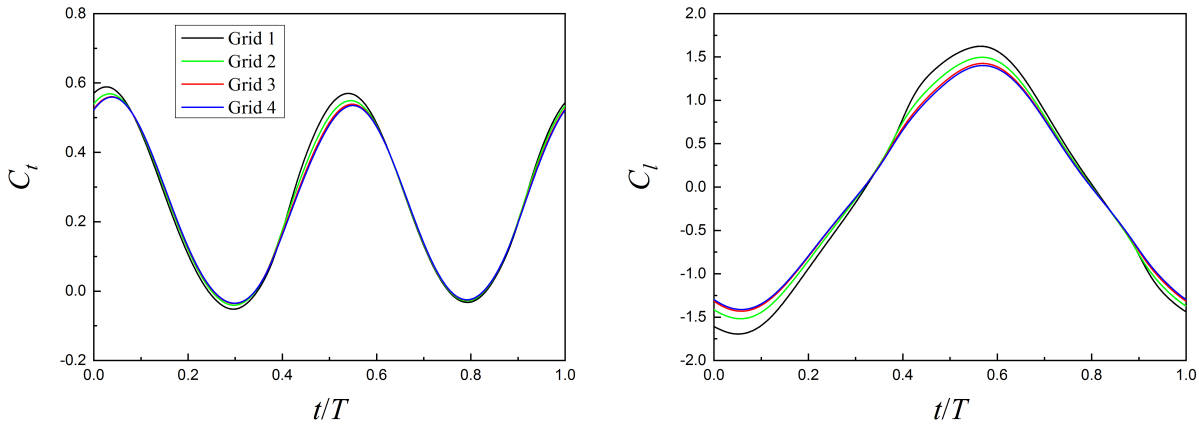

(a) Thrust coefficient (b) Lift coefficient

Figure 2-14 Time-varying force coefficients over one oscillatory cycle with different grids (Time step is fixed as a constant value during the simulation).

2.4.2 Uncertainty analysis

Numerical uncertainties with respect to both time step and grid size were analyzed using the correlation factor method (Stern et al., 2001; Wilson et al., 2001). Three solutions with systematic temporal and spatial refinement were performed. When the uncertainty analysis with respect to one input parameter is carried out, all other input parameters are kept as the constant values. The numerical setup for the uncertainty analysis is shown in Table 2-4, in which the uniform refinement ratio of 2 and $\sqrt{2}$ for the time step and grid size are used, respectively. The satisfactory independence with respect to time and space can be obtained in Figure 2-15, which presents the variation of thrust coefficients over one oscillatory cycle.

Table 2-4 Time-step and grid-size setup for the uncertainty analysis.

Setup	**Grid Cell** ($r_G = \sqrt{2}$)	**Time Step** ($r_T = 2$)
Fine (S_1)	96404	4×10^{-5}
Medium (S_2)	48186	8×10^{-5}
Coarse (S_3)	24060	1.6×10^{-4}

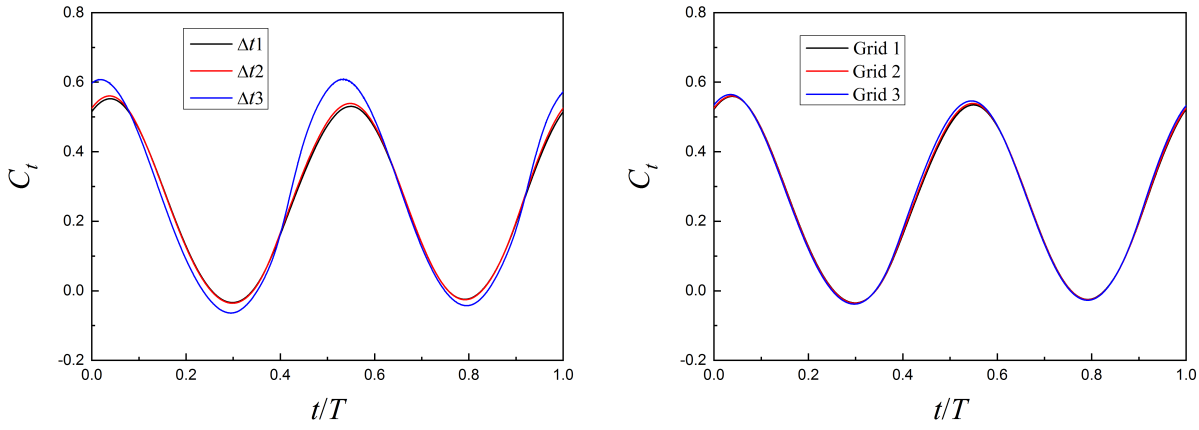

(a) Temporal convergence (b) Spatial convergence

Figure 2-15 Time-varying thrust coefficient over one oscillatory cycle with different setups.

The current study follows the procedure by Stern et al. (2006) to estimate the numerical uncertainties with respect to the time step and grid size. Time-averaged thrust and power coefficients are selected as the integral variables to perform the uncertainty calculation. It is assumed that iterative errors are negligible compared with the time-step and grid-size convergence errors in this study. Therefore, the numerical errors are decomposed into the contributions from the time step and grid size. The variations of thrust and power coefficients between fine, medium and coarse solutions for *k*-th input parameter can be calculated as:

$$\varepsilon_{k_{21}} = S_2 - S_1 \tag{2.45}$$

$$\varepsilon_{k_{32}} = S_3 - S_2 \tag{2.46}$$

The convergence ratio is defined as the changes between the medium-fine and coarse-medium solutions:

$$R_k = \frac{\varepsilon_{k_{21}}}{\varepsilon_{k_{32}}} \tag{2.47}$$

where S_1, S_2 and S_3 denote the solution from the fine, medium and coarse input parameter, respectively. Convergence ratio is employed to determine the convergence conditions, which include: (i) monotonic convergence ($0 < R_k < 1$), (ii) oscillatory convergence ($R_k < 0$; $|R_k| < 1$), (iii) monotonic divergence ($R_k > 1$), (iv) oscillatory divergence ($R_k < 0$; $|R_k| > 1$).

For the condition (ii), numerical uncertainties are predicted by bounding the error based on oscillation with maximum and minimum solutions. The errors and uncertainties cannot be estimated for condition (iii) and (iv). With respect to the condition (i), numerical errors and uncertainties are estimated by generalized Richardson extrapolation, which provides the estimate for one-term numerical error and order of accuracy as following equations:

$$\delta^*_{RE_{k1}} = \frac{\varepsilon_{k_{21}}}{r_k^{p_k} - 1} \tag{2.48}$$

$$p_k = \frac{\ln(\varepsilon_{k_{32}} / \varepsilon_{k_{21}})}{\ln(r_k)} \tag{2.49}$$

where r_k is the uniform refinement ratio for k-th input parameter. A correction factor is employed to account for the effect of higher-order terms for the error and uncertainty estimates defined as:

$$C_k = \frac{r_k^{p_k} - 1}{r_k^{p_{kest}} - 1} \tag{2.50}$$

where p_{kest} is an estimate for the limiting order of accuracy. An improved error estimate can be obtained based on the multiplication of equation 2.48 by the correction factor:

$$\delta^*_k = C_k \delta^*_{RE_{k1}} \tag{2.51}$$

The uncorrected uncertainty U_k and corrected uncertainty U_{kc} are estimated by following equations depending on the distance of solutions to the asymptotic range:

$$U_k = \begin{cases} (9.6(1-C_k)^2 + 1.1)\left|\delta^*_{RE_{k1}}\right| & \left|1-C_k\right| < 0.125 \\ (2\left|1-C_k\right| + 1)\left|\delta^*_{RE_{k1}}\right| & \left|1-C_k\right| \geq 0.125 \end{cases} \tag{2.52}$$

$$U_{kc} = \begin{cases} (2.4(1-C_k)^2 + 0.1)\left|\delta^*_{RE_{k1}}\right| & \left|1-C_k\right| < 0.25 \\ (\left|1-C_k\right|)\left|\delta^*_{RE_{k1}}\right| & \left|1-C_k\right| \geq 0.25 \end{cases} \tag{2.53}$$

The current numerical uncertainty with respect to time step and grid size are presented in Tables 2-5 and 2-6, respectively. Results indicated that the time-averaged thrust coefficient has a certain sensitivity for the time-step resolution, while the time-averaged power coefficient tends to be more sensitive to the grid-size resolution. Reasonably low level of uncertainty referring to both time step and grid size was obtained for two integral coefficients. The maximum uncertainty level of 3.19% was lied in the time-averaged thrust coefficient in time-step convergence calculation.

Table 2-5 Numerical uncertainty for the time step.

Variable	Solution			Convergence Ratio	Uncertainty		
	S_{T1}	S_{T2}	S_{T3}	R_T	δ^*_T (%S_{T1})	U_T (%S_{T1})	U_{Tc} (%S_{T1})
C_T	0.2490	0.2520	0.2577	0.5267	0.3979	3.1900	0.9307
C_P	0.3895	0.4023	0.5173	0.1111	1.0937	1.7773	0.6836

Table 2-6 Numerical uncertainty for the grid size.

Variable	Solution			Convergence Ratio	Uncertainty		
	S_{G1}	S_{G2}	S_{G3}	R_G	δ_G^* (%S_{G1})	U_G (%S_{G1})	U_{Gc} (%S_{G1})
C_T	0.2508	0.2520	0.2542	0.5616	0.4876	0.8985	0.1345
C_P	0.3946	0.4023	0.4202	0.4263	1.9379	2.4360	0.4980

2.4.3 Validation of numerical model

The first benchmark experiment is selected as the study conducted by Anderson et al. (1998), which measured propulsive characteristics of a single oscillating foil with fully imposed heaving and pitching motion. Figure 2-16 presents the comparison of time-averaged thrust and power coefficients between current simulations and experimental measurements. The configuration has a heaving amplitude of 0.75c and the pitch-leading phase angle of 90 degrees. The effective AoA is set as a constant value of 15 degrees by adjusting the pitching amplitude and oscillating frequency.

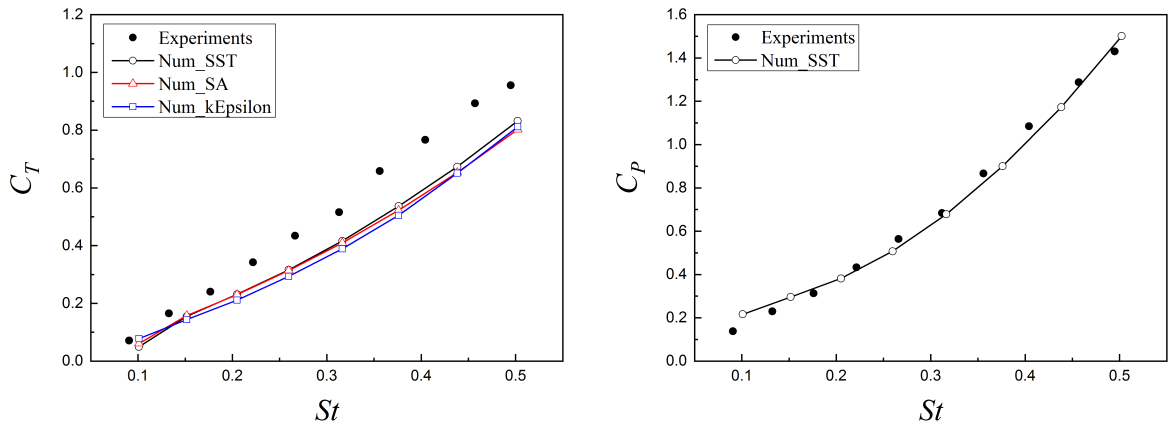

(a) Thrust coefficient (b) Power coefficient

Figure 2-16 Comparison of time-averaged propulsive coefficients for fully prescribed single foil between current predictions and experimental measurements by Anderson et al. (1998).

It can be seen that the major discrepancy between the current results and experimental data is lied in the thrust calculation. A satisfactory agreement for the power coefficient was obtained indicating that tip vortex shedding due to three-dimensional effect is not the major contribution to this disagreement. In the current simulations, the thrust calculation was also performed using the Spalart-Allmaras turbulence model and k - ε turbulence model, as shown in Figure 2-16 (a). The negligible difference between three models suggests that the turbulent effect is not the dominant cause to the discrepancy. The disagreement of thrust coefficient between the current calculations and experimental measurements is mainly attributed to the mismatched baseline of zero horizontal force along the advance speed. According to Read et al. (2003), the data was initialized to zero after the carriage starts to move and before the oscillation of foil in the measurements by Anderson et al. (1998). It leads to an artificially

high value of mean thrust due to the exclusion of drag. In contrast, the current results were set as zero value before any motion of carriage and foil oscillation, which ensures that the drag acting on the foil will be included in the thrust calculation.

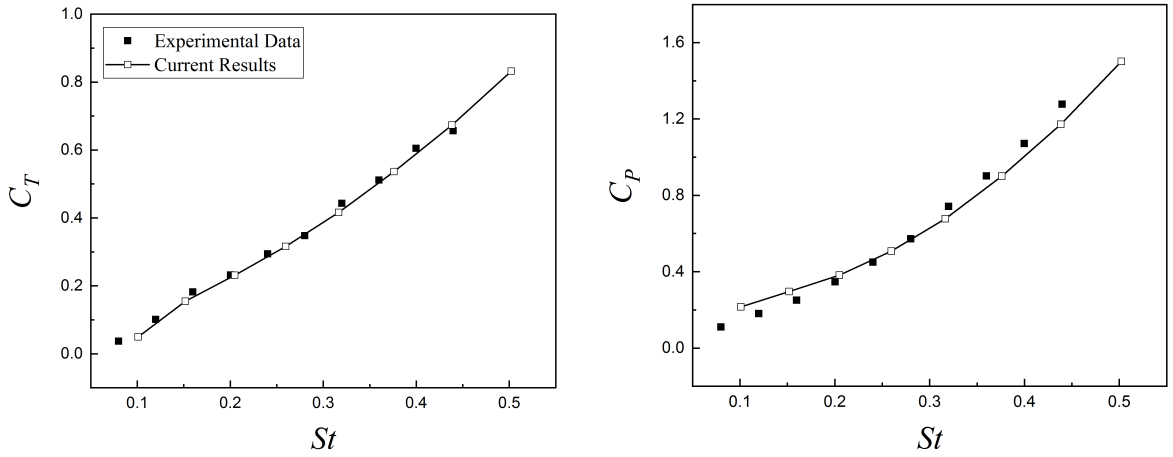

(a) Maximum AoA = 15 degrees (Left: Thrust coefficient, Right: Power coefficient)

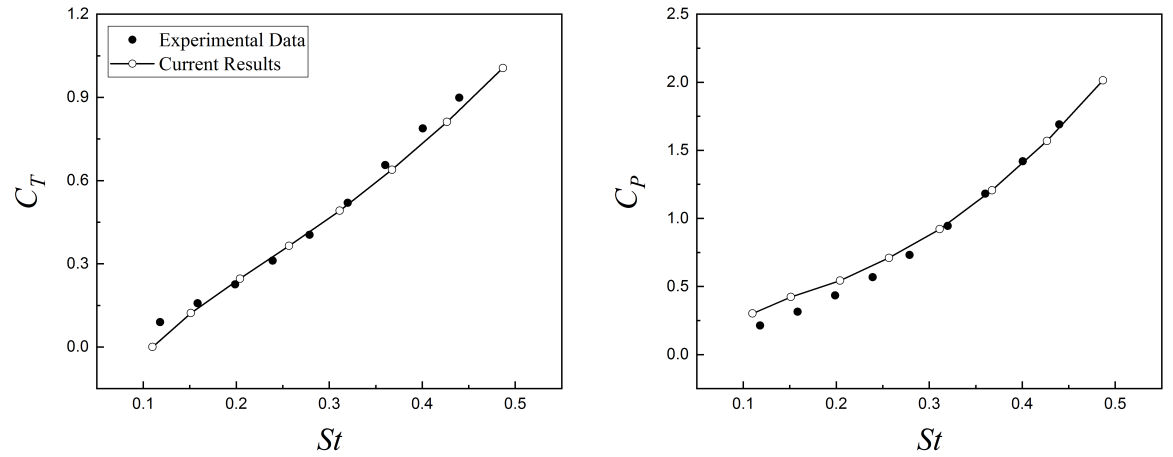

(b) Maximum AoA = 20 degrees (Left: Thrust coefficient, Right: Power coefficient)

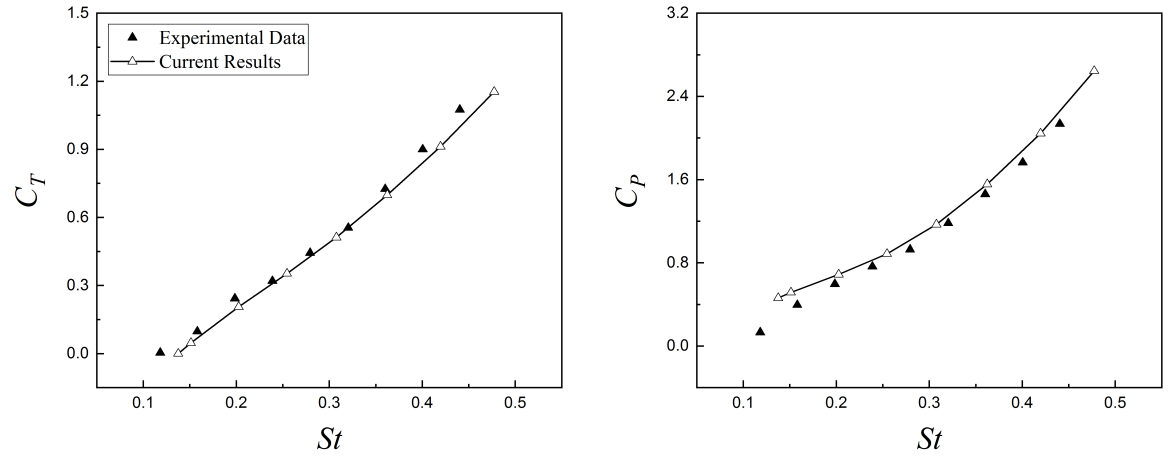

(c) Maximum AoA = 25 degrees (Left: Thrust coefficient, Right: Power coefficient)

Figure 2-17 Comparison of time-averaged propulsive coefficients for fully prescribed single foil between current predictions and experimental measurements by Read et al. (2003).

Therefore, the systematic experimental measurements by Read et al. (2003) are selected as the second baseline to conduct the comparisons of propulsive characteristics with the current predictions. A single fully prescribed oscillating foil with a heaving amplitude of 0.75c and pitch-leading phase of 90 degrees was considered in their experiments, in which the pitching amplitude and oscillating frequency are determined by the variation of maximum AoA. Figure 2-17 presents the comparisons of time-averaged thrust and power coefficients between the current computations and experimental data with three constant maximum AoAs. The satisfactory agreement between two results over the whole parametric range was observed in Figure 2-17, which implies a high accuracy and reliability of the current numerical model in the predictions of hydrodynamic characteristics of oscillating foils. In particular, a good quantitative agreement of current results with the experimental measurements with respect to the thrust coefficient is achieved by the established model.

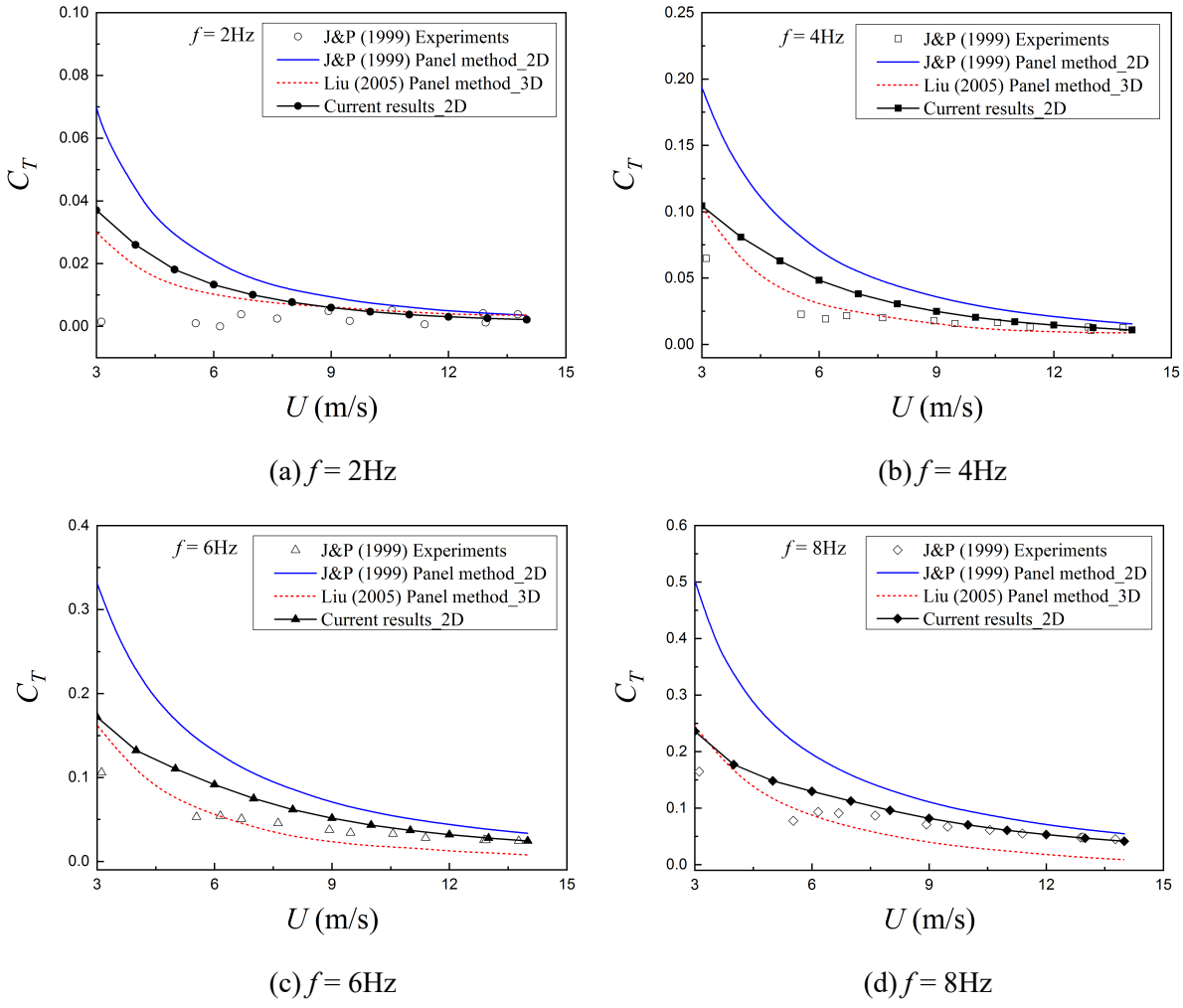

Figure 2-18 Comparison of time-averaged thrust coefficient for heave-only biplane configuration between current predictions and other results (Jones and Platzer, 1999; Liu, 2005b).

With respect to the biplane configuration, Jones and Platzer (1999) conducted a series of experimental measurements using both heave-only motion mode and dual motion mode (combined heave and pitch). This experimental study is selected as the third benchmark data to validate the current model. In their

experiment, the wing section is selected as the NACA0014 with a chord length of 64mm. Detailed geometry and motion parameters of this dual-foil configuration can be found in Jones and Platzer (1999).

For the heave-only motion mode, the mean distance between two foils and the heaving amplitude are set as 1.4c and 0.4c, respectively. In order to compare with inviscid results, the experimental data did not include steady-state drag, which is also removed from the current calculations. Figure 2-18 shows the comparisons of thrust coefficient with four oscillating frequencies, which also include the predictions by two-dimensional (Jones and Platzer, 1999) and three-dimensional (Liu, 2005b) panel method. For all four oscillating frequencies, the current thrust predictions have an acceptable agreement with the experimental measurements. Especially for the lightly loaded conditions corresponding to the high-speed regions, the current calculations have a better consistency with the experimental data over the results of panel method.

Indeed, the obvious discrepancy between calculations and measurements can be observed under heavily loaded conditions corresponding to the low-speed regions, in which three-dimensional panel method provides a better prediction compared with the current model. It can be observed that both current model and panel method tend to over-predict the thrust at the low advance speeds. Due to the relatively high aspect ratio of 20 in the experiment, the three-dimensional effect is unlikely to produce such a large discrepancy. However, for the low-speed regions the tip vortex shedding of finite-span foil may be more noteworthy, which is considered as the main reason that three-dimensional panel method shows a better agreement with measurements over the current calculations.

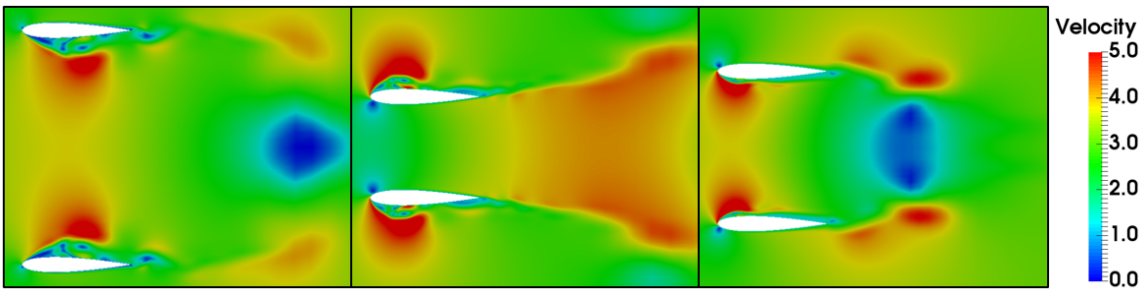

(a) $t = 0.2T$ (b) $t = 0.6T$ (c) $t = T$

Figure 2-19 Velocity contours of dual-foil heave-only configuration over one oscillatory cycle.

For the discrepancy between both calculations and the experimental data, the most likely cause is the severe flow separation and resulting stall. According to Liu et al. (2010), the critical AoA for a two-dimensional steady wing at the Reynolds number of 1000000 is about 12 degrees. However, the flow separation of unsteady oscillating foil will be delayed to about 20 to 25 degrees depending on the kinematics of oscillating foils (Akbari and Price, 2003). In this experiment, the maximum effective AoA for each oscillating frequency is 6.1, 12.1, 17.8, 23.2 degrees, respectively. A severe flow separation will occur under the maximum effective AoA of 23.2 degrees, which appears at the advance speed of 3m/s with the oscillating frequency of 8Hz. Figure 2-19 presents the velocity contours for this situation at three different instants over one oscillatory cycle, in which severe flow separation can be found in

both up-stroke and down-stroke of foil motion. Therefore, the discrepancy at the frequency of 8Hz between numerical calculations and experimental measurements is most substantial.

In addition, the effect of flexibility cannot be ignored in the experiment due to the high aspect ratio, which will increase the heaving amplitude of wing tip. However, the rigid body is employed in both current simulations and calculations by panel method, which is also partly responsible for the difference between calculations and measurements. Moreover, studies have shown that numerical simulations based on URANS model tend to underestimate the viscous drag and stall conditions, which also can be regarded as a potential cause that results in the underestimation of thrust by the current model over experimental data.

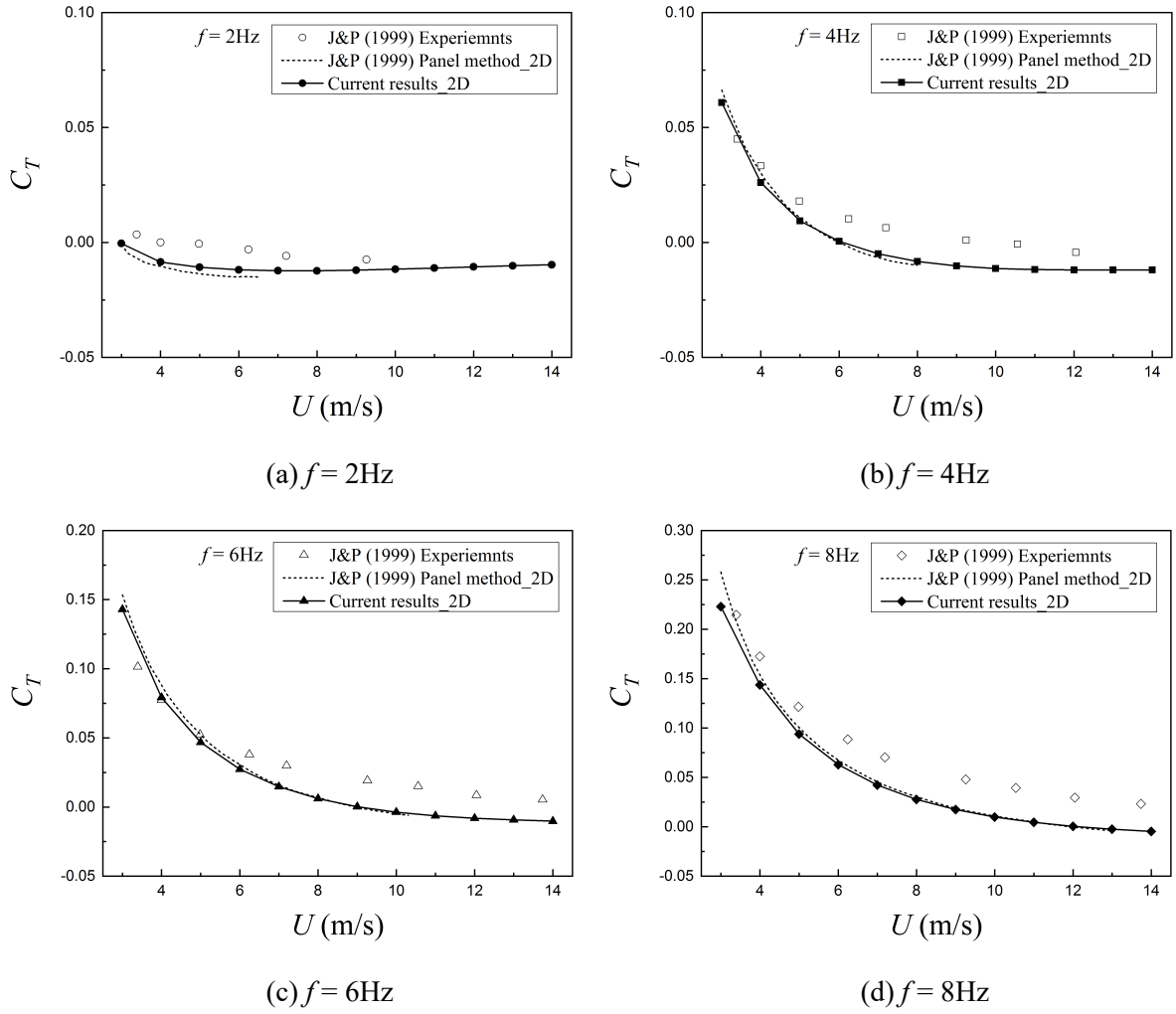

Figure 2-20 Comparison of time-averaged thrust coefficient for fully prescribed biplane configuration between current predictions and previous results by Jones and Platzer (1999).

For the dual motion mode characterizing as the combined heaving and pitching motion, the amplitude of pitch and heave are set as 5 degrees and 0.335*c*, respectively. The pivot axis is set at mid-chord position with a pitch-leading phase angle of 90 degrees. The comparison of time-averaged thrust coefficient between the current calculations and experimental data is presented in Figure 2-20, which also presents the computations by Jones and Platzer (1999) using two-dimensional panel method.

The results showed that both the current model and panel method tend to underestimate the thrust at relatively high advance speeds. For the heavily loaded conditions with lower speeds, a satisfactory agreement between the numerical results and experimental measurements can be observed. Especially, the current thrust predictions have a remarkably great agreement with the calculations using two-dimensional panel method (Jones and Platzer, 1999), which indicates that the three-dimensional effect and resulting tip-vortex behavior are partly responsible for the thrust underestimation of numerical calculations. Another likely reason for the discrepancy is the flexibility of wings since a relatively high aspect ratio of 20 is used in the experiments as noted before.

CHAPTER 3

Hydro-elasticity Characteristics of APWIGs

3.1 Effect of Torsional Spring Stiffness

The influence of spring stiffness on the propulsive performance of APWIGs was firstly investigated in this section. For the kinematics of oscillating foils, the heaving amplitude and oscillating frequency are fixed as 0.5*c* and 4Hz, respectively. The mean distance between two foils is selected as 1.8*c*. Herein, the spring stiffness in Nm/rad is directly used to represent the torsional flexibility for convenience.

3.1.1 Time-varying properties of kinematics and hydrodynamics

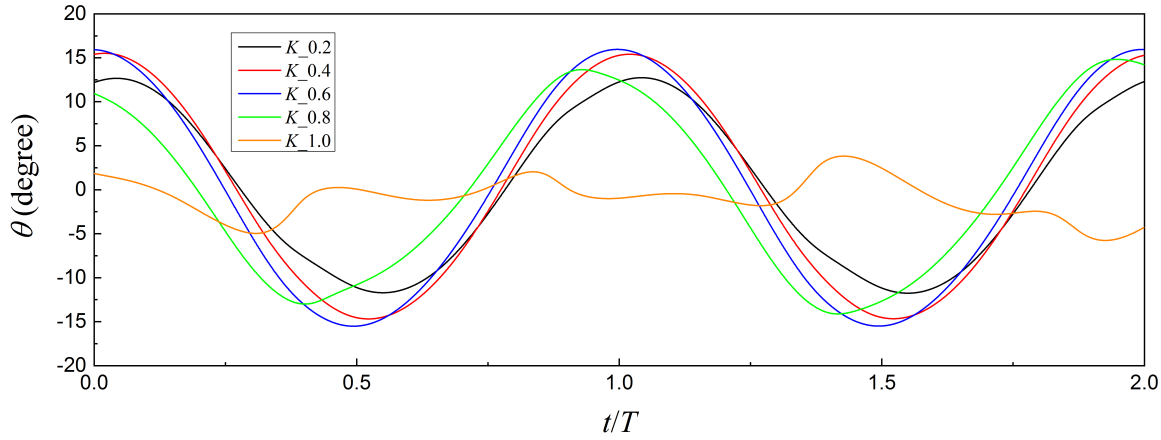

Figure 3-1 Time variation of pitching angle for APWIGs over two oscillatory cycles with different spring stiffness.

The time history of flow-induced pitching angle with different spring stiffness at advance speed of 2m/s is presented in Figure 3-1. As shown in this figure, the variation of flow-induced pitching angle is mainly affected by spring stiffness in the form of peak value and phase difference (pitch leads heave). At an extremely high stiffness, e.g., $K = 1.0$, the responsive pitching angle presents an aperiodic variation with a small maximum pitching angle. It was observed that the maximum pitching angle shows a first increasing and then decreasing trend with the decrease of spring stiffness.

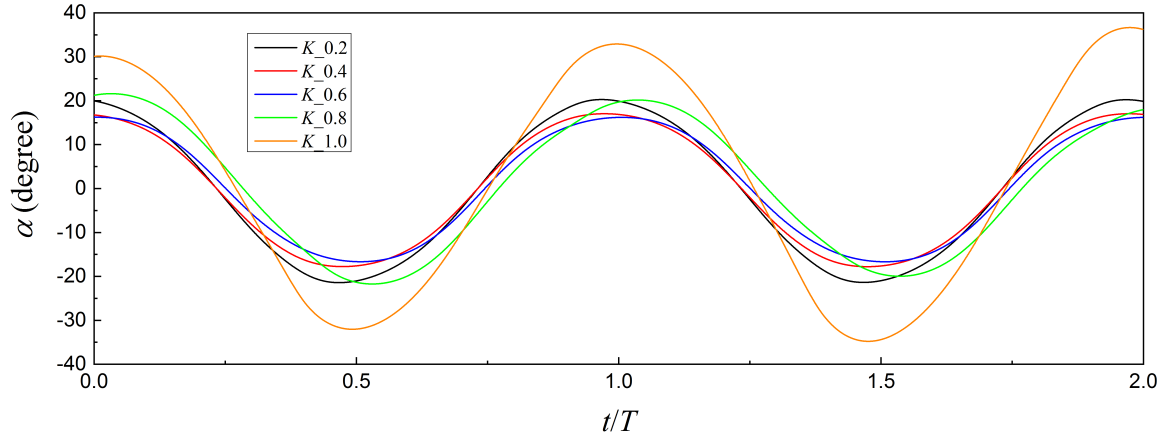

Figure 3-2 Time variation of effective AoA for APWIGs over two oscillatory cycles with different spring stiffness.

In general, the torsional spring with a high stiffness tends to restore the foils back to the horizontal plane more quickly, leading to a larger phase difference between imposed heave and passive pitch. The imposed heaving displacement will reach the maximum value at $t/T = 0.25$. Therefore, it can be seen that the phase difference drops consistently with the decrease of spring stiffness. Figure 3-1 also shows a sinusoidal-type variation profile for the pitching angle with an appropriate stiffness, e.g., $K = 0.6$.

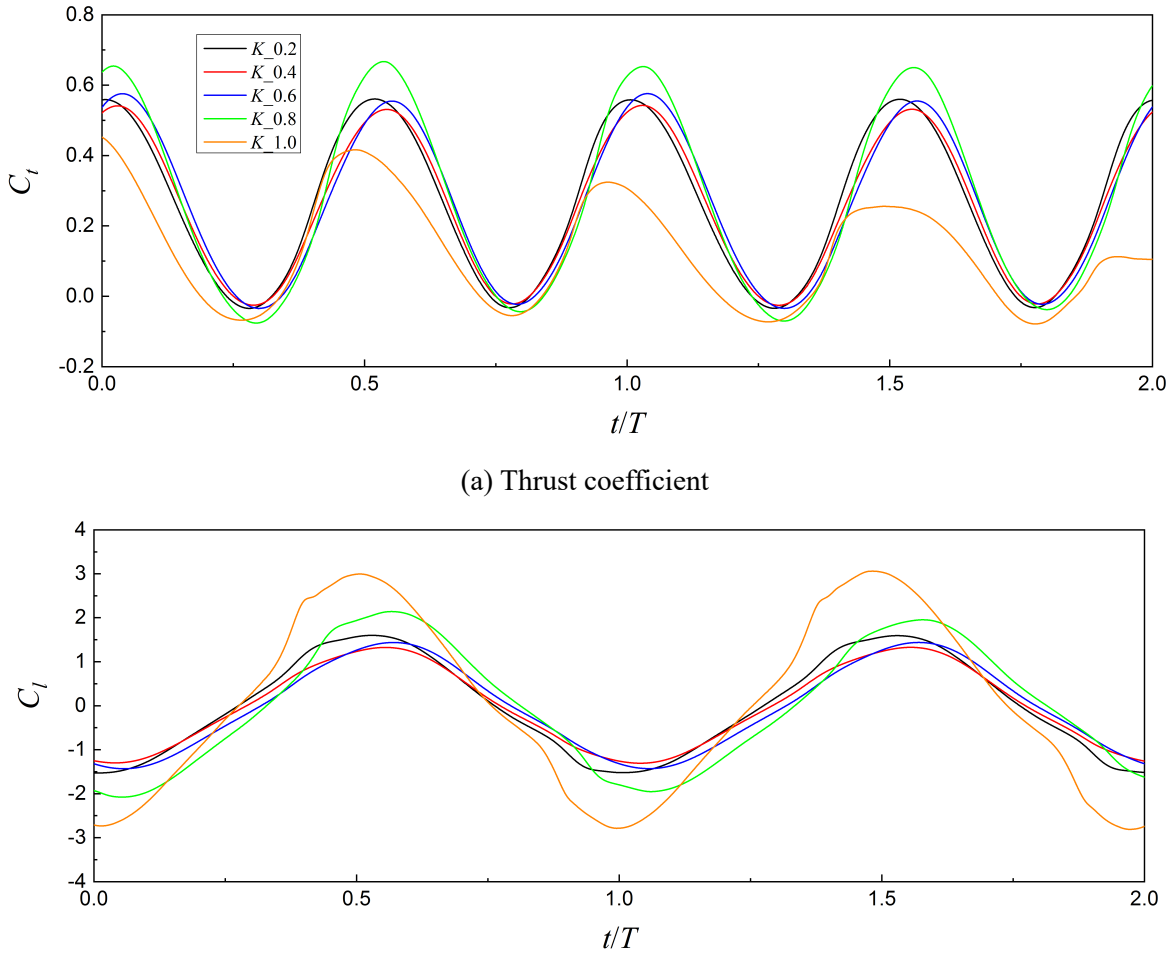

(a) Thrust coefficient

(b) Lift coefficient

Figure 3-3 Time variation of force coefficients for APWIGs over two oscillatory cycles with different spring stiffness.

The effective AoA is determined by the combination of effective advance speed and pitching angle, which has a critical influence on the thrust production. Figure 3-2 presents the time history of effective AoA with different spring stiffness at advance speed of 2m/s. A similar variation trend for the effective AoA can be observed in Figure 3-2 except for the stiffness of $K = 1.0$. As the results show, the largest peak value of pitching angle with a middle stiffness of 0.6 results in the smallest peak value of effective AoA. Therefore, an optimum spring stiffness for the APWGs can be found in principle, which will produce an appropriate effective AoA and satisfactory propulsive performance with less flow separation. The maximum effective AoA over 30 degrees was obtained by stiffness of 1.0, which will lead to the severe flow separation. Normally, the maximum effective AoA with different stiffness occurs around

t/T = 0, 0.5, 1.0, at which pivot axis of oscillating foils reaches the equilibrium position.

The time variation of thrust coefficient and lift coefficient with different spring stiffness at advance speed of 2m/s is presented in Figure 3-3. The oscillating foils with the extremely high spring stiffness (e.g., K = 1.0) produce the smallest thrust but largest lift, as shown in Figure 3-3. The foils with the stiffness of 0.2 and 0.8 almost produce the same maximum effective AoA but different phase angle. Only the largest thrust was observed for the spring stiffness of 0.8, which indicates the important role of phase difference between imposed heave and passive pitch on the propulsive performance. The lowest lift was found for the oscillating foils with the stiffness of 0.4, inducing a relatively small effective AoA and phase difference.

3.1.2 Time-averaged propulsive characteristics

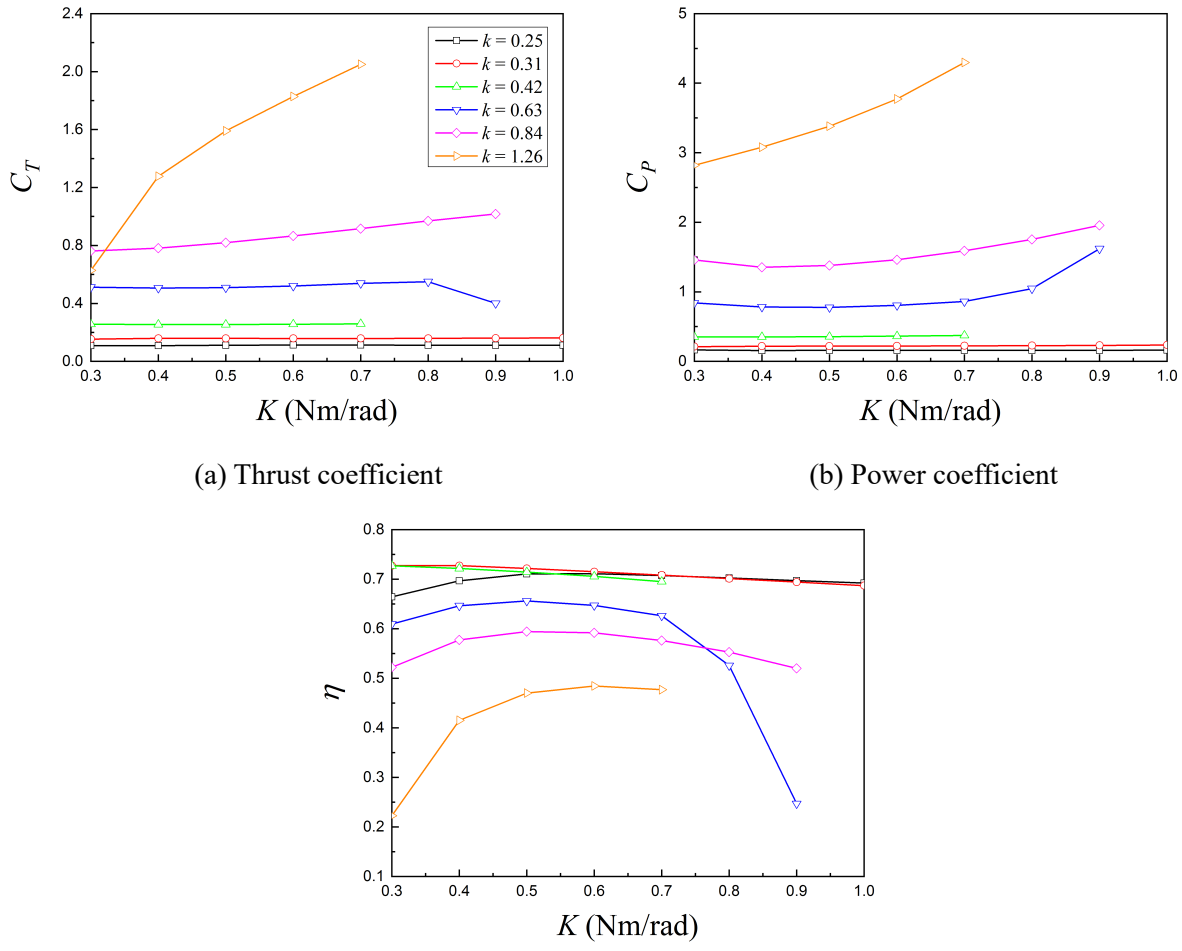

(a) Thrust coefficient

(b) Power coefficient

(c) Propulsive efficiency

Figure 3-4 Propulsive characteristics of APWIGs as a function of torsional spring stiffness with different reduced frequencies.

The comprehensive results for the effect of spring stiffness on the propulsive properties and locomotion characteristics of APWIGs at different advance speeds are presented in Figures 3-4 and 3-5, respectively. The considered scope of inflow conditions is summarized in Table 3-1.

Table 3-1 Parametric scope for investigation into torsional spring stiffness.

U (m/s)	1	1.5	2	3	4	5
Re	100000	150000	200000	300000	400000	500000
k	1.26	0.84	0.63	0.42	0.31	0.25

It was found that both the thrust coefficient and power coefficient show a general increasing trend with the larger spring stiffness, as shown in Figure 3-4 (a) and (b). The propulsive efficiency is presented in Figure 3-4 (c), in which maximum efficiency of 72.7% at the advance speed of 4m/s with the stiffness of 0.3 was obtained. For the large advance speeds, the propulsive efficiency of APWIGs tends to maintain a relatively high value around 70% with a wide range of spring stiffness. It also can be seen that the propulsive efficiency is less sensitive to the high advance speed.

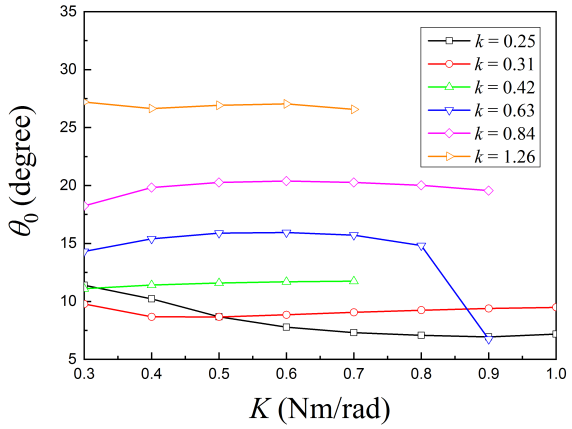

(a) Maximum pitching angle

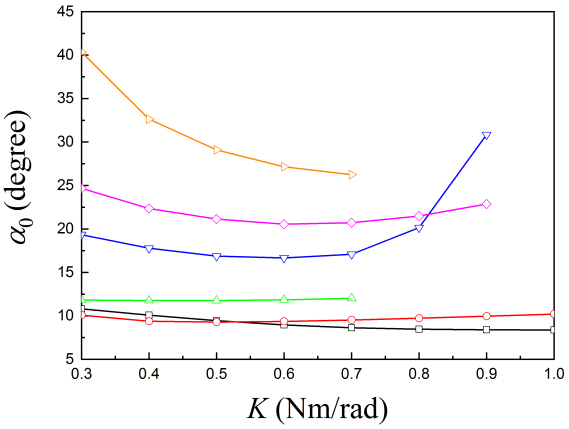

(b) Maximum effective AoA

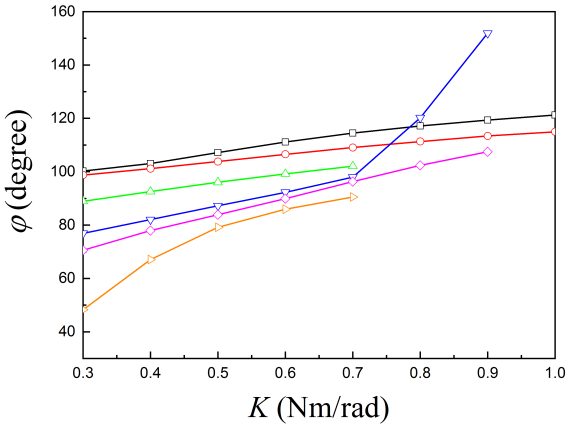

(c) Phase angle between pitch and heave

Figure 3-5 Locomotion characteristics of APWIGs as a function of torsional spring stiffness with different reduced frequencies.

However, the efficiency of APWIGs show a significant sensitivity to both spring stiffness and advance speed under large reduced frequencies corresponding to low advance speeds. A similar behavior was also obtained by Thaweewat et al. (2018) using a single auto-pitch oscillating foil propulsor. This is

mainly because the relatively large pitching angle and effective AoA were created at a small advance speed, as shown in Figure 3-5 (a) and (b). As a result, the optimum stiffness for the highest propulsive efficiency can be found evidently at low advance speeds in Figure 3-4 (c). The maximum efficiency at reduced frequency of 0.63, 0.84, 1.26 is 65.6%, 59.4%, 48.4%, respectively. It also should be noted that the optimum stiffness tends to decrease slightly with the increase of advance speed.

The maximum effective AoA of 40.3 degrees can be observed in the results with the advance speed of 1m/s and the stiffness of 0.3. The flow separation and stall are inevitable on this situation due to the dramatically larger effective AoA than dynamic-stall angle. Therefore, the lowest propulsive efficiency of 22.2% was recorded in this case. Both maximum pitching angle and effective AoA below 12 degrees at large speed regions (e.g., U = 3, 4, 5m/s) can be observed, which produce the satisfactory efficiency of around 70%. Taking for example at speed of 2m/s, the best propulsive performance occurs with the stiffness of 0.5, which leads to the pitching angle of 15.9 degrees, effective AoA of 16.9 degrees and phase difference of 87.2 degrees, respectively.

Overall, for the current parametric space the APWIGs with the torsional spring stiffness between 0.5 to 0.7 tends to produce a relatively high propulsive efficiency, in which the range of effective AoA is located between 9 to 17 degrees. As shown in Figure 3-5 (c), the pitch-leading phase difference increases when the spring stiffness and advance speed become larger. Both experimental and numerical studies have reported that a single oscillating foil under a fully prescribed motion tends to produce the highest efficiency with the phase difference around 90 degrees (Tuncer and Platzer, 2000; Read et al., 2003). For APWIGs in the current study, optimal efficiency performance can be obtained when the flow-induced pitch leads the imposed heave by the phase angle of 85 to 110 degrees depending on the advance speed.

3.2 Dynamics and Performance with Frequency Ratio

As an indication of non-dimensional spring stiffness, the ratio of natural frequency over oscillating frequency is employed to distinguish the locomotion states and depict the performance metrics. In this section, the influence of frequency ratio on the dynamic responses and resulting hydrodynamic behaviors of APWIGs were comprehensively demonstrated.

3.2.1 Setup of numerical domain

The size of computational domain is shown in Figure 3-6, which a horizontal length of 30c and a vertical height of 20c. The minimum distance between oscillating foil and boundaries of computational domain is larger than 8c. The foil section is selected as the NACA0012 with a chord length of 0.2m for the current simulations. The mean distance between two foils of biplane configuration is 1.2c with a counter-phase heaving amplitude of 0.3c for each foil. The spring-based pitching axis is located at 0.25

chord position from the leading edge. The frequency of prescribed heaving motion is fixed as 4Hz.

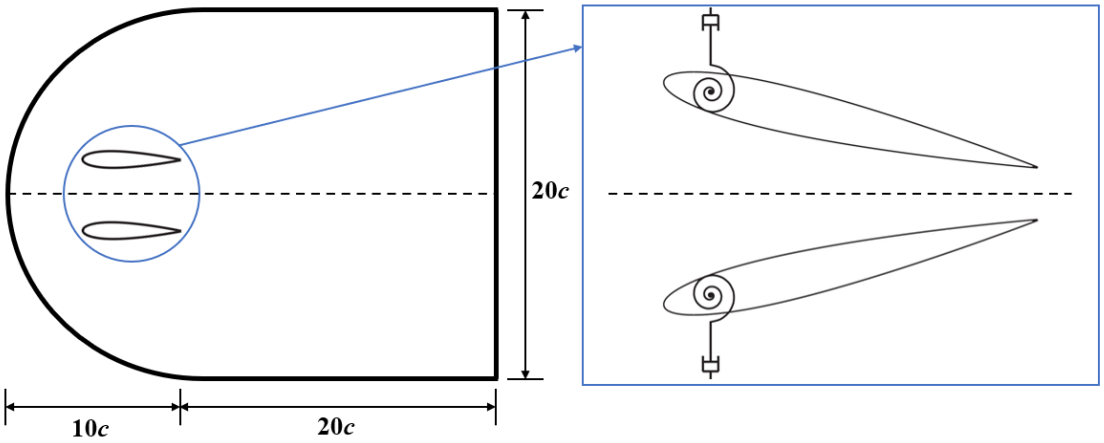

Figure 3-6 Schematic of computational domain for investigation into the frequency ratio.

To show the capability of different approaches for the boundary layer modelling, a comparison of time-averaged thrust coefficient between current predictions and experimental measurements by Read et al. (2003) was performed. As can be seen from the results in Figure 3-7, a general satisfactory agreement was obtained for over the whole range of Strouhal number. The simulation of boundary layer was performed by two numerical approaches, including the laminar model and SST k-ω turbulence model. As Figure 3-7 shows, the results of these two models show a negligible difference indicating that the laminar model can provide a satisfactory hydrodynamic prediction under certain flow conditions. Since the current parametric scope leads to low-to-moderate Reynolds numbers, the simulations in this section were conducted using the laminar model.

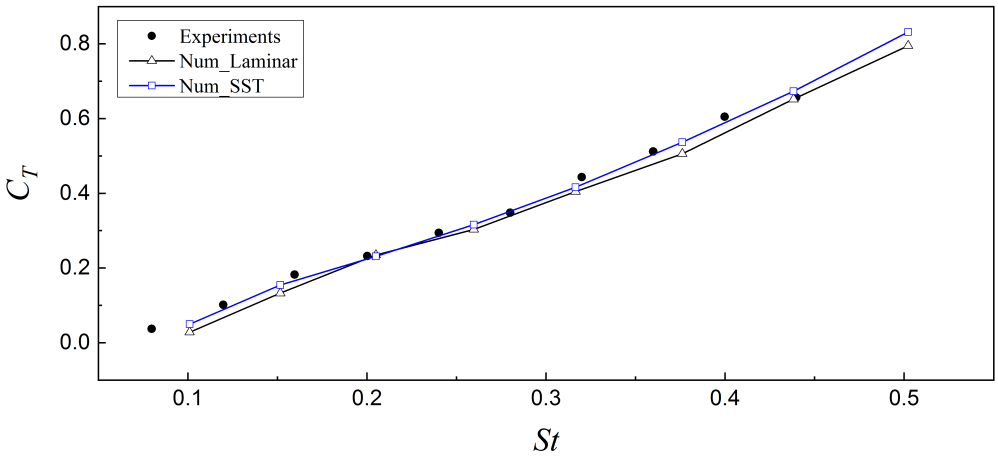

Figure 3-7 Comparison of time-averaged thrust coefficient between current results and experimental measurements by Read et al. (2003).

3.2.2 Dynamical behaviors

The torsional spring stiffness indicating the lumped torsional flexibility is the most important parameter to determine the locomotion and hydrodynamic behaviors of auto-pitch configuration. According to

Zhang et al. (2010), two dynamic responses of auto-pitch configuration depending on frequency ratio λ_F can be identified when the plate reaches a periodic-flow state. A forward movement can be observed with $\lambda_F > 1$, while the plate performs a backward movement when $\lambda_F \leq 1$.

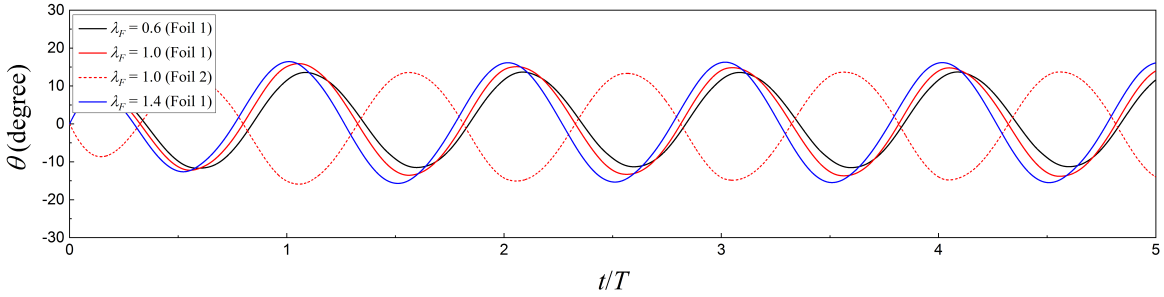

Figure 3-8 Time variation of pitching angle for APWIGs over five oscillatory cycles with different frequency ratios.

Hence, a range of 0.6 to 1.6 for λ_F was considered in the current simulations. Since the dynamic responses of APWIGs are highly sensitive to frequency ratio at the high advance speeds, a relatively narrow range of advance coefficient from 3 to 6 was selected in this section to avoid the non-periodic-flow state. Figures 3-8 and 3-9 presents the time history of dynamic responses and hydrodynamic features for APWIGs at the advance coefficient of 4.

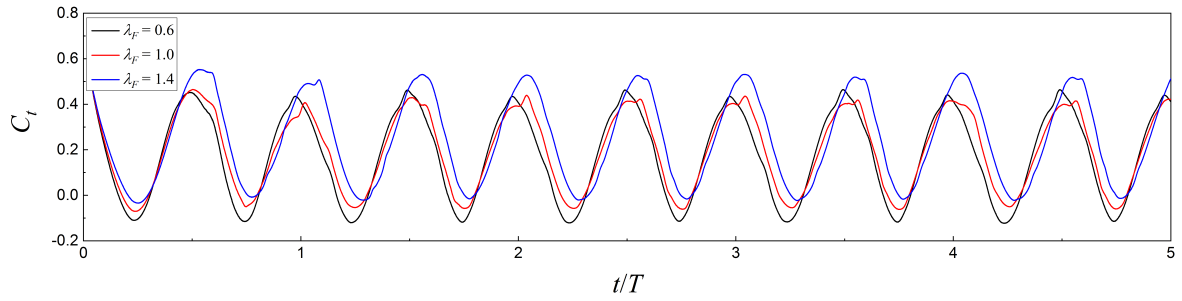

(a) Thrust coefficient

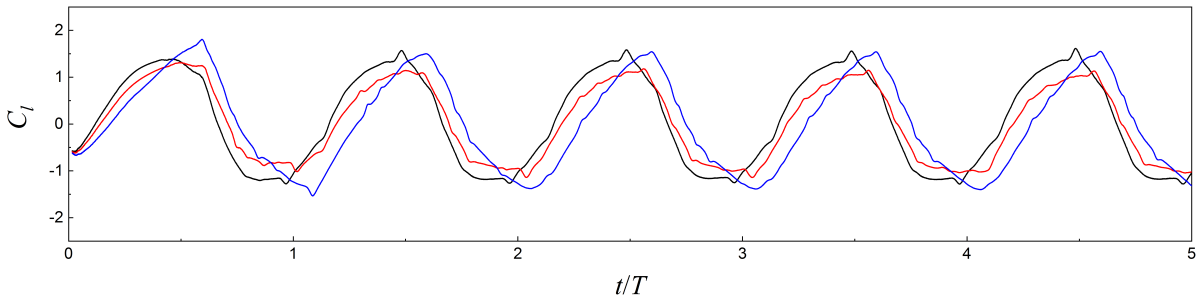

(b) Lift coefficient

Figure 3-9 Time variation of force coefficients for APWIGs over five oscillatory cycles with different frequency ratios.

The results show that APWIGs tends to reach a periodic-flow state after the third oscillatory cycle. As can be seen from Figure 3-8, the flow-induced pitching angle of APWIGs presents a sinusoidal-like

profile when each foil reaches the stable periodic state, which has an identical frequency with the prescribed heaving motion. One foil can be considered as the mirror image of another foil as their dynamic responses are symmetrical with respect to the imaginary ground plane. It was found that the frequency ratio has a significant effect on both the maximum pitching angle and pitch-leading phase difference. As a result, the hydrodynamic characteristics of APWIGs is highly dependent on the frequency ratio, as shown in Figure 3-9.

3.2.3 Propulsive performance

Contours of dynamic responses and propulsive performance for APWIGs as a function of advance coefficient and frequency ratio are presented in Figures 3-10 and 3-11, respectively. As can be seen in Figure 3-10 (a), a general trend of first increase and then decrease for maximum flow-induced pitching angle was obtained when the frequency ratio consistently increases. With the increase of advance speed, the amplitude of passively pitching motion of APWIGs tends to decrease consistently. A similar trend related to the maximum effective AoA with the change of forward speed and frequency ratio can be observed in Figure 3-10 (a). The numerical results of Figure 3-10 (b) present a trend of consistent increase for pitch-leading phase difference with the increase of frequency ratio since a stiffer torsional spring tends to restore each foil back to the equilibrium position more quickly. The advance coefficient shows a relatively slight effect on the phase angle especially for the high advance speed.

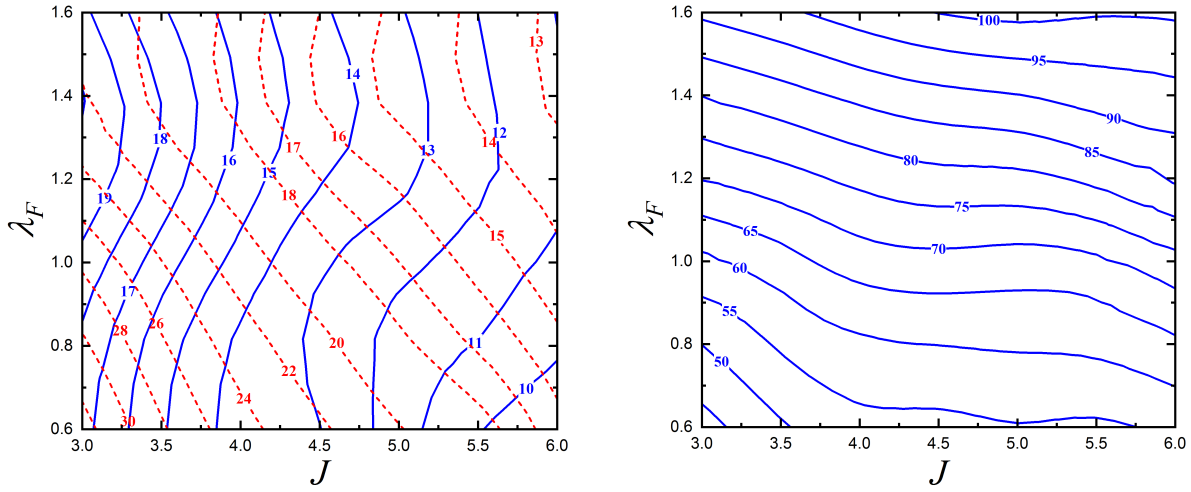

(a) Maximum pitching angle and effective AoA (b) Pitch-leading phase angle

Figure 3-10 Contours of dynamic responses for APWIGs as a function of advance coefficient and frequency ratio.

With respect to the propulsive characteristics, it was found that APWIGs can produce a forward thrust within the whole considered parametric space, even for the frequency ratio less than one, as shown in Figure 3-11 (a). Several reasons can be identified for such a behavior, including a relatively small heaving amplitude of 0.3*c*, elastic pitching axis of 0.25*c* from leading edge and produced WIG effect by counter-phase biplane configuration. All these factors can stabilize the locomotion state of APWIGs to lie in a thrust-producing regime over the whole range of frequency ratio.

Figure 3-11 (b) presents an increasing trend of propulsive efficiency with the increase of forward speed for APWIGs. More importantly, the frequency ratio shows a significant influence on the propulsive performance of APWIGs. A propulsive efficiency of over 60% can be achieved by APWIGs under a certain flow condition. A relatively low efficiency was obtained with the small frequency ratio and advance coefficient, which corresponds to the maximum effective AoA of around 30 degrees in Figure 3-10 (a). Since the effective AoA of around 30 degrees is larger than the dynamic-stall angle of oscillating foil, severe flow separation is the main reason for the inferior propulsive performance of APWIGs, as shown at the left bottom of Figure 3-11 (b). Current computations indicate that the frequency ratio of APWIGs within the range of 1.1-1.4 tends to produce a satisfactory propulsive performance, which results in the dynamic responses including the maximum effective AoA below 20 degrees and pitch-leading phase difference of around 80 degrees. The optimum range of frequency ratio for APWIGs also agrees with the regime of forward movement predicted by Zhang et al. (2010).

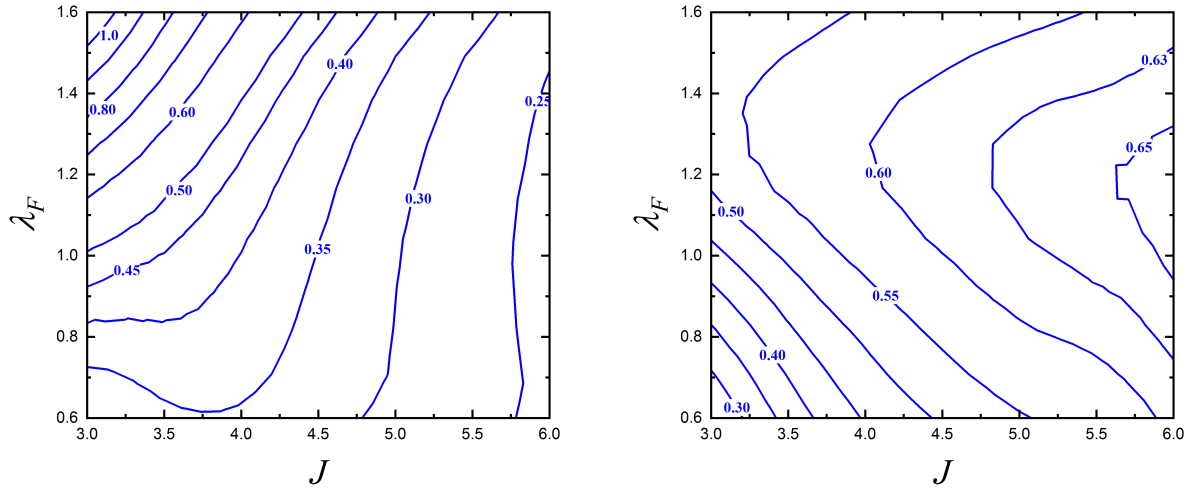

(a) Time-averaged thrust coefficient (b) Propulsive efficiency

Figure 3-11 Contours of propulsive performance for APWIGs as a function of advance coefficient and frequency ratio.

3.3 Vortex Structures and Wake Patterns for APWIGs

The hydrodynamic performance of oscillating foils is highly relevant to corresponding flow behaviors. Thus, a clear identification of vortex structures and wake pattens is essential. The instantaneous vortex contours of three representative cases with a constant spring stiffness of 0.6 over one oscillatory cycle are presented in Figures 3-12, 3-14 and 3-16, respectively. The advance speed of each case is 1m/s, 2m/s and 4m/s with the effective AoA of 27.2, 16.7 and 9.4 degrees, producing a propulsive efficiency of 48.5%, 64.7% and 71.5%, respectively. The corresponding total thrust coefficient of each case is shown in Figures 3-13, 3-15 and 3-17, respectively.

As the results show, obvious flow separation and leading-edge vortex shedding can be observed for the

case of 1m/s. Considering the upper foil, the leading-edge vortex starts to appear on the inside surface of foil when it lies in the upstroke. It causes the decrease of thrust coefficient before the pivot axis reaches the maximum displacement at $t = 0.25T$. After that, the foil begins the downstroke until the distance between two pivot points reaches the minimum value, producing an outside-surface leading edge vortex. During this process, the thrust coefficient starts to drop after an increase to its maximum value at $t = 0.55T$. Then, the foil starts another upstroke back to the initial position along with the increase of thrust coefficient.

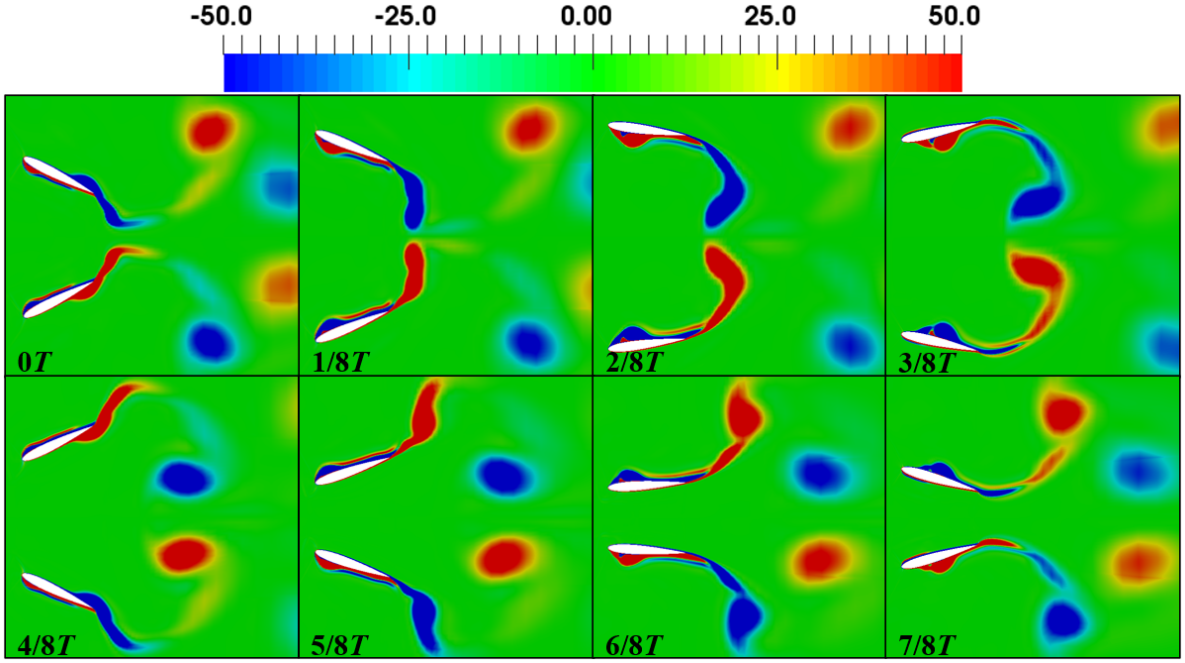

Figure 3-12 Vorticity contours of APWIGs at eight instants over one oscillatory cycle for the reduced frequency of $k = 1.26$.

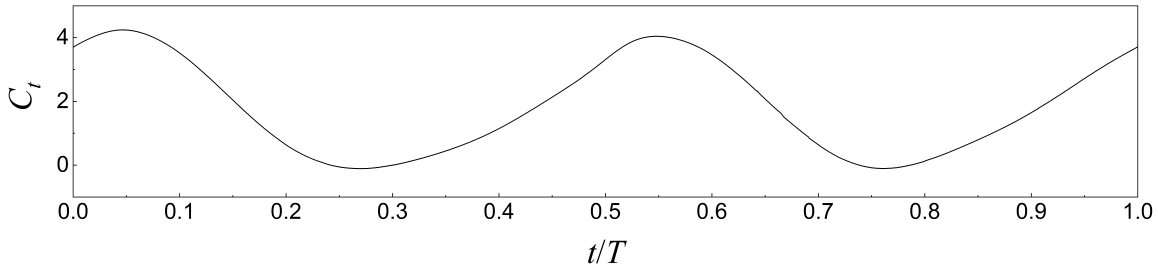

Figure 3-13 Time history of thrust coefficient for APWIGs over one oscillatory cycle for the reduced frequency of $k = 1.26$.

Basically, the peak of thrust coefficient appears at the instant after the oscillating foil goes through each quarter cycle. As the results suggest, the leading-edge vortex interacts with the trailing edge of foil before it sheds into the wake. Such a complicated interaction has a significant influence on the pressure distribution of body surface, and hence the hydrodynamic forces acting on the foils. After the vortices shed from the trailing edge, the separate vortex pair can be observed on the wake. The relatively low flow speed and vortices interaction are main causes for this wake characteristic.

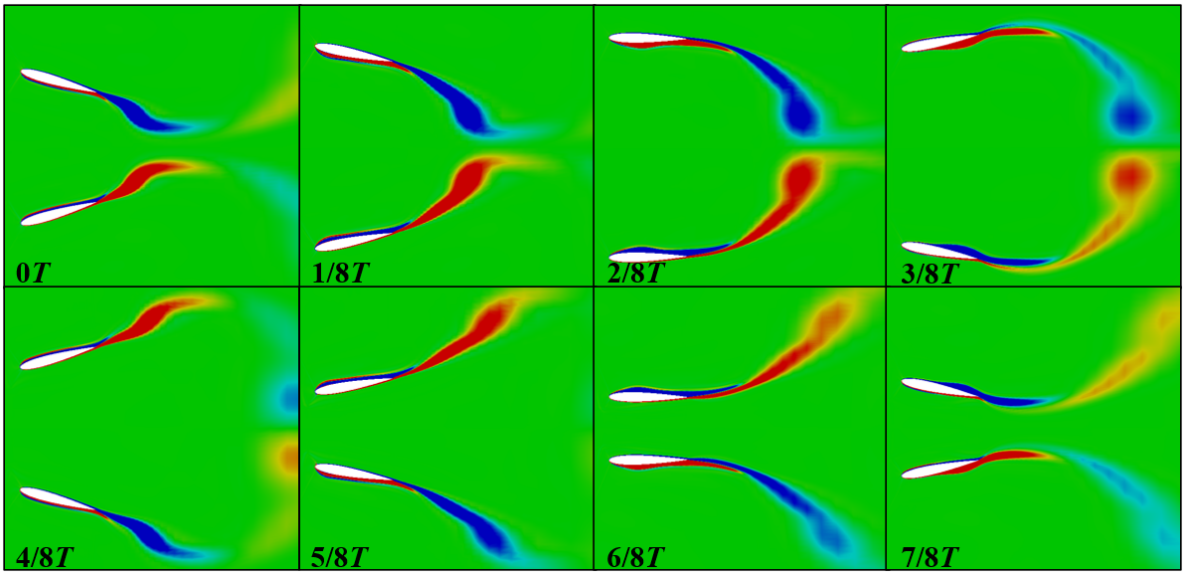

Figure 3-14 Vorticity contours of APWIGs at eight instants over one oscillatory cycle for the reduced frequency of $k = 0.63$.

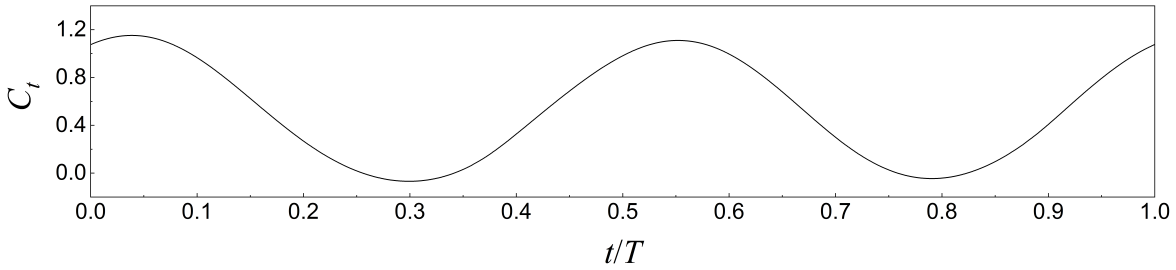

Figure 3-15 Time history of thrust coefficient for APWIGs over one oscillatory cycle for the reduced frequency of $k = 0.63$.

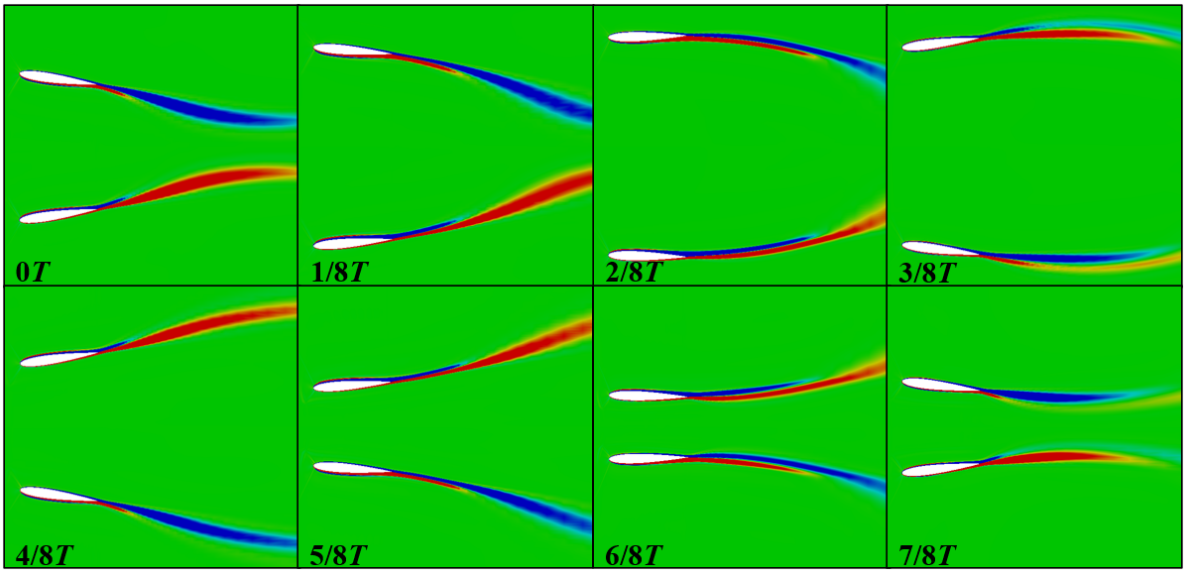

Figure 3-16 Vorticity contours of APWIGs at eight instants over one oscillatory cycle for the reduced frequency of $k = 0.31$.

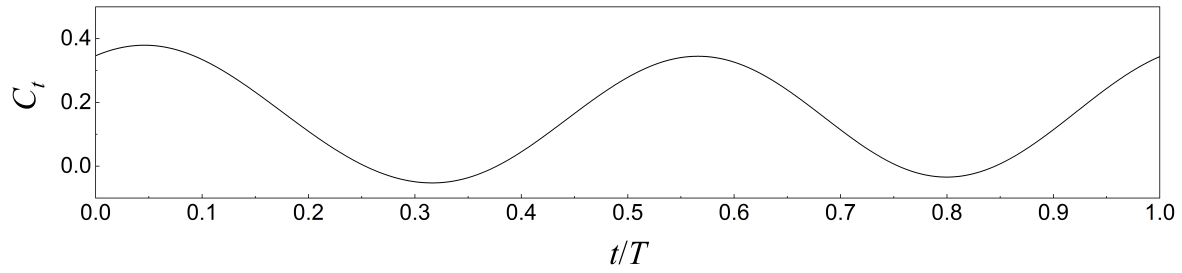

Figure 3-17 Time history of thrust coefficient for APWIGs over one oscillatory cycle for the reduced frequency of $k = 0.31$.

For the cases of 2m/s and 4m/s, the wake vortices tend to be stretched dramatically due to the relatively intense downstream flow. More importantly, the leading-edge vortex shedding is much less due to the small effective AoA and resulting highly attached flow on the foil surface. Based on the ground plane and resulting WIG effect, the wake structures of upper foil can also be considered as the mirror image of that of lower foil. There is another vortices interaction between the wake structure of two foils along the produced ground plane for APWIGs. Particularly, two wake structures behind the trailing edge have the minimum distance when the foils reach the maximum stroke, while the wake vortices of each foil tend to move apart from each other as two foils arrive at the closest position.

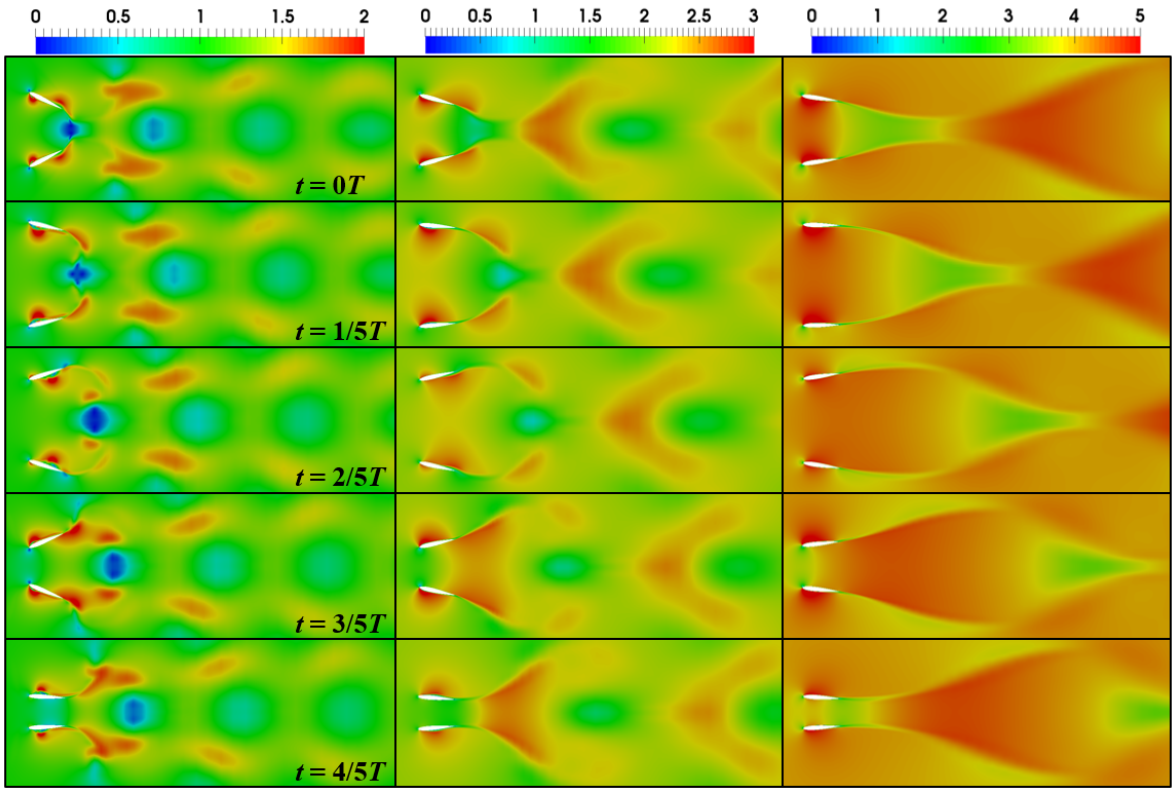

(a) $U = 1$m/s ($k = 1.26$) (b) $U = 2$m/s ($k = 0.63$) (c) $U = 4$m/s ($k = 0.31$)

Figure 3-18 Velocity contours of APWIGs over one oscillatory cycle at different advance speeds.

The corresponding velocity contours over one oscillatory cycle for these three cases are presented in Figure 3-18. Apparent velocity surplus can be observed in the wake profiles for all three reduced

frequencies, which indicates the thrust-producing characteristics of APWIGs. More specifically, the surplus region of velocity tends to appear separately along wake of each foil at the low speed. But for the relatively high advance speed, the momentum surplus of wake tends to concentrate on the single zone along the equilibrium plane between two foils. The thrust-producing vortex street along the wake of each foil has a significant effect on the velocity behaviors. Considering each foil at the advance speed of 1m/s, since the upper row of vortices has a counter-clockwise direction and the lower row of vortices rotates clockwise (Figure 3-12), a narrow jet-like region for the velocity field can be produced along the centerline of both upper and lower foil.

3.4 Concluding Remarks

The hydro-elasticity characteristics of APWIGs was numerically investigated in this section. Firstly, the effect of torsional spring stiffness on the propulsive performance of APWIGs was directly simulated. It was found that both the pitching angle and phase difference between imposed heave and flow-induced pitch are determined by the attached torsional spring. The time variation of pitching motion was found to resemble a sinusoidal profile with an appropriate stiffness. After a continuous increase with the less rigid torsional spring, the maximum pitching angle starts to drop slightly with the further decrease of stiffness due to influence of upstream flow. However, the phase difference that passive pitch leads prescribed heave shows an increasing trend when both advance speed and torsional spring stiffness become larger.

In general, the propulsive characteristics of APWIGs show a high sensitivity to relatively low advance speed that has a strong influence on the resulting effective AoA. Under certain loaded conditions, an optimum torsional spring stiffness can be found to produce the best propulsive performance. Constant high efficiency over 70% with a relatively wide range of operating speed was obtained in the current study. It was suggested that APWIGs tends to provide an outstanding propulsive performance with a torsional spring that can result in the effective AoA of 9 to 17 degrees and phase difference of 85 to 110 degrees under certain conditions.

To further identify the dynamic responses and hydrodynamic behaviors of APWIGs with the variation of torsional flexibility, the frequency ratio defined as the ratio of natural frequency over oscillating frequency is employed to characterize the spring stiffness. It was noted that the frequency ratio has a significant effect on both the dynamic responses and propulsive characteristics. Simulations suggested that the forward-motion regime and stable locomotion state with periodic dynamical behaviors can only be realized by a specific range of frequency ratio. APWIGs employing a frequency ratio in the range of 1.1 to 1.4 tends to produce a consistently high propulsive efficiency under different forward speeds. The contours of performance metrics show that an optimal regime can be found to maximize the thrust production and propulsive efficiency. Such a numerical database also provides a reference for the

parameter selection and property analysis of APWIGs.

Identification of vortex structures around the foil surface and flow patterns in the wake for APWIGs offers the insights into the relationship between the hydrodynamic performance and flow behaviors. The evolution of vortex shedding along both leading edge and trailing edge implies that the peak of thrust coefficient tends to appear at the instant after the oscillating foil goes through each quarter cycle. The interaction between the vortices shedding from the leading edge and vortex structures appear at the trailing edge results in the complicated characteristics of hydrodynamic forces. Owing to the self-controlled pitch, the flow separation and dynamic stall of APWIGs are substantially reduced.

CHAPTER 4

Two-dimensional Parametric Study for APWIGs

4.1 Setup of Parametric Scope

It is essential to address the effect of all relevant parameters for the performance optimization of oscillating foil propulsors. Thus, a two-dimensional parametric study on the propulsive characteristics APWIGs was performed in this section. The primary objective is to present a reliable database as the reference for the design, optimization and prototyping of APWIGs system. The size of computational domain with a horizontal length of 50*c* and a vertical height of 40*c* was implemented for the parametric study, as shown in Figure 4-1.

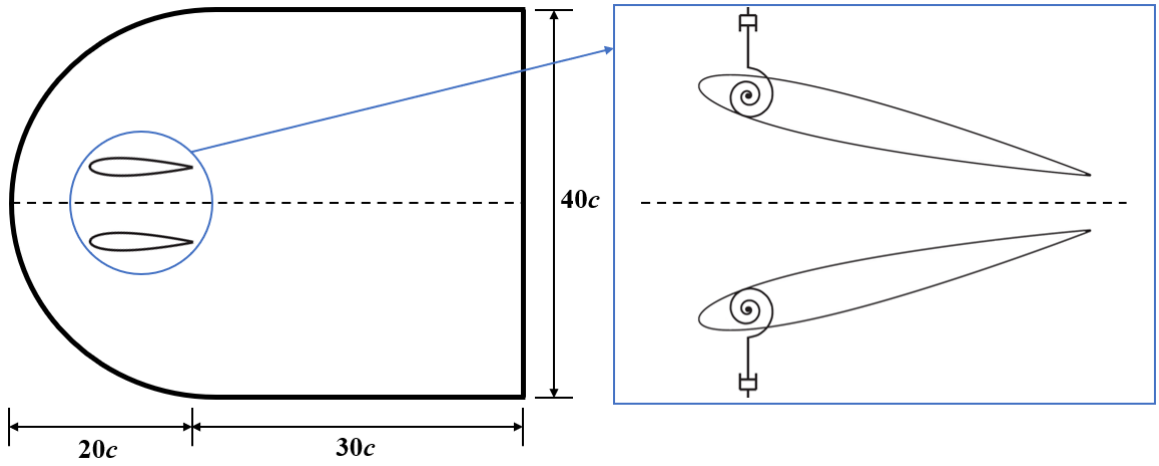

Figure 4-1 Schematic of computational domain for the parametric study.

The geometry and kinematic parameters of interest in the current study include the advance speed characterizing as inflow velocity, oscillating frequency, torsional spring stiffness, heaving amplitude, position of elastic pitching axis from the leading edge and equilibrium distance between two foils. A complete scan over the parametric space by considering every parameter combination is not feasible for the viscous simulations due to extremely high computing cost. Therefore, the influence of each parameter was investigated individually in the current study.

The computational scope for each parameter is presented in Table 4-1. The advance speed around 2m/s is commonly used for the underwater vehicles. Hence, the flow conditions for the parametric study are selected as the range from 1m/s to 3m/s. It should be noted that the definition of advance coefficient includes multiple geometry and motion parameters. For convenience, the advance speed with the unit of m/s was directly used to indicate the flow condition in this section. Three flow speeds of 1m/s, 2m/s and 3m/s were taken into consideration, which produce the corresponding Reynolds number of 100000, 200000 and 300000, respectively.

The selection of oscillating frequency should take into account the feasibility of installed actuator. In general, a relatively high oscillating frequency should be employed for the oscillating foils in air, while the oscillating foils in water use a low-to-moderate oscillating frequency. The range of torsional spring stiffness needs to be tested to achieve the stable locomotion state for implemented kinematics. Herein,

the non-dimensional spring coefficient was used to represent the torsional flexibility. For the purpose of propulsion, the position of elastic pitching axis of oscillating foils is smaller than one-third chord length from the leading edge in general. The range of heaving amplitude and distance between two foils need to consider the mesh motion of current numerical model. Both extremely high heaving amplitude and dramatically small gap between two foils may lead to the severe mesh deformation, and hence reduce the reliability and accuracy of simulations. In addition, the selection of these two parameters should consider the installation and operation of APWIGs for the target vehicles.

Table 4-1 The scope of computational parameters in the parametric study.

Parameters	**Non-dimensional**	**Computational Scope**
Advance speed (m/s)	Re	1m/s, 2m/s, 3m/s
Oscillating frequency (Hz)	k	0.31, 0.63, 0.94
Torsion spring stiffness (Nm/rad)	K^*	0 ~ 1.6
Heaving amplitude (m)	h_0/c	0.1, 0.2, 0.3, 0.4, 0.5
Position of pitching axis (m)	b_0/c	0.1, 0.15, 0.2, 0.25, 0.3, 1/3
Distance between two foils (m)	d_0/c	1.2 ~ 6

4.2 Investigation into Oscillating Frequency

The investigation into the influence of oscillating frequency on the propulsive characteristics of APWIGs was firstly performed. Herein, three oscillating frequencies were considered including 2Hz, 4Hz, 6Hz, which lead to the corresponding reduced frequencies of 0.31, 0.63, 0.94, respectively. Since the torsional flexibility is highly relevant to the kinematics of APWIGs, the variation of stiffness coefficients is also taken into account in the computations.

4.2.1 Time variation of flow-induced pitching motion

The time history of flow-induced pitching angle and effective AoA with different reduced frequencies are presented in Figures 4-2, 4-3 and 4-4, respectively. When using a relatively high spring stiffness at the medium reduced frequency, the time variation of flow-induced pitching angle tends to be chaotic due to the imbalance between hydrodynamic moments by the surrounding flow and restoring moments by the attached spring. It can be seen that the dynamic responses of APWIGs are more sensitive to the attached torsional spring at a low oscillating frequency, while much larger spring stiffness should be employed in the situation of high reduced frequency to produce the reasonable kinematics.

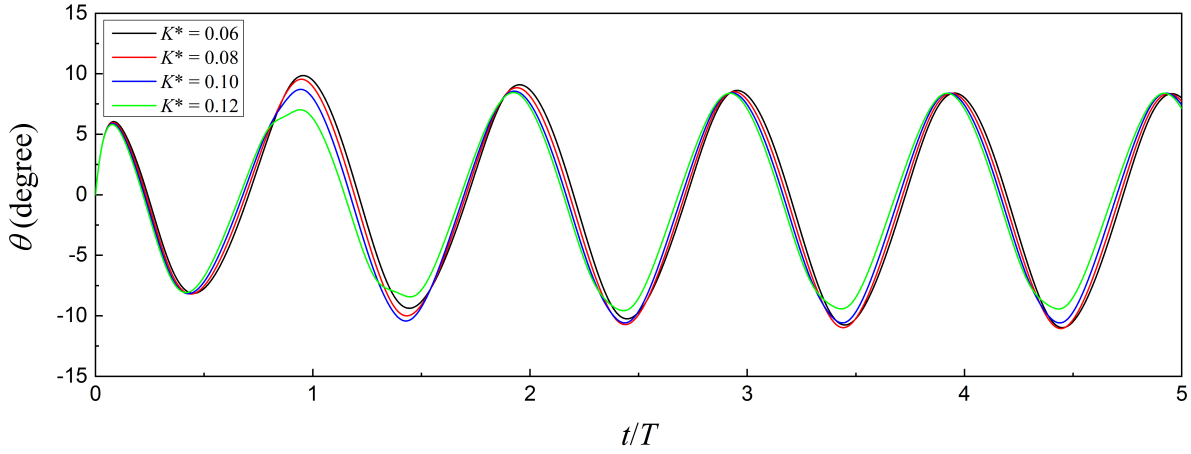

(a) Flow-induced pitching angle

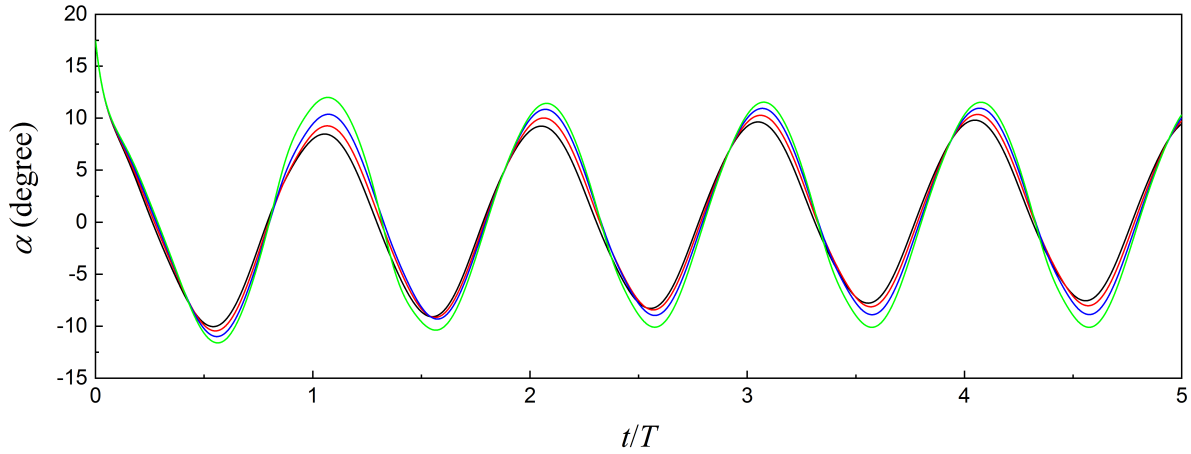

(b) Effective AoA

Figure 4-2 Time variation of dynamic responses for APWIGs over five oscillatory cycles with different spring stiffness at the reduced frequency of $k = 0.31$.

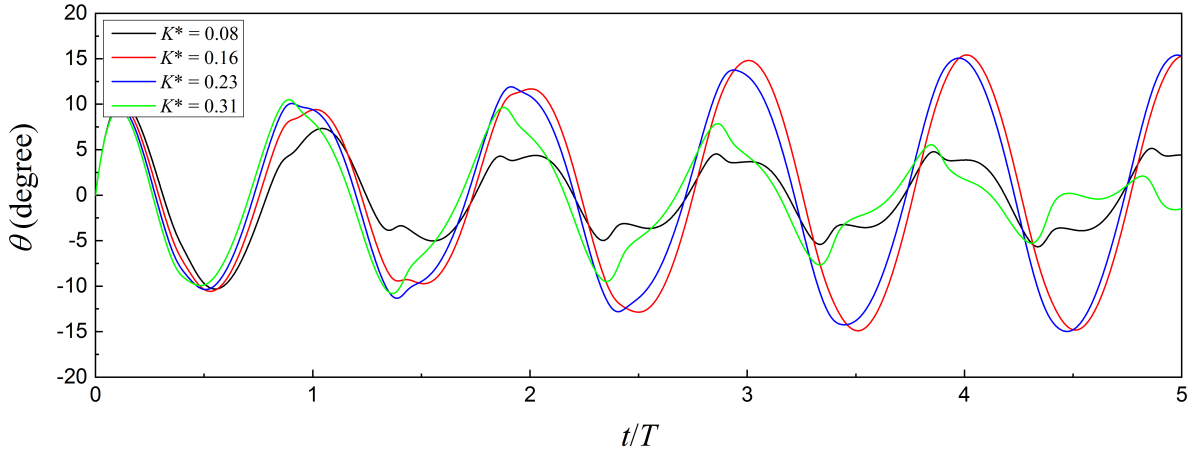

(a) Flow-induced pitching angle

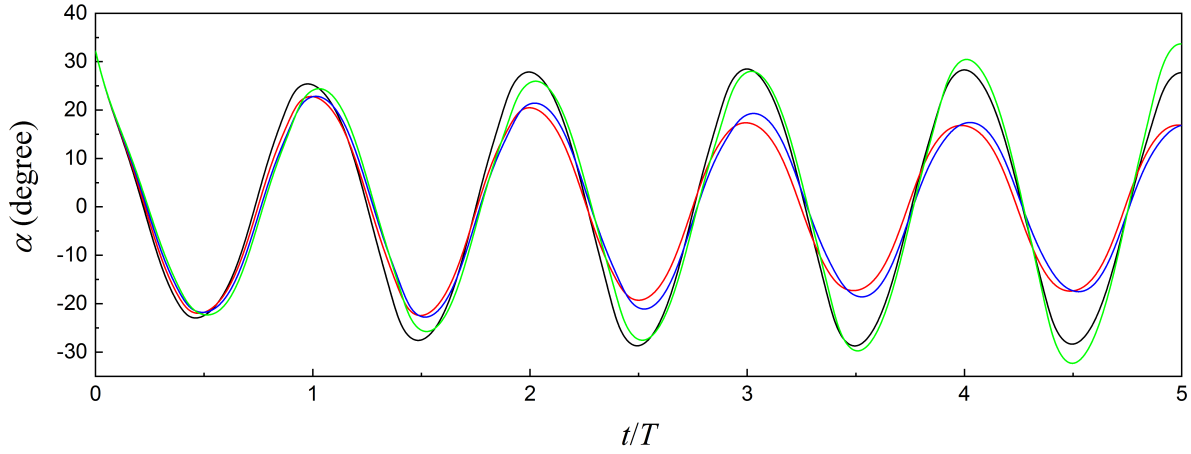

(b) Effective AoA

Figure 4-3 Time variation of dynamic responses for APWIGs over five oscillatory cycles with different spring stiffness at the reduced frequency of $k = 0.63$.

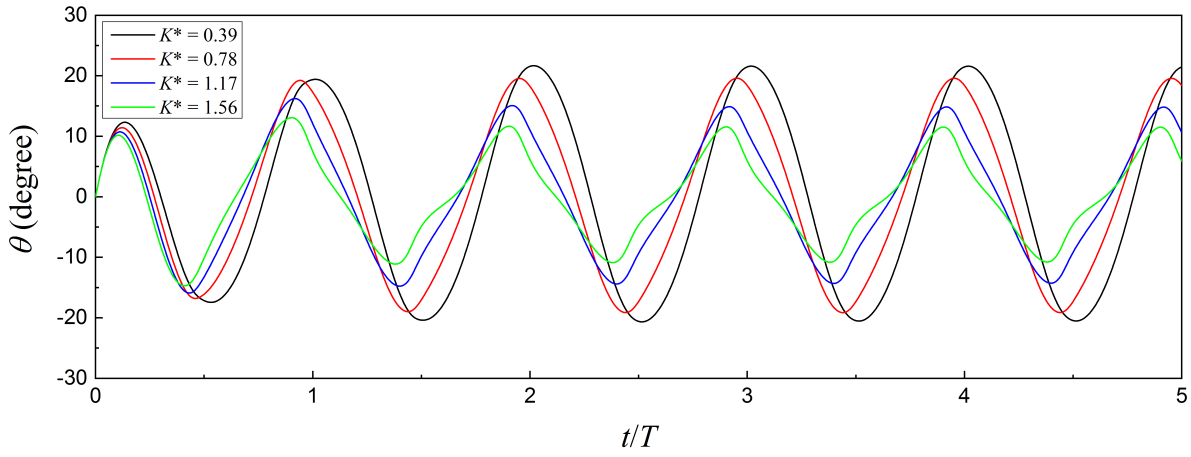

(a) Flow-induced pitching angle

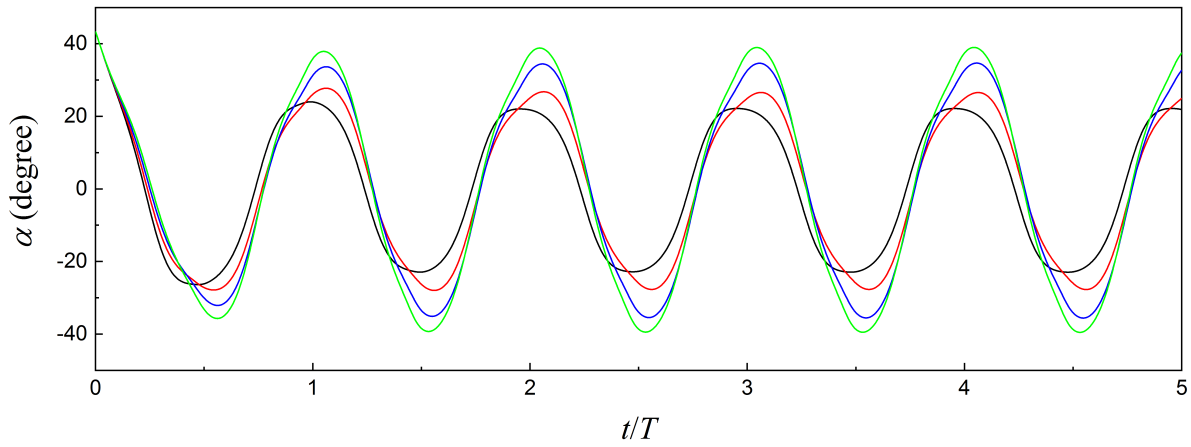

(b) Effective AoA

Figure 4-4 Time variation of dynamic responses for APWIGs over five oscillatory cycles with different spring stiffness at the reduced frequency of $k = 0.94$.

4.2.2 Time variation of hydrodynamic characteristics

Figures 4-5, 4-6 and 4-7 present the time variation of force coefficients for APWIGs with different oscillating frequencies. Two peaks of time-varying thrust over one cycle can be seen for all cases, in which the second peak is lower than the first one. With respect to the lift coefficient, there is a single peak in the time series over one cycle. Both maximum thrust and lift coefficient show an increasing trend with a higher oscillating frequency.

In addition, the time series of force coefficients present more complicated features when the reduced frequency is higher due to the corresponding evident vortex shedding. It should be noted that the torsional spring stiffness plays an extremely important role in the hydro-elasticity characteristics of APWIGs at all three oscillating frequencies. Therefore, it is necessary to perform an in-depth study on the propulsive performance of APWIGs based on the different oscillating frequencies as a function of stiffness coefficient.

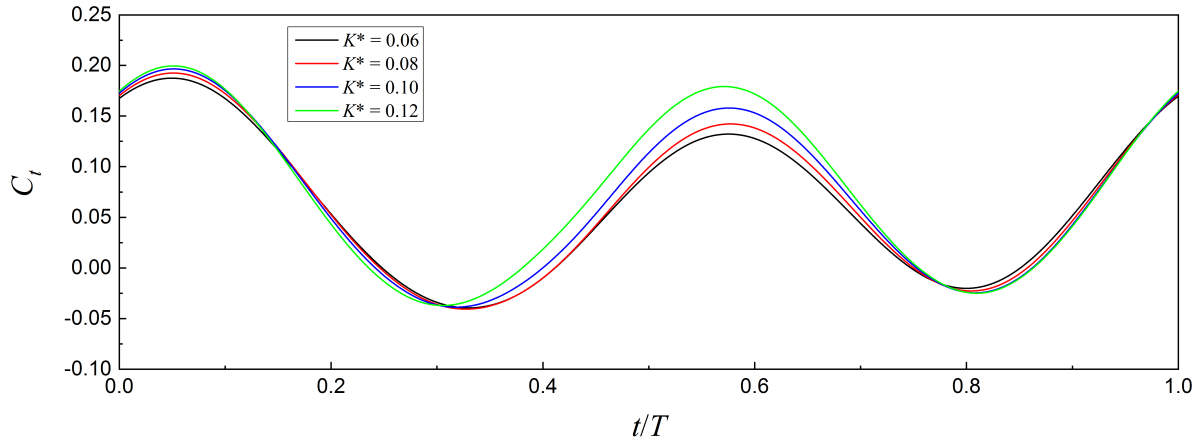

(a) Thrust coefficient

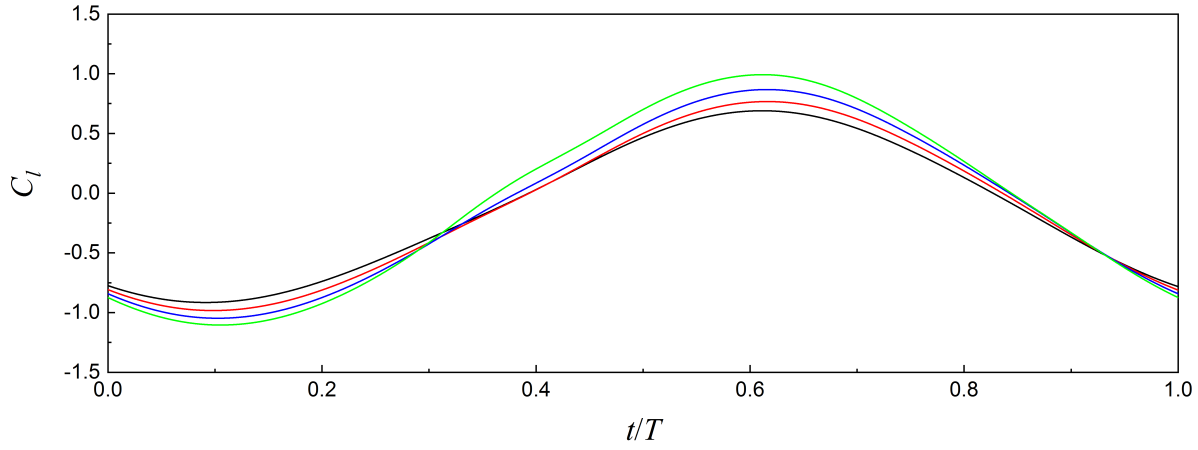

(b) Lift coefficient

Figure 4-5 Time variation of force coefficients for APWIGs over five oscillatory cycles with different spring stiffness at the reduced frequency of $k = 0.31$.

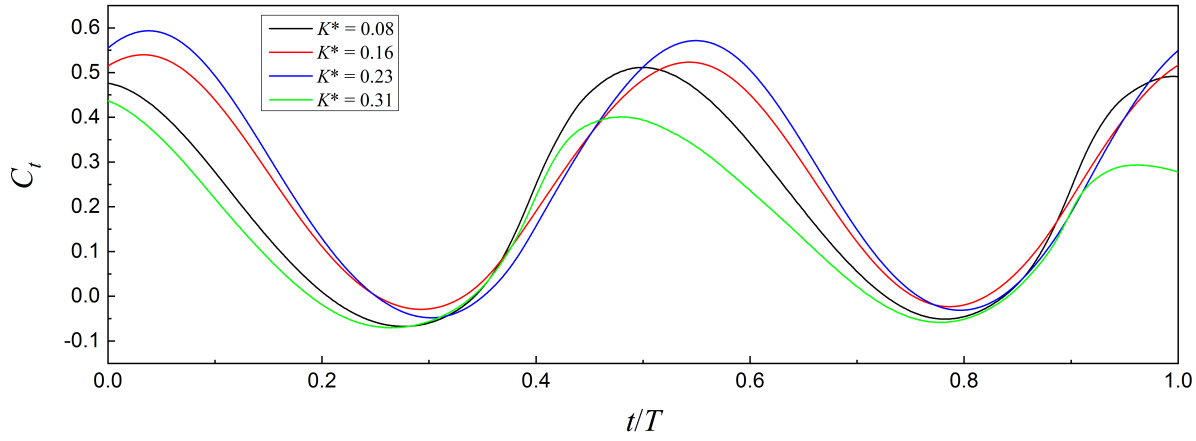

(a) Thrust coefficient

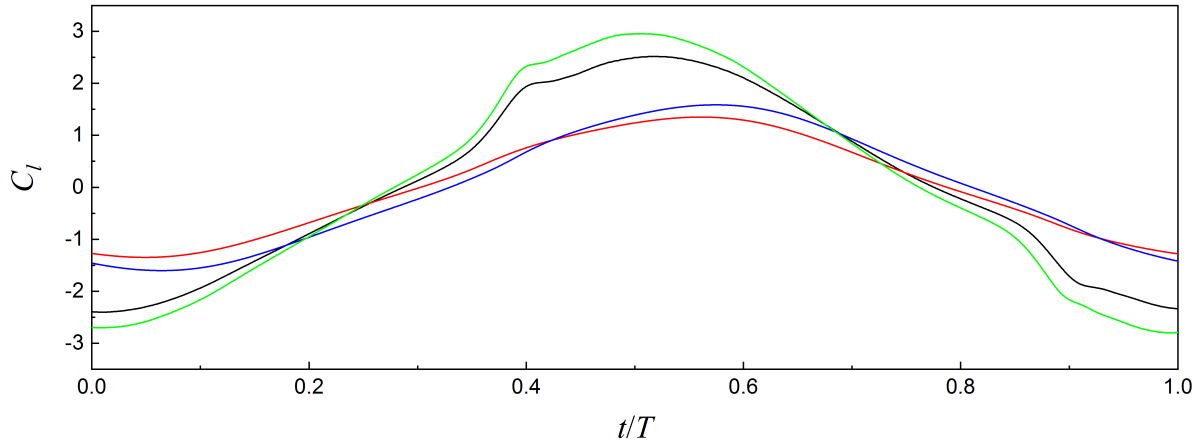

(b) Lift coefficient

Figure 4-6 Time variation of force coefficients for APWIGs over five oscillatory cycles with different spring stiffness at the reduced frequency of $k = 0.63$.

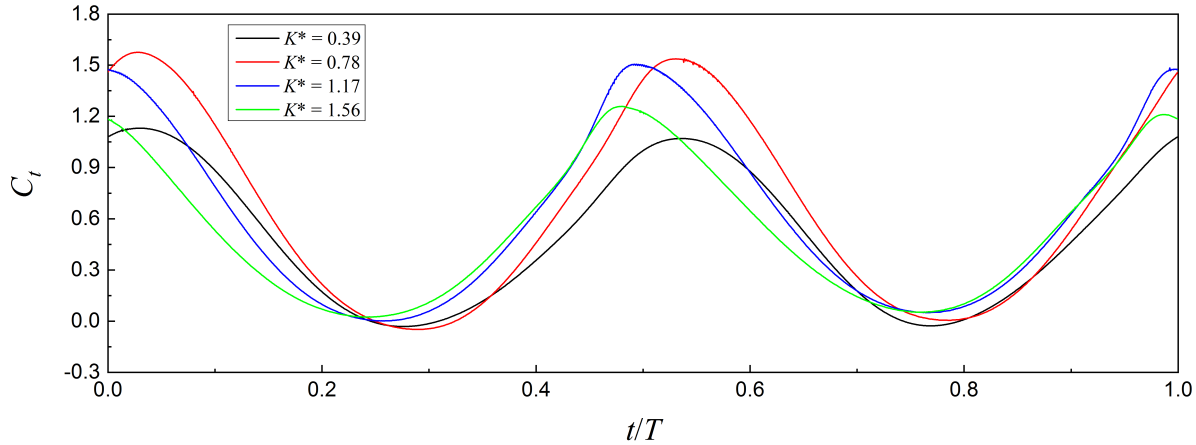

(a) Thrust coefficient

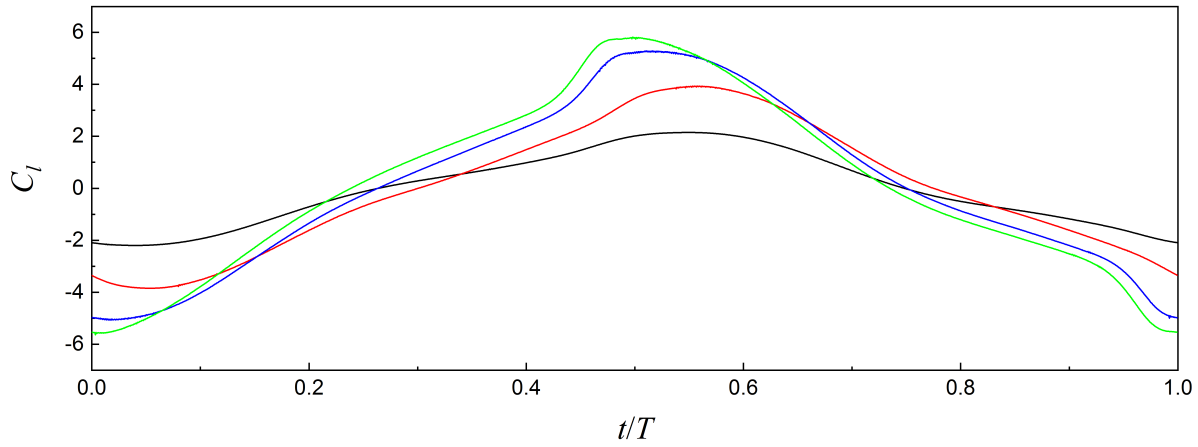

(b) Lift coefficient

Figure 4-7 Time variation of force coefficients for APWIGs over five oscillatory cycles with different spring stiffness at the reduced frequency of $k = 0.94$.

4.2.3 Kinematic features and propulsive performance

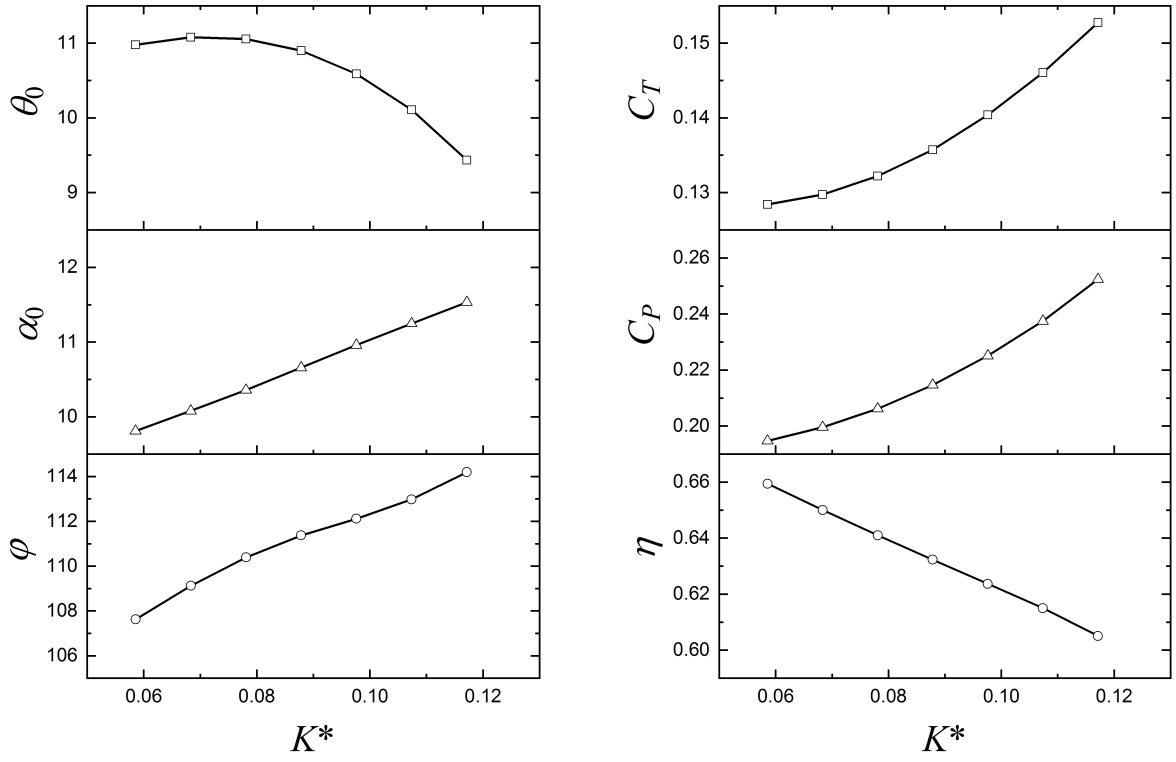

(a) Locomotion properties (b) Propulsive performance

Figure 4-8 Propulsive characteristics of APWIGs as a function of torsional spring stiffness at the reduced frequency of $k = 0.31$.

The peak of flow-induced pitching angle, maximum effective AoA and pitch-leading phase difference for APWIGs at three reduced frequencies are presented in Figures 4-8 (a), 4-9 (a) and 4-10 (a), respectively. As the results show, the maximum pitching angle shows an increasing trend with a larger

spring stiffness, while it starts to drop with the further increase of stiffness coefficient. The maximum pitching angle of APWIGs at three reduced frequencies are 11.1, 15.2 and 20.9 degrees, respectively. The corresponding peak of effective AoA at reduced frequencies of 0.63 and 0.94 show an opposite trend with respect to the pitching angle. After a rapid decrease with an increase of stiffness coefficient, the peak of effective AoA starts to increase consistently when the spring stiffness is larger than a critical value. In contrast, the maximum effective AoA at the reduced frequency of 0.31 shows a consistently increasing trend with a stiffer torsional spring.

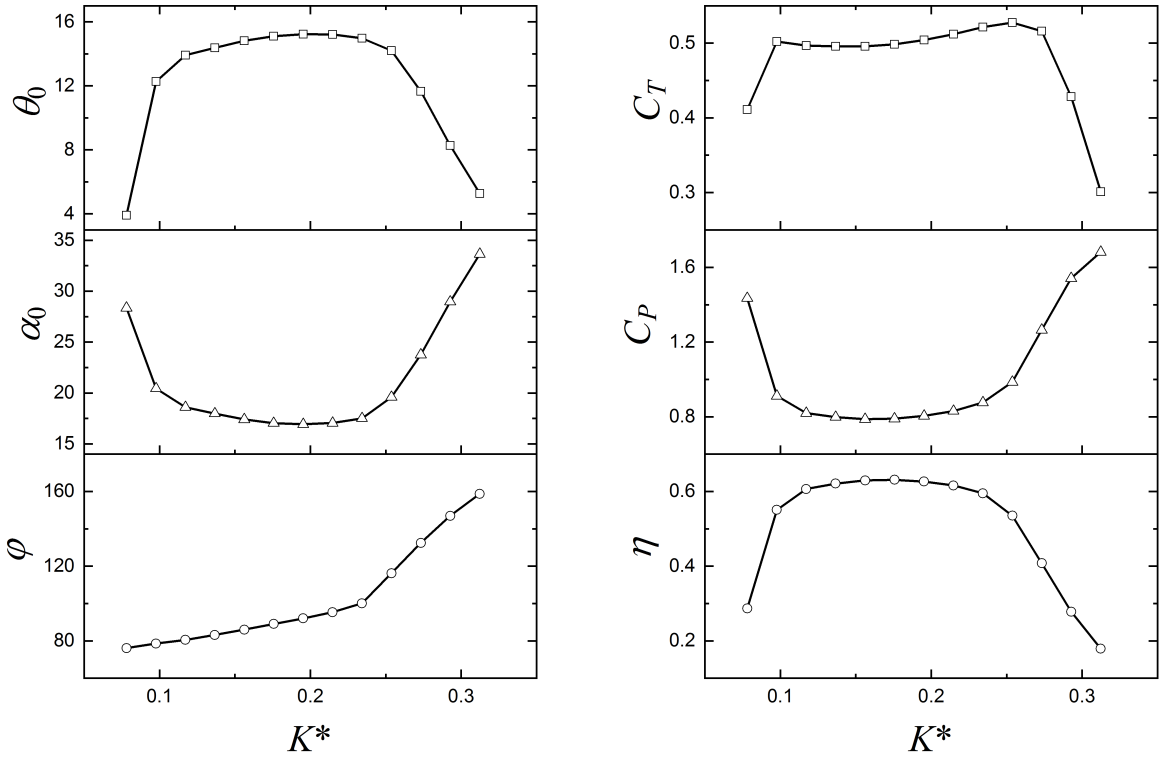

(a) Locomotion properties (b) Propulsive performance

Figure 4-9 Propulsive characteristics of APWIGs as a function of torsional spring stiffness at the reduced frequency of $k = 0.63$.

The peak of resulting effective AoA at three oscillating frequencies are 11.5, 33.6 and 39.5 degrees, respectively. It was indicated that the flow separation and corresponding stall are inevitable for some cases at a relatively high reduced frequency. In addition, the sustained growth in the phase angle between the flow-induced pitch and actively imposed heave can be seen with an increase of spring stiffness. This is attributed to that the attached torsional spring with a larger stiffness tends to restore the oscillating foil towards the equilibrium position within a shorter period of time. In general, both flow-induced pitching angle and corresponding effective AoA tends to become larger when the reduced frequency is higher. However, the pitch-leading phase difference shows a low sensitivity towards the oscillating frequency. It varies within a relatively wide range between 60 and 160 degrees depending on the torsional spring stiffness.

The propulsive performance of APWIGs with different oscillating frequencies as a function of stiffness

coefficient is presented in Figures 4-8 (b), 4-9 (b) and 4-10 (b), respectively. At the low reduced frequency, both time-averaged thrust and power coefficients show an increasing trend with an increase of spring stiffness. However, the propulsive efficiency tends to decrease consistently when the stiffness coefficient becomes larger. Due to the maximum effective AoA being below 15 degrees at the reduced frequency of 0.31, a satisfactory propulsive performance with the efficiency of over 60% was obtained for the considered range of spring stiffness. With respect to the relatively high reduced frequency, an initial rise in the time-averaged thrust with an increase of spring stiffness can be seen, which is followed by a rapid drop when the stiffness coefficient further increases. In contrast, the time-averaged power follows the trend that decrease firstly but then rise rapidly when the stiffness coefficient continues to increase. As a result, an obvious peak in efficiency at the reduced frequencies of 0.63 and 0.94 can be found in Figures 4-9 (b) and 4-10 (b). In other words, an optimum spring stiffness that produces the highest propulsive efficiency can be found for the APWIGs at a given oscillating frequency.

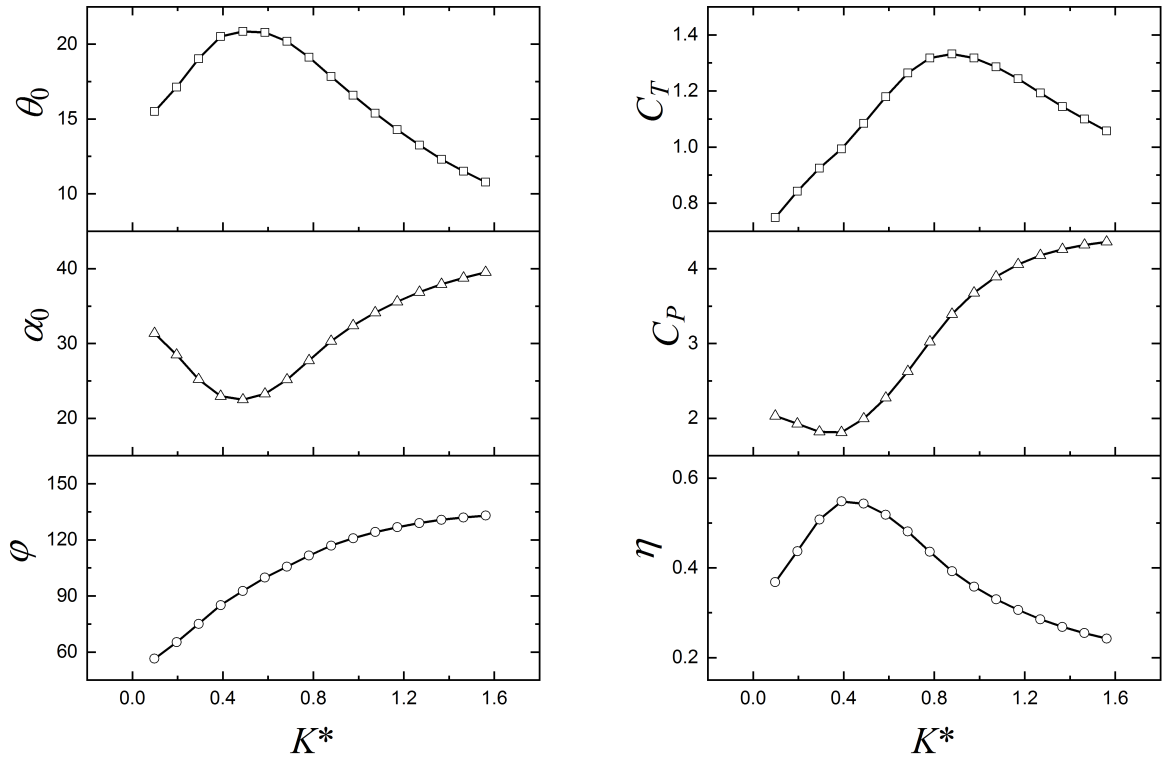

(a) Locomotion properties (b) Propulsive performance

Figure 4-10 Propulsive characteristics of APWIGs as a function of torsional spring stiffness at the reduced frequency of $k = 0.94$.

The maximum efficiency for the reduced frequencies of 0.31, 0.63, 0.94 are 65.9%, 63.1% and 54.8%, respectively. The corresponding stiffness coefficients are 0.06, 0.18 and 0.39, which occurred at a pitch-leading phase angle of 107.6, 89.0 and 85.1 degrees. It was found that a torsional spring stiffness that produces the pitch-leading phase difference of 85-110 degrees depending on advance speed tends to provide a satisfactory performance for APWIGs, which agrees well with the previous results. It should be noted that all the maximum effective AoAs for the highest efficiency at three reduced frequencies

are below 25 degrees, indicating that an attached flow around the foil surface is one of the crucial factors to ensure the satisfactory propulsive performance for APWIGs. Basically, such a propulsor at the larger oscillating frequency tends to produce higher forward thrust and require more input power, while the optimal efficiency shows a consistent drop with the increase of reduced frequency.

4.2.4 Flow patterns due to variation of oscillating frequency

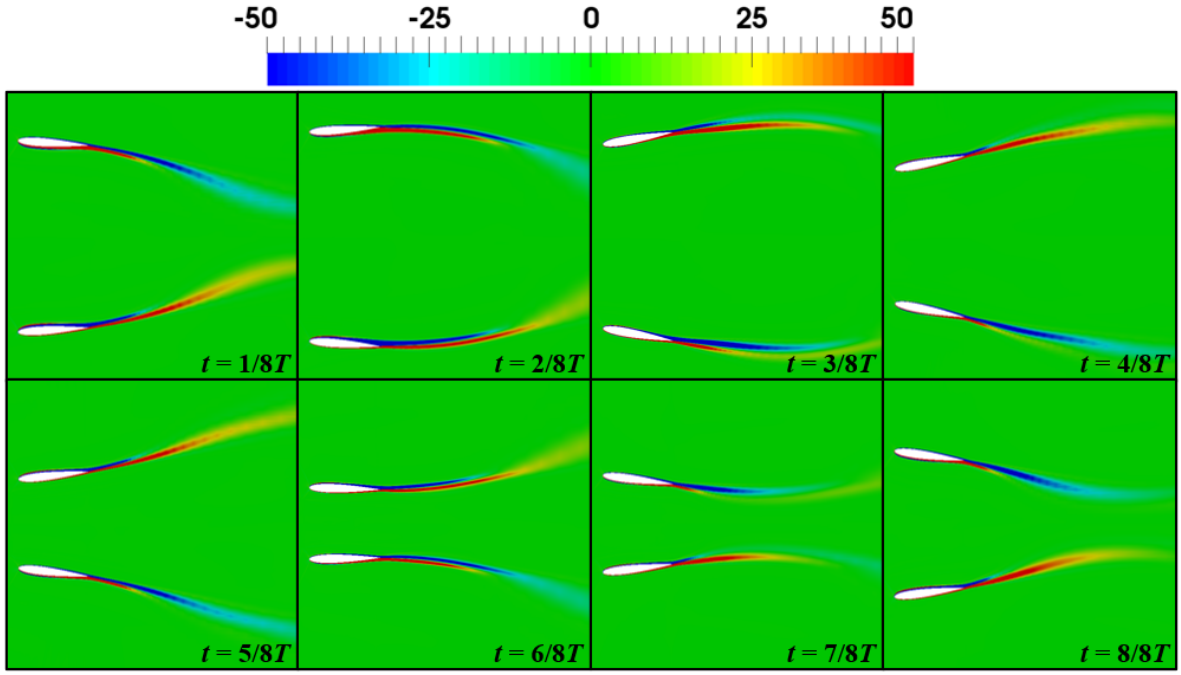

Figure 4-11 Vorticity contours of APWIGs at eight instants over one oscillatory cycle for the oscillating frequency of 2Hz (k = 0.31).

The vortex evolution and shedding over one oscillatory cycle for APWIGs with three reduced frequencies are presented in Figures 4-11, 4-12 and 4-13, respectively. For each situation, the stiffness coefficient is selected as the value that produces the highest propulsive efficiency. Since the reduced frequency is a direct measurement for the ratio of oscillating velocity along the vertical direction over forward advance speed, a smaller value of reduced frequency indicates a lower effective AoA during the operation of APWIGs. Consequently, the high attachment of surrounding flow for both leading edge and trailing edge can be seen for the case of k = 0.31 due to the maximum effective AoA below the dynamic-stall angle. With respect to the reduced frequencies of 0.63 and 0.94, the vortex shedding around both leading edge and trailing edge can be captured in the current simulations. Based on the results shown in Figures 4-8 (b), 4-9 (b) and 4-10 (b), it is reasonable to conclude that the massive leading-edge vortex shedding as well as the corresponding interaction of vortices between the leading edge and trailing edge will change the pressure distribution along the body surface and cause some energy loss, which thus are unfavorable to the propulsive performance of APWIGs.

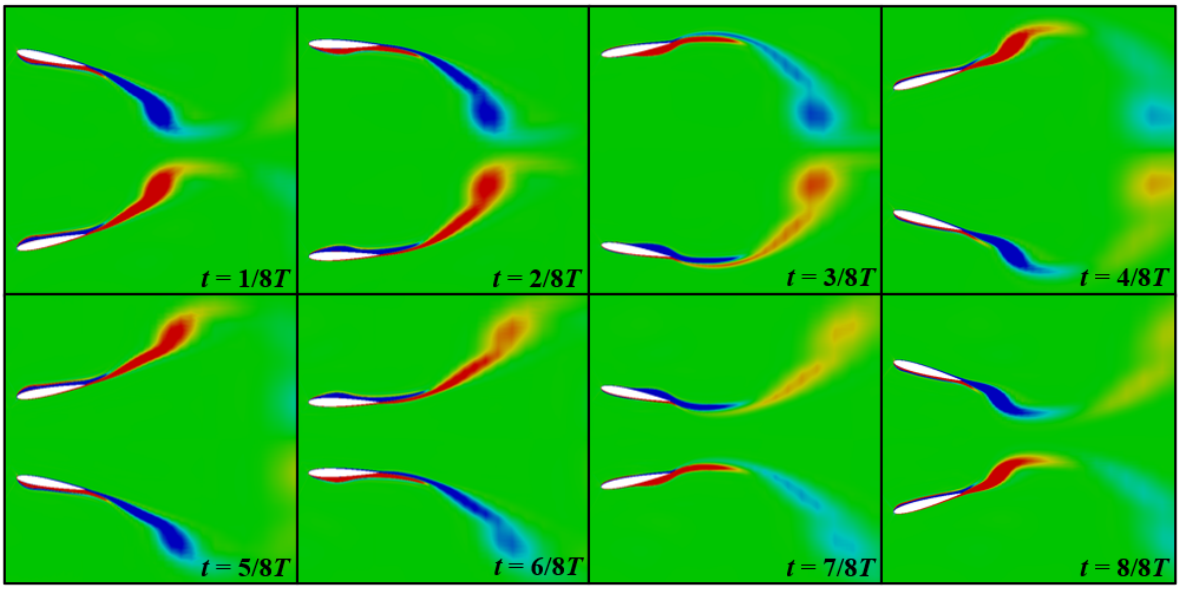

Figure 4-12 Vorticity contours of APWIGs at eight instants over one oscillatory cycle for the oscillating frequency of 4Hz (k = 0.63).

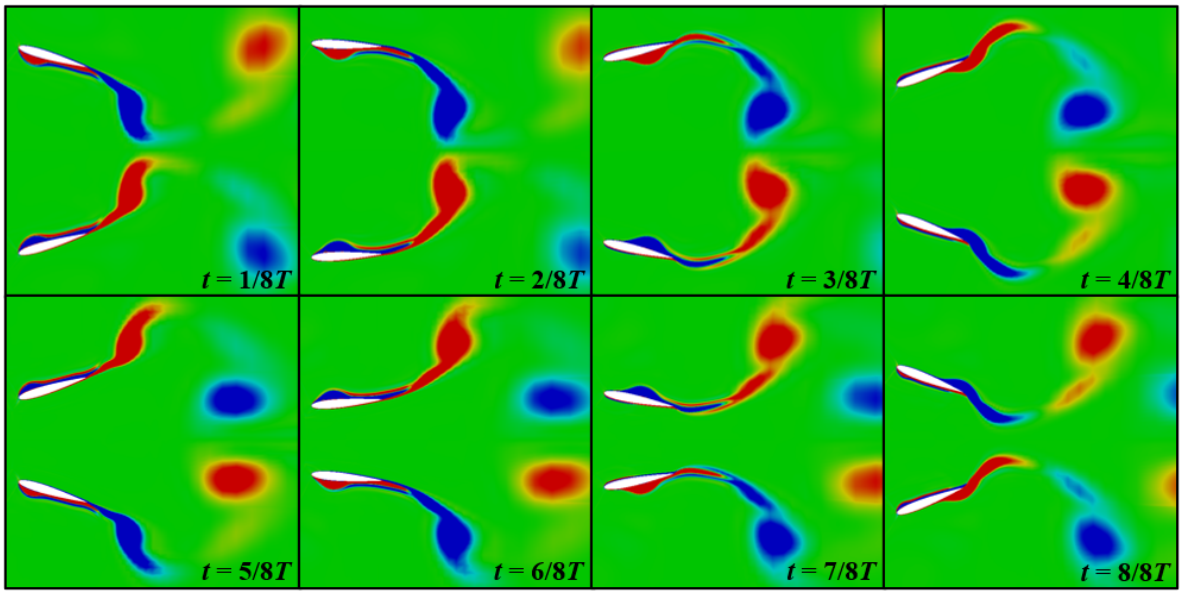

Figure 4-13 Vorticity contours of APWIGs at eight instants over one oscillatory cycle for the oscillating frequency of 6Hz (k = 0.94).

A typical process of vortex shedding for APWIGs was clearly recorded by the simulation with a reduced frequency of 0.94, as shown in Figure 4-13. During the upstroke of the first periodic quarter, the leading-edge vortices start to grow along the inside surface of each oscillating foil. Then, the generated vortices tend to arrive at mid-chord position when each foil reaches the maximum displacement. After that, the foils begin to perform downstroke motion, in which the produced vortices move further towards downstream and finally shed into wake from the trailing edge as the elastic pitching axis of each foil reaches the equilibrium position again. When two foils cross the equilibrium plane to move further

towards each other, the leading-edge vortices start to appear at the outside surface of each foil. In the same manner, these vortices will move towards the downstream during the upstroke of the last periodic quarter and shed into wake from the trailing edge when the oscillating foils return to initial position.

In the current simulations, the red and blue colors denote the vortices with the anticlockwise and clockwise directions, respectively. Considering the upper oscillating foil, results showed that an anticlockwise vortex is generated during the first half oscillatory cycle, while the motion in the second half cycle produces a clockwise vortex. The vortex behaviors of the lower foil can be considered as the mirror image of the upper foil with respect to the resulting ground plane. More importantly, the reverse Kármán vortex street can be obtained for each oscillating foil of APWIGs, which is characterized as the combination of a row of anticlockwise vortices above the symmetry plane and a row of clockwise vortices below the symmetry plane. Such a wake pattern was also reported by Tuncer and Kaya (2003) using a biplane flapping foil propulsion system with prescribed oscillating mechanism. It is worth noting that a reverse Kármán vortex street can induce a velocity surplus along the centerline of each foil indicating the thrust production.

4.3 Effect of Heaving Amplitude

It is well-established that the heaving amplitude has an apparent effect on the propulsive characteristics of oscillating foils. The relationship between the dynamic responses of foil and this kinematic parameter is also significant for the auto-pitch configuration. In the current simulations, a moderate range of heaving amplitude was considered including five values of h_0/c = 0.1, 0.2, 0.3, 0.4 and 0.5.

4.3.1 Time-varying dynamic responses

Figure 4-14 presents the time history of flow-induced pitching angle with different heaving amplitudes. It can be seen that the maximum pitching angle consistently increase when the heaving amplitude becomes larger. The sinusoidal-like profile for the passive pitch is constantly maintained with the variation of heaving amplitude. In addition, the heaving amplitude has no influence on the phase difference between the induced pitch and the prescribed heave for APWIGs.

4.3.2 Time-averaged propulsive performance

The propulsive characteristics of APWIGs with the variation of heaving amplitude are presented in Figure 4-15. As the results show, the time-averaged thrust shows a continuous increase with the rise of non-dimensional heaving amplitude for all three advance speeds. Especially, the APWIGs tends to produce the drag with an extremely low heaving amplitude, as shown in cases of 1m/s and 2m/s using the heaving amplitude of 0.1c.

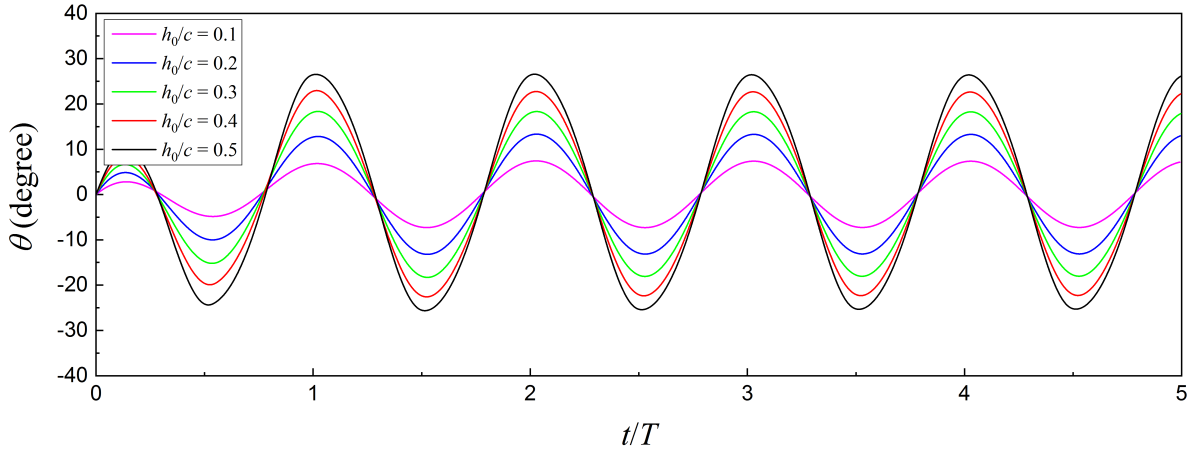

(a) $U = 1.0$m/s

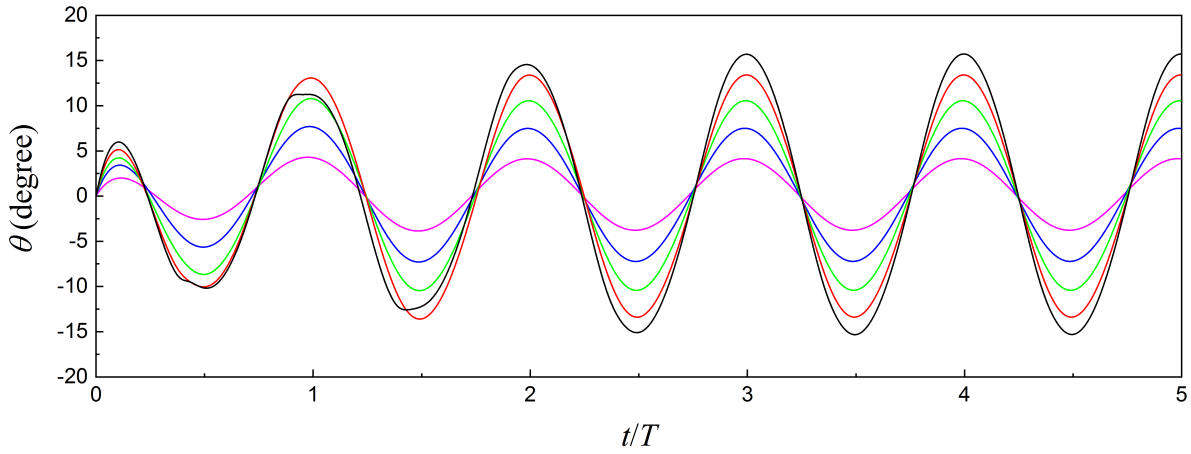

(b) $U = 2.0$m/s

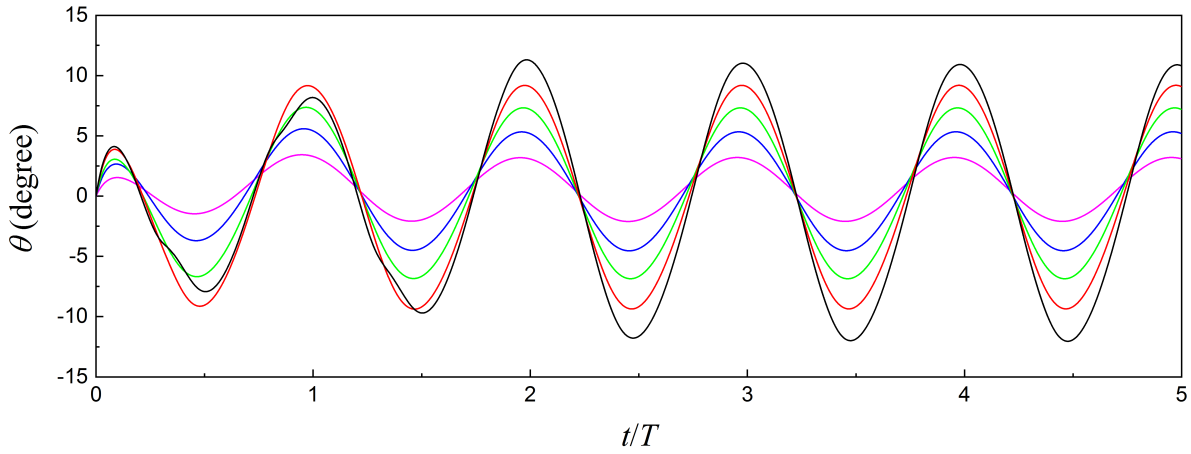

(c) $U = 3.0$m/s

Figure 4-14 Time variation of flow-induced pitching angle for APWIGs over five oscillatory cycles with different heaving amplitudes for three advance speeds.

The propulsive efficiency shows a more complicated trend with respect to the effect of heaving amplitude. It should be noted that the drag-producing cases were not presented in Figure 4-15 (b) due to the corresponding negative efficiency. For the advance speeds of 1m/s and 2m/s, the propulsive efficiency shows a trend that first increase and then decrease with the increase of heaving amplitude.

Within the current parametric range, the efficiency at advance velocity of 3m/s continuously increase when the APWIGs has a higher heaving amplitude. The highest propulsive efficiency of APWIGs for three advance speeds is 54.3%, 64.7 and 68.9%, which are produced by the heaving amplitudes of 0.3*c*, 0.4*c* and 0.5*c*, respectively. It is reasonable to conclude that an optimum heaving amplitude can be found for the APWIGs producing the highest efficiency at a given flow condition. In addition, the optimum heaving amplitude tends to increase with a larger advance speed. It should be noted that the considered heaving amplitudes in the current simulations are relatively small due to the limitation of dynamic mesh. The different performance characteristics and higher efficiency can be expected for the oscillating foil propulsors when employ a large heaving amplitude, as indicated in Anderson et al. (1998).

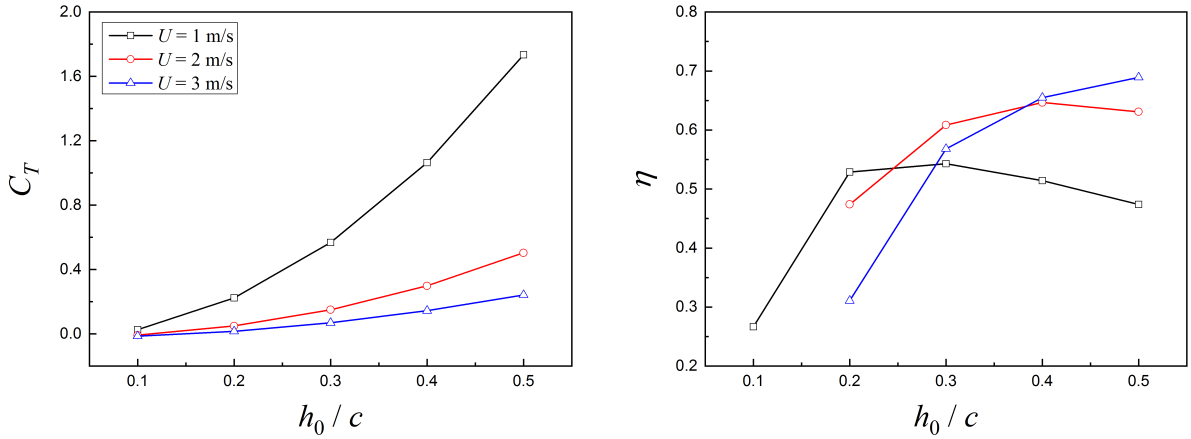

(a) Thrust coefficient (b) Propulsive efficiency

Figure 4-15 Effect of heaving amplitude on the propulsive performance of APWIGs.

4.4 Position of Elastic Pitching Axis

The studies in the existing literature indicated that the position of pitching pivot of oscillating foil propulsors tends to be closer to the leading edge, while the oscillating foils for energy harvesting are more likely to employ a position of pitching pivot in the middle of chord length or being closer to the trailing edge. With respect to the auto-pitch configuration, a relatively large distance of elastic pitching axis to the leading edge may result in the chaotic flow-induced pitching motion. A common setup for the position of pitching axis of oscillating foil propulsors is 1/3*c* from the leading edge in the relevant literature, such as Read et al. (2003). In the current computations, six positions of elastic pitching axis from the leading edge of oscillating foil were taken into consideration including the 0.1*c*, 0.15*c*, 0.2*c*, 0.25*c*, 0.3*c* and 1/3*c*.

4.4.1 Time-varying dynamic responses

The time variation of flow-induced pitching angle with different positions of elastic pitching axis at the advance speed of 3m/s is presented in Figure 4-16. It can be seen that the elastic-axis position has an

apparent influence on both pitching angle and pitch-leading phase difference. The comprehensive results with respect to the maximum pitching angle and phase difference for APWIGs with the variation of elastic-axis position at three advance speeds are presented in Table 4-2. As the results show, the peak of flow-induced pitching angle tends to firstly increase and then decrease with the rise of distance between the leading edge and elastic pitching axis for all three advance speeds. However, the pitch-leading phase difference shows a generally increasing trend with a larger elastic-axis distance from the leading edge. Overall, the flow-induced pitching motion tends to produce a lowest peak of pitching angle at the 0.25 chord position from the leading edge, which thus has a significant effect on the maximum effective AoA. As indicated in the preceding section, the pitch-leading phase angle within the range of 85 to 110 degrees for APWIGs tends to produce a higher propulsive efficiency. Results showed that the elastic-axis position from the leading edge within the range of 1/4c to 1/3c tends to result in a desired phase difference.

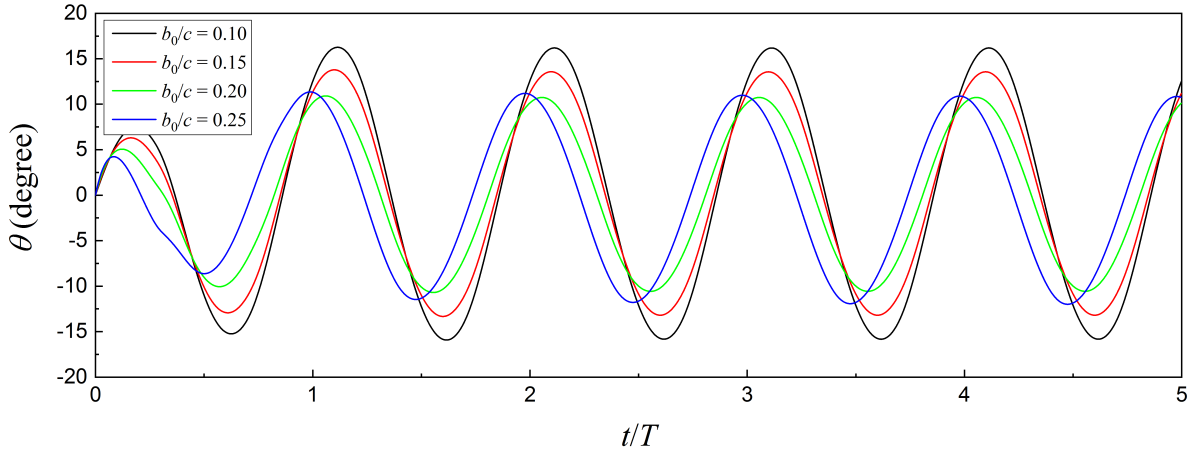

Figure 4-16 Time variation of flow-induced pitching angle for APWIGs over five oscillatory cycles with different positions of elastic pitching axis at the advance speed of U = 3m/s.

Table 4-2 Peak of flow-induced pitching angle and pitch-leading phase difference with five positions of elastic pitching axis.

b_0/c	U = 1m/s		U = 2m/s		U = 3m/s	
	θ_0 (degree)	φ (degree)	θ_0 (degree)	φ (degree)	θ_0 (degree)	φ (degree)
0.10	30.44	12.92	40.48	21.87	15.83	48.15
0.15	32.41	34.92	45.26	16.20	13.19	54.08
0.20	26.72	62.71	9.19	34.08	10.56	70.14
0.25	25.48	85.68	15.55	91.74	11.99	99.21
0.30	26.31	98.92	20.77	107.77	-	-
1/3	28.18	107.59	21.55	109.06	-	-

4.4.2 Time-averaged propulsive performance

The effect of elastic-axis position on the propulsive performance of APWIGs is presented in Figure 4-17. Basically, APWIGs at the advance speeds of 1m/s and 2m/s tends to produce the drag when the distance of elastic pitching axis from the leading edge is below 0.2*c*. With the further movement of pivot axis towards the mid-chord position, the time-averaged thrust at the advance speed of 1m/s shows a continuously increasing trend, while the case of 2m/s produces the maximum thrust with an elastic pitching axis of 0.25 chord position from the leading edge. With respect to the advance velocity of 3m/s, a general increase in time-averaged thrust can be seen when the elastic pitching axis becomes farther to the leading edge. It should be noted that the flow-induced pitching motion tends to be chaotic and aperiodic for the speed of 3m/s when the elastic-axis position from the leading edge is beyond 0.25*c*. Therefore, the numerical results at speed of 3m/s with the elastic pitching axis of 0.3 and 1/3 chord positions from the leading edge were not presented.

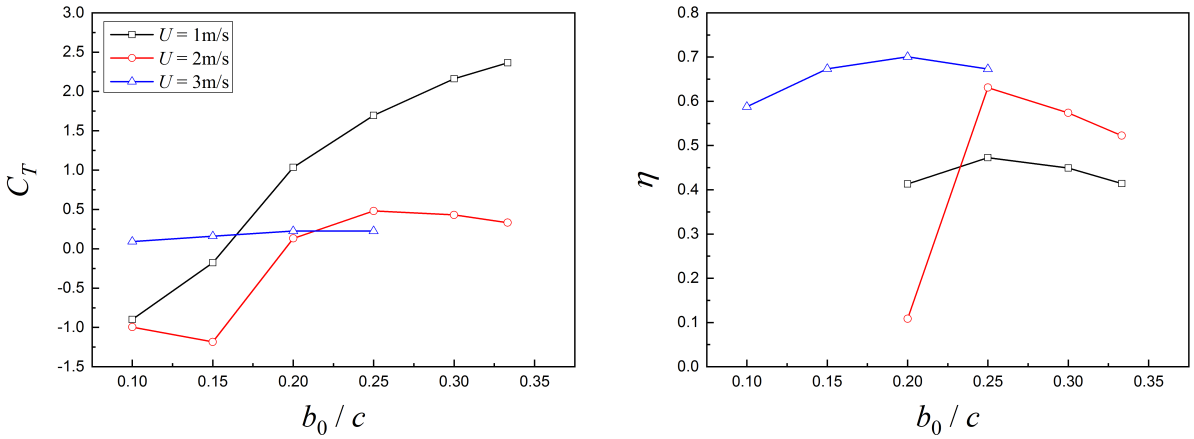

(a) Thrust coefficient (b) Propulsive efficiency

Figure 4-17 Effect of position of elastic pitching axis on the propulsive performance of APWIGs.

With respect to the propulsive efficiency, its trend of first increase and then drop with the increase of elastic-axis distance from the leading edge is shown in Figure 4-17 (b). As can be seen from the numerical results, the propulsive efficiency at the advance speed of 2m/s with an elastic pitching axis of 0.2 chord position from the leading edge shows a sudden drop. Figure 4-18 presents the comparison of time variation of flow-induced pitching angle with two positions of elastic pitching axis at the advance speed of 2m/s. It was found that the aperiodic and consistently declining pitch is the main reason for the sudden drop of propulsive performance with an elastic pitching axis of 0.20*c*.

Current calculations indicate that the flow-induced pitching motion of APWIGs tends to be unstable with an extremely close position of elastic pitching axis from the leading edge depending on advance speeds. The maximum efficiencies for three advance speeds are 47.2%, 63.1% and 70.1%, which are obtained by the elastic pitching axis of 0.2 and 0.25 chord position from the leading edge. Generally, the elastic pitching axis around 0.25 chord position from the leading edge tends to produce a satisfactory

performance at the low speeds. As to a relatively high advance velocity, the elastic pitching axis around 0.2 chord position from the leading edge should be used for the optimal efficiency of APWIGs.

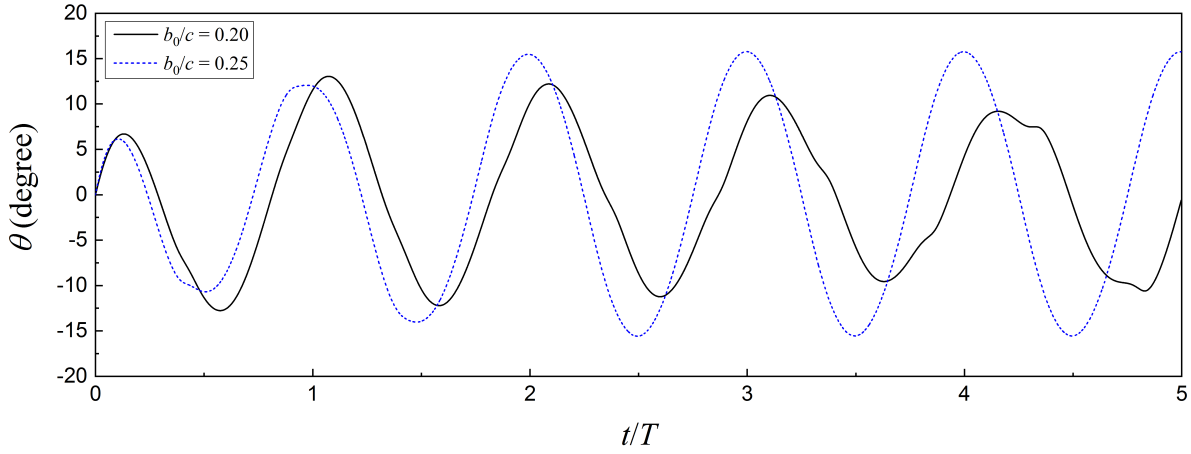

Figure 4-18 Time variation of flow-induced pitching angle for APWIGs over five oscillatory cycles with two positions of elastic pitching axis at the advance speed of U = 2m/s.

4.5 Wing-in-ground Effect of APWIGs

The WIG effect as a result of counter-phase biplane oscillating foil configuration is regarded as a favorable factor for the improvement of thrust production and propulsive efficiency. Such an effect tends to be more dominant when the distance between two foils becomes smaller. In the current study, the equilibrium distance between two foils d_0/c was employed to characterize the WIG effect, which covers a relatively wide range from 1.2 to 6.

4.5.1 Time-varying dynamic responses

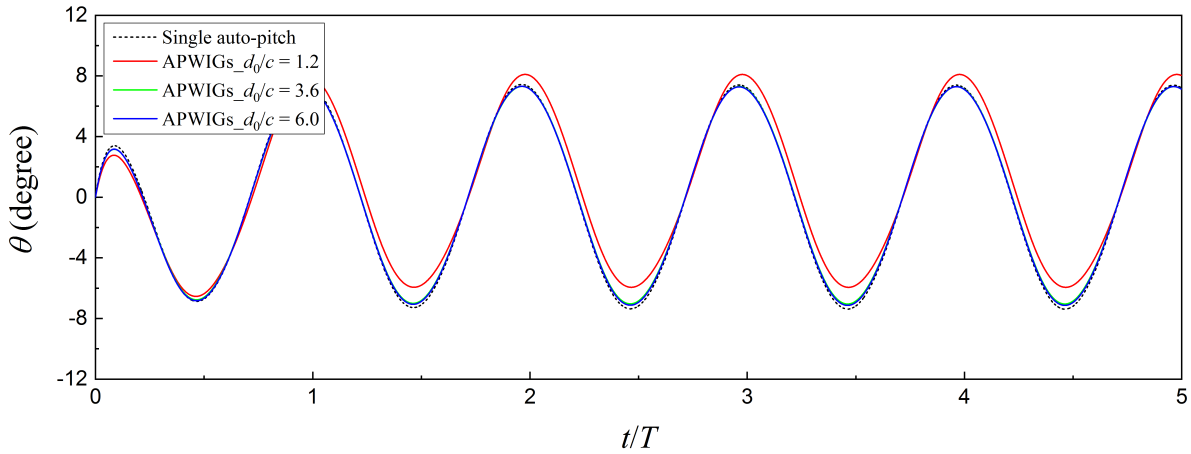

Figure 4-19 Time variation of flow-induced pitching angle for APWIGs over five oscillatory cycles with different equilibrium distances between two foils at the advance speed of U = 3m/s.

For the effect of equilibrium distance between two foils, a direct comparison of propulsive performance

of APWIGs with the single auto-pitch configuration was performed. A medium heaving amplitude of 0.3*c* was employed for this part of calculation. Figure 4-19 shows the time history of flow-induced pitching angle with different equilibrium distances between two foils at the advance speed of 3m/s. As the results show, the pitching motion of APWIGs tends to be consistent with that of single auto-pitch configuration when the equilibrium distance is relatively large. Compared with the pitching variation of single auto-pitch oscillating foil, the resulting WIG effect tends to increase the flow-induced pitching angle during the upstroke and decrease the value at the downstroke. It can be observed that the variation of equilibrium distance has a less influence on the pitch-leading phase difference.

4.5.2 Time-averaged propulsive performance

The influence of equilibrium distance between two foils on the propulsive performance of APWIGs is presented in Figure 4-20. The blue dashed lines denote the results of single auto-pitch configuration. Note that the thrust coefficient of APWIGs is the average of that for each foil. As the results show, the time-averaged thrust tends to consistently increase with the decrease of equilibrium distance between two foils. When the equilibrium distance is larger than 5*c*, the generated thrust agrees to a fixed value, which is still larger than that of the single oscillating foil. It was suggested that the maximum time-averaged thrust generated by each foil of APWIGs is about 1.5 times that of single oscillating foil.

A similar trend was found in the characteristics of propulsive efficiency, as shown in Figure 4-20 (b). A higher efficiency can be obtained for APWIGs when one foil is set closer to another one. The propulsive efficiency of APWIGs finally converges to around 53% with the equilibrium distance of over 5*c*. It can be seen that there is a constant increase of 2% in propulsive efficiency for APWIGs over the single auto-pitch configuration even though the equilibrium distance between two foils is considerably large. The maximum increase of around 12% in propulsive efficiency was obtained by the produced WIG effect, in which the APWIGs employs an equilibrium distance of 1.2*c*.

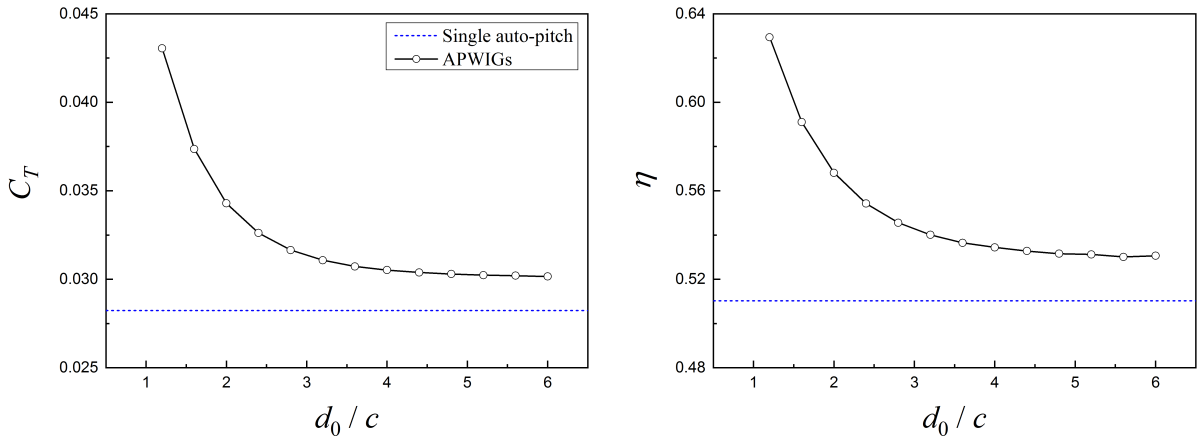

(a) Thrust coefficient (b) Propulsive efficiency

Figure 4-20 Wing-in-ground effect with the variation of equilibrium distance between two foils on the propulsive performance of APWIGs.

4.6 Concluding Remarks

A parametric study on the propulsive performance of APWIG was conducted to analyze the effect of individual geometry and kinematic parameters. The considered parameters include the advance speed, oscillating frequency, torsional spring stiffness, heaving amplitude, position of elastic pitching axis from the leading edge and equilibrium distance between two foils. The selection of computational scope for each parameter is based on the range of interest in the engineering applications, feasibility of established numerical model and computing cost. This section aims to provide a two-dimensional database as a reference for the performance optimization of APWIGs.

The investigation into the effect of oscillating frequency on the propulsive characteristics provides significant insights into the thrust-producing mechanism of APWIGs. The flow separation around the oscillating foils tends to be mild at a low reduced frequency, which is attributed to the relatively small effective AoA. With respect to a high reduced frequency, obvious vortex shedding along both leading edge and trailing edge can be captured by the current model. A typical reverse Kármán vortex street characterizing as a row of anticlockwise vortices above the symmetry plane and a row of clockwise vortices below the symmetry plane was obtained in the wake of each oscillating foil for APWIGs. It was believed that such a vortex pattern induces a momentum surplus in the downstream appearing as a jet-like wake profile.

The oscillating frequency was found to be dominant for both dynamic responses and propulsive performance of APWIGs. It was also noted that the torsional spring stiffness plays an extremely important role in the hydro-elasticity characteristics of APWIGs for different oscillating frequencies. A relatively high torsional flexibility is appropriate for a large oscillating frequency, while the APWIGs with a low oscillating frequency requires a modest torsional spring stiffness to achieve the stable locomotion state. In general, the propulsive efficiency of APWIGs shows a decreasing trend with an increase of reduced frequency. With a fixed oscillating frequency and a given flow condition, an optimum spring stiffness can be found to produce the highest propulsive efficiency for APWIGs.

The current results demonstrated that the heaving amplitude and mean distance between two foils have a significant effect on the peak of flow-induced pitching angle, while the phase difference shows a negligible sensitivity to these two parameters. The propulsive efficiency tends to increase firstly and then decrease with a consistent increase of heaving amplitude, which indicates that there is an optimum value generating the best propulsive performance. The propulsion performance presents a steady growth with the decrease of mean distance between two foils, owing to the enhancement of WIG effect. Within the current parametric space, it was found that the thrust production by APWIGs is 1.5 times that of a single auto-pitch configuration, and the maximum efficiency improvement due to the WIG effect is approximately 12%.

The position of the elastic pitching axis was found to be a dominant parameter to determine the dynamic

responses of auto-pitch oscillating foil configuration. Both the pitch-leading phase difference and the maximum passive pitching angle of APWIGs show an obvious sensitivity to this parameter. In particular, it was found that the elastic-axis position from the leading edge beyond 0.25 chord length tends to produce a chaotic and aperiodic flow-induced pitching motion when the advance speed is relatively high, resulting in a poor propulsion performance. Current results showed that the 0.2 to 0.25 chord position from the leading edge can produce a desirable performance depending on advance speeds.

In summary, the dynamic responses and propulsive characteristics of APWIGs show a high dependence on several key parameters. Based on indications by the current parametric study, it can be conjectured that the APWIGs propulsion system with the self-adjusted pitch and WIG effect is capable of achieving a satisfactory propulsive performance by employing an appropriate combination of relevant geometry and kinematic parameters.

CHAPTER 5

Comparative Study between Different Configurations

5.1 Configuration Setup of Comparative Study

To demonstrate the superiority of APWIGs in both thrust production and efficiency enhancement, a direct comparison of propulsive performance between current configuration of interest and other widely examined oscillating foil propulsors in the existing literature was performed. The considered oscillating foil propulsors in the comparative study include the single auto-pitch oscillating foil, biplane heave-only oscillating foil configuration and biplane fully-prescribed oscillating foil configuration. The kinematics for each configuration is presented in Table 5-1.

Table 5-1 Kinematic setup of various configurations in the comparative study.

Configurations	Kinematics	Features
APWIGs	Active heave + Passive pitch	WIG effect & Flow-induced pitch
Single auto-pitch	Active heave + Passive pitch	Simple geometry
Biplane heave-only	Active heave + No pitch	Simple control mechanism
Biplane fully-prescribed	Active heave + Active pitch	Adjustable parameters

As indicated before, the configuration of APWIGs is characterized as a biplane arrangement with the actively imposed heaving motion and flow-induced pitching motion restrained by the attached torsional spring. The single auto-pitch oscillating foil has the same kinematics with APWIGs but employs a simple geometry. The comparison between these two configurations is used to show the WIG effect on the propulsive characteristics. It should be noted that the torsional spring stiffness for the auto-pitch configuration is selected as a value that produces optimal performance for all comparisons.

The biplane heave-only oscillating foil configuration attracts the certain attention due to the relatively simple locomotion. This system only needs one actuator to actively impose the heaving motion, which implies that the corresponding control mechanism is highly straightforward. Since it does not have the degree of freedom in rotation, the biplane heave-only oscillating foil configuration may encounter the issue of zero effective AoA and resulting zero start-up thrust when it operates in the still water.

To address this problem, the pitching motion of oscillating foils needs to be introduced to generate an initial effective AoA. The biplane fully-prescribed oscillating foil configuration with the combined heaving and pitching motion requires two actuators for the motion control of each foil, resulting in three locomotion parameters including the heaving amplitude, pitching amplitude, phase angle between heave and pitch. As both heaving motion and pitching motion are actively imposed, the relevant parameters and corresponding kinematics for this configuration are highly adjustable. However, the relatively complicated control mechanism and significant dependence on the flow condition can be identified for the biplane fully-prescribed oscillating foil configuration.

5.2 Comparison with Single Auto-pitch Oscillating Foil

The propulsive performance of APWIGs was firstly compared with the single auto-pitch oscillating foil configuration to highlight the superiority of biplane arrangement and resulting WIG effect. The single auto-pitch oscillating foil propulsor has been widely modelled and explored, such as Zhang et al. (2010), Xiao et al. (2014) and Thaweewat et al. (2018). In the current comparison, the completely same kinematic and geometry setup were implemented for these two configurations except for the number of foils. The heaving amplitude is fixed at the 0.5*c*. The oscillating frequency is selected as the 4Hz. The equilibrium distance between two foils for APWIGs is set as 1.8*c*.

The comparison of thrust coefficient and propulsive efficiency between APWIGs and single auto-pitch configuration is presented in Figure 5-1. APWIGs shows a slight increase compared with single auto-pitch configuration in terms of thrust coefficient. However, the WIG effect can be observed by the comparison of efficiency between APWIGs and single auto-pitch oscillating foil. The APWIGs presents a higher propulsive efficiency over whole speed range compared with that of single auto-pitch configuration, especially for the relatively large advance speed resulting in a small reduced frequency. When the advance speed is larger than a critical value, the efficiency of single auto-pitch oscillating foil propulsor starts to drop dramatically. However, the APWIGs tends to keep a nearly constant high efficiency and show a trend of independence of speed at the large speed region, suggesting APWIGs has a wider applied range of operating speed compared with single-foil configuration.

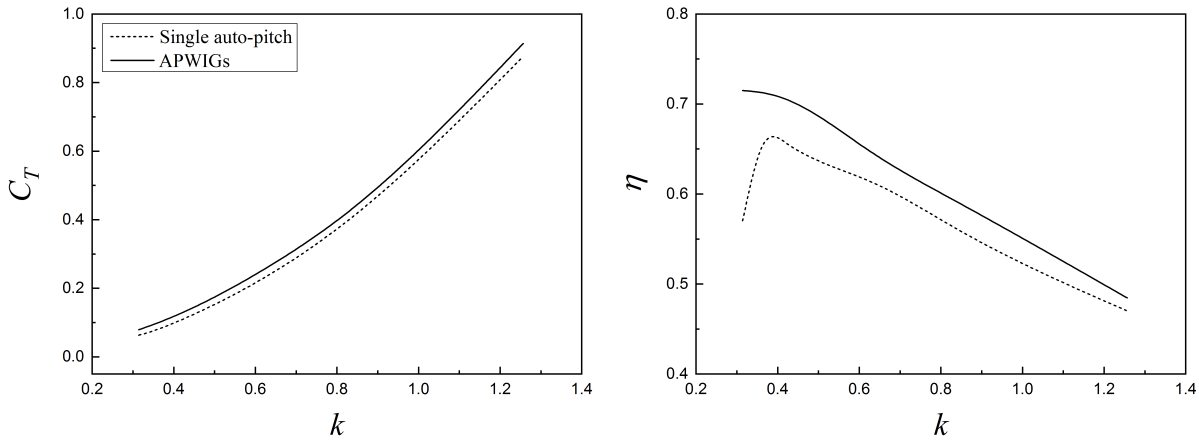

(a) Thrust coefficient (b) Propulsive efficiency

Figure 5-1 Comparison of propulsive performance between APWIGs and single auto-pitch oscillating foil configuration.

The unstable pitching motion of single auto-pitch configuration at the relatively high advance speeds is considered as the main reason for such a behavior. Figure 5-2 presents the comparison of time history of pitching angle over one oscillatory cycle between APWIGs and single auto-pitch configuration. When the advance speed is relatively low corresponding to a high *k*, both APWIGs and single foil show a stable and periodic pitching variation. At the relatively high advance speeds, APWIGs still can

maintain a stable pitching motion due to the biplane arrangement, while the pitching angle of single foil shows an irregular time variation and obvious discrepancy with that of APWIGs. Such a non-periodic and unstable pitching variation dramatically reduces the time-averaged thrust for the single auto-pitch configuration, and hence leads to the drop of efficiency at a lower reduced frequency. At the reduced frequency of 0.31, the efficiency of these two configurations is 71% and 57%, respectively. It was suggested that the efficiency increase by the WIG effect is about 14% for this case.

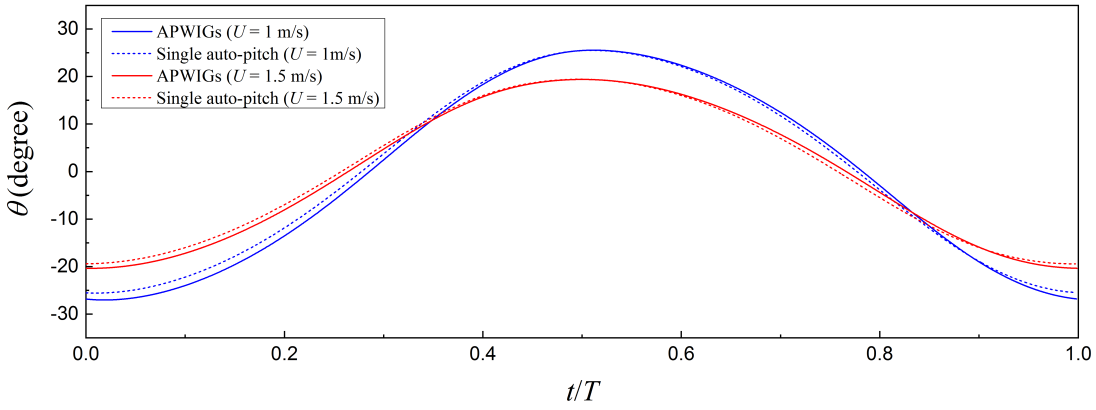

(a) Low advance speed

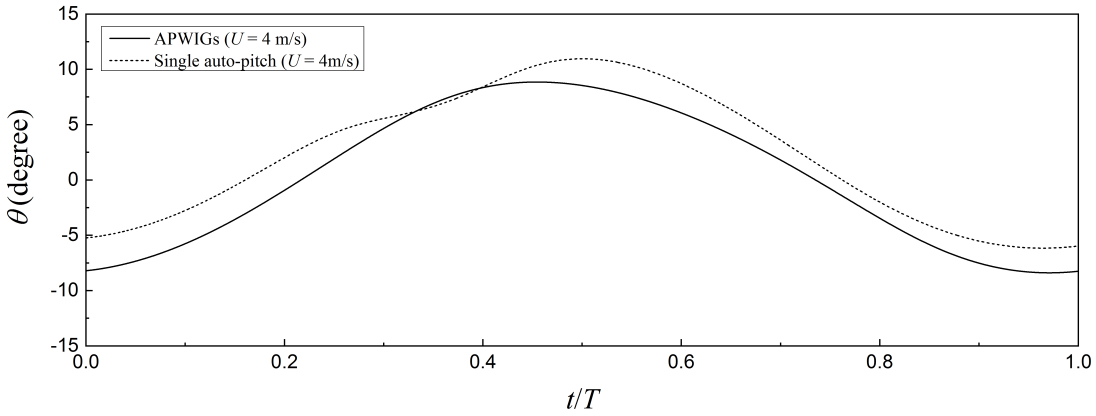

(b) High advance speed

Figure 5-2 Comparison of flow-induced pitching angle over one oscillatory cycle between APWIGs and single auto-pitch oscillating configuration.

5.3 Comparison with Biplane Heave-only Configuration

The comparison of propulsive characteristics between APWIGs and biplane heave-only configuration is employed to demonstrate the importance of pitching motion. The pioneering studies on the biplane configuration with heave-only motion were conducted by Jones et al. (1997) and Liu (2005b). The kinematics for this subsection is characterized as the heaving amplitude of 0.5c, oscillating frequency of 4Hz, and mean distance between two foils of 1.8c.

5.3.1 Start-up thrust generation

At the start-up point, i.e., sudden acceleration, oscillating foils using the heave-only mechanism may produce insufficient thrust due to the constant AoA of 90 degrees. The flow separation and stall angle at the start-up speed can be reduced substantially by adding a self-controlled pitch. For the start-up computation, a uniform flow with zero inlet velocity is initialized for the whole domain at first, and then the heaving motion of each foil is activated. The time variation of generated thrust over the first oscillatory cycle is compared between APWIGs and dual-foil heave-only propulsor in Figure 5-3. A relatively high torsional spring stiffness of 2Nm/rad was used in this case to avoid extremely large pitching angle. As the results show, the APWIGs produces a larger thrust over whole oscillatory cycle compared with the heave-only configuration. The time-averaged thrust over the first oscillatory cycle for APWIGs and dual-foil heave-only propulsor is 44.6N and 10.5N, respectively. By adding a spring-based pitching flexibility, the APWIGs can produce more than quadrupled time-averaged thrust than heave-only mode at the sudden acceleration.

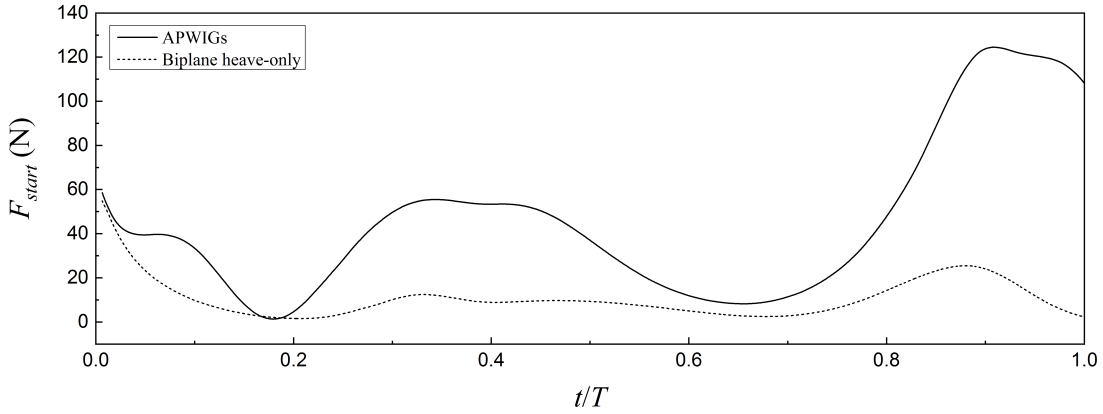

Figure 5-3 Comparison of start-up thrust generation at the first oscillatory cycle between APWIGs and biplane heave-only oscillating foil configuration.

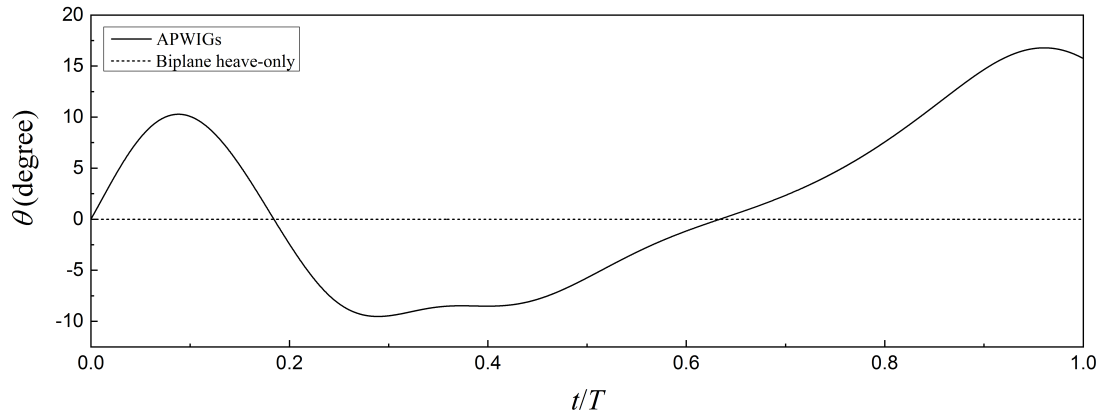

Figure 5-4 Comparison of pitching angle at the first oscillatory cycle between APWIGs and biplane heave-only oscillating foil configuration.

The time variation of pitching angle for two configurations is shown in Figure 5-4. Compared with the constant zero pitching angle produced by the prescribed heave-only mode, the pitching motion of APWIGs is adjusted automatically by flow around the oscillating foils and generates an effective AoA less than 90 degrees within the certain period.

5.3.2 Propulsive performance

The comparison of propulsive characteristics between APWIGs and biplane heave-only oscillating foil configuration is shown in Figure 5-5. An evident advantage of the produced thrust and propulsive efficiency for the auto-pitch configuration over the oscillating foil propulsor with a heave-only motion was observed. The maximum increase of around 50% in propulsive efficiency can be identified by introducing a flow-adapted pitching motion. Figure 5-5 suggests that the oscillating foil using the single heaving oscillation cannot provide the satisfactory propulsive performance.

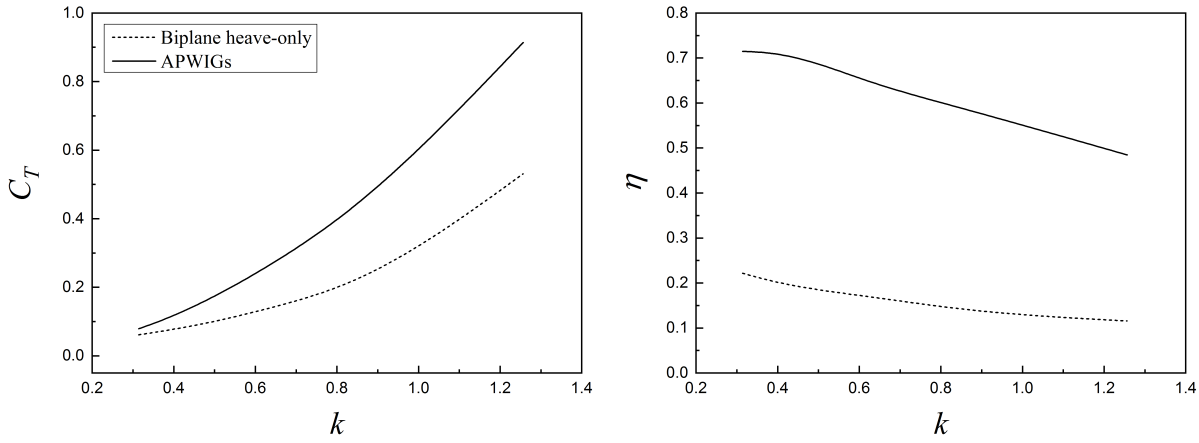

(a) Thrust coefficient (b) Propulsive efficiency

Figure 5-5 Comparison of propulsive performance between APWIGs and biplane heave-only oscillating foil configuration.

5.3.3 Flow patterns

The evolution and shedding of vortices over one oscillatory cycle for APWIGs and biplane heave-only propulsor at the speed of 2m/s resulting in a reduced frequency of 0.63 are shown in Figure 5-6. The maximum effective AoA for two configurations is 16.7 and 32.1 degrees, respectively. It means that the flow separation and resulting stall for dual-foil heave-only configuration are unavoidable. As the results show, the vortex contours of first foil are nearly symmetrical to that of second foil about the ground plane between two foils. Clear vortex structures around the foils were captured by the current numerical model, which significantly affect the propulsive performance of oscillating foils.

For the APWIGs, the smooth trailing-edge vortex shedding shows a good flow attachment on the foil surface. However, due to such a large resulting effective AoA for the dual-foil heave-only configuration, both the trailing-edge vortex shedding and the dynamic-stall vortex shedding around leading edge can

be observed over the whole oscillatory cycle. Based on the comparison of performance between two configurations, it was believed that the leading-edge vortex shedding may lead to a part of energy loss and have an unfavorable effect on thrust production of oscillating foils. In terms of wake characteristics, the APWIGs tends to produce a series of pure wake structures and dissipate quickly. But for the dual-foil heave-only propulsor, the wake structures are much more complicated and spread more widely due to the influence of dynamic-stall vortex shedding. Similar trend of wake features for biplane heave-only configuration were recorded experimentally by Jones et al. (2002a).

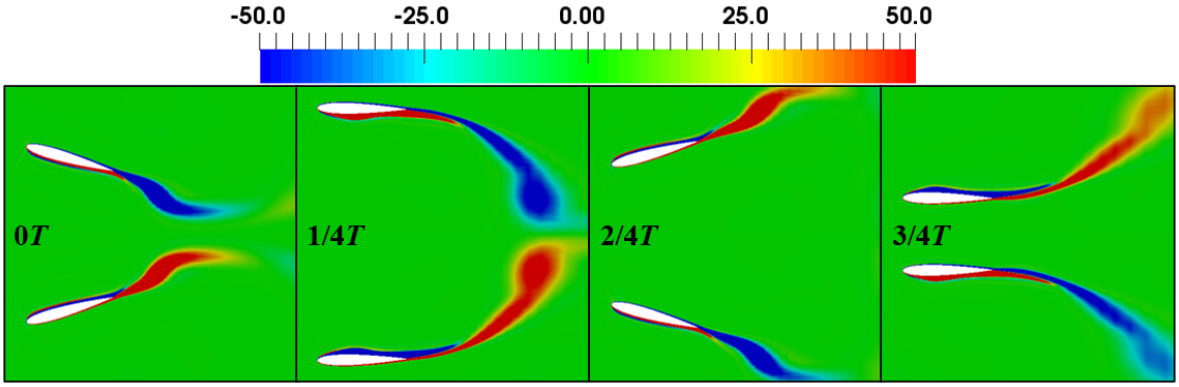

(a) APWIGs

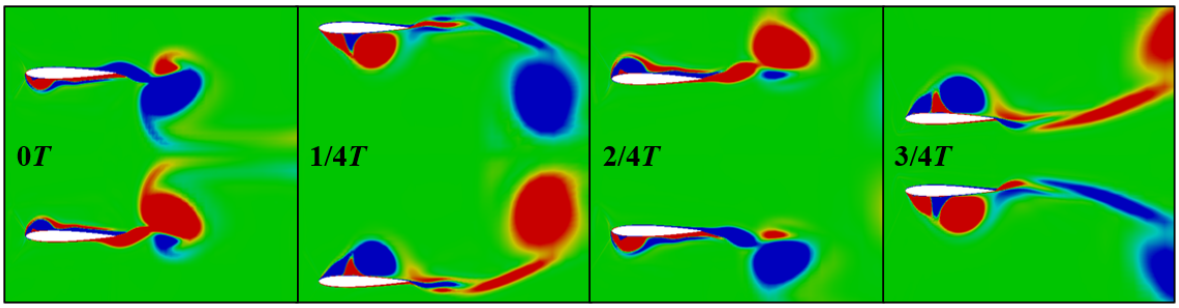

(b) Biplane heave-only configuration

Figure 5-6 Comparison of vortex contours at four instants between APWIGs and biplane heave-only oscillating foil configuration.

5.4 Comparison with Biplane Fully-prescribed Configuration

To signify the superiority of flow-adapted pitching mechanism, the performance comparison between APWIGs and biplane fully-prescribed oscillating foil configuration with different pitching amplitudes was conducted. The propulsive characteristics of biplane fully-prescribed configuration have been extensively examined by Jones and Platzer (1999), Jones et al. (2001) and Tuncer and Kaya (2003). To ensure the validity of comparison, the selection of pitching amplitudes for biplane fully-prescribed configuration was to cover the flow-induced pitching variation of APWIGs. Since the maximum flow-induced pitching angle for APWIGs is less than 30 degrees within the current parametric scope, three

pitching amplitudes are broadly tested for the fully-prescribed configuration including 10 degrees, 20 degrees and 30 degrees. The pitch-leading phase angle for the fully prescribed system is fixed at 90 degrees. In addition, the kinematics for two configurations were remained consistent with a heaving amplitude of 0.5c, oscillating frequency of 4Hz, and mean distance between two foils of 2c.

5.4.1 Propulsive performance

Figure 5-7 presents the comparison of propulsive efficiency as a function of advance coefficient between APWIGs and the fully imposed configuration with a rigid shaft. As the results show, the maximum efficiency of APWIGs is 68.9% at the advance coefficient of 5.87, while the peak of efficiency for the fully prescribed system is 72.9%, 69.0%, 56.4% with pitching amplitudes of 10, 20, 30 degrees, respectively. For the rigid-foil configuration, the propulsive performance tends to drop rapidly after the advance number is larger than a certain value depending on the pitching amplitude. However, by adding a spring-based pitching elasticity, the APWIGs achieves the propulsive efficiency over 60% within a much wider range of advance coefficient compared with the fully imposed mechanism. In addition, it can be seen that the efficiency curve of APWIGs tends to connect all the peaks of rigid-foil configuration with different pitching amplitudes, which was also numerically reported by Thaweewat et al. (2018) for a single oscillating foil.

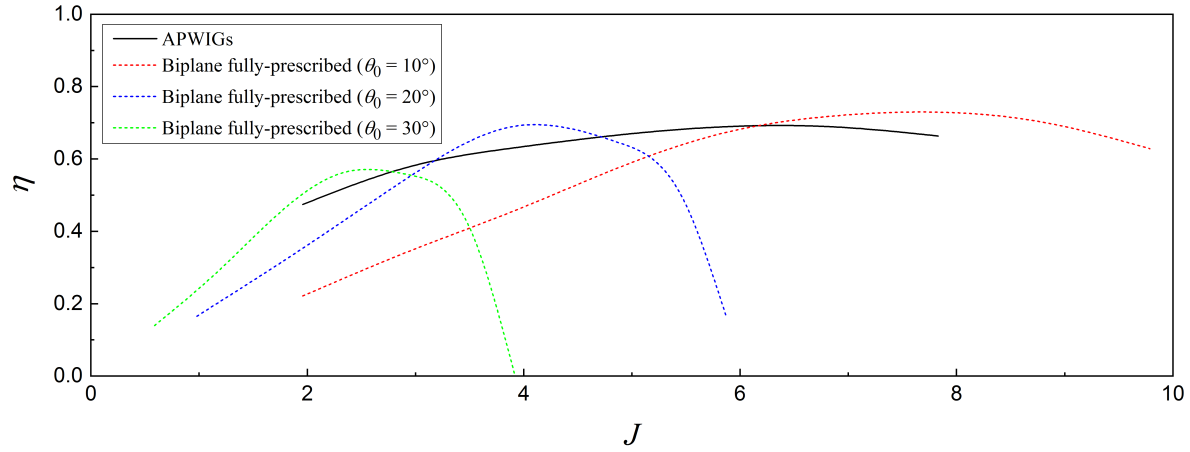

Figure 5-7 Comparison of propulsive performance between APWIGs and biplane fully-prescribed oscillating foil configuration with different pitching amplitudes.

5.4.2 Dynamic responses of APWIGs

Such a propulsive characteristic is mainly attributed to the different responding mechanisms to the flow separation and resulting stall by two propulsion systems. Basically, the instantaneous effective AoA of the fully prescribed configuration is determined by the given kinematic parameters since the surrounding flow has no influence on the foil motion. In contrast, the time-varying pitching angle of APWIGs is adjusted by the flow forces acting on the oscillating foils, which can substantially reduce the maximum effective AoA and hence the flow separation during operation.

Figure 5-8 presents the time variation of flow-induced pitching angle and corresponding effective AoA over five oscillatory cycles for APWIGs. It can be seen that the maximum pitching angle of APWIGs show a decreasing trend with an increase of advance coefficient. The peaks of effective AoA at the advance coefficient of 1.96, 3.92, 5.87, 7.83 are 27.0, 16.4, 12.0, 10.9 degrees, respectively. In general, the stall angle for an unsteady oscillating foil will be delayed to approximately 20 to 25 degrees depending on the kinematics of configuration (Akbari and Price, 2003). Consequently, the severe flow separation can be avoided by the self-controlled pitching motion of APWIGs within a relatively wide range of advance coefficient. Considering the rigid-foil configuration with the pitching amplitude of 10 degrees, the maximum effective AoA at four advance coefficients are 41.5, 22.1, 12.7 and 7.4 degrees, respectively. Obviously, the severe flow separation is inevitable at the advance coefficient of 1.96 due to the extremely large effective AoA of 41.5 degrees, which produces a relatively poor propulsive performance as shown in Figure 5-7. Therefore, it is reasonable to conclude that the limitation of applicable speed range for the fully prescribed configuration can be greatly improved by the APWIGs with a proper spring stiffness.

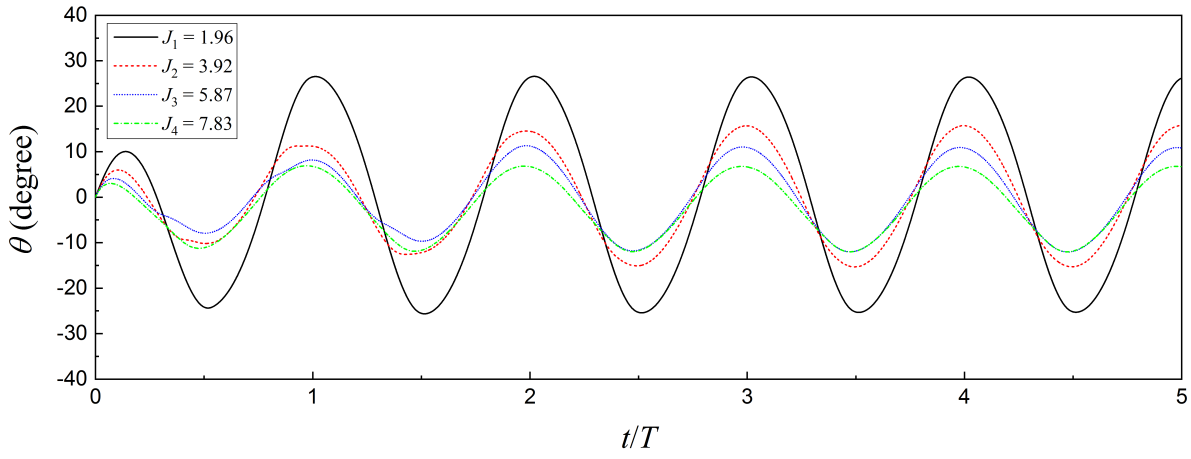

(a) Flow-induced pitching angle

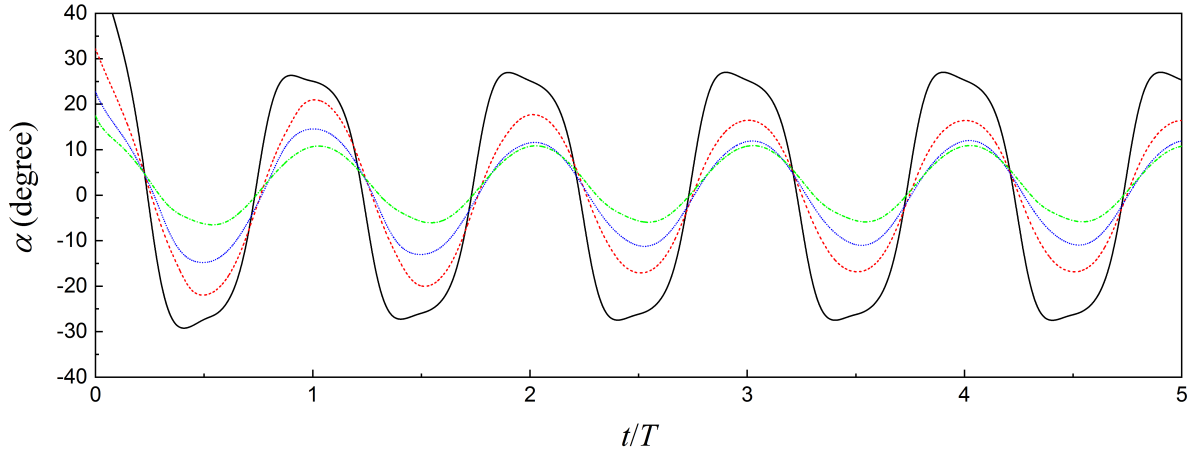

(b) Effective AoA

Figure 5-8 Time variation of dynamic responses for APWIGs at different advance speeds.

5.4.3 Flow behaviors and wake profiles

To further investigate the inherent thrust-producing mechanism for APWIGs, Figures 5-9, 5-10 and 5-11 present the velocity contours in m/s over one oscillatory cycle at three advance speeds, respectively. The velocity surplus can be seen along the wake of each case. Such a jet-like region of velocity field is mainly attributed to the generated reverse Kármán vortex streets.

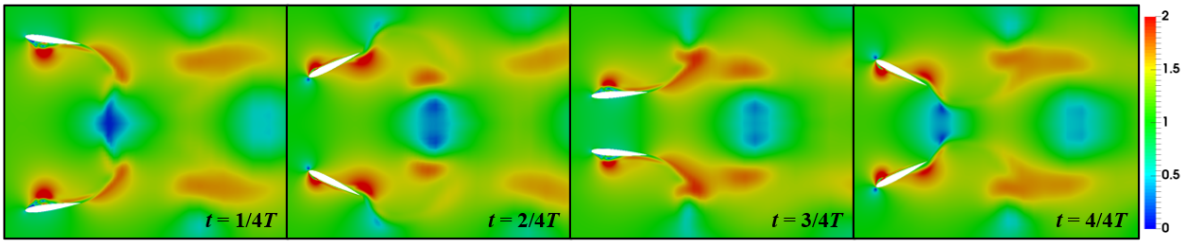

Figure 5-9 Velocity contours of APWIGs at four instants over one oscillatory cycle for the advance speed of $J = 1.96$.

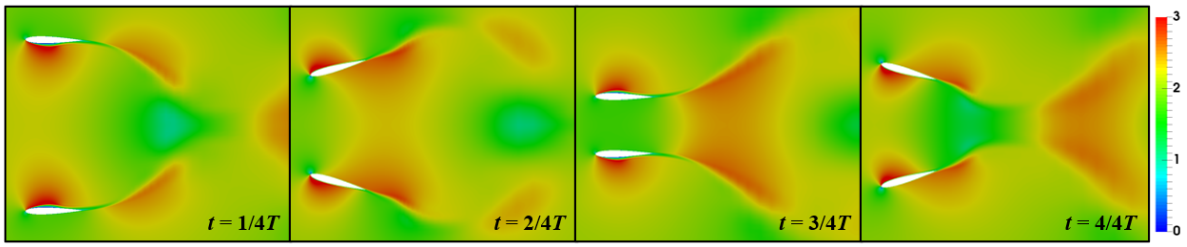

Figure 5-10 Velocity contours of APWIGs at four instants over one oscillatory cycle for the advance speed of $J = 3.92$.

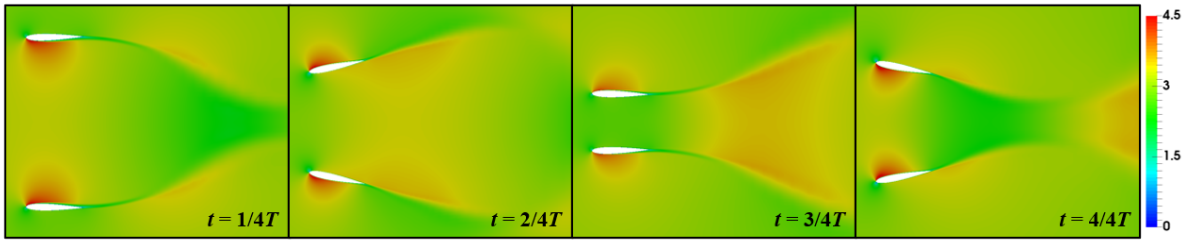

Figure 5-11 Velocity contours of APWIGs at four instants over one oscillatory cycle for the advance speed of $J = 5.87$.

For the low advance speeds, the flow separation along both leading edge and trailing edge can be found due to the high instantaneous effective AoA, which results in the relatively low efficiency of 47.4% for APWIGs. When the APWIGs operates at a high advance coefficient, the highly attached flow along the leading edge of foils was found. Only slight flow separation along the trailing edge can be seen. It has been indicated that the leading-edge vortex behaviors have a significant effect on the thrust-producing characteristics of oscillating foils (Platzer et al., 2008). Results suggested that a constantly high

propulsive efficiency can be obtained for APWIGs operating at a relatively high advance speed due to the low flow separation and plain vortex behaviors along the leading edge.

The time-averaged wake profiles for horizontal velocity corresponding to Figures 5-9, 5-10 and 5-11 are presented in Figures 5-12, 5-13 and 5-14, respectively. The cross-section probes are set at one and half chord length downstream of the trailing edge. It can be seen that a narrow profile of wake jet is generated along the downstream of each foil, while the equilibrium plane between two foils appears a velocity deficit. The wake profile of one foil is symmetric to that of another foil with respect to the produced ground plane. In addition, the wake jet of each oscillating foil tends to be slenderer with the increase of advance coefficient. Such a wake velocity profile provides a much more straightforward demonstration towards the physical mechanism of thrust generation for APWIGs. The stable operation of the propulsion system at a given flow condition can always produce a momentum surplus over an oscillatory cycle, which inherently leads to the forward thrust production.

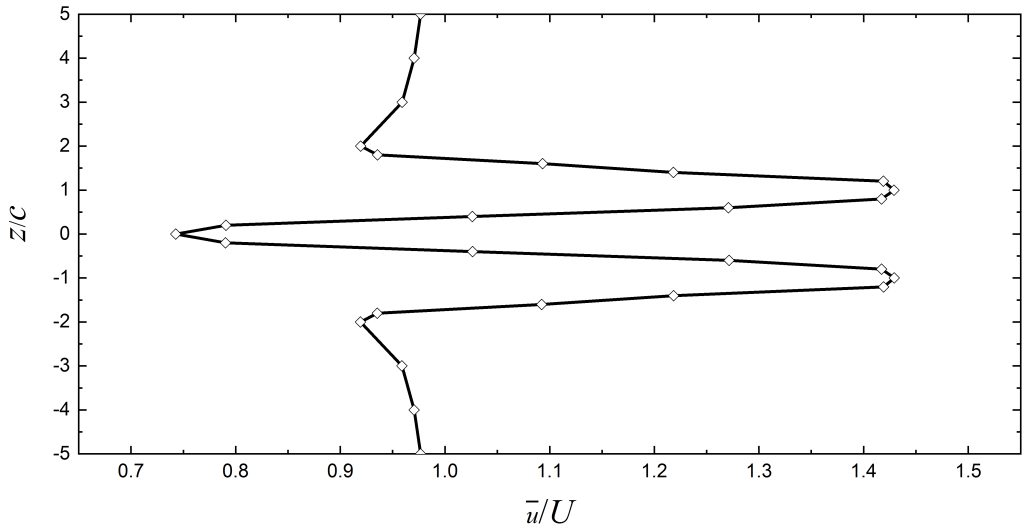

Figure 5-12 Downstream time-averaged velocity profile of APWIGs for the advance speed of $J = 1.96$.

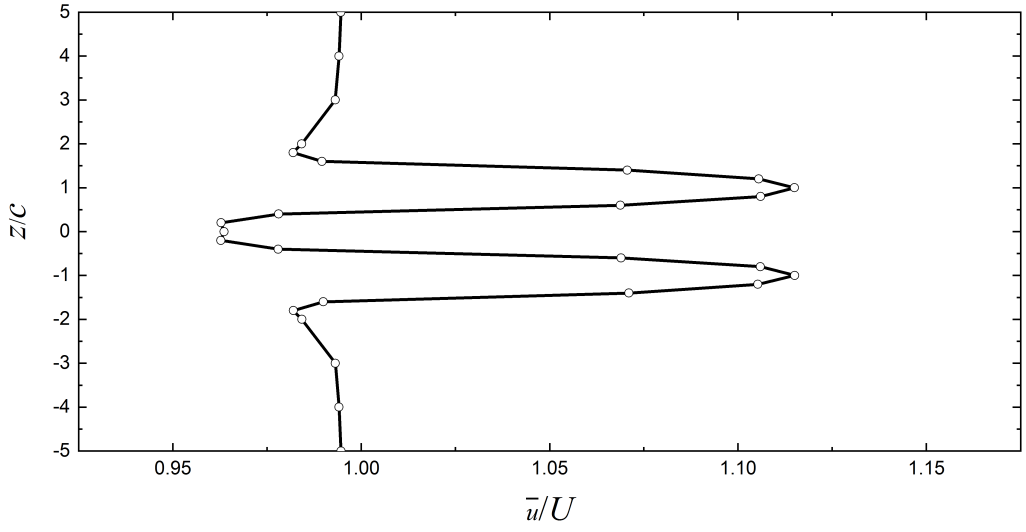

Figure 5-13 Downstream time-averaged velocity profile of APWIGs for the advance speed of $J = 3.92$.

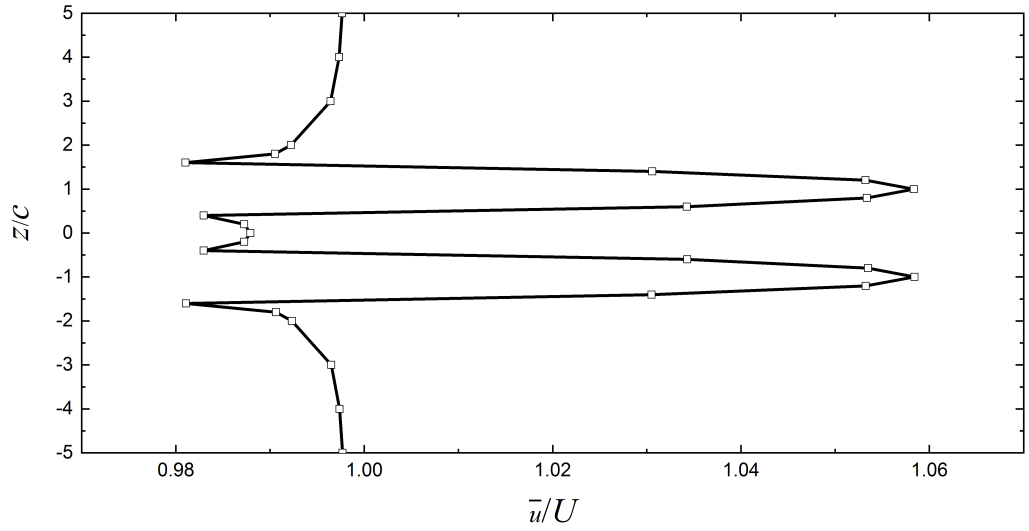

Figure 5-14 Downstream time-averaged velocity profile of APWIGs for the advance speed of $J = 5.87$.

5.5 Indication of Superiority for APWIGs

The comprehensive comparison of performance metrics involving four concerned configurations was performed to highlight the credibility of APWIGs as a marine propulsor. To confirm the validity of preceding implications under different scales, a chord length of 0.2m was employed for the current simulations. The frequency of actively imposed oscillation was selected as 4Hz. The mean distance between two foils and heaving amplitude were set as $1.2c$ and $0.3c$, respectively. The range of 5 to 15 degrees for the pitching amplitude of biplane fully-prescribed configuration was taken to cover the maximum flow-induced pitching angle of APWIGs. Both the hydrodynamic characteristics and flow features were considered in this systematic comparison.

5.5.1 Propulsive performance

Sections 5.5.1 and 5.5.2 have been removed for copyright or proprietary reasons. They have been published in: Wang, J., Lui, P., Chin, C., He, G., 2020. Auto-pitch wing-in-ground effect oscillating foils for marine propulsion. The 30th International Ocean and Polar Engineering Conference, ISOPE-2020. International Society of Offshore and Polar Engineers.

Figure 5-15 Comprehensive comparison of propulsive characteristics between various configurations at the function of advance speed.

5.5.2 Vortex structures and wake patterns

(a) APWIGs

(b) Single auto-pitch configuration

(c) Biplane heave-only configuration ($\theta_0 = 0°$)

(d) Biplane fully-prescribed configuration ($\theta_0 = 15°$)

Figure 5-16 Downstream time-averaged velocity profile for different configurations.

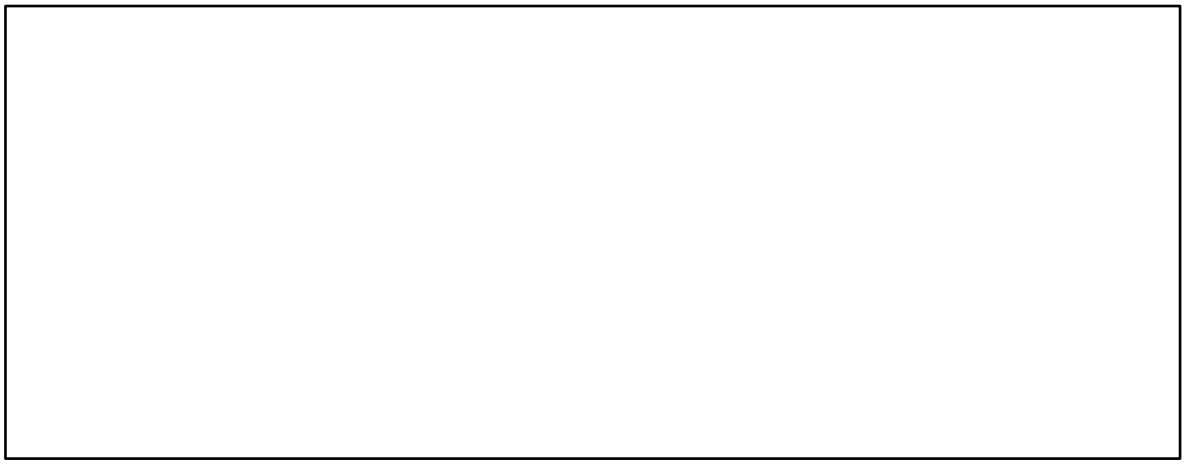

Figure 5-17 Schematic of thrust-producing vortical structure in the wake of oscillating foil.

(a) APWIGs (b) Single auto-pitch configuration

(c) Biplane heave-only configuration ($\theta_0 = 0°$) (d) Biplane fully-prescribed configuration ($\theta_0 = 15°$)

Figure 5-18 Vortical contours in the wake of oscillating foils for different configurations at four instants over one oscillatory cycle.

5.5.3 Summary of performance metrics

To clearly highlight the superior advantages of APWIGs, the performance metrics for considered oscillating foil configurations in the current simulations are summarized in Table 5-2. Since the propulsive performance of oscillating foils is highly correlated to flow behaviors, the properties in terms of both hydrodynamic characteristics and flow structures were demonstrated for each configuration.

For the APWIGs system, two major advantages over other configurations can be identified. Firstly, it can generate a satisfactory propulsive performance with the efficiency of over 70%. Secondly, it tends to be independent of advance speed. It also should be noted that the torsional spring stiffness needs to be tested for the specific flow conditions implying additional manufacturing cost and difficulty. The single auto-pitch oscillating foil has the same advantages with that of APWIGs. However, the single oscillating foil generally suffers from the issue of lateral forces which may lead to the vibration and instability for the target vehicle. These lateral forces can be balanced by a biplane configuration with the counter-phase heaving motion.

The biplane heave-only configuration has the modest demand for the system actuators due to its straightforward kinematics. Nevertheless, the inferior propulsive performance produced by this system indicates that the single oscillating mechanism is not appropriate for the propulsion application of oscillating foils. Furthermore, it also encounters the issue of start-up thrust generation in the still water. By introducing an actively imposed pitching motion, the biplane fully-prescribed oscillating foil configuration can achieve a relatively high propulsive efficiency. The fully prescribed pitching and heaving motion implies the flexibility of parameter adjustment, while it also results in the difficulty of performance optimization and complicated governing mechanism for system actuators. In addition, the biplane fully-prescribed oscillating foil configuration is highly sensitive to the advance speed which significantly reduces its universality of practical application.

The downstream time-averaged velocity profile along the equilibrium centerline of configuration is an indication of either thrust-producing regime or drag-producing regime. The single oscillating foil produces an individual velocity surplus in the downstream flow without any deficit feature. The velocity profile for the biplane configuration has two surplus features and one deficit feature. The maximum velocity surplus is captured in the downstream flow of biplane fully-prescribed configuration which corresponds to the identified highest efficiency for this system under a certain condition. The vortex structures tend to shed from the trailing edge for the oscillating foils using combined heaving and pitching motion, while apparent vortex shedding from both leading edge and trailing edge can be identified for the heaving oscillating foil system. The severe vortex behaviors for the biplane heave-only configuration agree well with the hackly profile of downstream time-averaged velocity. Hence, the smooth time-averaged velocity profile for other three configurations can be attributed to the modest vortex shedding. Since four oscillating foil configurations achieve a thrust-producing regime, the reverse Kármán vortex street was observed in the wake of all oscillating foils. The severe vortex

shedding by heave-only motion also leads to a highly complicated wake flow pattern. The structure of wake vortices behind each foil of APWIGs is different from that of single auto-pitch oscillating foil due to the vortex interactions. The flow-adapted pitching mechanism was found to generate the smoothest flow pattern in the wake implying the satisfactory hydrodynamic performance.

Table 5-2 Summary of performance metrics for four oscillating foil configurations.

Characteristics		**APWIGs**
Propulsion	Advantages	High efficiency and independence of advance speed
	Disadvantages	Optimization of torsional spring stiffness
Flow	Velocity Profile	Two large velocity surplus and one small velocity deficit
	Vortex Shedding	Modest vortex shedding from trailing edge
	Wake Pattern	Two sets of reverse Kármán vortex street with smooth profile
Characteristics		**Single auto-pitch configuration**
Propulsion	Advantages	High efficiency and independence of advance speed
	Disadvantages	Stiffness optimization and instability due to the lateral forces
Flow	Velocity Profile	One large velocity surplus and no velocity deficit
	Vortex Shedding	Modest vortex shedding from trailing edge
	Wake Pattern	One set of reverse Kármán vortex street with smooth profile
Characteristics		**Biplane heave-only configuration**
Propulsion	Advantages	Modest requirement for system actuator
	Disadvantages	Low efficiency and zero start-up thrust
Flow	Velocity Profile	Two small velocity surplus and one large velocity deficit
	Vortex Shedding	Severe vortex shedding from both leading and trailing edges
	Wake Pattern	Two sets of reverse Kármán vortex street with stretched profile
Characteristics		**Biplane fully-prescribed configuration**
Propulsion	Advantages	High efficiency and flexible adjustment
	Disadvantages	High sensitivity to flow conditions and kinematic parameters
Flow	Velocity Profile	Two large velocity surplus and one moderate velocity deficit
	Vortex Shedding	Modest vortex shedding from trailing edge
	Wake Pattern	Two sets of reverse Kármán vortex street with smooth profile

5.6 Concluding Remarks

A comparative investigation into the propulsive characteristics between APWIGs and other widely examined configurations in the literature was performed. In addition to APWIGs, the considered systems for the comparison include the single auto-pitch oscillating foil configuration, biplane heave-only oscillating foil configuration and biplane fully-prescribed oscillating foil configuration with different pitching amplitudes. Due to the close relationship between propulsive performance and vortex behaviors, the superior advantages of APWIGs over other configurations were highlighted in terms of both hydrodynamic properties and flow behaviors.

The comparison of APWIGs with the single auto-pitch oscillating foil configuration indicates that the biplane arrangement with generated WIG effect tends to produce the higher thrust and efficiency than that of single oscillating foil. Especially under the lightly loaded conditions, the APWIGs still can maintain a relatively high efficiency, while the efficiency of single auto-pitch configuration begins to drop dramatically. The maximum increase of 14.5% in efficiency by the WIG effect was obtained in the current parametric scope. The vortex structures along the foil surface and the downstream time-averaged velocity profile of each foil for APWIGs were found to be similar to that of single auto-pitch configuration. However, the slight difference of wake pattern was identified between two configurations due to the vortex interactions of biplane arrangement.

The oscillating foils using single heaving motion generally have the issue of start-up thrust generation, which can be resolved by adding a pitching motion. Results suggested that APWIGs can produce more than four times thrust over the biplane heave-only configuration at the start-up speed, since the flow separation is substantially reduced by a flow-induced pitch. With respect to a wide range of operating speed, the significant advantages of APWIGs over heave-only mode were also obtained in terms of thrust production and propulsive efficiency. The severe vortex shedding from both leading edge and trailing edge was numerically visualized for the biplane heave-only configuration, which corresponds to the complex profile of time-averaged momentum surplus implying the thrust production.

It was found that the APWIGs can maintain a satisfactory efficiency within a wider range of advance speed over fully imposed system with a rigid shaft. By attaching a torsional spring to the pivot axis of each foil, the APWIGs can adjust the maximum pitching angle to adapt different loaded conditions, which will reduce the effective AoA and thus decrease the flow separation during operation. Although the maximum efficiency is produced by the biplane fully-prescribed configuration under certain conditions, this propulsion system shows a high dependence on the advance speed. The feature of low sensitivity to advance speed for APWIGs presents a significant potential to operate within the large scope of flow conditions. Such a characteristic can be attributed to the highly attached flow around the oscillating foils using the flow-adapted pitch and the smooth vortex structures in the wake. In general, the APWIGs promises a better choice over other commonly studied oscillating foil configurations for marine propulsion due to the highlighted advantages in various aspects.

CHAPTER 6

Three-dimensional Effect of Biplane Configurations

6.1 Numerical Setup

A series of three-dimensional numerical simulations on the WIG effect oscillating foil propulsor were performed in this section. The first focus is to explore the effect of aspect ratio on the hydrodynamic characteristics and wake topology of WIG effect configuration with fully prescribed kinematics, namely imposed heave and pitch. By testing an adequately large range of aspect ratio, the aim is to provide the relevant recommendations for the aspect ratio selection of biplane configuration in the real flow. The second focus is lied in the performance analysis of three-dimensional APWIGs. Herein, it is intended to extend the previous two-dimensional works to a three-dimensional situation and provide fundamental insights into the hydrodynamic characteristics of finite-span APWIGs.

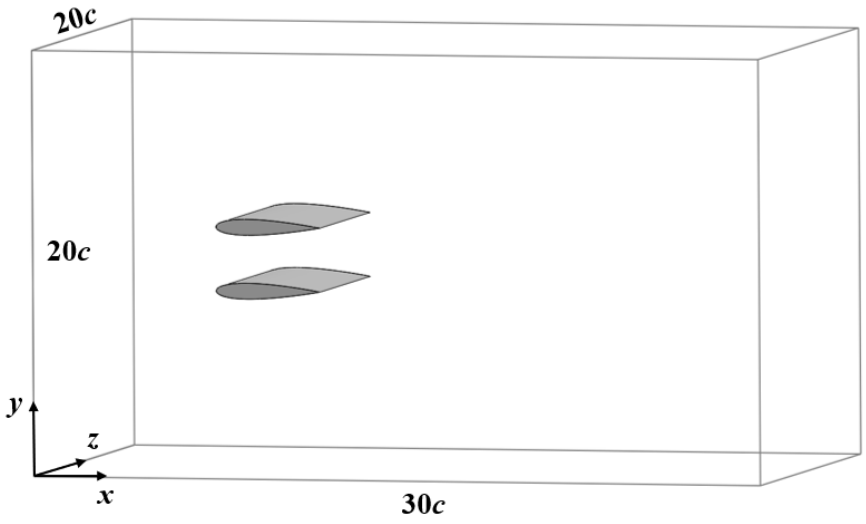

Figure 6-1 Schematic of three-dimensional computational domain for biplane configuration.

The three-dimensional computational domain for the biplane configuration is presented in Figure 6-1, which has a size of 30*c*×20*c*×20*c*. To improve the computing efficiency, the boundary condition of symmetry plane between two foils was employed to cut one half of the computational domain. In addition, other three lateral boundaries were also set as the symmetry plane to minimize the influence of borders of numerical model. Thus, the actual computational domain and corresponding mesh distributions for the current three-dimensional simulations are shown in Figure 6-2 with a dimension of 30*c*×10*c*×20*c*. The three-dimensional structured grid with refined region around foil was employed for this computation.

The parameters for the three-dimensional simulations were set as the following description if not particularly specified. The cross-section of the foil is selected as the NACA 0015. The density ratio of the structure over fluid is taken as 15 to achieve a satisfactory numerical stability. The Reynolds number based on the chord length is 200000. The mean distance between two foils and heaving amplitude are 2*c* and 0.4*c*, respectively. The pitching amplitude is 10 degrees for the prescribed configuration with a constant phase shift of 90 degrees between imposed pitch and heave. The pitching axis is set at 0.25 chord position from the leading edge. The oscillating frequency is selected as 4Hz for all cases. This

parameter setup was chosen because such a combination tends to produce a high performance based on preceding two-dimensional simulations.

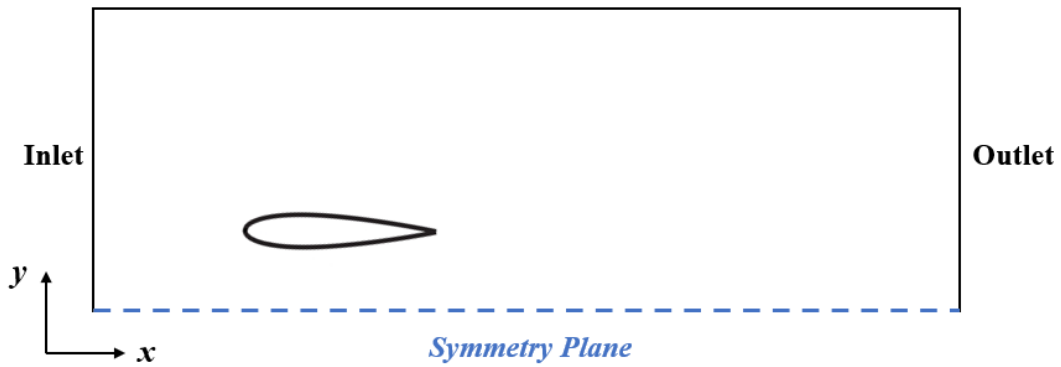

(a) Computational domain

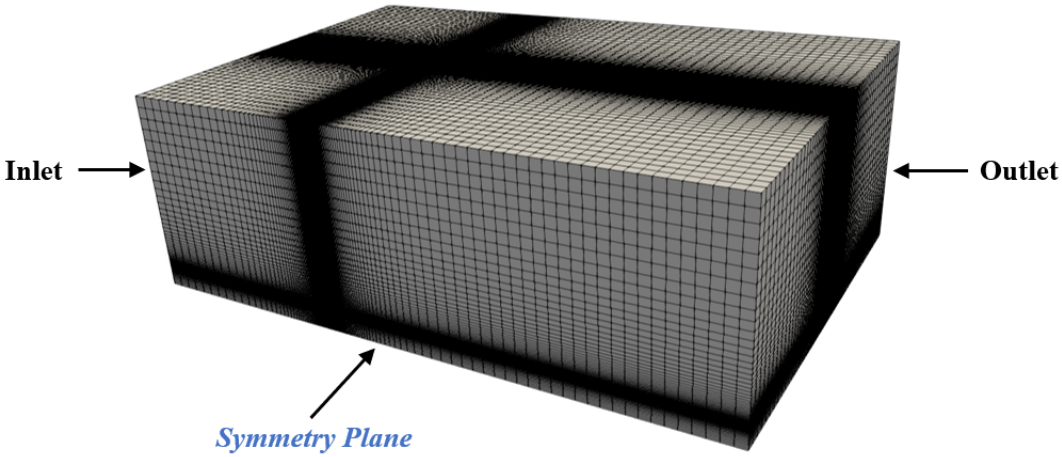

(b) Mesh distributions

Figure 6-2 Computational domain and mesh distributions using a symmetry plane in the three-dimensional simulations.

6.2 Effect of Aspect Ratio

The oscillating foil with a finite span is expected to show a significant difference with a two-dimensional case for both hydrodynamic features and vortex structures due to the three-dimensional effect. The focus of this part is to demonstrate the influence of aspect ratio on the propulsive performance of WIG effect oscillating foil propulsor. The fully prescribed configuration was employed to simplify the problem. Current computations cover a wide range of aspect ratio from 1 to 10.

6.2.1 Time-varying hydrodynamic characteristics

The typical time history of force coefficients for a three-dimensional biplane configuration (AR = 2)

using fully prescribed motion over four oscillatory cycles is shown in Figure 6-3. A two-dimensional case is also plotted in this figure as a reference. The results indicated that both two-dimensional and three-dimensional cases tend to produce the steady thrust and lift by each foil from the third oscillatory cycle. Hence, all numerical simulations were monitored over four cycles to ensure that the periodic state is achieved for each case. Note that the time-averaged results are calculated by the data of the last cycle. Both two-dimensional and three-dimensional oscillating foils nearly generate the forward thrust over whole oscillating cycle while the finite-span foil produces a smaller positive peak of thrust coefficient compared to the infinite-span foil. The same manner can be seen in the time history of lift coefficient in which a three-dimensional oscillating foil tends to decrease the lift production.

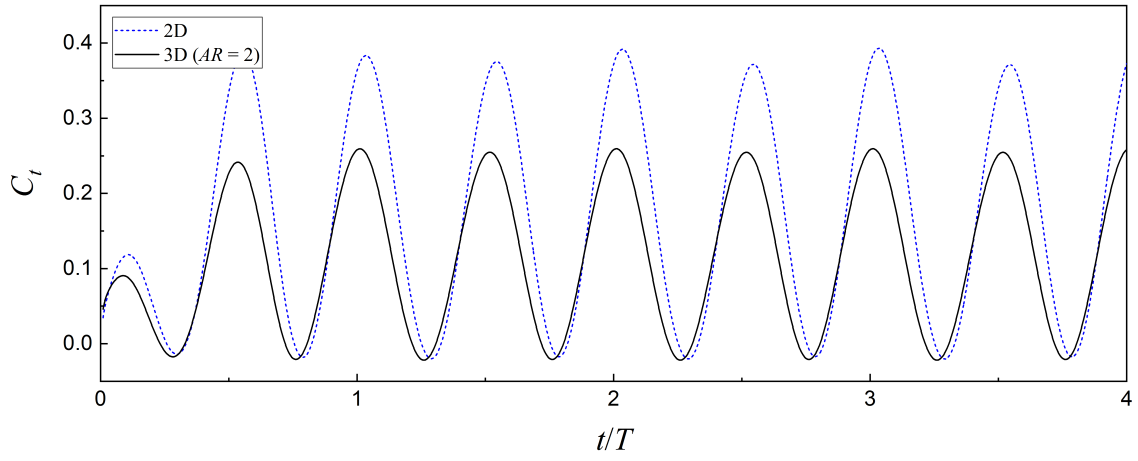

(a) Thrust coefficient

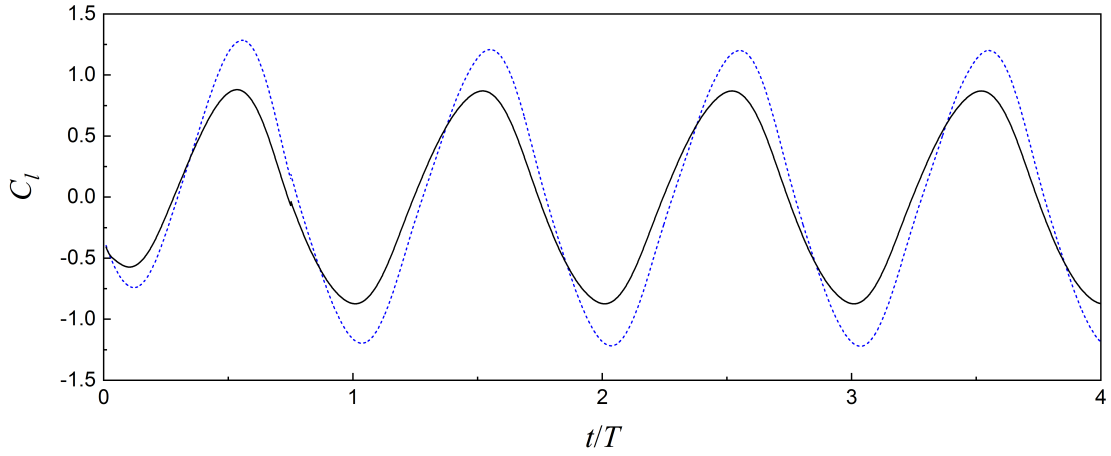

(b) Lift coefficient

Figure 6-3 Time history of force coefficients for three-dimensional biplane fully-prescribed configuration within four oscillatory cycles (Two-dimensional results are included for comparison).

The discrepancy of time-varying force coefficients between two-dimensional and three-dimensional cases are mainly due to the different vortex structures. A two-dimensional oscillating foil with the assumption of infinite span has a uniform vortex pattern along the spanwise direction. However, a finite-span oscillating foil tends to generate the distorted vortex structures around the spanwise area as a result of wing-tip influence. Such distorted vortex patterns significantly change the pressure distribution of

foil surface and hence the overall hydrodynamic characteristics. The wing-tip vortex shedding for a three-dimensional oscillating foil is another reason for the difference since such a flow behavior can induce the drag and decrease the lift. Additionally, the finite-wing effect with the downwash induced velocity is partly responsible for the force differences between two-dimensional and three-dimensional computations as in the steady hydrodynamics.

Figure 6-4 presents the time variation of force coefficients for the fully prescribed configuration with different aspect ratios. It can be seen from the results that the lower peak values of the thrust coefficient tend to be independent of the aspect ratio, while the upper peak shows a decreasing trend as the aspect ratio decreases. With respect to the lift coefficient, both lower and upper peak values tend to increase with a larger span length. The computational results plotted in Figure 6-4 show that the force coefficients of the finite-span oscillating foil are inclined to the results of two-dimensional case when the aspect ratio becomes higher. It is interesting to find that the variation of the aspect ratio also influences the phase difference of force coefficients. An oscillating foil with a smaller aspect ratio tends to reach the peak value of forces at an earlier time instant compared to the foil with a larger aspect ratio.

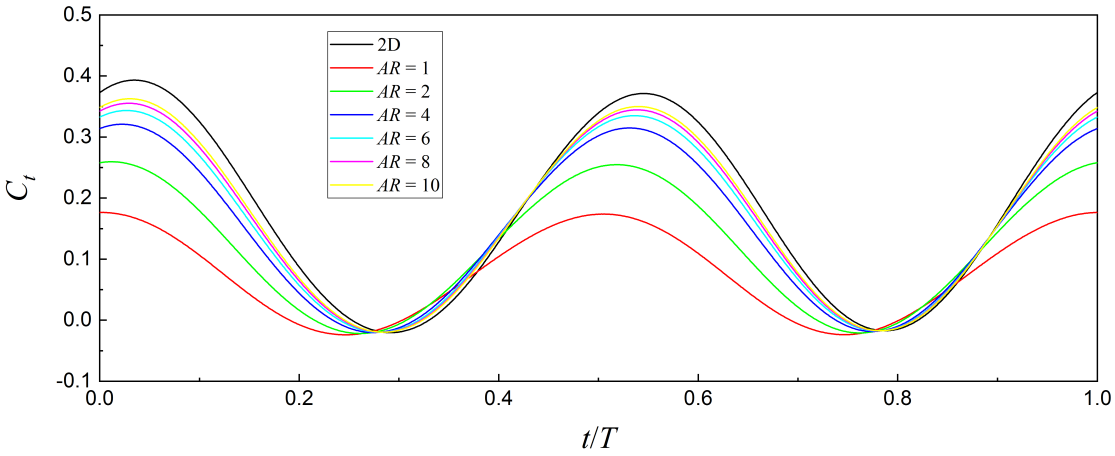

(a) Thrust coefficient

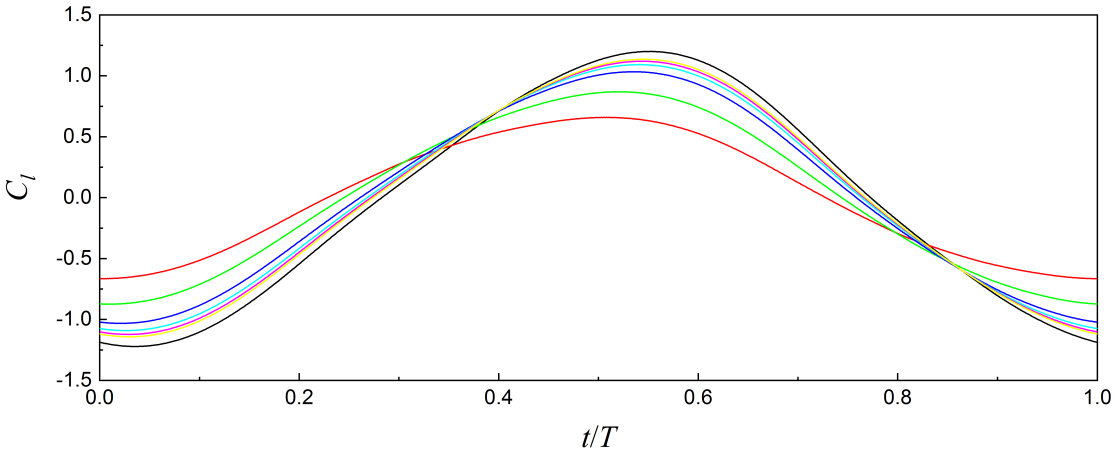

(b) Lift coefficient

Figure 6-4 Time-varying force coefficients for biplane fully-prescribed configuration with different aspect ratios over one oscillatory cycle.

Figure 6-5 shows the time variation of pitching angle and effective AoA for the biplane configuration employing a prescribed pitching motion. The profile of AoA was found to be similar with the sinusoidal pitching motion. The instantaneous maximum AoA is 16.7 degrees that occurs at the 0T and 0.5T. Such a modest value of maximum AoA implies little flow separation on the foil surface since the stall angle of an unsteady oscillating foil can be delayed to over 20 degrees depending on kinematics. Comparison of Figure 6-5 with the time variation of force coefficients in Figure 6-4 shows that both thrust and lift reach the peak value when the maximum AoA appears, especially for the low-aspect-ratio case.

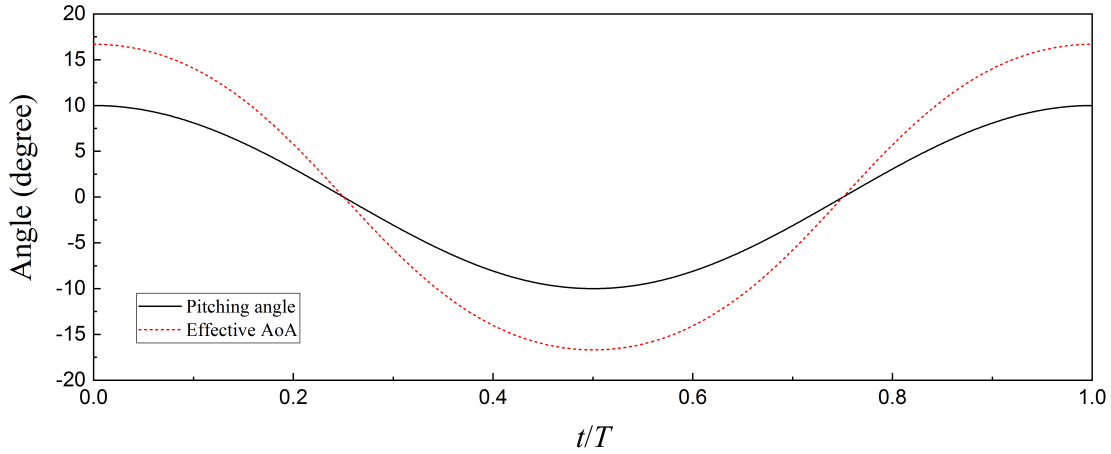

Figure 6-5 Time variation of pitching angle and effective AoA for biplane fully-prescribed configuration over one oscillatory cycle.

6.2.2 Time-averaged propulsive performance

The propulsive performance of fully prescribed biplane configuration with variation of aspect ratio is provided in Figure 6-6, in which the left figure presents the time-averaged thrust coefficient and the right figure shows the propulsive efficiency. The results of two-dimensional case are also presented in this figure denoted by a dashed line for direct comparison. The time-averaged thrust and propulsive efficiency are the direct consequences of time variation of hydrodynamic forces over one oscillatory cycle. Due to the absence of wing tips, the two-dimensional simulations show a higher performance prediction over the results by all considered aspect ratios.

As the results show, the three-dimensional effect tends to reduce both forward thrust and propulsive efficiency. The time-averaged thrust coefficient and propulsive efficiency for the two-dimensional case are 0.36 and 60.13%, respectively. With the decrease of the aspect ratio, the generated thrust and propulsive efficiency of the finite-aspect-ratio oscillating foil shows a significant decreasing trend. It can be expected that the propulsive performance of three-dimensional foil employing an adequately large span length will level off to the two-dimensional predictions. Such a significant degradation of performance for the low-aspect-ratio oscillating foil compared to the infinite-span foil is mainly attributed to the spanwise vortex behaviors. For a relatively high aspect ratio, there is a region around the midspan where both leading-edge and trailing edge vortex shedding resemble the two-dimensional

flow pattern. As a result, the propulsion characteristics of high-aspect-ratio oscillating foils approximate to two-dimensional situation. With respect to a low aspect ratio, the three-dimensional vortex structures at the midspan have an apparent discrepancy compared with the two-dimensional vortices, leading to the difference of propulsive characteristics over either high-aspect-ratio foil or infinite-span foil.

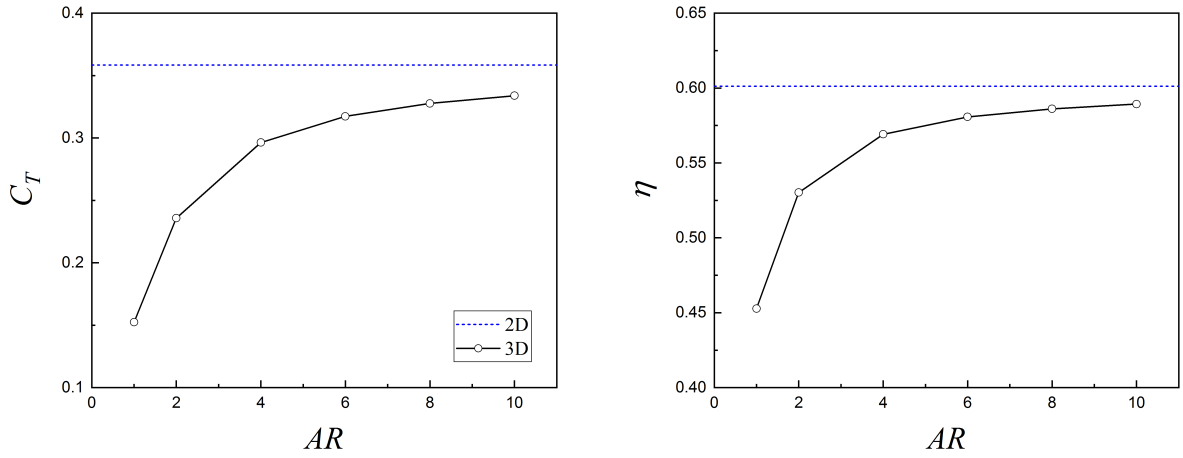

(a) Thrust coefficient (b) Propulsive efficiency

Figure 6-6 Propulsive performance of three-dimensional biplane fully-prescribed configuration with different aspect ratios (Two-dimensional results are included for comparison).

The efficiency drops of 14.85% and 1.20% were reported here compared to the two-dimensional computation for the finite-aspect-ratio foil of AR = 1 and 10, respectively. Such a significant decrease in efficiency for the low-aspect-ratio oscillating foil compared with the infinite-span foil is mainly attributed to the evident spanwise vortex behaviors, which will be discussed in the subsequent part. It should be noted that the drop of 3.22% in efficiency was observed for the finite-aspect-ratio foil of AR = 4, which is an acceptable loss with the consideration of increasing manufacturing cost and installation difficulty using a larger aspect ratio. Thus, it is reasonable to recommend a range of aspect ratio from 3 to 5 for the engineering application of WIG effect oscillating foil propulsors.

6.2.3 Vortex topologies of fully-prescribed configuration

The vortical contours for two-dimensional fully prescribed biplane configuration over one oscillatory cycle is presented in Figure 6-7, in which the clockwise and anticlockwise vortices are denoted by blue and red color, respectively. Good flow attachment can be observed around the foil surface due to the maximum effective AoA being below the dynamic-stall angle. The wake structure in the downstream of each oscillating foil is characterized as a reverse Kármán vortex street. The velocity surplus can be induced along the centerline by this vortex pattern indicating the thrust production. When the two foils get close to each other in the counter-phase motion, an imaginary ground plane can be generated between them. Thus, the vortices shed from the upper foil tend to interact with the vortices originated from the lower foil with same direction when they move towards the downstream due to the resulting WIG effect.

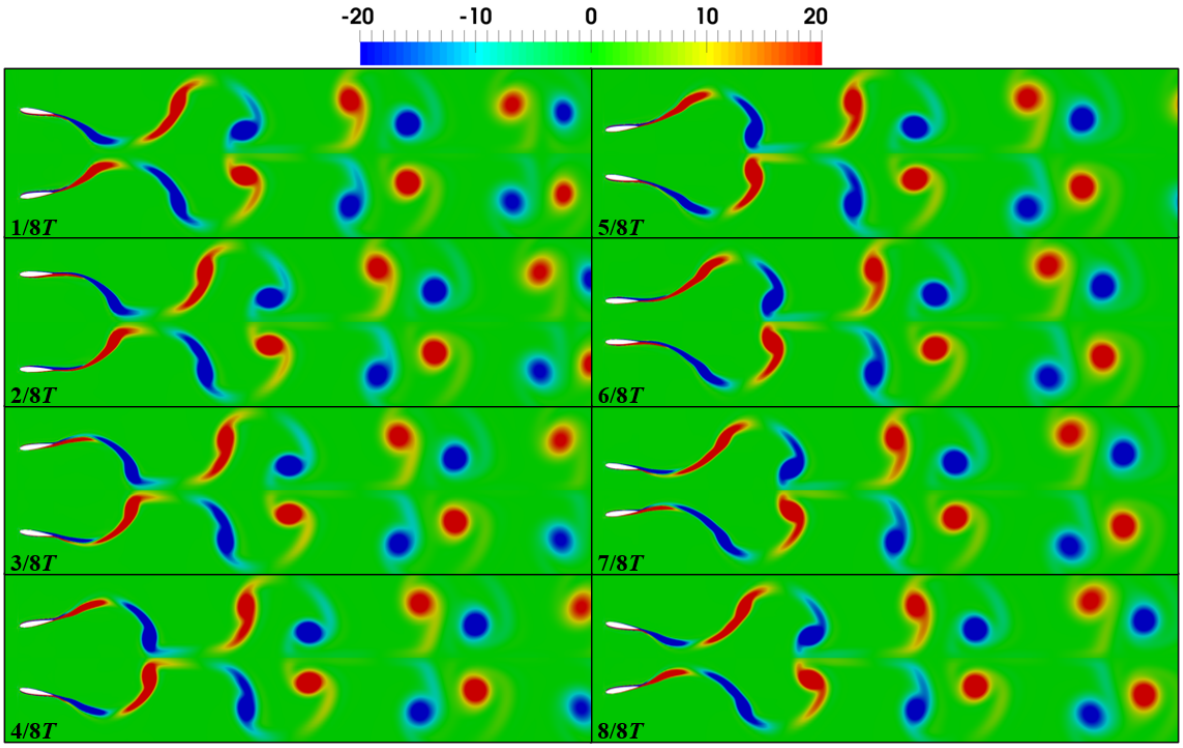

Figure 6-7 Wake vortical contours at eight instants over one oscillatory cycle for two-dimensional biplane fully-prescribed configuration.

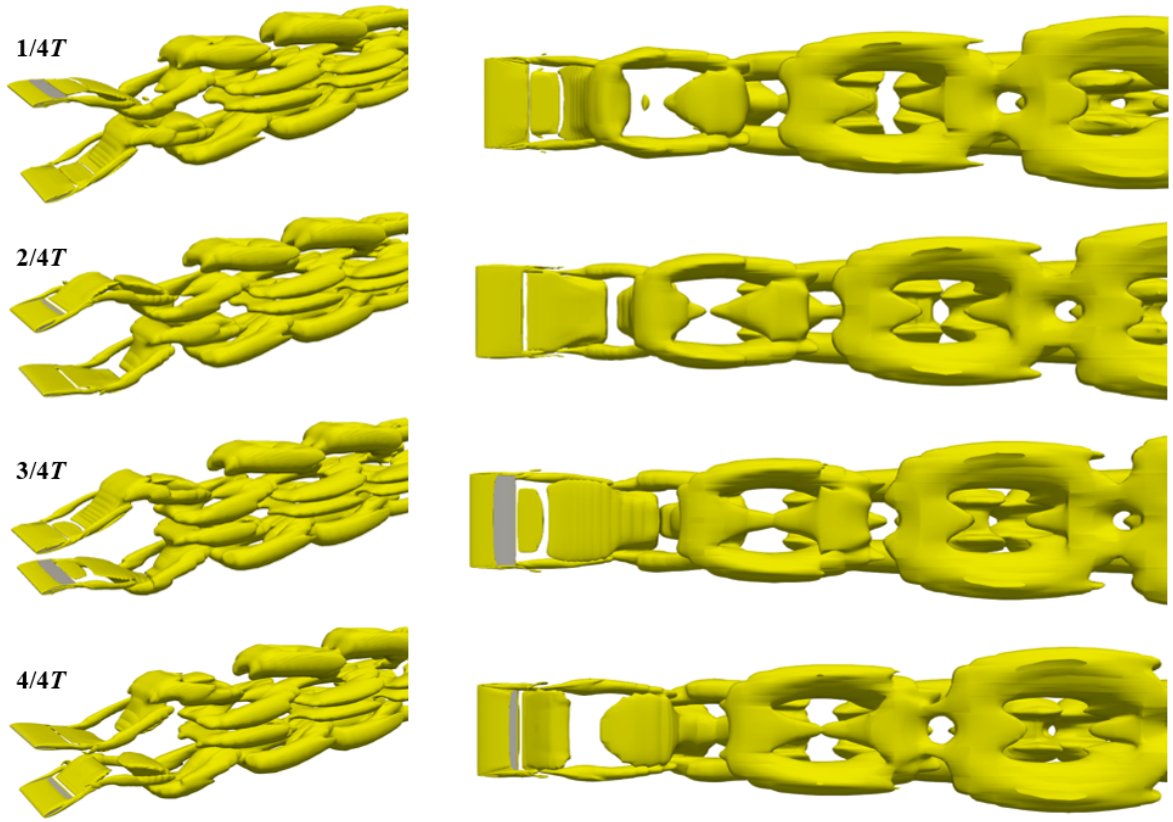

Figure 6-8 Vortex topologies identified using $Q = 0.05$ for biplane fully-prescribed configuration with $AR = 2$ over one oscillatory cycle (Left: Perspective view, Right: Top view).

The detailed process of vortex shedding and evolution for a two-dimensional case has been provided in preceding sections. Here, the main attention is concentrated on the three-dimensional vortex structure and wake topology for the WIG effect configuration. In the current study, the Q-criterion (Hunt et al., 1988) was used to identify the three-dimensional vortex topology which is defined by the iso-surface of the second invariant of the velocity gradient tensor Q. The iso-surface of $Q = 0.05$ was employed in the current three-dimensional vortex visualization that follows the setup by Deng et al. (2014). The vortex topologies for the aspect ratio of 2 over one cycle is shown in Figure 6-8, in which the low-aspect-ratio characteristics still dominate. The left column presents the perspective view and the right column provides the top view.

Although several common features including the vortex shedding from the trailing edge and satisfactory flow attachment around foil surface can be observed between infinite-span foil and finite-span foil, it was found that the three-dimensional vortex structures have little resemblance to the wake pattern of the two-dimensional oscillating foil. Such a characteristic indicates that the two-dimensional insights may not serve well for the actual three-dimensional flow. It can be seen from the perspective view that the wake topology of a finite-span oscillating foil is characterized as two sets of vortex rings that moves towards the downstream along the centerline of each foil. From the top view of vortex topology, the spanwise length of each vortex ring increases as the vortices further convect to the downstream.

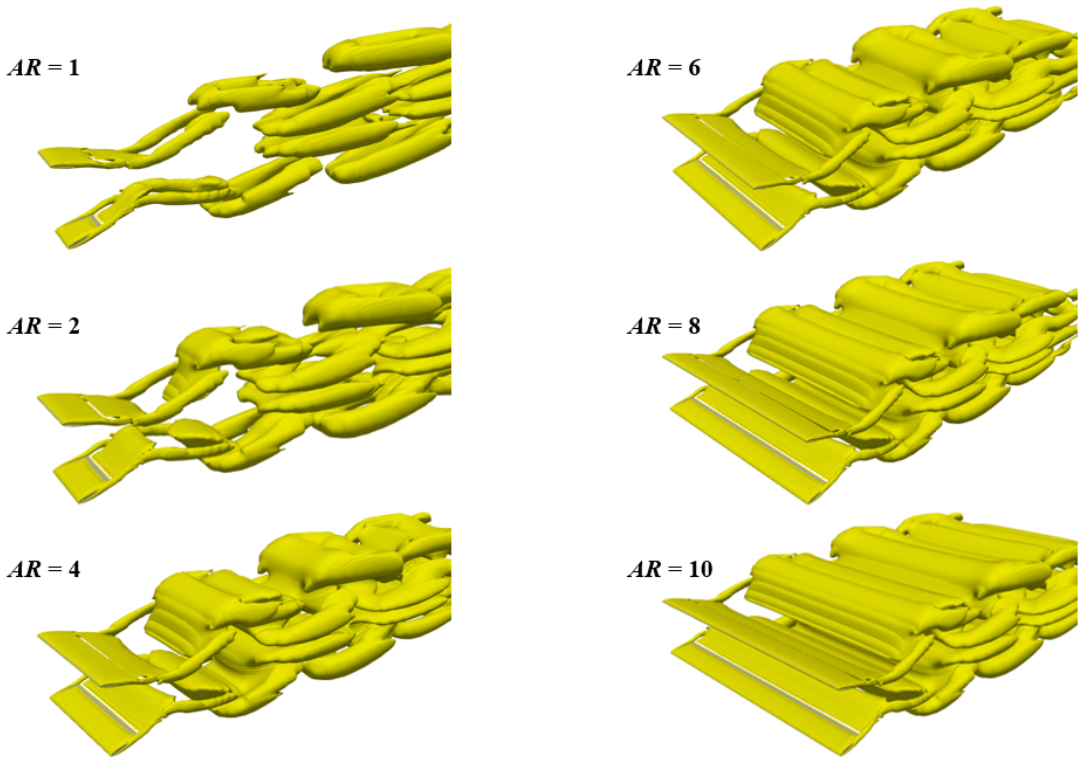

(a) Perspective view

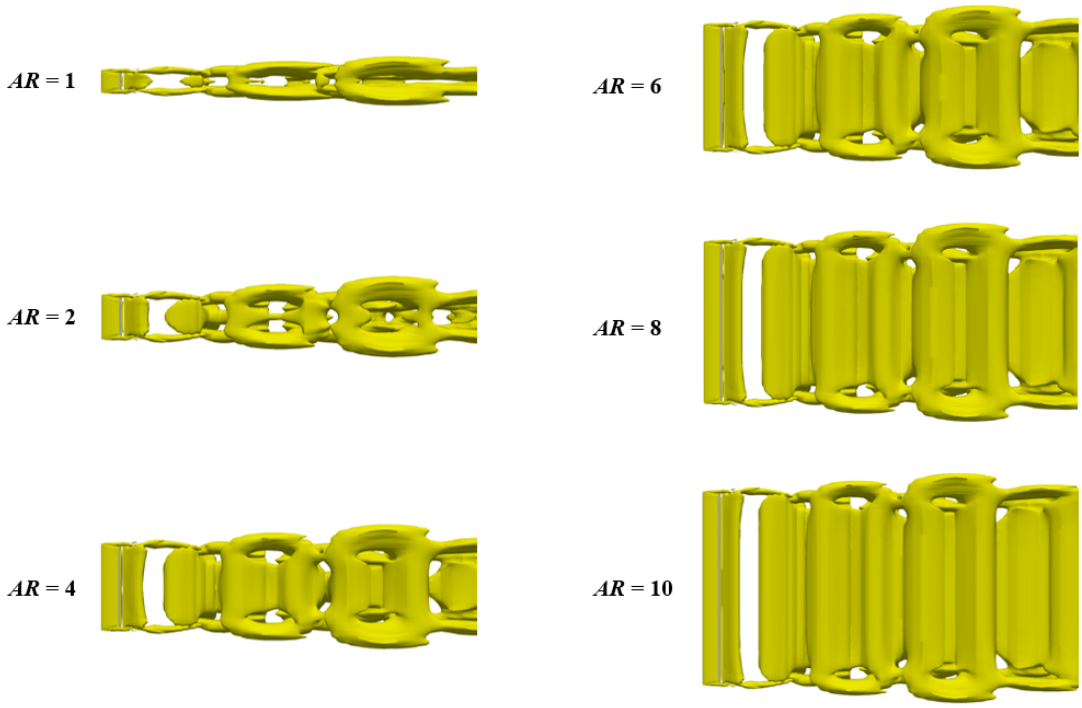

(b) Top view

Figure 6-9 Vortex topologies identified using Q = 0.05 for biplane fully-prescribed configuration with different aspect ratios at the instant of maximum thrust coefficient.

The formation of a vortex ring starts from the vortex shedding on the outside surface of the trailing edge when the foil performs upstroke motion in the first periodic quarter. At the same time, the wing-tip vortices start to grow and shed on the spanwise tips in the same manner. During downstroke motion of the second periodic quarter, two wing-tip vortices are associated by the trailing-edge shedding vortex. With two foils moving further towards each other in the third periodic quarter, the two wing-tip vortices tend to connect the other one. Thus, an evident vortex loop can be observed in the fourth periodic quarter when the foils start to conduct the upstroke motion again. As the generated vortex loop continues to convect towards the flow downstream, its profile gradually evolves as a ring-like shape. It should also be noted that one vortex ring tends to partially join the neighbor vortex ring along the direction of incoming flow. Considering the upper oscillating foil in the biplane configuration, the upper sequence of vortex ring presents a moderate oblique angle to the wake centerline while the lower sequence of vortex ring tends to be parallel to the wake centerline due to the produced WIG effect.

The wake topology for the fully prescribed biplane configuration with different aspect ratios is shown in Figure 6-9. The instant in this figure corresponds to the appearance of the first peak value for the thrust coefficient in Figure 6-4 (a). It can be seen from the top view that the length of vortex ring in streamwise direction remains constant with the variation of aspect ratio, while the spanwise length tends to increase as the aspect ratio increases. Two evident features with the variation of aspect ratio can be identified from the perspective view in Figure 6-9 (a). Firstly, each vortex ring in wake of the low-aspect-ratio foil (AR = 1, 2) tends to be isolated, whereas a connected sequence of vortex ring can be

observed for the larger aspect ratio (AR = 4, 6, 8, 10). Secondly, the leading-edge vortices on the high-aspect-ratio foil (AR = 4, 6, 8, 10) are stretched only around the regions of spanwise tips. For the low-aspect-ratio foil (AR = 1, 2), the whole leading-edge vortices deformed along the spanwise direction. It is conjectured that the wing-tip influence is the main cause for these two features with different aspect ratios. For a low-aspect-ratio case, the vortex onset, shedding and evolution at the midspan are highly affected by the wing-tip vortices since the distance between the tip and midspan is relatively small. The vortex behaviors around the midspan of high-aspect-ratio oscillating foils tend to maintain the features with a less influence of wing-tip vortices. Hence, compared to large-span oscillating foils, the leading-edge and trailing-edge vortex structures of oscillating foils with a small aspect ratio are more likely to be stretched to the distorted pattern and merged into an isolated vortex loop by the wing-tip vortices.

Results indicated that such the low-aspect-ratio characteristics are dominant when the aspect ratio of oscillating foil is less than 4. It was believed that these low-aspect-ratio vortex behaviors are responsible for the significant drop in propulsive performance compared to the two-dimensional case. Overall, the satisfactory boundary attachment around both leading edge and trailing edge was observed for all aspect ratios which is considered as an indication of less flow separation. Two-dimensional simulations are commonly used to explore the propulsive characteristics of oscillating foil propulsors due to the low computational cost. Based on the current results, it is recommended that the propulsion performance by two-dimensional computations should be taken a certain discount depending on the target aspect ratio to ensure the validity and reliability of analysis.

6.3 Hydro-elasticity Characteristics

The APWIGs configuration using an elastic pitching axis is considered as a preferable option for the marine propulsion over fully prescribed system due to several advantages, which has been confirmed in preceding two-dimensional study. For an oscillating foil employing an elastic pitching pivot, the torsional spring stiffness is the most important parameter that determines both dynamic responses and hydrodynamic characteristics. Thus, the effect of spring stiffness for APWIGs was investigated by a constant low-aspect-ratio foil (AR = 2), in which the three-dimensional effect is still dominant. The primary motivation in this part is to examine whether the insights of hydrodynamics and kinematics for the two-dimensional APWIGs are applicable for three-dimensional situations.

6.3.1 Dynamic responses and hydrodynamic characteristics

The typical time series of flow-induced pitching angle and force coefficients for the three-dimensional APWIGs are presented in Figure 6-10, in which a two-dimensional case is also provided for comparison. Like the fully prescribed configuration, both pitching angle and hydrodynamic forces of APWIGs tend to reach a steady state after the third oscillatory cycle. Results indicated that the finite-span foil has a

smaller maximum flow-induced pitching angle compared to the two-dimensional prediction. A same manner was observed with respect to the force coefficients that the three-dimensional effect tends to reduce both thrust and lift production for APWIGs. A slight phase discrepancy between the two-dimensional and three-dimensional computations for force coefficients was observed in Figure 6-10.

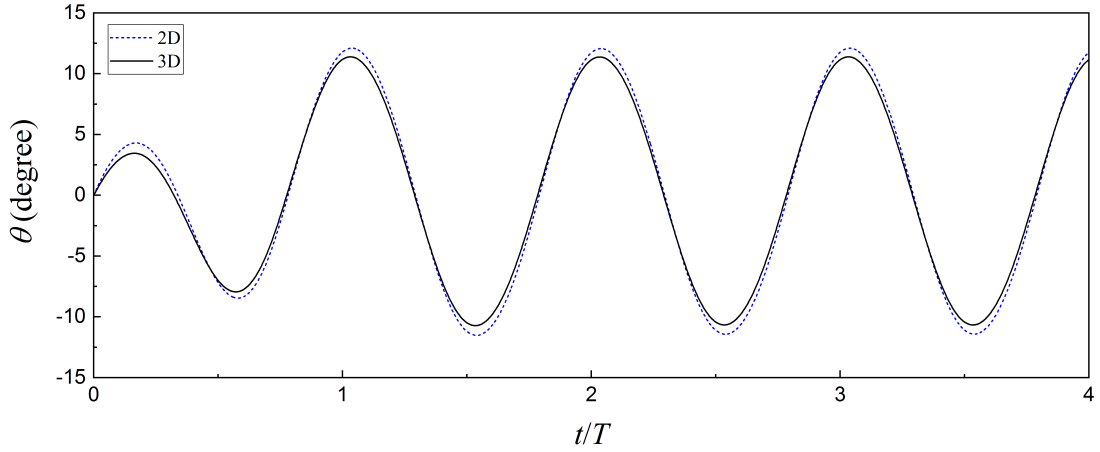

(a) Flow-induced pitching angle

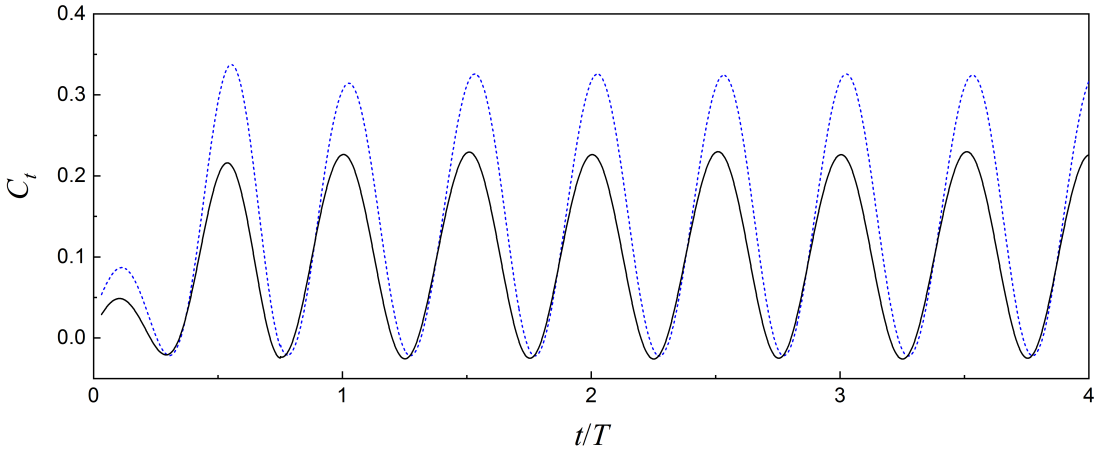

(b) Thrust coefficient

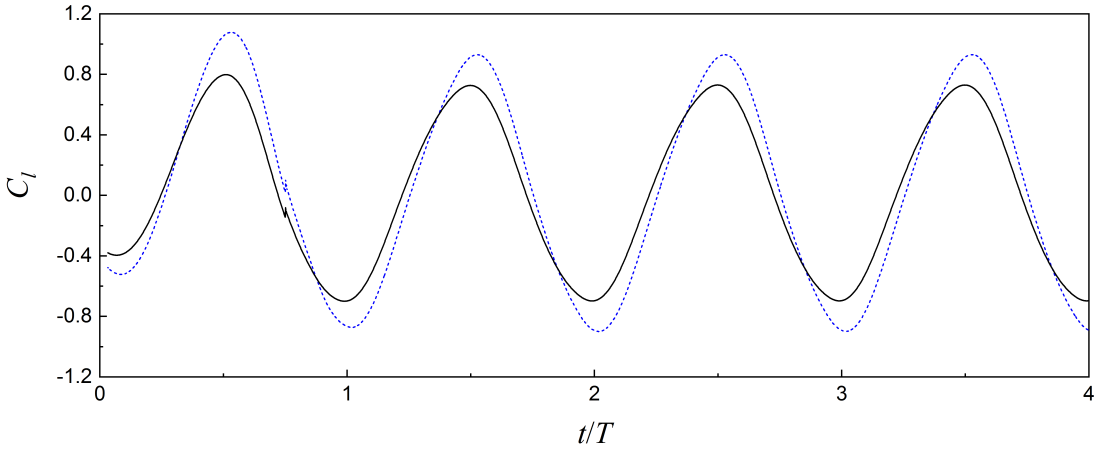

(c) Lift coefficient

Figure 6-10 Time history of flow-induced pitching angle and force coefficients for three-dimensional APWIGs within four oscillatory cycles (Two-dimensional results are included for comparison).

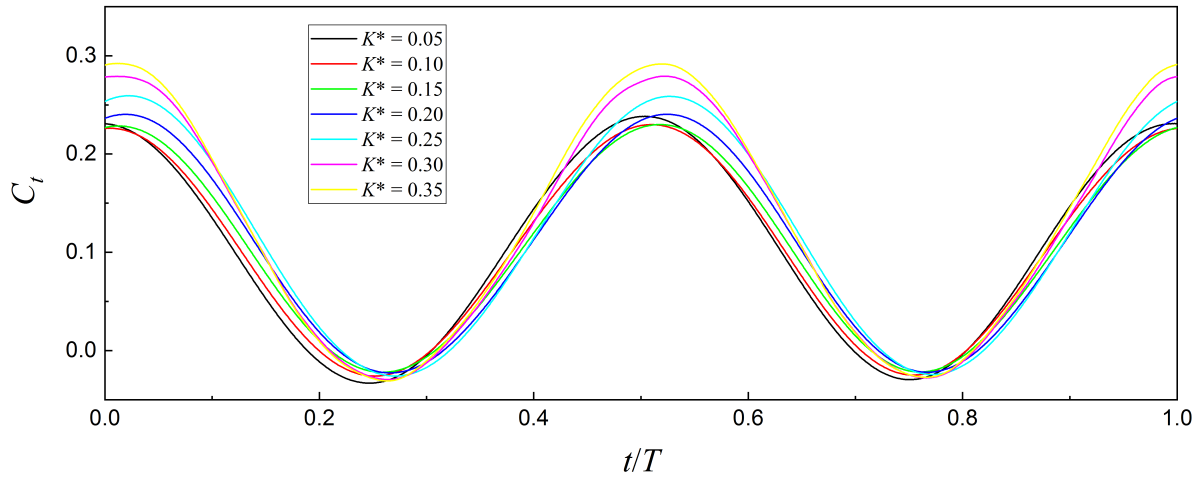

(a) Thrust coefficient

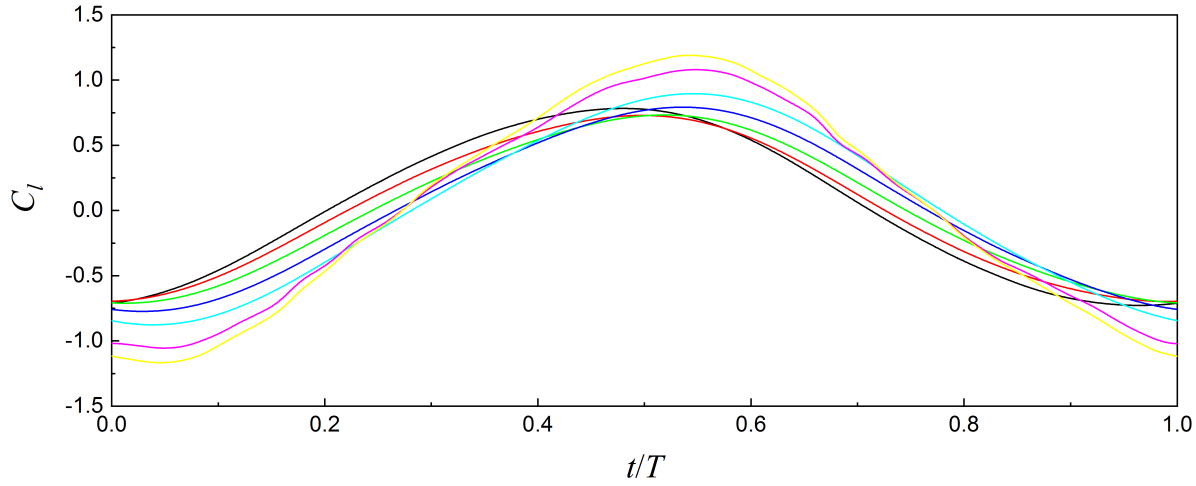

(b) Lift coefficient

Figure 6-11 Time-varying force coefficients for three-dimensional APWIGs with different torsional spring stiffness over one oscillatory cycle.

The time variations of force coefficients and dynamic responses for the three-dimensional APWIGs with different torsional spring stiffness over one oscillatory cycle are presented in Figures 6-11 and 6-12, respectively. It can be seen from the results that the torsional spring has a significant influence on both flow-induced kinematics and propulsion characteristics. When a relatively large stiffness ($K^* > 0.10$) is employed for APWIGs, an increasing trend with respect to the peak values of force coefficients can be observed as the torsional spring stiffness increases. However, the feature of larger maximum force coefficients produced by $K^* = 0.05$ than the prediction of $K^* = 0.10$ was also reported in Figure 6-11. Such a behavior is because the hydrodynamic moments of surrounding flow acting on the oscillating foil with an elastic support dominates the kinematics over the restoring moments as an adequately small spring stiffness is used. When a relatively large spring stiffness ($K^* = 0.30, 0.35$) is employed, the less-smooth profiles were observed for the time series of lift coefficient, which is due to the rapid flow-induced pitch and resulting complicated vortex topology with a stiffer spring.

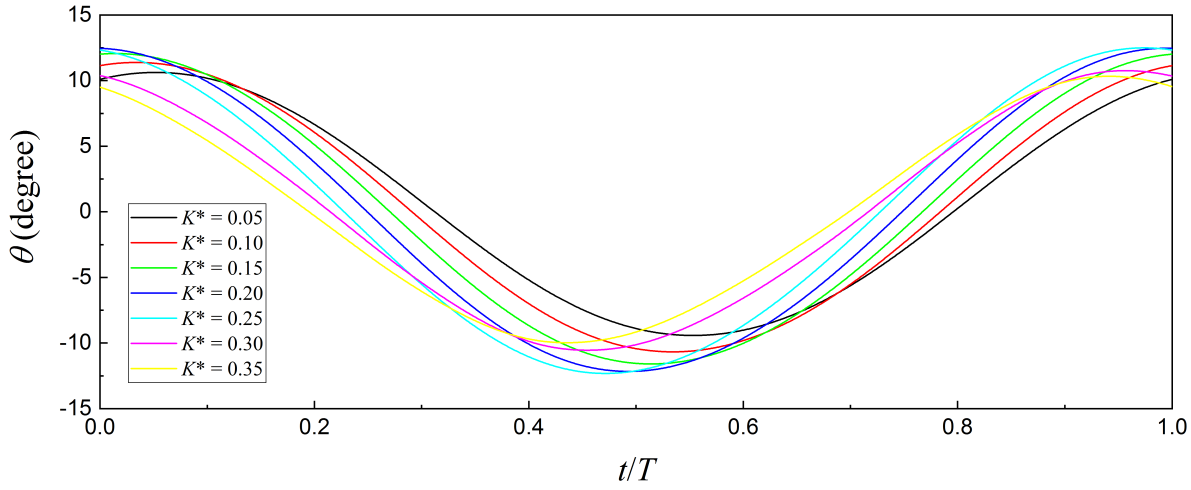

(a) Flow-induced pitching angle

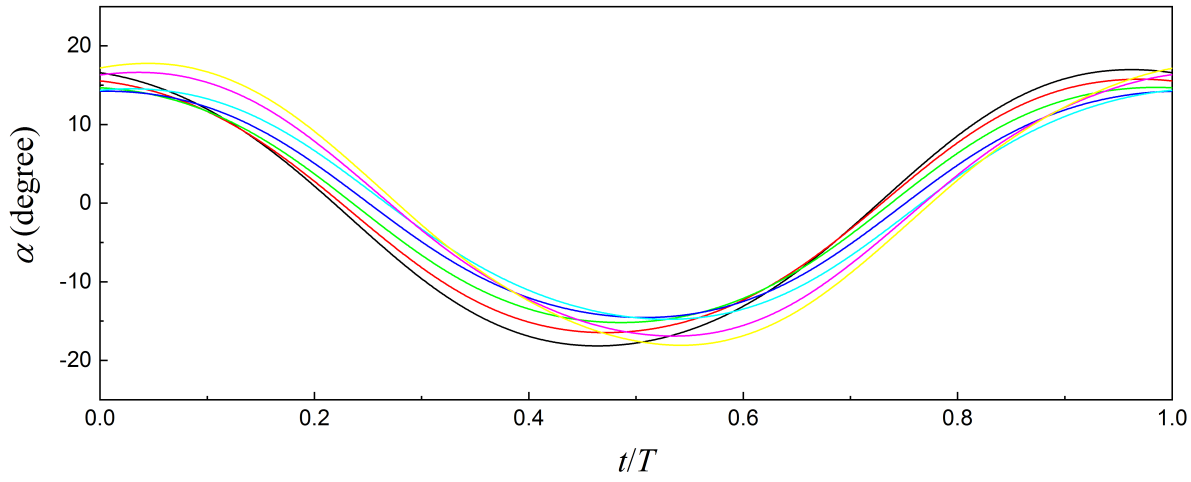

(b) Effective AoA

Figure 6-12 Time-varying dynamic responses for three-dimensional APWIGs with different torsional spring stiffness over one oscillatory cycle.

Figure 6-12 presents the time variations of dynamic responses for the three-dimensional APWIGs with different torsional spring stiffness over one oscillatory cycle. Results suggested that both peak values and phase difference of dynamic responses are dominated by the torsional spring stiffness. The maximum flow-induced pitching angle and resulting effective AoA in Figure 6-12 are summarized in Table 6-1, in which the variation of pitch-leading phase difference with varying spring stiffness is also provided. As the results show, the trend of first increase and then decrease with respect to the maximum flow-induced pitching angle was found as the spring stiffness increases for both two-dimensional and three-dimensional cases. In contrast, the peak values of the effective AoA presents an initial drop with the increase of spring stiffness, which is followed by a trend of rise when the spring stiffness further increases. The maximum pitching angle appears at the K^* = 0.25 for both two-dimensional (12.9 degrees) and three-dimensional (12.5 degrees) predictions. A less evident discrepancy was observed between them due to a relatively small heaving amplitude was employed in the current computations. As a result, the corresponding peak values of the effective AoA also present a slight difference between

a finite-span foil and infinite-span foil that occur at the $K^* = 0.05$.

A consistent increasing trend with respect to the pitch-leading phase difference was reported for both two-dimensional and three-dimensional cases as the spring stiffness rises. Such a behavior is reasonable because a stiffer torsional spring will restore the oscillating foil towards the centerline more quickly. It should also be noted that the three-dimensional effect tends to increase the pitch-leading phase difference slightly compared to an infinite-span foil.

Table 6-1 Maximum flow-induced pitching angle, peak value of effective AoA and pitch-leading phase difference for APWIGs with different torsional spring stiffness.

	K^*	**0.05**	**0.10**	**0.15**	**0.20**	**0.25**	**0.30**	**0.35**
2D	θ_0	11.420	12.098	12.581	12.852	12.881	12.751	12.398
	α_0	17.391	15.897	14.716	14.046	14.025	14.626	15.685
	φ	69.552	75.888	82.800	89.712	96.624	103.536	110.448
3D	θ_0	10.621	11.382	12.061	12.466	12.495	10.758	10.328
	α_0	18.153	16.463	15.182	14.547	14.772	16.904	18.076
	φ	70.704	77.616	84.816	92.592	100.368	106.416	113.040

6.3.2 Effect of torsional spring stiffness

The comparison of propulsive performance as a function of torsional spring stiffness between the two-dimensional and three-dimensional predictions is presented in Figure 6-13. As the results show, the time-averaged thrust coefficient for a finite-span foil tends to decline first and then rise when the spring stiffness consistently increases. In contrast, an initial increase in propulsive efficiency with a larger spring stiffness can be observed for the three-dimensional case, which is followed by a rapid drop as the torsional spring becomes further stiffer. This characteristic indicates an optimum torsional spring stiffness can be found for the three-dimensional APWIGs that produces the highest propulsive performance. The same manner of hydro-elasticity characteristics for the two-dimensional case was reported in Figure 6-13, which can also be confirmed by the preceding predictions.

An evident discrepancy can be seen between two lines in Figure 6-13, in which the three-dimensional effect tends to reduce both thrust production and propulsive efficiency compared to the two-dimensional results. An averaged drop of around 10% in efficiency was observed in Figure 6-13 (b) due to the influence of finite span, while this discrepancy will extend to approximately 13% with a larger spring stiffness. The apparent drop in propulsive performance for a three-dimensional foil with relatively large spring stiffness can be explained by the corresponding severe vortex behaviors, which will be demonstrated in the following part. It should also be noted that the optimum spring stiffness of three-dimensional foil is slightly larger than that of two-dimensional case. The optimum stiffness for the

infinite-span foil is K^* = 0.10 that produces the highest efficiency of 67.22%, while the maximum efficiency of 58.01% is produced by K^* = 0.15 for the finite-span foil. Although several different features can be identified, the general hydro-elasticity characteristics of two-dimensional configuration is highly relevant to the three-dimensional APWIGs for the current parametric space.

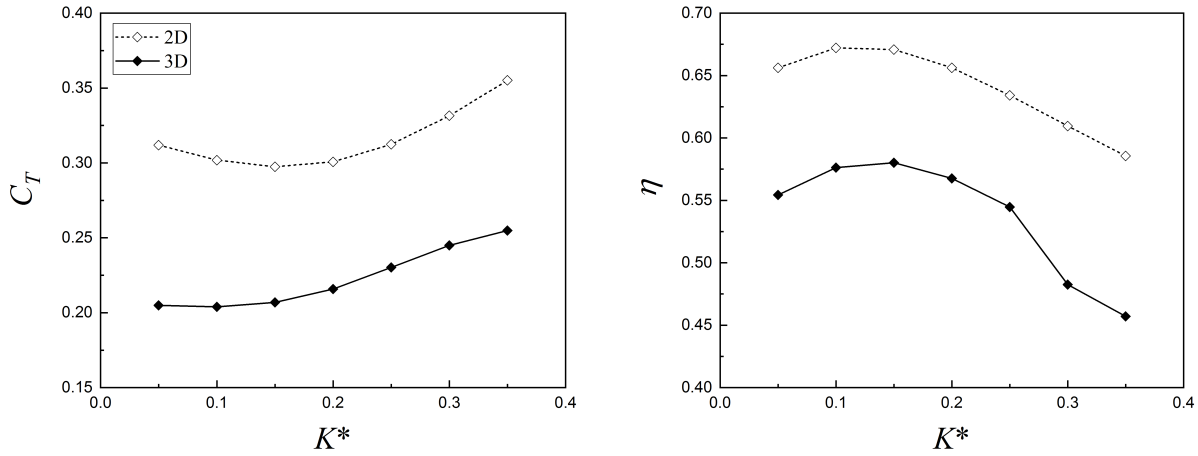

(a) Thrust coefficient (b) Propulsive efficiency

Figure 6-13 Propulsive performance of three-dimensional APWIGs with different torsional spring stiffness (Two-dimensional results are included for comparison).

6.3.3 Vortex topologies of APWIGs

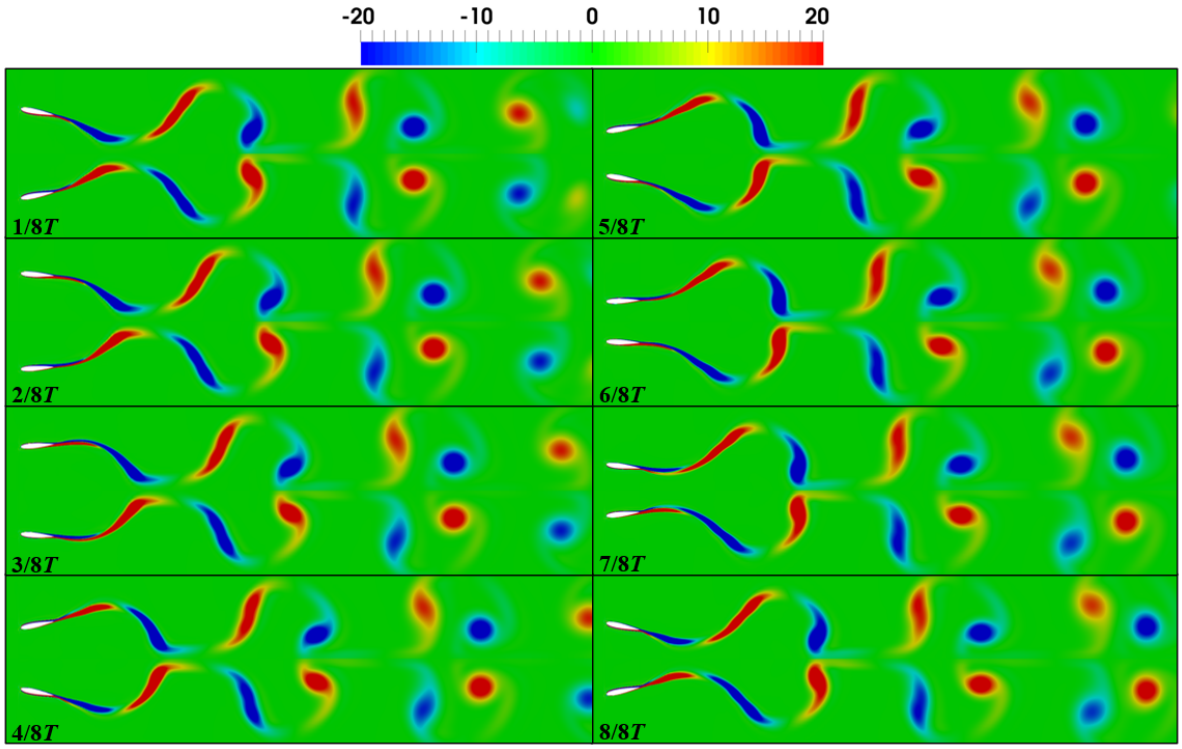

Figure 6-14 Wake vortical contours at eight instants over one oscillatory cycle for two-dimensional APWIGs (K^* = 0.10).

The vortical contours of the two-dimensional APWIGs at eight instants over one oscillatory cycle is shown in Figure 6-14. The torsional spring stiffness used in this figure is K^* = 0.10 that produces the highest propulsive efficiency in Figure 6-13 (b). The corresponding time series of thrust and lift coefficients are presented in Figure 6-15.

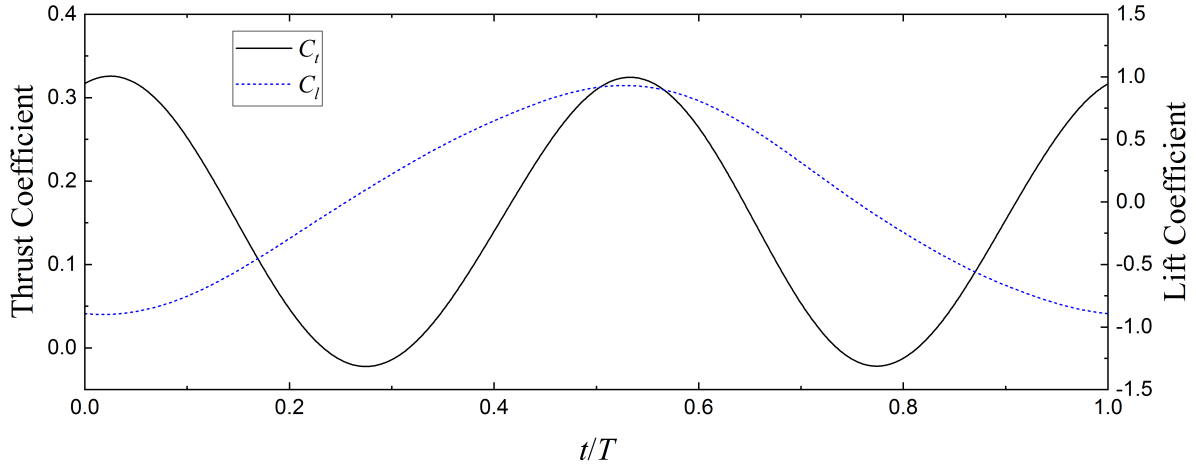

Figure 6-15 Time variation of force coefficients for two-dimensional APWIGs with K^* = 0.10 over one oscillatory cycle.

The compact attachment of surrounding flow can be observed on both leading edge and trailing edge of each foil in Figure 6-14. Like the fully prescribed configuration, a same wake pattern of reverse Kármán vortex street was numerically visualized in the downstream of each elastic-support foil. Results indicated that the wake vortices of the two-dimensional APWIGs tend to dissipate more rapidly compared to the fully prescribed configuration in Figure 6-7.

Three-dimensional wake topologies for the APWIGs with different torsional spring stiffness identified by Q = 0.05 are presented in Figures 6-16, 6-18 and 6-20, respectively. Four instantaneous instants are provided over one oscillatory cycle. Figures 6-17, 6-19 and 6-21 correspond to the time-varying thrust and lift coefficients. In the same manner, the three-dimensional vortex topology of APWIGs in the wake of each foil is characterized as two sets of intertwined vortex rings.

It can be seen that the torsional spring stiffness plays a significant role in wake topology of APWIGs. The attached leading-edge vortices were observed for APWIGs with a modest torsional spring stiffness (K^* = 0.05, 0.20), which also presents the moderate trailing-edge vortex shedding. In contrast, the highly detached vortices and severe flow separation around both leading edge and trailing edge were observed for the APWIGs using a relatively large spring stiffness (K^* = 0.35). In addition, the sequence of vortex ring in Figures 6-16 and 6-18 (K^* = 0.05 and 0.20) is much smoother compared to the prediction of K^* = 0.35. The possible cause is due to the relatively large pitching velocity generated by an adequately stiff torsional spring, which leads to the increase of local Reynolds number and hence the dominance of turbulence effect. On the other hand, the considerably high pitching velocity of trailing edge also prompts the flow separation and tends to produce complicated vortex structures. The less

stable time series of lift coefficient for K^* = 0.35 in Figure 6-21 is an indication of severe vortex behaviors. It should also be noted that the negative peak of time-varying lift coefficient for three spring stiffness is slightly smaller than the positive peak values due to the WIG effect.

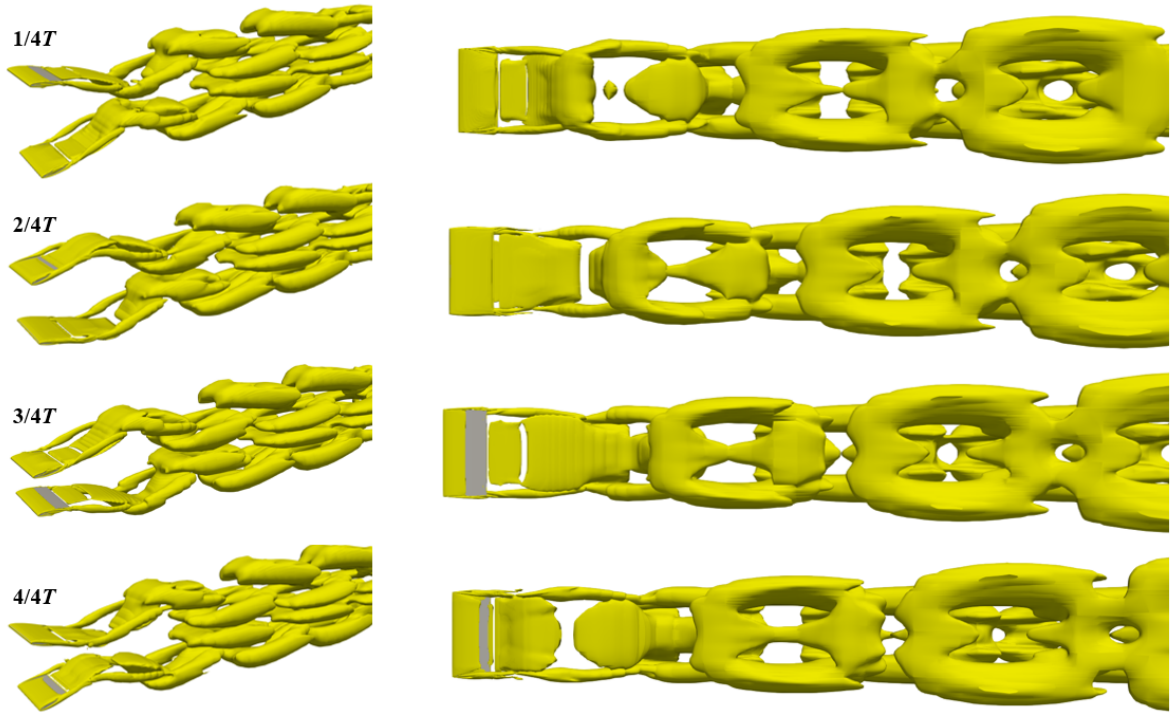

Figure 6-16 Vortex topologies identified using Q = 0.05 for three-dimensional APWIGs with K^* = 0.05 over one oscillatory cycle (Left: Perspective view, Right: Top view).

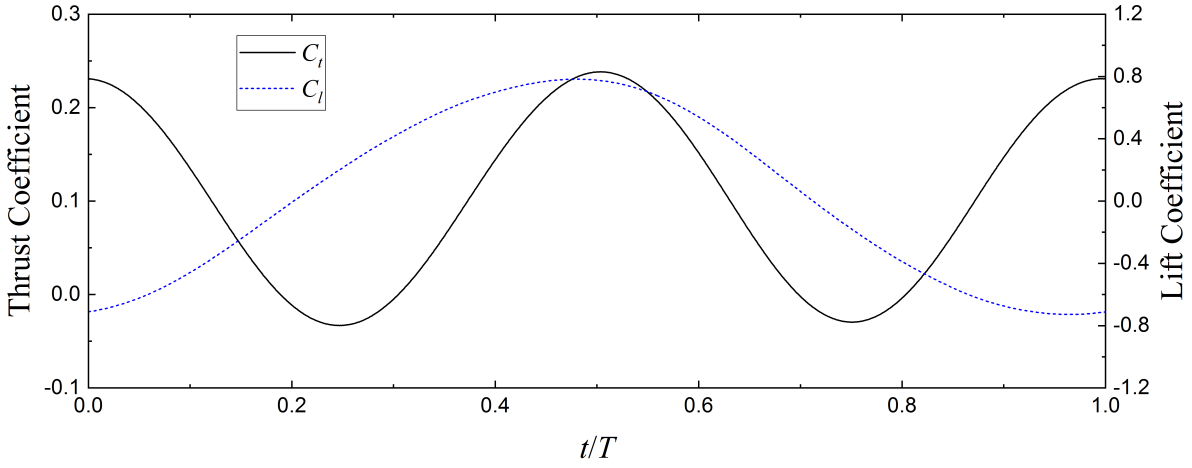

Figure 6-17 Time variation of force coefficients for three-dimensional APWIGs with K^* = 0.05 over one oscillatory cycle.

Considering the vortex topologies of APWIGs with K^* = 0.20 in Figure 6-18, an oblique angle of each vortex ring to the wake centerline was observed in the outside vortex-ring sequence. Therefore, the induced flow is expected to have a net component along the streamwise direction, which is an indication of the thrust production for the three-dimensional oscillating foils. Such a vortex profile was previously

reported by Dong et al. (2006) using a single oscillating foil, which has a high accordance with the current predictions.

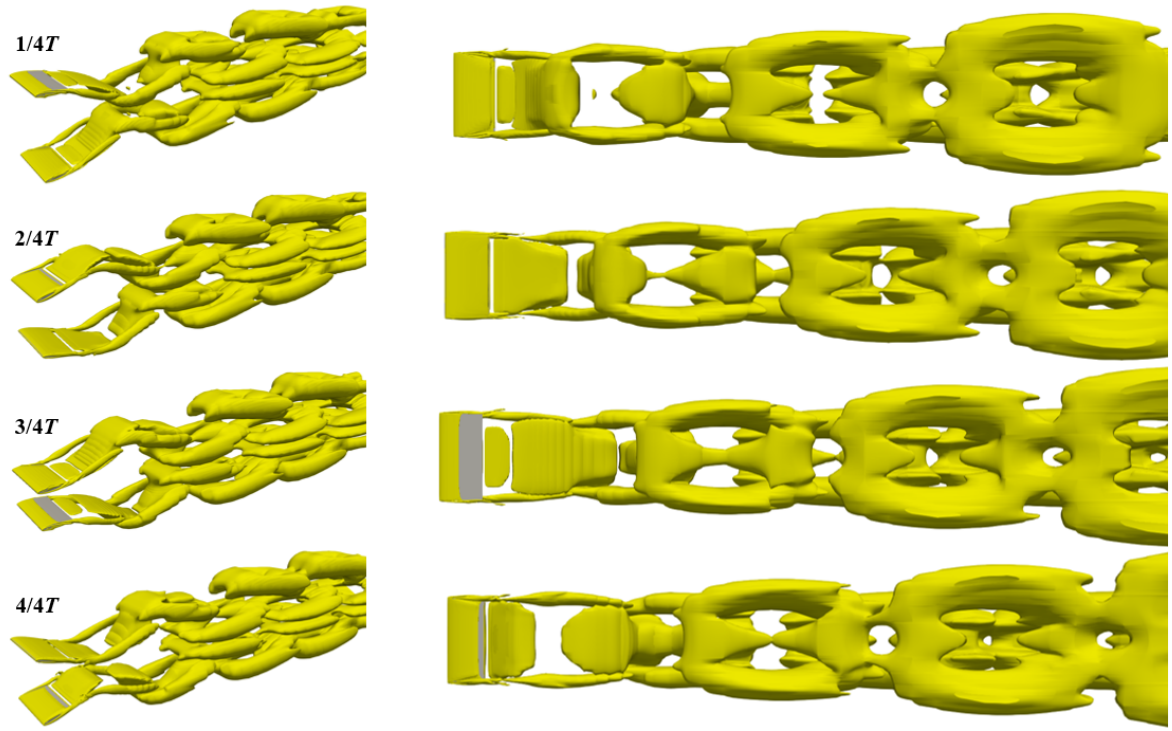

Figure 6-18 Vortex topologies identified using $Q = 0.05$ for three-dimensional APWIGs with $K^* = 0.20$ over one oscillatory cycle (Left: Perspective view, Right: Top view).

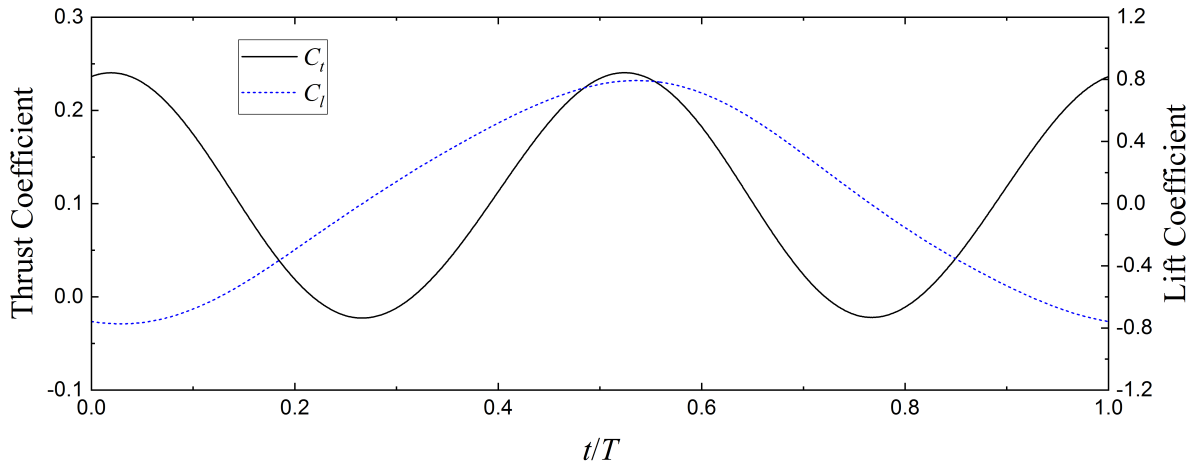

Figure 6-19 Time variation of force coefficients for three-dimensional APWIGs with $K^* = 0.20$ over one oscillatory cycle.

The mechanism of vortex topology of finite-span foil has the little resemblance to the two-dimensional flow pattern characterizing as a reverse Kármán vortex street for a thrust-producing oscillating foil. Comparison of vortex structures between the fully prescribed configuration in Figure 6-8 and APWIGs in Figure 6-18 shows that the detached leading-edge vortices by the rigid pivot is more apparent than

an elastic-support pitching axis. The efficiency of 56.76% was numerically recorded by the APWIGs configuration, which is slightly higher compared to the efficiency of 53.03% by the fully prescribed system. Based on the current computations, a flow-adapted pitching motion for the three-dimensional oscillating foil is expected to have advantages over a rigid shaft in efficiency improvement.

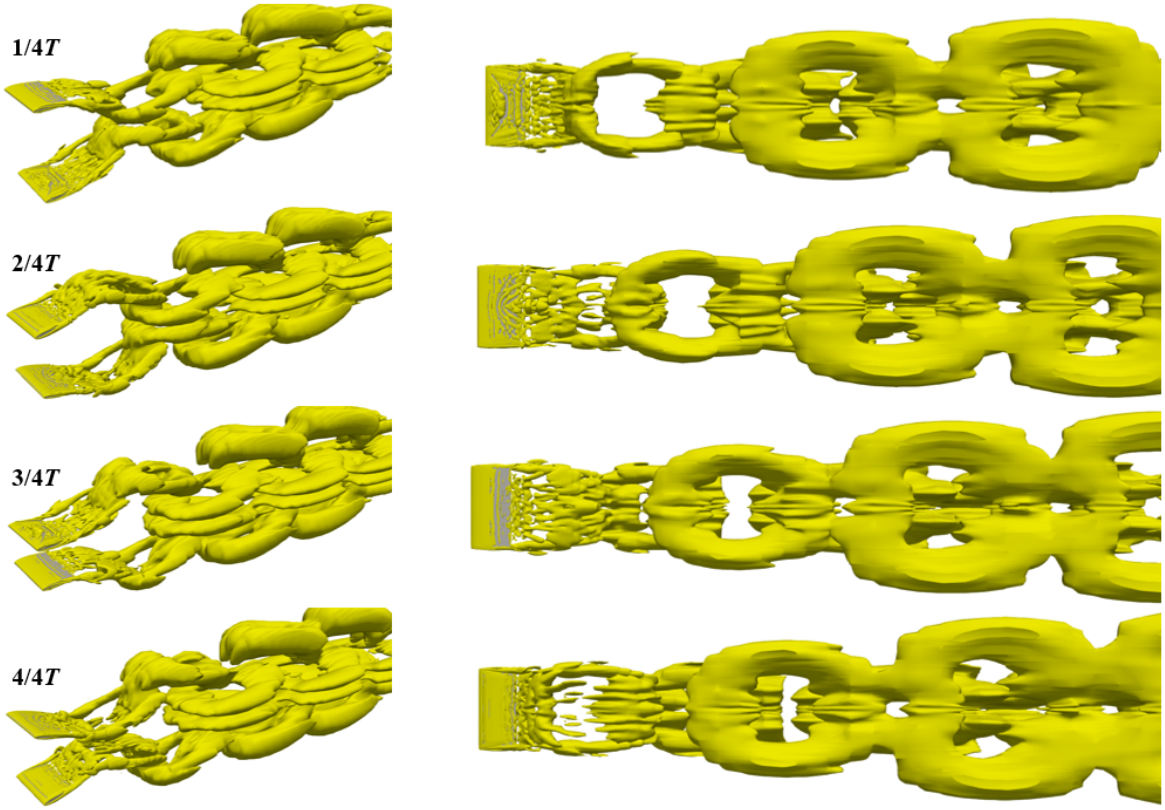

Figure 6-20 Vortex topologies identified using $Q = 0.05$ for three-dimensional APWIGs with $K^* = 0.35$ over one oscillatory cycle (Left: Perspective view, Right: Top view).

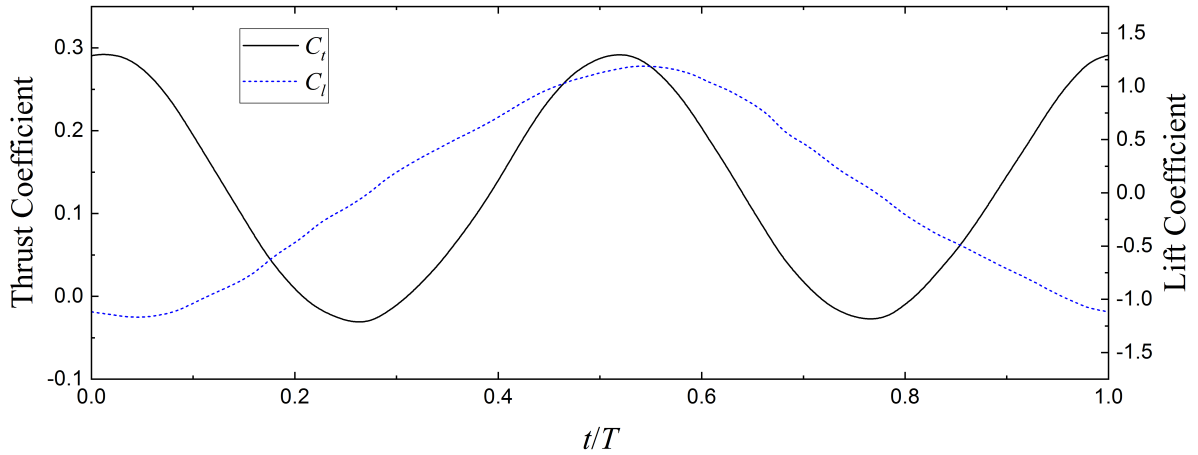

Figure 6-21 Time variation of force coefficients for three-dimensional APWIGs with $K^* = 0.35$ over one oscillatory cycle.

6.4 Concluding Remarks

The three-dimensional computations with respect to propulsive characteristics of WIG effect oscillating foil propulsor were performed in this section. Two different configurations were considered to study the effect of aspect ratio and hydro-elasticity characteristics, respectively. Firstly, the fully prescribed motion mode was employed to investigate the effect of three-dimensionality by covering an adequately large range of aspect ratio from 1 to 10. Secondly, a low-aspect-ratio foil (AR = 2) was applied to the APWIGs with a flow-adapted pitching motion to explore the influence of torsional spring stiffness. Both configurations can produce a WIG effect by the counter-phase heaving oscillation that benefits the improvement of propulsive performance. The comprehensive demonstration and analysis in the hydrodynamic performance of these configurations were presented. The three-dimensional vortex topologies were numerically visualized by the iso-surface of the second invariant of the velocity gradient tensor (Q-criterion), which aims to provide the insights into the mechanism of thrust production for the finite-span oscillating foils.

Results of fully prescribed biplane configuration showed that the three-dimensional effect tends to reduce both thrust production and propulsive efficiency. The maximum drop of 14.85% in efficiency was reported for AR = 1 compared to the two-dimensional prediction. With the increase of aspect ratio, the propulsive performance of the finite-span oscillating foils tends to approach the two-dimensional case. Based on the modest efficiency drop of 3.22% for AR = 4, the recommendation of aspect ratio from 3 to 5 is reasonable for the engineering application of three-dimensional WIG effect oscillating foil propulsor considering the compromise between decreasing efficiency and increasing manufacturing cost. The wake topology of finite-span oscillating foils is characterized as two sets of intertwined vortex rings that convect downward along the wake centerline of each foil. The vortex evolution indicates that the formation of vortex ring originates from a vortex loop constituted by a trailing-edge shedding vortex and two stretched wing-tip vortices. With the rise of aspect ratio, the spanwise length of wake profiles for a finite-span oscillating foil shows an increasing trend while the streamwise length of each vortex ring tends to keep constant.

The primary interest of APWIGs lies in the comparison of hydro-elasticity characteristics between two-dimensional and three-dimensional cases. It was shown that the propulsive efficiency of three-dimensional APWIGs presents an initial increase with a larger torsional spring stiffness, which is followed by a rapid drop as the spring stiffness continues to increase. Thus, an optimum torsional spring stiffness can be found to produce the highest propulsive performance for the three-dimensional APWIGs configuration. Such a characteristic for the finite-span foil has a high accordance compared to an infinite-span foil, indicating that the hydro-elasticity characteristics of the APWIGs configuration by the two-dimensional computations is reasonably relevant to the three-dimensional case within the current parametric space. An averaged drop of around 10% in efficiency was observed for the APWIGs configuration due to the finite-span effect, whereas the drop tends to extend with a larger spring stiffness.

Two apparent features with respect to the vortex topology of three-dimensional APWIGs can be identified in the current simulations. The oblique angle of outside vortex rings to the wake centerline implies that a net induced flow component can be produced along the streamwise direction, which is an indication of thrust production for a finite-span oscillating foil. In addition, the torsional spring stiffness shows a significant influence on the characteristics of vortex structures for the APWIGs configuration, which present the evident trailing-edge vortex shedding and severe flow separation with an adequately large spring stiffness. In the current three-dimensional computations, the higher propulsive performance for APWIGs was numerically reported over the fully prescribed biplane configuration. The elastic-support oscillating foil was found to be a preferable option for marine propulsion over the rigid-shaft system even for the real finite-span flow.

CHAPTER 7

Design Procedure of APWIGs for Marine Propulsion

7.1 General Introduction

The design of marine propulsion systems is a multi-disciplinary engineering process which usually employs multiple research tools including the theoretical analysis, CFD computations and experimental measurements. The development of a universal propulsion system for different marine vehicles and various operating environments is highly challenging, indicating that the thruster design process should be closely correlated to requirements of target vehicle and corresponding deployment conditions. The long-term studies and a wealth of application experiences regarding conventional propulsion systems may provide significant insights into the development of novel marine propulsors.

7.1.1 Background of marine propulsion systems

The widely applied propulsion systems for marine vehicles include the fixed pitch propellers, controllable pitch propellers, ducted propellers, podded and azimuthing propulsors, waterjet propulsion and paddle wheels (Carlton, 2018). The fixed pitch propeller is the most common propulsion device that generally operates in either mono-block or built-up forms. The design types and sizes of fixed pitch propeller covers a large application range from small high-speed patrol craft to large container ships. The controllable pitch propeller allows the change of blade pitch for different loading conditions, differing from the fixed pitch propeller with a single operational variable of rotational speed. The controllable pitch propeller has a wide application in vessels including tugs, trawlers and ferries.

The ducted propeller generally consists of two principal components: an annular duct with the aerofoil cross-section and a propeller with either fixed or controllable pitch. There are two types of duct form including the accelerating duct and decelerating duct. The accelerating duct accelerates the flow inside the duct to increase the thrust and efficiency, while the decelerating duct reduces the flow speed inside the duct to relieve the issue of cavitation. The podded and azimuthing propulsor is a combination of fixed pitch propeller and an electric drive motor housed in the pod. This type of propulsion system can provide directional thrust and satisfactory maneuvering properties. The sited position of drive motor forms the difference between azimuthing propulsors and podded propellers.

The operational principle of waterjet propulsion is to draw the fluid through a ducting system using an internal pump, and then expel the fluid aft at a high velocity. The forward thrust is mainly produced by the momentum increase imparted to the fluid. The waterjet propulsion device is widely applied to the thrust generation for small high-speed crafts. The paddle wheel is an antiquated propulsion device equipped with a feathering float system which appears before the screw propellers. This type of propulsion device has almost disappeared except for few specific applications of lakes and river vehicles. Additionally, the novel propulsion systems such as oscillating foils (or flapping wings) provide an alternative to the above conventional propulsion systems for thrust generation of both ship and AUV.

For a long time in the past, the primary design objective of propulsion systems is to maximize the

efficiency. However, with the augment of vessel speeds and loading conditions over recent decades, the issue of cavitation has attracted an increasing interest in the propulsion community. Hence, the design process of propulsion systems for modern marine vehicles generally employs the trade-off design principle to compromise the multiple performance metrics including the thrust coefficient, propulsive efficiency, structural strength, cavitation, vibration, noise, etc. Based on this design principle, one or more dominant factors need to be weighted additionally for specialized requirements. More details with respect to the design principle of conventional propulsion systems can be referred to Carlton (2018).

The design process for a given propulsion problem is a continuous loop consisting of a number of phases (Kerwin and Hadler, 2010). Since each phase interacts with the other, the continuous loop can be completed only when all design phases are satisfied. In general, a design process of marine propulsion system is made up of the definition of problem, preliminary design phase, detail design phase, and evaluation of the design. The definition of problem may be changed with the proceeding of design process. The preliminary design phase is to develop the basic design using fundamental knowledge. The detail design phase involves a series of theoretical analysis and model tests. The evaluation of the design is conducted during the initial sea trials of vessels. One may find more details regarding the design and analysis loop of marine propulsors in Kerwin and Hadler (2010).

7.1.2 Design procedure of screw propeller

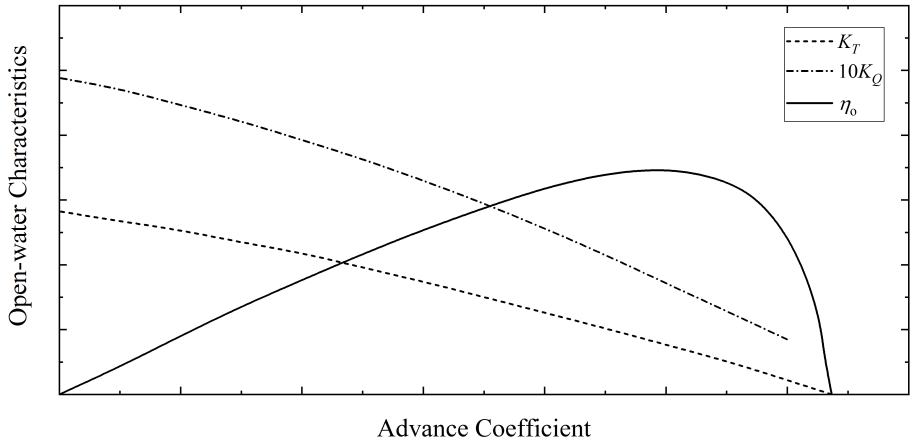

Figure 7-1 A sketch demonstration of open-water propulsive characteristics for a fixed pitch propeller.

A typical design procedure for the screw propellers that has been well developed and widely applied over decades is presented to inspire the design of novel propulsion systems. The primary performance metrics for a screw propeller are thrust coefficient and propulsive efficiency. Figure 7-1 presents a sketch demonstration of open-water propulsive characteristics for a fixed pitch propeller, in which the K_T, K_Q and η_o represent the thrust coefficient, torque coefficient and open-water efficiency, respectively. It is noted that the thrust coefficient is inversely proportional to the advance coefficient, while there exists a maximum value for efficiency with the variation of advance coefficient. Such a trend is generally applicable to any marine propellers that have the similar geometric form. Hence, one of the

major objectives for propeller design is to make the operation of propulsion system to approach this operating condition with maximum efficiency.

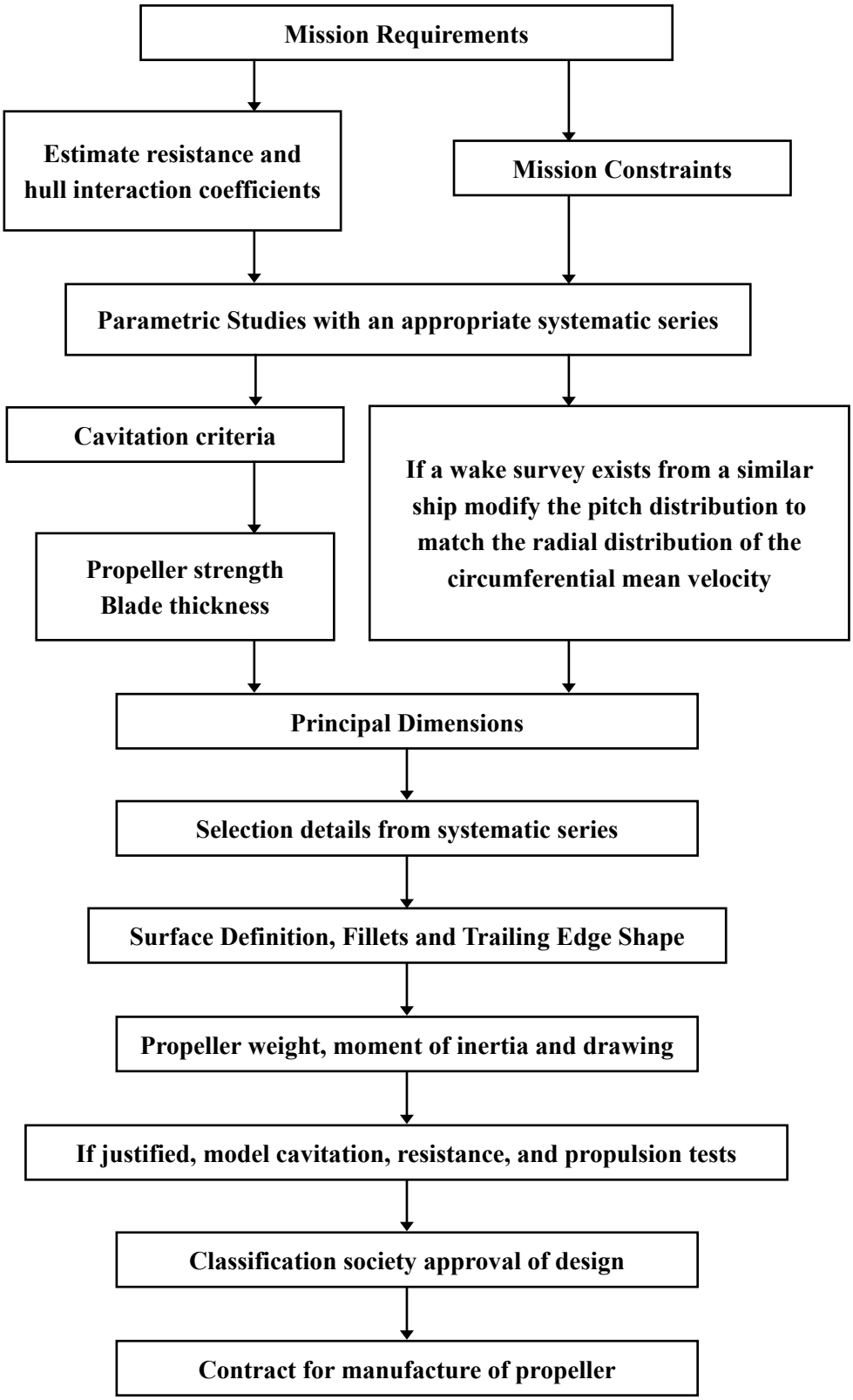

Figure 7-2 A typical design procedure for the screw propeller employing systematic propeller series (Kerwin and Hadler, 2010).

The parameter selection of marine propellers is generally achieved by either open-water tests or computational analysis using circulation theory. The design using open-water tests is based on the experimental results of a systematic series of propellers. A number of design parameters are considered in the model tests, such as pitch ratio, section shape and blade area. In these experimental tests, a parent model with the given geometry properties is chosen first. After that, a number of models that have the same features but different pitch ratios are built. These models are then tested in a towing tank as a function of advance ratio. There are many well-known propeller series such as the B-screw series by Maritime Research Institute of the Netherlands (MARIN), which are widely applied to the conventional merchant ships. The design employing circulation theory requires much more input information compared with the first approach. To obtain the optimal performance, an iteration process is involved during the computational analysis. It is noted that the propeller design based on the circulation theory tends to overestimate the propulsive efficiency compared with experimental data from the open-water tests. Additionally, several choices need to be made to determine other characteristics, such as propeller diameter, number of revolutions, number of blades, blade outline, skew, camber and AoA.

The detail design of propellers involves a procedure of analysis and optimization, which largely depends on the available information and computational capabilities. A typical design process for marine propellers using systematic propeller series was summarized by Kerwin and Hadler (2010), as shown in Figure 7-2. The required information for the design of systematic propeller series includes the primary features of target vessel, effective power, engine power and rated RPM, vessel speed and all restrictions. The typical flow diagram for the design process of propellers using circulation theory can be referred to Kerwin and Hadler (2010). It should be noted that the design process of propellers may vary to some extent to satisfy the specific performance requirements for different vessels.

7.1.3 Propulsion application of oscillating foils

The propulsion device using oscillating foils for marine vehicles have been explored over many years, which is considered as one of most promising novel propulsion systems to substitute the conventional screw propellers. Since the oscillating foil propulsor is still under development and the majority of relevant mechanisms remain unclear, the available applications for this novel propulsion system mostly lie in the phase of conceptual design.

A general layout for the application of oscillating foils propulsor in biplane configuration propelling a surface ship is demonstrated in Figure 7-3. The propulsion system using two horizontal foils with the counter-phase heave is installed at the stern of vehicle to provide the forward thrust. The pitching motion of each foil can be implemented as either prescribed mode using the actuator or flow-adapted rotation based on the torsional spring. In addition, two vertical wings with adjustable inflow angle are mounted at the rear end of oscillating foils to generate directional forces and hence achieve maneuverability.

A typical application of oscillating foil propulsion system for underwater vehicles is demonstrated in

Figure 7-4, which is developed by Liu (2005a) in the form of technical invention. This propulsion device consists of a primary system installed at the rear end of vehicle and a set of auxiliary systems mounted to the body of vehicle. All propulsion systems employ a biplane oscillating foil configuration, in which the heaving motion is actively imposed and the pitching motion is controlled by the damping setup. The primary propulsion system at the rear end of vehicle is used to generate the forward thrust. The auxiliary propulsion systems on the body of vehicle are employed to produce the directional forces at any angle, and thus achieve a superb maneuverability.

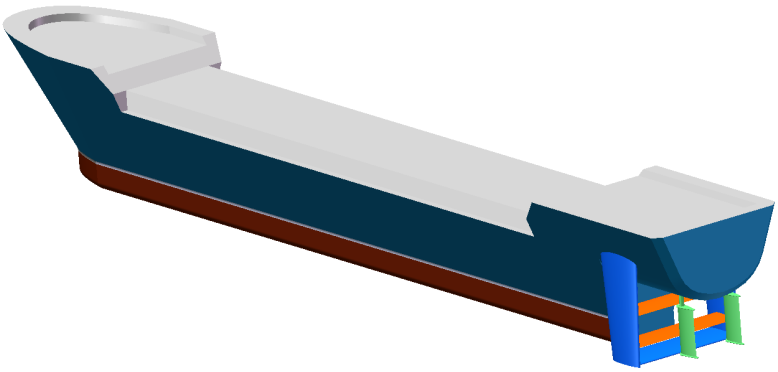

(a) Perspective view

(b) Back view (c) Front view

Figure 7-3 Schematic of oscillating foil propulsor in biplane configuration for a surface ship.

The studies on the design of oscillating foil propulsors in literature mainly focus on the optimization of geometry and kinematic parameters, which can be generally classified into four groups. The first type is characterized as the parametric studies using boundary element method that is less computationally expensive (Politis and Tsarsitalidis, 2014). The second type employs the multi-objective evolutionary algorithm coupled with a flow solver or an experimental apparatus to optimize the performance metrics of oscillating foils (Milano and Gharib, 2005; Oyama et al., 2009; Culbreth et al., 2013). The third type uses the adjoint-based approach coupled with a numerical model to solve the optimization problem with a large parameter space (Xu and Wei, 2016). The last type integrates two or more computational methods with different physical fidelity into a single framework to optimize the performance metrics (Willis et al., 2008; Zheng et al., 2013).

Yang et al. (2018) demonstrated a typical design process for a novel propulsion device using oscillating foils, which undergoes several stages including the conceptual design, preliminary design, structural design, fabrication, test and refinement. Such a design loop has been proved to be a realistic and valid pathway for the development of oscillating foil propulsion systems. In the stage of conceptual design, the initial design parameters such as foil geometry and oscillating frequency are determined. After that,

the tentative studies using both theoretical and experimental methods are conducted in the stage of preliminary design, which aims to analyze the hydrodynamic characteristics and further detail the geometry and kinematic features. The structural design is then employed to analyze the structural and power properties, which is generally performed by means of CFD computations. A prototype can be obtained after the process of fabrication. At this point, a practical test is required to examine the corresponding capability and performance metrics. A refinement with adjustment of parameters is used to close the design loop that is repeated until the specialized requirements are satisfied. It should be noted that the design process for different oscillating foil configurations is highly changeable depending on specific geometry arrangement and kinematic implementation.

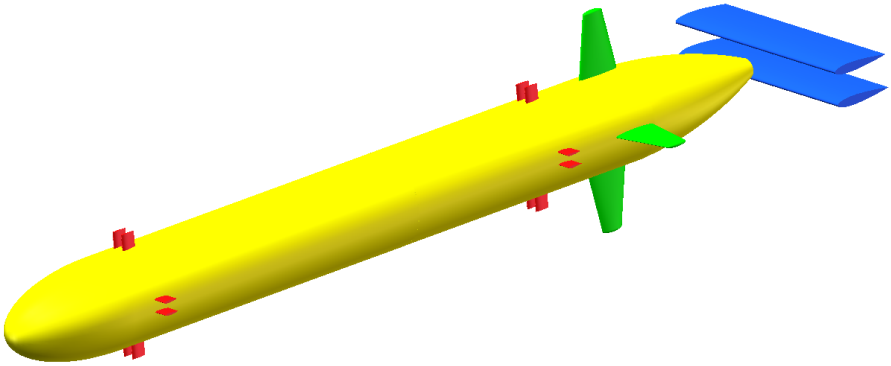

(a) Perspective view

(b) Back view (c) Front view

Figure 7-4 Oscillating foil propulsor in biplane configuration for AUV (Liu, 2005a).

In addition to optimization of performance metrics, the design process of oscillating foil propulsor needs to take various restrictions into account to satisfy the required mission profile of target vehicle. Unlike the screw propellers, the oscillating foil propulsion systems generally have less possibility to encounter the issue of cavitation due to the relatively low velocity of foils. However, other limitations in various aspects are involved in the design procedure to ensure the feasibility and reliability of developed propulsion system. The common considerations for the design of propulsion systems include the propulsion machinery, manufacture, component number, size constraint, interaction with target vehicles, install position and orientation, etc.

The propulsion machinery is usually characterized as one or more mechanical actuators to achieve the specified degrees of freedom of motion. Most of the oscillating foils for marine propulsion employs the NACA profile to define cross-section, indicating that the corresponding manufacture demanding is less

complex compared to screw propellers. The consideration of component number involves both the number of foils for each propulsion unit and the number of propulsion units for the target vehicle. The size constraint and interaction with vehicles may need to take various factors into consideration and make the compromise between performance metrics and engineering practice. The install position and orientation mainly depend on the role of propulsion systems in the vehicle motion. The propulsion system that are used to generate the forward thrust is generally installed at the rear end of target vehicle, while oscillating foils for the production of maneuvering forces tend to be mounted on the front position with either specified orientation or adjustable pivot shaft.

7.2 Design Approaches of APWIGs

For almost all propulsion problems, there is no single design solution to a given vehicle. To provide a reference for the application of APWIGs, three approaches were proposed to perform the design of this novel propulsion system for different operating situations. It should be noted that the current study only focuses on the selection of relevant parameters for performance optimization. The detailed issues such as the mechanical implementation and product manufacture are beyond the scope of this section. Additionally, all three design approaches require systematic numerical computations, implying the experimental verification is warranted for the developed propulsion system by each approach.

7.2.1 Design geometry and kinematic parameters

Table 7-1 Considered parameters in the design process of APWIGs.

Parameters	Description	Restriction
k	Oscillating frequency (Hz)	Actuator power and capability
h_0/c	Heaving amplitude (m)	Actuator power and capability
K^*	Torsional spring stiffness (Nm/rad)	Rigidity of torsional spring
b_0/c	Position of pitching axis (m)	Locomotion stability
d_0/c	Distance between two foils (m)	Collision of trialing edges
AR	Span length (m)	Operating space and flexibility

For most of propulsion design cases, the advance speed is determined by the mission profile of target vehicle. Hence, six parameters are taken into account during the design procedure of APWIGs, which is summarized in Table 7-1. The design problem of APWIGs for the current study is characterized as the optimization of these six parameters that aims to satisfy the requirements of mission profile and maximize the propulsive performance. In general, the selection of these relevant parameters depends on both practical restrictions and influence on the performance metrics. The practical restrictions can

be employed to narrow the space of tested parameters, while the finalization of parameter set will refer to the corresponding propulsive characteristics.

The APWIGs propulsion device has an actively prescribed heaving motion that is imposed by the actuator for each foil. Thus, the range of oscillating frequency and heaving amplitude are restricted by the actuator power and capability. In particular, an extremely high oscillating frequency is not feasible for marine propulsion due to relatively large resistance in water. The heaving amplitude may also be limited by the dimension of target vehicle and install position. The initial scope for these two kinematic parameters is provided by basic information and mission profile before further optimization.

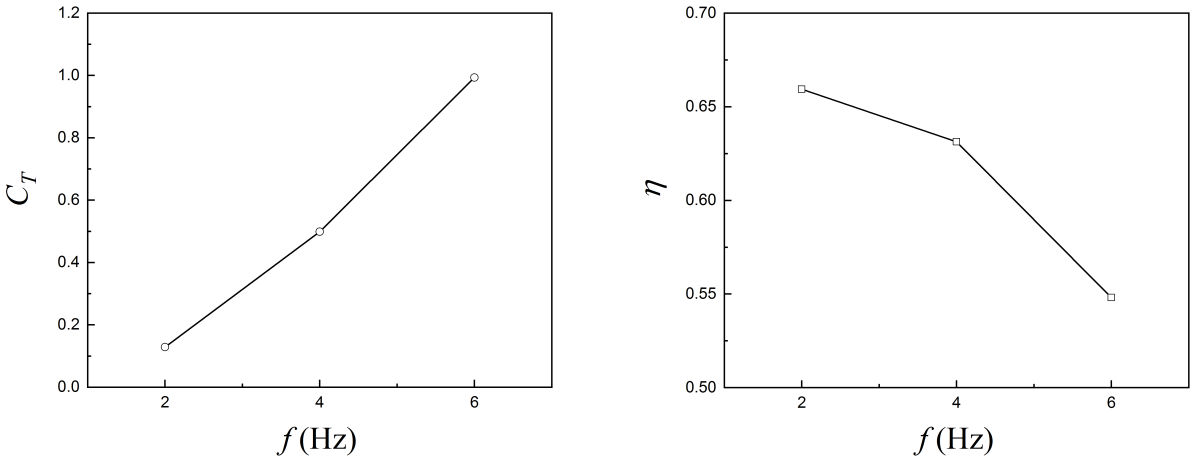

(a) Thrust coefficient (b) Propulsive efficiency

Figure 7-5 Propulsive performance of APWIGs with the variation of oscillating frequency.

The general trend for the propulsive performance of APWIGs with the variation of oscillating frequency and heaving amplitude are presented in Figures 7-5 and 7-6, respectively. It was noted that the thrust coefficient increases when these two parameters become larger. The propulsive efficiency is inversely proportional to the oscillating frequency, while there is an optimum heaving amplitude that generates the maximum efficiency.

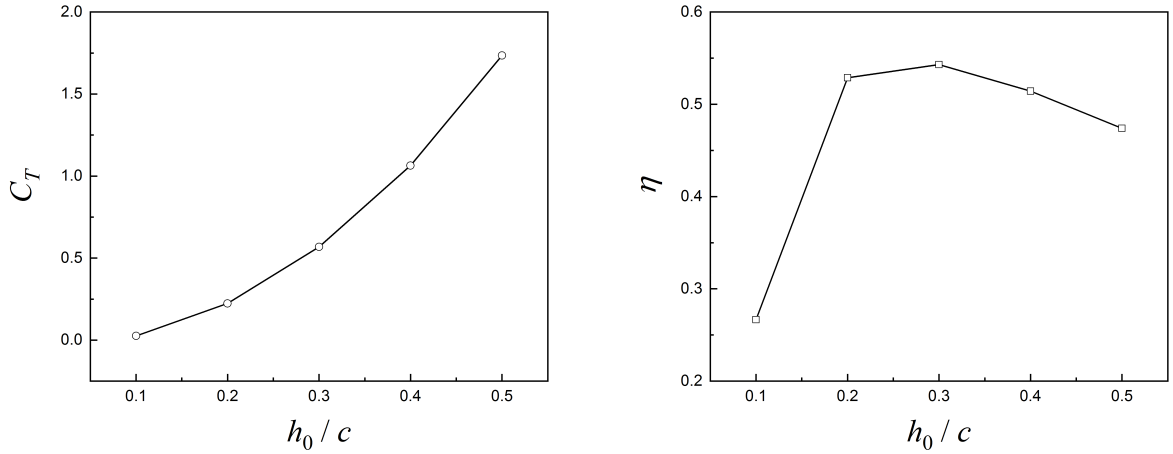

(a) Thrust coefficient (b) Propulsive efficiency

Figure 7-6 Propulsive performance of APWIGs with the variation of heaving amplitude.

The torsional spring stiffness is one of most important parameters for oscillating foil configuration with a flow-adapted pitching motion. It has a significant influence on both locomotion characteristics and propulsive performance. In engineering practice, this parameter is implemented by the rigidity of torsional spring based on the indications of optimization. Figure 7-7 presents the typical propulsive characteristics of APWIGs with the variation of torsional spring stiffness. It can be noted that both thrust coefficient and propulsive efficiency tend to increase first and then decrease with the augment of spring stiffness, implying there exists an optimum torsional spring stiffness.

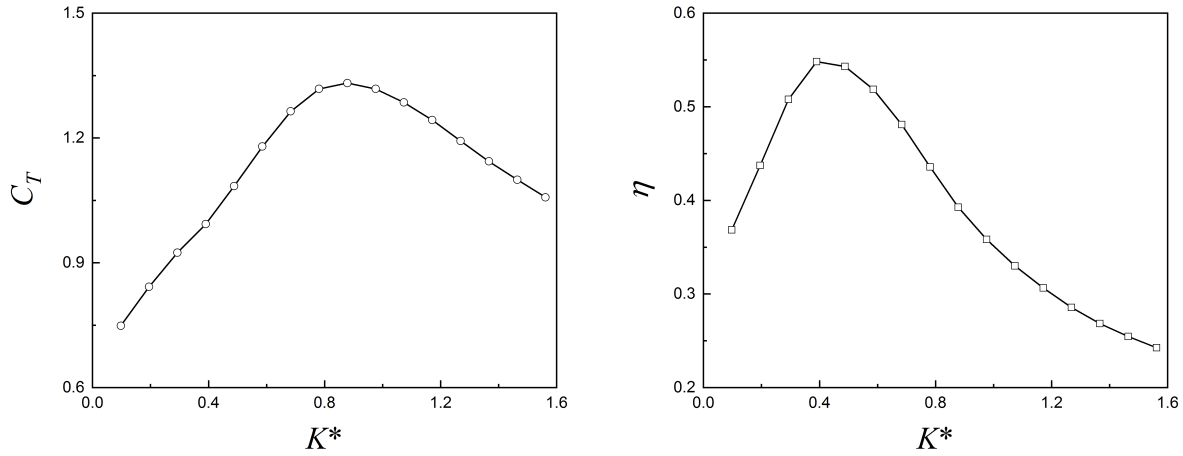

(a) Thrust coefficient (b) Propulsive efficiency

Figure 7-7 Propulsive performance of APWIGs with the variation of torsional spring stiffness.

The position of elastic pitching axis was found to have a critical effect on the dynamic responses of auto-pitch configuration. The APWIGs may produce an unstable locomotion state when the distance of pitching axis from the leading edge is larger than one third of chord length. The performance metrics of APWIGs with the variation of position of pitching axis is shown in Figure 7-8, in which the propulsive efficiency is not plotted for the drag-producing values. It was found that the thrust coefficient presents an increasing trend when the pitching axis move away from the leading edge. The maximum efficiency is achieved by the position of pitching axis at the quarter of chord length.

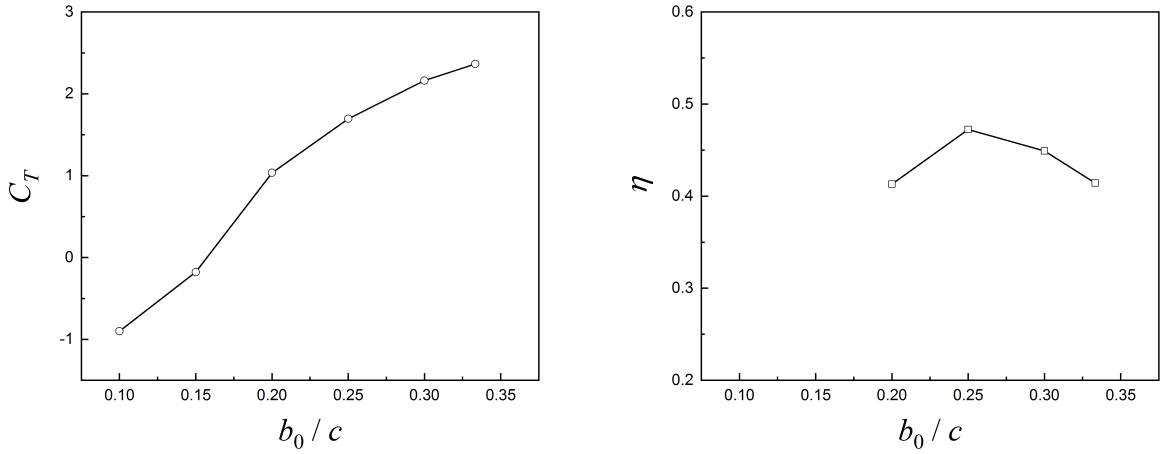

(a) Thrust coefficient (b) Propulsive efficiency

Figure 7-8 Propulsive performance of APWIGs with the variation of position of pitching axis.

In order to avoid the collision of two foils for biplane configuration, the setup of equilibrium distance needs to take the kinematics into consideration. This collision is more likely to occur at the end position of foils implying that the maximum displacement of trailing edge should be considered carefully. For oscillating foil propulsors, the higher span length requires larger operating space and more manufacture cost. Additionally, dramatically high aspect ratio may result in the issue of spanwise flexibility, which tends to increase the possibility of structural failure and decrease the propulsive performance. The effect of spanwise flexibility is not dominant for a low-aspect-ratio foil although corresponding performance is inferior due to the significant three-dimensional effect.

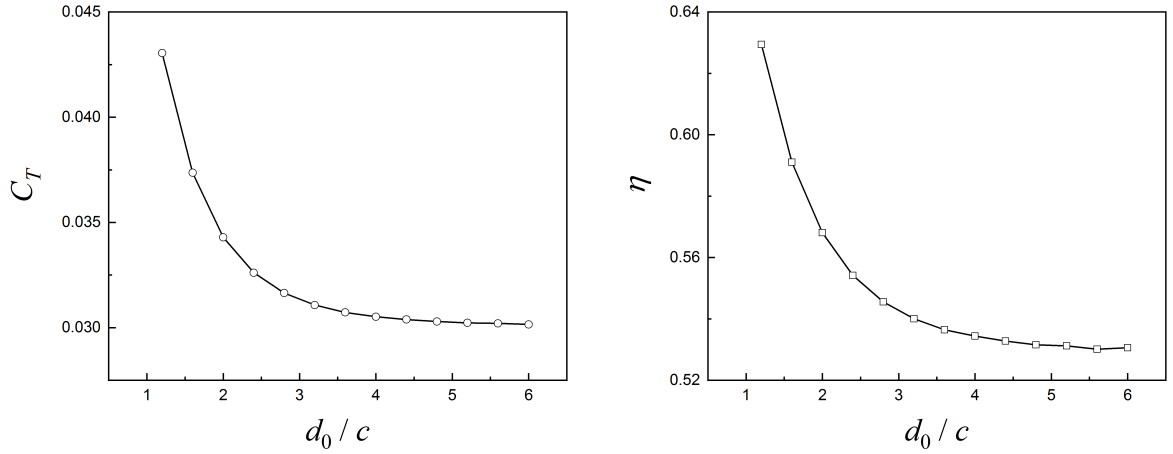

(a) Thrust coefficient (b) Propulsive efficiency

Figure 7-9 Propulsive performance of APWIGs with the variation of distance between two foils.

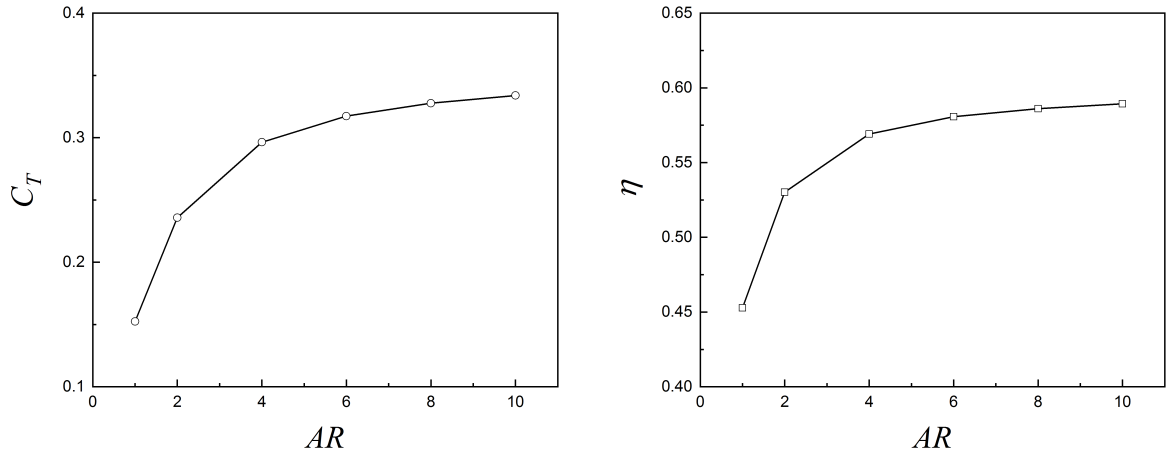

(a) Thrust coefficient (b) Propulsive efficiency

Figure 7-10 Propulsive performance of APWIGs with the variation of aspect ratio.

The general propulsive characteristics of APWIGs with the variation of distance between two foils and aspect ratio are demonstrated in Figures 7-9 and 7-10, respectively. It was indicated that the propulsive performance is inversely proportional to the equilibrium distance of biplane configuration due to the enhancement of WIG effect with a small gap between two foils. The performance metrics was identified to consistently increase with the augment of aspect ratio, which is attributed to the less low-aspect-ratio effect around span and wing tip. Since the influence of distance between two foils and aspect ratio on

the performance metrics of APWIGs is relatively simple, these two parameters are generally considered and examined during latter phases of design procedure.

7.2.2 Objectives of design process

Parameter selection of thrusters is a typical optimization problem with multi-objective design process. For a marine propulsion system using oscillating foils, the design process generally has two objectives including the maximization of forward thrust and maximization of efficiency (or minimization of input power). It should be noted that these two objectives contradict with each other implying that a trade-off between thrust production and propulsive efficiency (or input power) needs to be made.

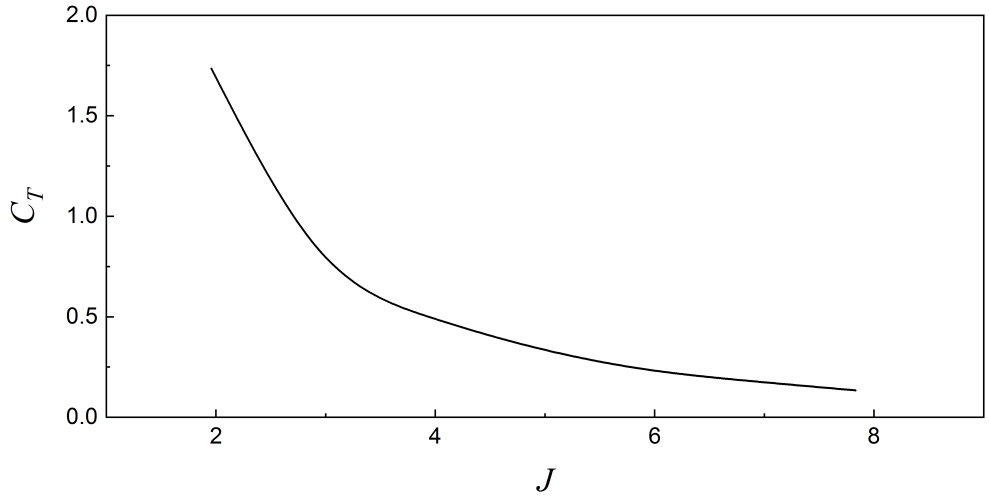

(a) Thrust coefficient

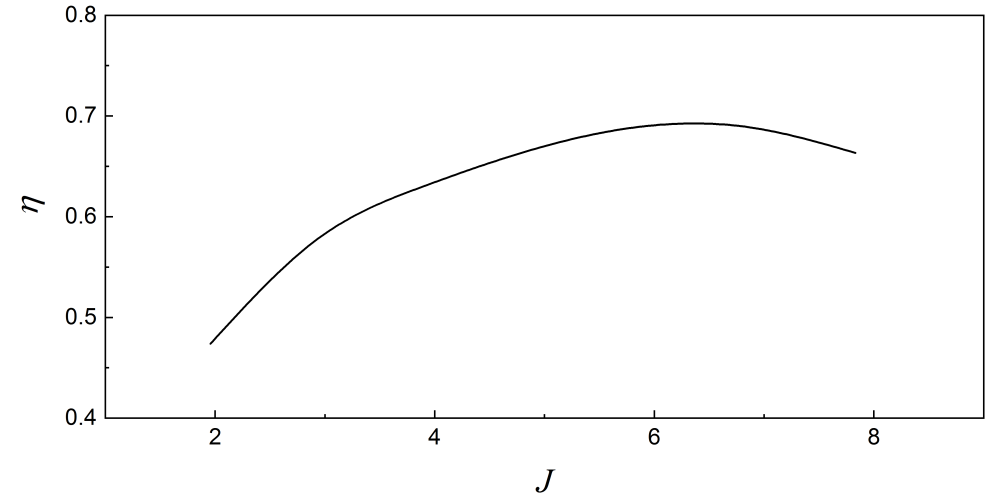

(b) Propulsive efficiency

Figure 7-11 General propulsive characteristics of APWIGs as a function of advance speed.

The general propulsive properties of APWIGs as a function of advance coefficient are presented in Figure 7-11. It was found that the thrust coefficient shows a decreasing trend with the increase of

advance speed, while the propulsive efficiency tends to increase first and then decrease when the advance speed consistently augments. Such a feature generally agrees well with the trend of open-water propulsive characteristics for a screw propeller. However, the plateau of propulsive efficiency for APWIGs was found to have a much wider range compared with that of screw propellers, which indicates that the APWIGs has a potential to operate near the optimal condition. The design objectives of the current optimization problem with respect to APWIGs are chosen as the maximization of time-averaged thrust coefficient and propulsive efficiency. The design objectives are considered throughout whole design procedure bounded by the range of design parameters and applied constraints.

7.2.3 Low-fidelity design method

For the propulsion problem with a moderate search space, a low-fidelity design method was proposed to perform the parameter optimization of APWIGs. This method is suitable for the scenario that a modest number of parameters are involved and the primary interest lies in the search for the highest performance. In particular, the low-fidelity design method can be applied to the phase of preliminary design after the initial assessment of considered parameters in conceptual design. The comprehensive parameter search by this approach is crucial for further refinement of design parameters.

Since an exhaustive parameter sweep based on CFD calculations is required, a numerical model that is computationally cheap is essential for the low-fidelity design method. Hence, the computer program named oscillating foil boundary element method (OSFBEM) was selected as the key module for the design procedure of low-fidelity design method. The OSFBEM based on the time-domain panel method was developed by Liu (1996) to simulate the unsteady flow around oscillating foils. This computing program has been proved to be a reliable tool in predicting hydrodynamic characteristics of oscillating foils with the wide applications to the studies on both propulsors and energy harvesters (Liu, 2005b; Liu et al., 2010; Liu, 2015). The numerical program of OSFBEM has a high computing efficiency at the expense of physical fidelity, suggesting that this program is an ideal choice to conduct the parameter exploration for the current low-fidelity design method.

The design procedure for the parameter optimization of APWIGs using the low-fidelity design method is presented in Figure 7-12. The details of each phase in this flow diagram are described as follows:

- The design process starts with the mission profile that provides specific requirements and essential information for target vehicle, including the principal dimensions, operating speed, data of model tests, engine power, etc.
- The number of concerned parameters during the design procedure is estimated by taking the imposed restrictions into consideration, such as the propulsor size.
- Based on the initial analysis and assessment, the range of each design parameter is determined to bound the search space and narrow the computing scope.

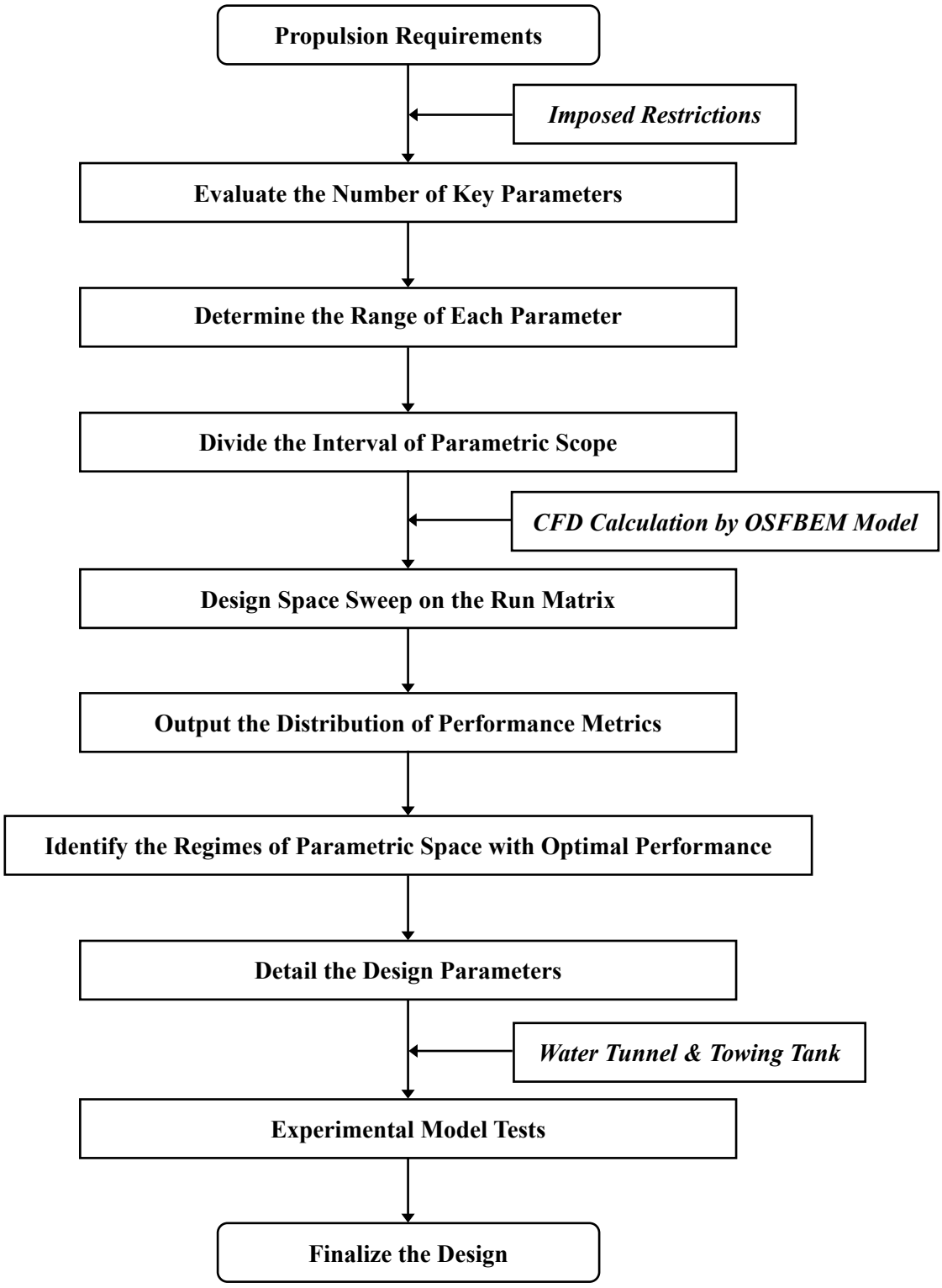

Figure 7-12 Flow diagram for the design of APWIGs using low-fidelity design method.

- According to the extent of correlation for each parameter to hydrodynamic characteristics, the parametric scope is divided by a certain interval to generate a run matrix.
- The design space sweep based on the CFD calculations using the computing program of OSFBEM is performed on the generated run matrix.

- The distribution of performance metrics for APWIGs is obtained as a raw database, which is then handled and analyzed by various post-processing tools.
- The regimes in search space with optimal or near-optimal performance are identified based on the distribution of performance metrics.
- The details of design parameters are determined by balancing the propulsive performance and engineering feasibility, which are used to prepare for fabrication.
- Systematic experimental model tests are conducted in both water tunnel and towing tank to verify the propulsive performance and capability of designed APWIGs.
- The set of design parameters are finalized if all mission requirements are satisfied.

The low-fidelity design method is regarded as the most straightforward approach to perform parameter optimization of APWIGs. This method is expected to provide a comprehensive parameter search by covering a certain number of design parameters and a moderate scope of parametric space, indicating that there is a high possibility to find the optimum parameter combination. The outputs of this design procedure are characterized as a series of charts for the hydrodynamic properties and a variety of contours for the distribution of performance metrics. Although the limited flow behaviors such as turbulence, separation of boundary layer and vortex shedding can be identified, the low-fidelity design method is capable of providing systematic information for propulsive characteristics of APWIGs which is essential for the parameter selection.

7.2.4 High-fidelity design method

For the design problems with a concentrated parametric space and bounded by a number of restrictions, the higher accuracy and reliability of evaluations may be required in the design process. In this scenario, a high-fidelity design method was developed to conduct the parameter optimization of APWIGs. This method is suitable for situations when the flow behaviors dominate the hydrodynamic characteristics and the effect of design parameters on the design objectives is one of primary interests. During the stage of mechanism analysis in the development loop of oscillating foil propulsors, the high-fidelity design method is an ideal choice to provide the insights into the appropriate parameter selection and ensure an accurate assessment of performance characteristics.

To provide precise evaluation for the design objectives, a Navier-Stokes solver is needed during the design procedure. Herein, the established and well-validated URANS model in previous sections was employed to act as the key module of design process. It can be conjectured that the satisfactory physical fidelity is preserved by the high-fidelity design method at the expense of computing efficiency. Since the simulations using the Navier-Stokes solver is computationally expensive, the exhaustive parameter sweep based on the high-fidelity design method is not feasible for most of design cases. The principal of the current high-fidelity design method is to determine the values of design parameters in sequence

according to the extent of correlation of each parameter to the hydrodynamic characteristics. It should be noted that the testing sequence of design parameters may vary depending on the specific mission requirements and imposed restrictions. The main merits of this design method are the high credibility of performance evaluation and various outputs of flow information. The shortcoming of this design method is also obvious which is the high possibility for the omission of optimum parameter combination with highest performance, as a result of that the design parameters are determined sequentially.

The design process of the high-fidelity design method for parameter optimization of APWIGs is shown in Figure 7-13. The interpretation for each phase of the flow diagram is summarized as follows:

- The mission profile specializes the propulsion problem that is bounded by various design requirements and general data of target vehicle.
- The importance of all involved design parameters is systematically evaluated by the extent of correlation of each parameter to the hydrodynamic characteristics.
- The sequence of parameter optimization is determined based on previous correlation evaluation. The generated parameter sequence with the order of priority of testing is different for various situations. The following descriptions represent a certain parameter sequence.
- The parametric scope for position of pitching axis is decided according to corresponding imposed restrictions. The propulsive performance of APWIGs as a function of position of pitching axis is firstly examined using two-dimensional URANS simulations while all other design parameters are remained constant.
- The parametric scope for heaving amplitude is decided according to corresponding imposed restrictions. By adopting the previous optimized parameters, the propulsive performance of APWIGs as a function of heaving amplitude is examined using two-dimensional URANS simulations while all other design parameters are remained constant.
- The parametric scope for distance between two foils is decided according to corresponding imposed restrictions. By adopting the previous optimized parameters, the propulsive performance of APWIGs as a function of distance between two foils is examined using two-dimensional URANS simulations while all other design parameters are remained constant.
- The parametric scope for aspect ratio is decided according to corresponding imposed restrictions. By adopting the previous optimized parameters, the propulsive performance of APWIGs as a function of aspect ratio is examined using three-dimensional URANS simulations while all other design parameters are remained constant.
- The oscillating frequency and spring stiffness are optimized at the same time. The relevant imposed restrictions generate a run matrix for these two parameters. Taking all other design parameters as the obtained optimum values, the performance metrics as a function of oscillating frequency and

spring stiffness are evaluated by three-dimensional URANS computations.

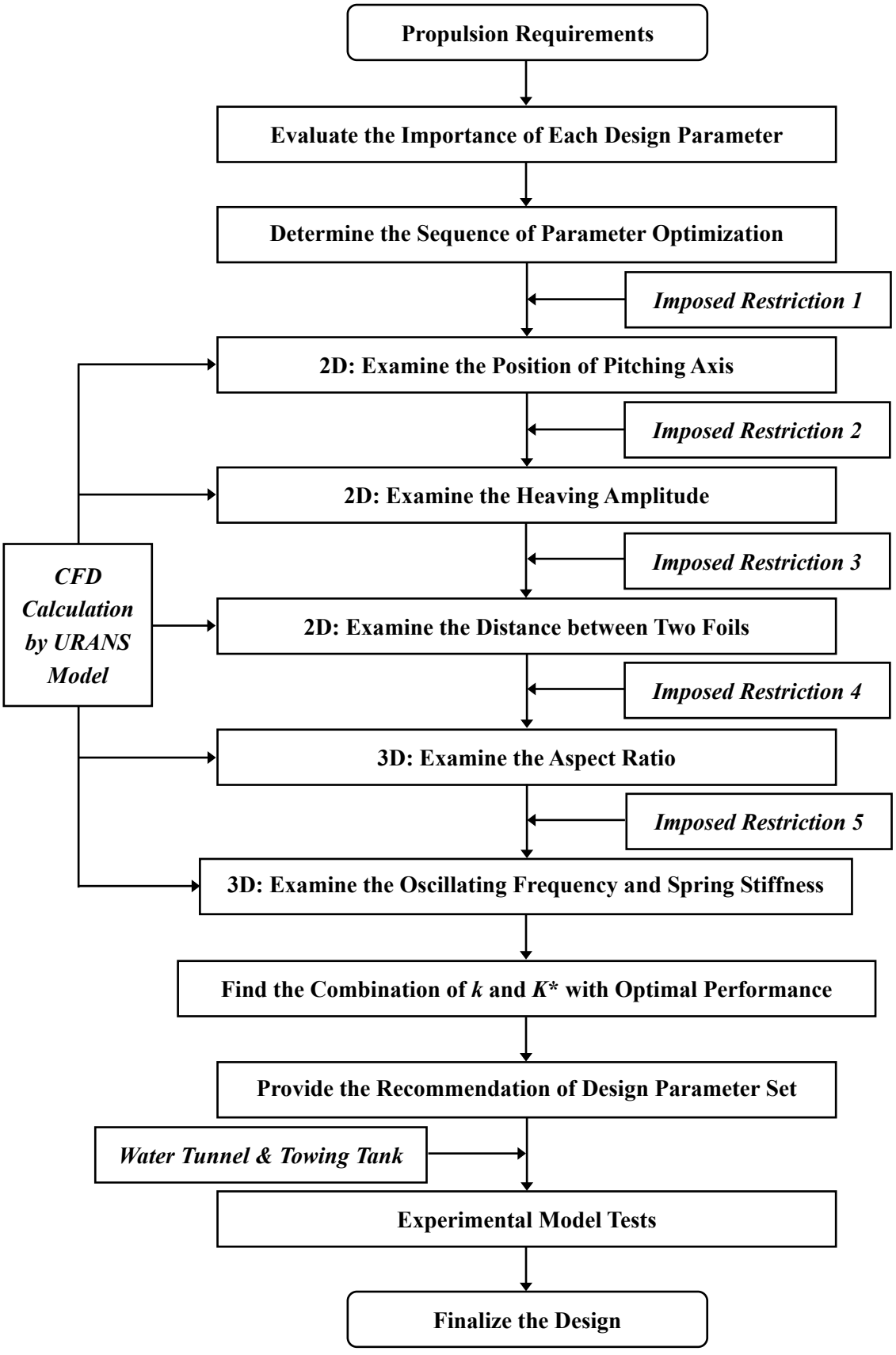

Figure 7-13 Flow diagram for the design of APWIGs using high-fidelity design method.

- The parametric regimes with the optimal propulsive performance are identified to determine the values of oscillating frequency and spring stiffness.
- Based on the previous optimized results, a recommendation of design parameter set is provided to guide the fabrication.
- A series of experimental tests are performed in both water tunnel and towing tank to verify the propulsion properties of designed APWIGs.
- All design parameters are finalized when the mission profile is fulfilled.

The high-fidelity design method is believed to provide the most reliable evaluation for the propulsive performance of APWIGs during the design process, even though it cannot cover all parameter subsets in the whole parametric space. The outputs of this design method are characterized as a series of characteristics charts indicating the individual effect of each parameter and comprehensive numerical visualizations indicating the details of flow field. In particular, the distribution contours of performance metrics with the variation of oscillating frequency and torsional spring stiffness can be obtained by this approach. Such the information is highly essential to guide the development of powerful and efficient APWIGs. The complicated flow features such as effect of viscosity, vortices behaviors and wake patterns are identified by high-fidelity design method, which can enhance fundamental understanding of physical mechanisms and hence contribute to the latter stages of design procedure.

7.2.5 Multi-fidelity design method

The design process for most of propulsion problems using oscillating foils involves a large number of design variables, which leads to an enormous search space. The exhaustive parameter sweep for such a design problem is not feasible even by a potential-flow-based solver. It is fairly challenging to resolve such propulsion problem by individual computational model. Inspired by the works of Willis et al. (2008) and Zheng et al. (2013), a multi-fidelity design method was developed to address propulsion design of APWIGs for general engineering problems with a large design space. Compared with aforementioned two design methods, the multi-fidelity design method is considered as a relatively integrated and thorough approach with a significant universality. This approach is believed to have the capability to conduct a comprehensive parameter optimization accompanying with the highly accurate and reliable performance evaluation.

The multi-fidelity design method consists of three key modules, including the OSFBEM solver, Navier-Stokes solver and optimization algorithm. A compromise between model fidelity and computational effort is made by integrating the OSFBEM solver developed by Liu (1996) and the Navier-Stokes solver established in the current study into a single computational framework. The widely used genetic algorithm (Holland, 1992) was selected as the optimization algorithm to perform the search of large parameter space. Generally, the genetic algorithm mimics the process of natural selection which starts with the creation of a series of initial individuals with randomly selected design parameters. The

performance metrics of these individuals are then evaluated by the given objective function. After that, the individuals with high fitness are propagated into the next generation, while the poor individuals are eliminated. In addition to these high-fitness individuals, the next generation is also filled with the novel individuals generated by various operators such as crossover and mutation. The optimization process is repeated until the converged criteria are satisfied. The individuals with the highest fitness are taken as the basis for the search of optimum design parameters when the genetic algorithm converges. It should be noted that several constraints are applied to the implementation of genetic algorithm, which is used to avoid the solutions without physical significance or beyond the considered parametric space. More details with respect to the genetic algorithm can be referred to Holland (1992).

The principal of multi-fidelity design method is to generate the design parameters for APWIGs by the coupling of genetic algorithm with OSFBEM solver, which is then systematically evaluated by the Navier-Stokes solver. This design procedure involves two loops including the initial variables optimization and design parameters refinement. In the inner loop of variables optimization, the created design parameters by genetic algorithm are transferred to the OSFBEM solver to assess the values of objective functions, and resulting performance metrics of these variables are in turn employed to guide the parameter selection in the module of genetic algorithm. In the outer loop of parameters refinement, the generated design parameters by genetic algorithm and OSFBEM solver are input to the module of Navier-Stokes solver to verify the corresponding performance metrics. If the design requirements are not satisfied, the parametric space is refined and the relevant design phases are repeated until the mission profile is completely attained. Such the optimization loops ensure that the designed geometry and kinematic parameters can achieve the expected propulsive performance for the target vehicle.

The design procedure using the multi-fidelity design method for the parameter optimization of APWIGs is indicated in Figure 7-14. Further details in the flow diagram are presented as follows:

- The mission profile with the propulsion requirements and general information of target vehicle is provided to define the design problem.
- All relevant geometry and kinematic parameters are selected as design variables. The optimization objective is taken as the weighted sum of multiple design objectives including the maximization of forward thrust and maximization of propulsive efficiency.
- The parameter search space is generated by imposing the various restrictions in both geometric consideration and locomotion aspect.
- The optimization loop is repeated by the information interchange between the optimization algorithm and OSFBEM solver until the converged criteria are satisfied. The generated high-fitness individuals with design variables are regarded as the basis of search for optimum solutions.
- The performance metrics of selected solutions are comprehensively evaluated by the Navier-Stokes solver. The design procedure moves on to the next phase if all requirements are satisfied, while the

design process is repeated with refined parameters when the mission profile is not completed.

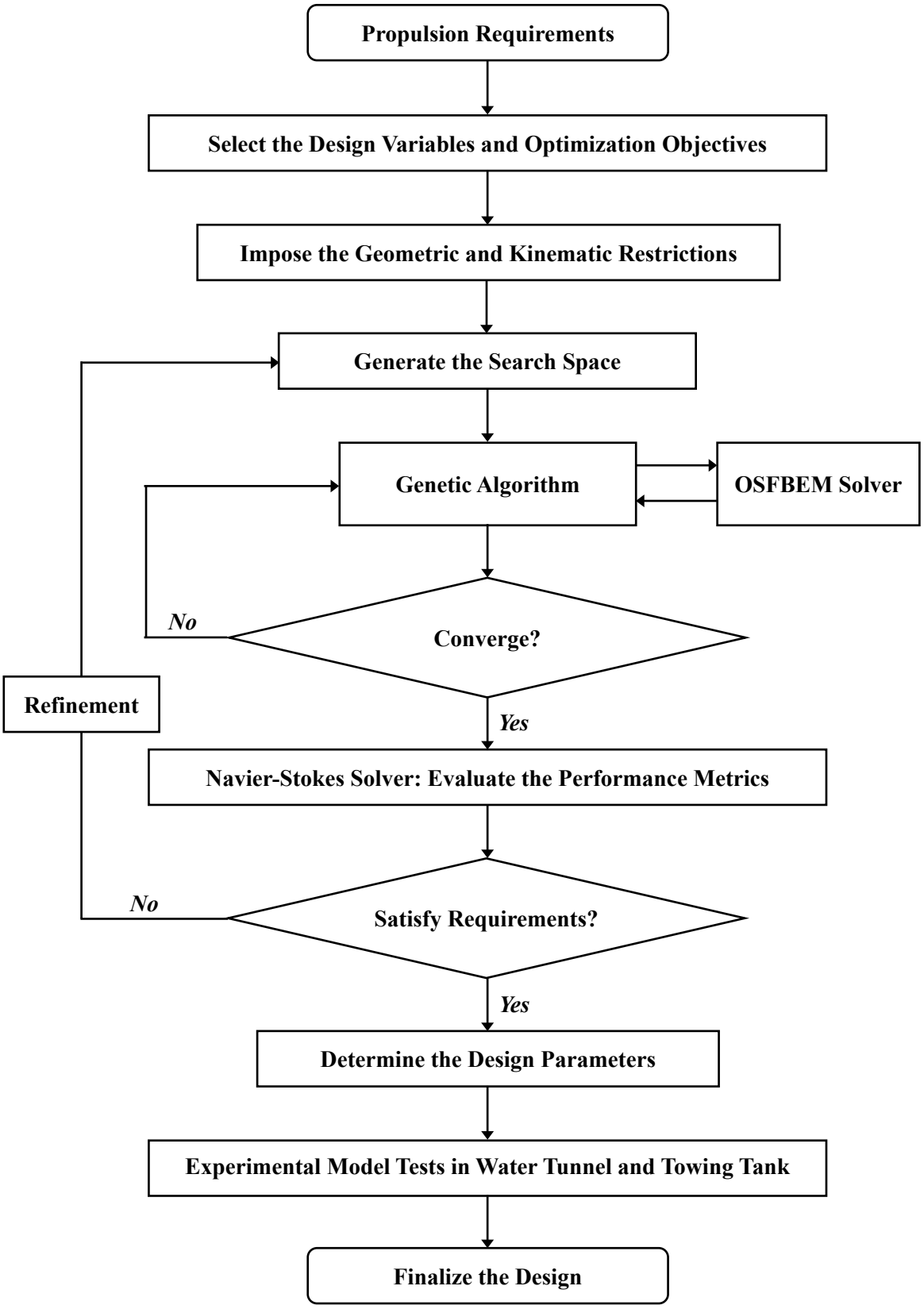

Figure 7-14 Flow diagram for the design of APWIGs using multi-fidelity design method.

- The set of design parameters for APWIGs are determined to provide guidance for the further fabrication and installation.
- A series of experimental model tests for the developed APWIGs system are conducted in both water tunnel and towing tank to verify the corresponding capability and performance.
- The design procedure is finalized with the optimized parameters when all propulsion requirements are achieved.

The multi-fidelity design method is considered as the most robust one among three design approaches since it both covers an adequately large search space and guarantees an accurate performance evaluation. The coupled optimization algorithm can significantly increase the possibility that the optimum or near-optimum solutions for APWIGs design are found within the parametric space. The multiple verifications of performance metrics by the potential-flow-based model, viscous-flow-based model and experimental tests can ensure the credibility of optimization results. The outputs of multi-fidelity design method are characterized as both comprehensive propulsion characteristics with variation of design parameters and detailed visualizations of flow field. The propulsion characteristics of APWIGs as a function of relevant parameters are used to analyze the performance distribution and identify the optimum regimes of parametric space, while the various visualizations with flow behaviors can provide insights into the correlation between optimization objectives and flow pattens. In general, the multi-fidelity design method provides an effective and reliable procedure to guide the design and development of APWIGs system for propulsion community.

7.3 Case Study on Propulsion of AUV

To enhance the interpretation of design procedure for APWIGs, a case study on the propulsion problem of a given AUV using the developed multi-fidelity design method was presented here. It should be noted that no computational results are included in this section due to the limitation of available computing resources. Herein, the primary objective is to illustrate the design principal and demonstrate the design process for the proposed multi-fidelity design approach.

7.3.1 Basic data of *nupiri muka* AUV

The autonomous underwater vehicles are unmanned robotic devices powered by a propulsion system. Owing to the significant mobility and increasing ability to carry multiple payloads, the AUV has been applied to a broad range of tasks, such as oceanographic surveys, bathymetric data collection, cable or pipeline inspection, environmental monitoring and route survey. A typical AUV generally consists of the pressure hull, propulsion system, power supply, communication system, navigation system and various sensors. It is worth noting that an efficient propulsion system with the ability to generate

directional forces is crucial for the deployment of AUV due to its high requirements regarding the endurance and maneuverability.

The current case study selects the *nupiri muka* AUV as the target vehicle to demonstrate the design procedure of APIWGs using the multi-fidelity design method. The name of *nupiri muka* means 'Eye of the Sea' in palawa kani that is the language of Tasmanian Aborigines. The *nupiri muka* AUV is an Explorer-class AUV which is constructed by International Submarine Engineering (ISE). The *nupiri muka* project is funded by the Australian Research Council (ARC) Special Research Initiative for Antarctic Gateway Partnership and Australian Maritime College (AMC), University of Tasmania (UTAS). The *nupiri muka* project aims to develop a research tool for data acquisition under ice shelf in the Antarctic, which has been successfully deployed in different environments to conduct a series of scientific missions by equipped instruments.

Table 7-2 Technical specifications of *nupiri muka* AUV.

Characteristic	Specification
Weight	1600 kg
Displacement	1600 kg
Length	6.25 m
Height	1.4 m (including antennas)
Beam	1.5 m (including fore planes)
Body Diameter	0.74 m
Turning Radius	10 m
Depth Capability	5000 m
Speed Capability	1.0-2.6 m/s
Normal Operating Speed	1.5 m/s
Power	Li-Ion Batteries (32 kWh)
Endurance	40 hours (300km)
Propulsion	Brushless DC motor driven propeller

The technical specifications with respect to the principal data and payload sections for *nupiri muka* AUV were described by Loh (2020) in detail. The major properties of *nupiri muka* AUV are summarized in Table 7-2. This vehicle has a capability to travel at the speed between 1.0-2.6m/s and dive to the depth of 5000m. The propulsion system employs a screw propeller to maintain a normal operating speed of 1.5m/s. In this section, an attempt to design an APWIGs thruster to propel the *nupiri muka* AUV by the multi-fidelity design procedure was performed. Rather than a computational work, the focus of this

case study was concentrated on a step-by-step guidance for the parameter selection of APWIGs.

Compared with a conventional propeller for AUV, the designed APWIGs is expected to achieve several advantages. Firstly, the APWIGs using an appropriate parameter combination has a bigger potential in performance maximization over a traditional propeller. Besides, the APWIGs shows a lower sensitivity to advance speed than screw propellers which usually experience a severe drop of performance at a relatively large forward speed. Moreover, unlike the conventional propellers, the APWIGs has a less possibility to encounter the issues of cavitation, noise, vibration and structural damage due to the simple geometry and motion. In addition, a higher maneuverability for AUV can be achieved by APWIGs compared to propellers owing to the operating mechanism of oscillating foils.

7.3.2 Design process of APWIGs

In order to develop a novel propulsion system for a marine vehicle, prerequisite conditions need to be satisfied before the start of design procedure. In addition to the presented technical specifications in Table 7-2, it is assumed that the required information such as the data of buoyancy and stability, hydrostatic properties and hydrodynamic characteristics for *nupiri muka* AUV are available based on the results of either model tests or CFD computations. The effective power from experimental measurements or computing estimations and the engine power determined by manufacturer should be explicitly indicated. Furthermore, all restrictions with respect to both geometric dimension and kinematic scope need to be pointed out clearly to ensure the validity of the designed propulsion system. In general, all preconditions including the technical specifications, required information and imposed restrictions for the vehicle are summarized to a mission profile coupling with the design objectives.

The biplane arrangement is taken as the basic configuration for APWIGs. The cross-section of each foil is selected as the NACA0012 profile. By referring to the ratio of vehicle dimension with propeller size, the chord length of foils is set as 0.4m that is approximately equal to the radius of propeller. This setup takes several issues into consideration such as the limitation of operating space, installation of propulsion system and vehicle stability. As indicated before, there are six design parameters that need to be considered during the design process of APWIGs, including the oscillating frequency (k), heaving amplitude (h_0/c), torsional spring stiffness (K^*), position of pitching axis (b_0/c), distance between two foils (d_0/c) and aspect ratio (AR). The design objectives for the current propulsion problem are characterized as the maximization of thrust coefficient and propulsive efficiency. Since the single-objective optimization algorithm is used in the current design procedure, such a design problem with multiple objectives is transformed into a single-objective problem by the weighted sum method.

The maneuverability with directional forces for *nupiri muka* AUV is assumed to be achieved by the auxiliary planes. Hence, the main focus is concentrated on the development of the primary propulsion system at the rear end of vehicle. Based on the previous multi-fidelity design method, the design procedure of APWIGs for *nupiri muka* AUV is demonstrated as follows:

1. The propulsion problem with indicated design requirements is well defined and assessed by a given mission profile for *nupiri muka* AUV. The design aims to develop an APWIGs system for this vehicle to provide the required forward thrust. The developed propulsion system should be capable of satisfying the listed performance specifications and having no obvious influence on the operation of vehicle.

2. The design variables are clearly identified. Since the effect of distance between two foils (d_0/c) and aspect ratio (AR) on the hydrodynamic characteristics of APWIGs are monotonous and straightforward, these two parameters are not involved in the optimization process. The AR is taken as a minimum recommended value of 3 by the previous discussion. The d_0/c is initially selected as a safe value that avoids the collision of two foils, which will be adjusted to the allowed minimum value after all other parameters are determined. The remaining parameters of k, h_0/c, K^* and b_0/c are regarded as the design variables to perform the parameter optimization.

3. For the optimization objectives, the optimized forward thrust for *nupiri muka* AUV should be at least larger than a certain value in which the vehicle can be propelled at the normal operating speed of 1.5m/s. The optimization objective of propulsive efficiency is to attain a result as high as possible. In order to employ the optimization algorithm, these two objectives are converted into a single objective using the weighted sum of them.

4. All imposed restrictions and technical specifications are comprehensively analyzed to evaluate the bounds of search space. The scope of oscillating frequency is limited by the actuator power. The principal dimensions and operating space of vehicle place a constraint in the heaving amplitude. The position of pitching axis should be set at the first half chord from the leading edge to ensure the locomotion stability of APWIGs. The setup of torsional spring stiffness has a relatively high freedom, the scope of which can be given by preliminary computations. Thus, a design space is generated based on evaluated bounds of these four variables.

5. Within the design space, a population of initial individuals with randomly selected design variables (k, h_0/c, K^*, b_0/c) are generated by the genetic algorithm. By transferring the parameters to OSFBEM solver, the performance metrics of these individuals are evaluated using the objective function. The individuals with high fitness are propagated into the next generation, which is filled by various operators. The coupling loop between genetic algorithm and OSFBEM solver is repeated until either the optimization criteria are satisfied or the number of generations reaches the maximum value.

6. After the genetic algorithm converges, the optimized results are generally characterized as a series of high-fitness individuals in the parametric space. Hence, a parameter subset with different variable combinations is obtained to represent the possible optimum or near-optimum solutions. These solutions are input to Navier-Stokes solver to verify corresponding propulsive performance of APWIGs. The combinations of design variables are taken as the basis for the parameters selection when all mission requirements are satisfied. The design procedure is moved back to the fourth phase to refine the search space if no qualified solutions are identified.

7. By taking into account the feasibility of practical operation, the most appropriate combination of design parameters among satisfactory individuals is taken as the solution of optimization problem. Thus, the parameter setup of APWIGs for prototype fabrication is determined by this optimized result with four design variables (k, h_0/c, K^* and b_0/c) and two directly selected parameters (d_0/c and AR).

8. A series of experiment validations are conducted to examine the credibility of developed APWIGs. Firstly, the propulsion tests for APWIGs model are performed in water tunnel independently to report the hydrodynamic characteristics and performance metrics. Secondly, the experimental measurements on APWIGs model installed at the rear end of vehicle model are carried out in the towing tank to demonstrate the comprehensive capability of this thruster. The design procedure is closed and the design parameters are finalized when the results of all model tests meet the mission requirements.

7.3.3 Recommendation of parameter setup

The current design process is expected to provide a parameter set suggesting the exact value of each design variable. Based on the multi-fidelity design method, a general recommendation for the parameter setup of APWIGs as the propulsion system of *nupiri muka* AUV is summarized in Table 7-3. The relevant parameters can be classified into three groups depending on selection principal. The characters of n_1, m_1, m_2, m_3 and m_4 in this recommendation list represent the values of corresponding parameters that are obtained by the optimization algorithm and computational solvers. These parameters are not explicitly provided as the solution of these values is beyond the scope of this section.

Table 7-3 The recommendation of parameter setup for APWIGs as the propulsor of *nupiri muka* AUV.

Parameters	Recommendation	Selection Principal
Section profile	NACA0012	Based on literature survey
Chord length	c = 0.4 m	Based on propeller size
Aspect ratio	AR = 3	Guided by simulations
Distance between two foils	$d_0/c = n_1$	Guided by simulations
Position of pitching axis	$b_0/c = m_1$	Optimization procedure
Heaving amplitude	$h_0/c = m_2$	Optimization procedure
Oscillating frequency	$k = m_3$	Optimization procedure
Torsional spring stiffness	$K^* = m_4$	Optimization procedure

Most of the studies on the oscillating foil propulsion in literature prefer a symmetric section profile such as NACA0012 or NACA0015. The difference of performance metrics for these two section profiles is expected to be negligible due to their highly similar geometry. A cross-section of NACA0012 for APWIGs of *nupiri muka* AUV is recommended by following this common style. The chord length is

taken as 0.4m by referring to the propeller size. The aspect ratio of 3 is recommended by referring to previous three-dimensional simulations. Thus, the geometric features of each foil for the designed APWIGs can be determined with these three parameters.

By using the multi-fidelity design method, the design parameters involved in optimization procedure are obtained by the modules of genetic algorithm and OSFBEM solver and verified by the module of Navier-Stokes solver. The recommended values for parameters of b_0/c, h_0/c, k and K^* are believed to produce an optimal or near-optimal performance satisfying the mission requirements of *nupiri muka* AUV. After the confirmation of these four parameters, the initial d_0/c is modified to an allowed minimum value by avoiding the collision of two foils which aims to maximize favorable WIG effect. It should be noted that the recommendation of parameter setup serves for the specialized vehicle and operating condition which needs to be regenerated for a different propulsion problem.

7.4 Concluding Remarks

The design methods for the development of APWIGs as the propulsor of marine vehicles were explored in this section. It should be noted that the current section only presents a conceptual demonstration without any computations due to the limitation of computing sources. A typical design process for conventional screw propellers in literature that have been well established was described to provide significant insights into the design procedure of novel propulsion systems. It was indicated that a given propulsion problem generally has multiple design solutions. To this end, three approaches with different model fidelity were proposed to address the design of APWIGs under various conditions.

The first approach is the low-fidelity design method that works for a moderate search space. The key module of this design method is the potential-flow-based OSFBEM solver, which has a high computing efficiency at the expense of physical fidelity. The principal of low-fidelity design method is to perform a design space sweep to find the optimum solution. The second approach is the high-fidelity design method that is suitable for the situations with a concentrated parametric space and a number of restrictions. A viscous-flow-based Navier-Stokes solver is used as the core of this design method. The evaluation of performance metrics by this approach is believed to be accurate but computationally expensive. The principal of high-fidelity design method is to determine the related parameters in sequence based on the dependency level of hydrodynamic characteristic on each parameter.

To handle a general propulsion problem with a large search space, a multi-fidelity design method was developed to conduct the parameter optimization of APWIGs. This design procedure is made up of three key modules including the genetic algorithm, OSFBEM solver and Navier-Stokes solver. The design process of multi-fidelity design method is characterized as an optimization loop and a refinement loop. All design variables are firstly optimized by the genetic algorithm, which employs the performance assessment by OSFBEM solver to select the high-fitness individuals. The possible optimum and near-

optimum solutions are then evaluated by the Navier-Stokes solver. The search space is refined to repeat the design procedure when the mission requirements are not satisfied.

In addition to applicable scenario, the difference of features and outcomes for three approaches are evident. The low-fidelity design method is expected to produce a systematic presentation of propulsion characteristics even though limited flow information can be provided. There is a high possibility that the optimum solution is obtained by this method since an exhaustive parameter sweep is involved. The various flow behaviors such as vortex shedding and wake patten can be identified by the high-fidelity design method in detail, which can enhance understanding for the effect of key parameters on the design objectives. The multi-fidelity design method is regarded as the most robust approach that is capable of providing both comprehensive evaluation of performance metrics and elegant information of flow field. Since it is proposed to handle the universal propulsion problems, the multi-fidelity design method has the highest potential to promote the practical application of APWIGs. To demonstrate the detailed process of multi-fidelity design method, a case study was conducted to develop an APWIGs system for the propulsion of an AUV, which attains a general recommendation of parameter setup.

CHAPTER 8

Conclusions

8.1 Research Summary

This thesis performed a numerical investigation into the propulsive performance of a novel oscillating foil propulsor named APWIGs. The propulsion device of APWIGs is characterized as the combination of biplane configuration with counter-phase heave and flow-induced pitch constrained by torsional springs. The biplane arrangement is expected to produce a favorable WIG effect, while the auto-pitch mechanism is capable of improving flow separation around the foil surface. The aim of this study is to explore the potential of APWIGs serving as a marine propulsor by systematic performance evaluation. A preliminary database of propulsion characteristics was built to guide the development of APWIGs. Key insights into the correlation between hydrodynamic characteristics and flow behaviors for oscillating foils were gained to enhance the understanding of involved flow physics.

The current study commenced with the establishment of a numerical model based on the open-source CFD platform *OpenFOAM*. The flow solver with the solution of Navier-Stokes equations was used to simulate the unsteady flow around oscillating foils. A six degrees of freedom motion solver in *OpenFOAM* toolbox was modified to compute semi-active kinematics of APWIGs in a computational domain with dynamic mesh. The effect of boundary layer was solved by the URANS method coupled with the wall functions. Comprehensive verification and validation were conducted to demonstrate the credibility of established numerical model.

The first focus of this thesis was the hydro-elasticity characteristics of APWIGs indicated by the influence of torsional spring stiffness. The general trend of propulsive performance was directly demonstrated by the non-dimensional spring stiffness. The frequency ratio was employed to distinguish the locomotion states and depict the distribution of performance metrics. Simulations on the hydro-elasticity characteristics of APWIGs sought to find an optimum spring stiffness leading to the stable locomotion and highest performance. Followed by that, a two-dimensional parametric study on the propulsive performance of APWIGs was conducted by taking various parameters into consideration. Based on a series of computations, it was aimed to provide significant insights into the effect of each parameter on both dynamic responses and hydrodynamic characteristics of APWIGs. Additionally, the flow behaviors were connected with corresponding hydrodynamic characteristics to gain implications in the high-performing operating mechanisms of APWIGs.

Subsequently, a comparative study of propulsive performance between APWIGs and widely examined configurations was performed to highlight the superiority of APWIGs for marine propulsion. In addition to current configuration of interest, three propulsion systems were involved in the comparison of performance metrics, including the single auto-pitch oscillating foil, biplane heave-only configuration and biplane fully-prescribed configuration. The comparison between APWIGs and single auto-pitch oscillating foil was employed to demonstrate the performance improvement as a result of beneficial WIG effect. The contrast of APWIGs with biplane heave-only configuration was performed to emphasize the significant role of rotation in start-up thrust generation. To indicate the advantage of

flow-adapted pitch, the difference of propulsion characteristics between APWIGs and biplane fully-prescribed configuration was examined extensively.

After that, a series of three-dimensional computations on performance metrics of biplane configuration were carried out to completely uncover the flow physics of oscillating foils in the real flow. The effect of aspect ratio on the hydrodynamic characteristics of WIG effect oscillating foil propulsors using fully prescribed kinematics was firstly studied. The previous two-dimensional investigation into the dynamic responses and propulsive performance of APWIGs was then extended to the three-dimensional situation. Herein, the efficiency degradation due to the low-aspect-ratio effect for biplane configuration and the hydro-elasticity characteristics of finite-span APWIGs were the primary interests. Furthermore, the wake topologies of three-dimensional oscillating foils were numerically visualized to demonstrate finite-span vortex features and compare with the flow patterns of infinite-span simulations.

Finally, the design procedure that aims to guide the parameter selection of APWIGs was explored. Three design approaches were proposed to address various mission requirements. For a narrow search space with a number of restrictions, a high-fidelity design method based on the current Navier-Stokes solver was developed by following the principal of determining the design parameters in sequence. To handle a moderate search space, an exhaustive parameter sweep was performed by a low-fidelity design method using a potential-flow-based solver. For the purpose of universality, a multi-fidelity design method was proposed to solve the propulsion problems with a large search space, which integrate an optimization algorithm, the potential-flow-based solver and the Navier-Stokes solver into a single computational framework. A case study on the application of APWIGs to an AUV was conducted to demonstrate the design process of the multi-fidelity design method in detail.

The primary significance of this study is lied in the first evaluation for the propulsive performance of APWIGs. To the best knowledge of the author, the oscillating foil configuration with the combination of auto-pitch mechanism and biplane arrangement has not been investigated in literature. Therefore, this work extends the technical solutions in the existing propulsion community and provides a promising alternative for marine propulsion. The established database for APWIGs is regarded as a valuable reference to analyze the role of each parameter and guide the performance optimization. The comprehensive performance analysis of APWIGs gains key insights into the physical mechanisms regarding the spring-based flexibility and WIG effect configuration. The extensive numerical visualizations with respect to various flow behaviors deepen the fundamental understanding in flow physics of oscillating foils. The current endeavor to develop a design procedure for APWIGs is capable of facilitating the practical application of novel propulsion systems.

8.2 Main Conclusions and Key Findings

On the basis of the presented computations and analyses, notable findings can be identified to highlight

the outcomes of this thesis. Owing to that, considerable conclusions were drawn to demonstrate the completion of research objectives and answer the research questions that initiated in the commencement of this work. In brief, the main conclusions and key findings are summarized as following descriptions, which significantly contributes to both academic area and engineering field.

- Numerical tool of performance prediction

  The established numerical model shows a satisfactory independence and a reasonably low level of numerical uncertainty with respect to both time step and mesh resolution. The current computations correlate well with available experimental data suggesting that this Navier-Stokes solver can provide accurate and reliable predictions of performance metrics for oscillating foil propulsors. The developed numerical tool has the capability to capture complicated flow phenomena and identify extensive fluid information.

- Influence of geometry and kinematic parameters

  The torsional spring stiffness plays a crucial role in both dynamic responses and propulsive performance of APWIGs. Under some conditions, there exists an optimum spring stiffness that produces the highest efficiency for auto-pitch configuration. Computational results showed that the forward-motion regime and stable locomotion state with periodic dynamical behaviors for APWIGs can only be achieved by an appropriate range of frequency ratio. The frequency ratio in the range of 1.1 to 1.4 was found to generate the optimal or near-optimal performance for APWIGs. The propulsion characteristics of APWIGs show a certain dependence on the operating conditions. The less stable locomotion behaviors and complex hydrodynamic properties were reported at either extremely low or dramatically high advance speeds.

  The propulsive efficiency of APIWGs presents a continuous decreasing trend with the increase of oscillating frequency, which significantly affect the resulting effective AoA and flow behaviors around foil surface. The position of pitching axis was found to have an obvious influence on both peak of flow-induced pitching angle and pitch-leading phase difference. Simulations indicated that the elastic pitching axis around 0.25 chord position from the leading edge tends to produce a satisfactory performance. The maximum passive pitching angle was observed to be highly sensitive to heaving amplitude, which shows a negligible influence on pitch-leading phase angle. The distance between two foils is employed to measure the WIG effect on the performance metrics of APWIGs. It was found that both thrust coefficient and propulsive efficiency are inversely proportional to the equilibrium distance between two foils. Within the attainable scope of this parameter, the maximum efficiency increase of over 10% was identified by current simulations.

  With an appropriate parameter combination, the APWIGs was found to be capable of achieving a high efficiency of over 70%. It is worth noting that such a high performance can be maintained in a relatively wide range of advance speed, indicating that the APWIGs has a potential to run at the optimum or near-optimum operating condition.

- Propulsion advantages of APWIGs

  It was indicated that the APWIGs produces a higher propulsive performance compared to single auto-pitch oscillating foil over the whole examined scope of operating speed, reporting a maximum efficiency increase of over 14% within the considered parametric space. A significant propulsion improvement by APWIGs over biplane heave-only configuration was observed in the current computations suggesting that the introduce of pitching motion is highly essential. Especially, the APWIGs was found to generate more than four times thrust over biplane heave-only configuration at the start-up stage. The propulsive characteristics of biplane fully-prescribed configuration were noted to have an extremely high sensitivity to advance speeds. In contrast, the APWIGs was found to be capable of maintaining a satisfactory performance over a relatively large scope of operating speed, implying that the mechanism of spring-based elastic axis with flow-adjusted pitch significantly outperforms the setup of rigid shaft using imposed rotation.

  The numerical simulations showed that the vorticity behaviors of APWIGs are characterized as the mild leading-edge vortex shedding and apparent trailing-edge vortex shedding. A typical reverse Kármán vortex street with the combination of a row of anticlockwise vortices above the wake centerline and a row of clockwise vortices below the wake centerline was identified in the downstream region of APWIGs. Such wake patterns can induce a momentum surplus behind each foil which provides a strong evidence for the thrust-producing mechanism of APWIGs. It was noted that the satisfactory propulsive performance by oscillating foils generally corresponds to the slight leading-edge vortex behaviors and less stretched vortex structures in wake. Such flow patterns were found to be attained by the moderate values of effective AoA.

  In general, the APWIGs was found to outperform all examined oscillating foil configurations owing to the favorable WIG effect by counter-phase biplane arrangement and the substantial reduction of flow separation by flow-adapted pitching mechanism, indicating that the APWIGs promises a valid option for marine propulsion.

- Three-dimensional effect

  The finite-span effect was found to significantly decrease the propulsive performance of WIG effect propulsors. The maximum efficiency drop of approximately 15% was observed for the case of $AR = 1$. It was noted that the three-dimensional effect dominates hydrodynamic characteristics of oscillating foils with an aspect ratio of below 2. The modest efficiency decrease of about 3% for $AR = 4$ indicates that the recommendation of aspect ratio within the range of 3-5 is reasonable for the WIG effect propulsors by taking into account the trade-off between propulsive performance and manufacturing cost.

  The hydro-elasticity characteristics of three-dimensional APWIGs were found to be highly analogical to two-dimensional simulations with an averaged efficiency loss of around 10%, as a result of low-aspect-ratio effect. The propulsion superiority of finite-span APWIGs was confirmed

by the comparison with fully prescribed biplane configuration, implying that the APWIGs outperforms other oscillating foil propulsors even in the real three-dimensional flow.

Wake topologies suggested that the flow patterns of finite-span oscillating foils are characterized as two sets of intertwined vortex rings, differing from the wake structures of two-dimensional simulations. The spring stiffness was found to have a significant effect on the trailing-edge vortex behaviors of APWIGs. Numerical visualizations identified the vortex shedding along both leading and trailing edges, as well as around the wing tips for three-dimensional WIG effect propulsors.

- Exploration of design procedure

  It was indicated that there is no single design procedure for a propulsion problem employing the oscillating foils. The design process with the parameter selection has a high dependence on the specific mission requirements and imposed restrictions. A multi-fidelity design method was found to be a promising approach to develop the APWIGs system. This design method has the capability to address a general propulsion problem with a large search space. The feasibility of multi-fidelity design method was demonstrated by a case study on the application of APWIGs to an AUV.

8.3 Future Work

Although significant progress regarding the performance analysis of APWIGs and notable advance in the understanding of oscillating foil characteristics have been made by completed works, several limitations can be identified in this study. Improvements with respect to both capability of numerical tool and fidelity of physical model are expected for further insights into the relevant problems.

To overcome the restrictions of the current model, further development of sharp tools with sophisticated numerical modelling techniques are necessary. A relatively large density ratio between body and fluid was used in the current study to ensure numerical stability. The modelling of fluid-structure interaction with the strong coupling scheme is required to study the small-density-ratio related dynamics, such as the effect of inertia. The current simulations were limited to the cases with moderate heaving amplitudes and distance between two foils since severe mesh deformation may result in poor predictions. In order to explore the influence of large heaving amplitude and small gap of two foils, more robust dynamic mesh approaches should be implemented, of which the overset mesh is a notable technique. For the purpose of more insights into fluid physics governing the hydrodynamic characteristics of oscillating foils, advanced turbulence models such as LES should be utilized to solve the behaviors of boundary layer. In particular, challenges remain for the numerical solution of complex flow mechanisms including the severe flow separation and transition from laminar to turbulent flow.

A certain simplification for a given problem is rational in the stage of preliminary study. However, the relevant factors and potential effects should be taken into account in the later works to approach a real

scenario. For the current study on APWIGs, the propulsion system was simulated separately in a model scale. The presented case study on the application of APWIGs to an AUV through the proposed design method did not involve any computations. To pave the way for engineering practice, the interaction between APWIGs and target vehicle should be explored to provide a complete evaluation on the capability of this novel propulsor. Due to the different scaling trends of key parameters, the investigations into the scaling effect with full-scale APWIGs is required for subsequent works. In particular, the case study associated with the systematic computations on the application of APWIGs to marine vehicles are highly suggested to verify the feasibility of multi-fidelity design method. This requires the integration of different codes into a single framework and substantial simulations based on powerful computing resources.

Additionally, a number of issues still remain a challenge for the complete understanding in thrust-producing mechanisms and flow physics of oscillating foils, which are difficult to be adequately covered by the current study in a given timeframe. To further enhance the knowledge regarding the oscillating foil characteristics, it is recommended that the investigation into APWIGs can be extended to the following areas in the future works.

The comprehensive experimental investigations into both propulsive performance and flow details of APWIGs are significantly required. Especially, the force measurements and flow visualizations by well-designed apparatus for biplane oscillating foil configuration are quite limited in literature. There are plenty of three-dimensional features for oscillating foil propulsion that are yet to be fully understood. Of particular importance are the onset and evolution of spanwise vortices as well as the wing-tip vortex shedding which highly affect the performance metrics of oscillating foils. The influence of endplate in relieving the finite-span effect for the improvement of hydrodynamic characteristics is another much less noted issue. The effect of foil geometry regarding both cross-section and spanwise shape on the propulsive properties and flow patterns of APWIGs remains to be explored.

The general issues such as cavitation, vibration and instability that affect the operation of target vehicles should be considered in further studies on APWIGs. Numerical simulations coupling with specialized modelling schemes can contribute to the understanding of these flow behaviors, while experimental information is capable of providing significant insights into the control mechanisms for these problems. It is noted that the flow behaviors regarding vortex-vortex and wing-vortex interactions for oscillating foils are still inadequately understood. Further investigations into the manipulation of vortex structures are recommended to refine the knowledge for involved flow physics and improve the hydrodynamic performance of oscillating foil propulsors. Since the advantages of flexible foils have been widely indicated in literature, the comparison between APWIGs and biplane flexible oscillating foil configuration can be made to examine whether the lumped flexibility using the torsional spring or the uniform flexibility along chordwise direction is suitable for the thrust production. Additionally, the spanwise flexibility for APWIGs can be considered in future simulations to increase the modelling fidelity, especially for the high-aspect-ratio foils.

A systematic comparison of propulsion characteristics between APWIGs and screw propellers based on an appropriate similitude criterion is recommended to increase the credibility of this novel propulsor over the conventional propulsion systems. The influence of free surface on the propulsive performance of oscillating foils are still notably limited since most of the studies in literature mainly focus on the underwater vehicles. The current APWIGs is developed to serve for various marine vehicles, implying that the effect of free surface needs to be taken into consideration in the propulsion problem of surface ships. Although significant efforts have been made on the performance analysis and mechanism research of oscillating foil propulsors, there is still a lack of information with respect to engineering practice. To this end, the mechanical implementation regarding the torsional springs and heaving actuators, as well as the incorporation of propulsion system to target vehicles in the prototyping phase of APWIGs should be well programmed based on interdisciplinary methodology.

References

AKBARI, M. & PRICE, S. 2003. Simulation of dynamic stall for a NACA 0012 airfoil using a vortex method. *Journal of fluids and structures,* 17**,** 855-874.

ALBEN, S., WITT, C., BAKER, T. V., ANDERSON, E. & LAUDER, G. V. 2012. Dynamics of freely swimming flexible foils. *Physics of Fluids,* 24**,** 051901.

ANDERSEN, A., BOHR, T., SCHNIPPER, T. & WALTHER, J. H. 2017. Wake structure and thrust generation of a flapping foil in two-dimensional flow. *J Fluid Mech,* 812**,** R4.

ANDERSON, J., STREITLIEN, K., BARRETT, D. & TRIANTAFYLLOU, M. 1998. Oscillating foils of high propulsive efficiency. *Journal of Fluid Mechanics,* 360**,** 41-72.

ARORA, N., GUPTA, A., AONO, H. & SHYY, W. Propulsion of a plunging flexible airfoil using a torsion spring model. 33rd AIAA Applied Aerodynamics Conference, 2015. 3295.

ARORA, N., KANG, C. K., SHYY, W. & GUPTA, A. 2018. Analysis of passive flexion in propelling a plunging plate using a torsion spring model. *Journal of Fluid Mechanics,* 857**,** 562-604.

ARRANZ, G., FLORES, O. & GARCIA-VILLALBA, M. 2020. Three-dimensional effects on the aerodynamic performance of flapping wings in tandem configuration. *Journal of Fluids and Structures,* 94**,** 102893.

ASHRAF, M., YOUNG, J. & LAI, J. 2011. Reynolds number, thickness and camber effects on flapping airfoil propulsion. *Journal of Fluids and structures,* 27**,** 145-160.

AYANCIK, F., FISH, F. E. & MOORED, K. W. 2020. Three-dimensional scaling laws of cetacean propulsion characterize the hydrodynamic interplay of flukes' shape and kinematics. *Journal of the Royal Society Interface,* 17**,** 20190655.

AYANCIK, F., ZHONG, Q., QUINN, D. B., BRANDES, A., BART-SMITH, H. & MOORED, K. W. 2019. Scaling laws for the propulsive performance of three-dimensional pitching propulsors. *Journal of Fluid Mechanics,* 871**,** 1117-1138.

BARANNYK, O., BUCKHAM, B. J. & OSHKAI, P. 2012. On performance of an oscillating plate underwater propulsion system with variable chordwise flexibility at different depths of submergence. *Journal of Fluids and Structures,* 28**,** 152-166.

BARRETT, D. S. 1996. *Propulsive efficiency of a flexible hull underwater vehicle.* Massachusetts Institute of Technology.

BEAL, D., HOVER, F., TRIANTAFYLLOU, M., LIAO, J. & LAUDER, G. V. 2006. Passive propulsion in vortex wakes. *Journal of Fluid Mechanics,* 549**,** 385.

BELIBASSAKIS, K. A. & POLITIS, G. K. 2013. Hydrodynamic performance of flapping wings for augmenting ship propulsion in waves. *Ocean Engineering,* 72**,** 227-240.

BENKHEROUF, T., MEKADEM, M., OUALLI, H., HANCHI, S., KEIRSBULCK, L. & LABRAGA, L. 2011. Efficiency of an auto-propelled flapping airfoil. *Journal of Fluids and Structures,* 27**,** 552-566.

BERGOU, A. J., XU, S. & WANG, Z. J. 2007. Passive wing pitch reversal in insect flight. *Journal of Fluid Mechanics,* 591**,** 321.

BETZ, A. 1912. Ein Beitrag zur Erklaerung des Segelfluges. *Zeitschrift fur Flugtechnik und Motorluftschiffahrt,* 3**,** 269-272.

BIRCH, J. M. & DICKINSON, M. H. 2001. Spanwise flow and the attachment of the leading-edge vortex on insect wings. *Nature,* 412**,** 729-733.

BIRNBAUM, W. 1924. Das ebene Problem des schlagenden Flügels. *ZAMM ‐ Journal of Applied Mathematics and Mechanics/Zeitschrift für Angewandte Mathematik und Mechanik,* 4**,** 277-292.

BLONDEAUX, P., FORNARELLI, F., GUGLIELMINI, L., TRIANTAFYLLOU, M. S. & VERZICCO, R. 2005. Numerical experiments on flapping foils mimicking fish-like locomotion. *Physics of Fluids,* 17**,** 113601.

BøCKMANN, E. & STEEN, S. 2014. Experiments with actively pitch-controlled and spring-loaded oscillating foils. *Applied Ocean Research,* 48**,** 227-235.

BOUDREAU, M., GUNTHER, K. & DUMAS, G. 2019. Investigation of the energy-extraction regime of a novel semi-passive flapping-foil turbine concept with a prescribed heave motion and a passive pitch motion. *Journal of Fluids and Structures,* 84**,** 368-390.

BOUDREAU, M., PICARD-DELAND, M. & DUMAS, G. 2020. A parametric study and optimization of the fully-passive flapping-foil turbine at high Reynolds number. *Renewable Energy,* 146**,** 1958-1975.

BUCHHOLZ, J. H. & SMITS, A. J. 2006. On the evolution of the wake structure produced by a low-aspect-ratio pitching panel. *Journal of fluid mechanics,* 546**,** 433-443.

CARLTON, J. 2018. *Marine propellers and propulsion*, Butterworth-Heinemann.

CARR, Z. R., DEVORIA, A. C. & RINGUETTE, M. J. 2015. Aspect-ratio effects on rotating wings: circulation and forces. *Journal of Fluid Mechanics,* 767**,** 497-525.

CHAE, E. J., AKCABAY, D. T. & YOUNG, Y. L. 2013. Dynamic response and stability of a flapping foil in a dense and viscous fluid. *Physics of Fluids,* 25**,** 104106.

CHAO, L.-M., PAN, G., ZHANG, D. & YAN, G.-X. 2019. Numerical investigations on the force generation and wake structures of a nonsinusoidal pitching foil. *Journal of Fluids and Structures,* 85**,** 27-39.

CHEN, Y., GRAVISH, N., DESBIENS, A. L., MALKA, R. & WOOD, R. J. 2016. Experimental and computational studies of the aerodynamic performance of a flapping and passively rotating insect wing. *Journal of Fluid Mechanics,* 791**,** 1.

CHENG, H. K. & MURILLO, L. E. 1984. Lunate-tail swimming propulsion as a problem of curved lifting line in unsteady flow. Part 1. Asymptotic theory. *Journal of Fluid Mechanics,* 143**,** 327-350.

CHIMAKURTHI, S. K., TANG, J., PALACIOS, R., CESNIK, C. E. & SHYY, W. 2009. Computational aeroelasticity framework for analyzing flapping wing micro air vehicles. *AIAA journal,* 47**,** 1865-1878.

CHOPRA, M. 1974. Hydromechanics of lunate-tail swimming propulsion. *Journal of Fluid Mechanics,* 64**,** 375-392.

CHOPRA, M. 1976. Large amplitude lunate-tail theory of fish locomotion. *Journal of Fluid Mechanics,* 74**,** 161-182.

CHOPRA, M. & KAMBE, T. 1977. Hydromechanics of lunate-tail swimming propulsion. Part 2. *Journal of Fluid Mechanics,* 79**,** 49-69.

CONNELL, B. S. & YUE, D. K. 2007. Flapping dynamics of a flag in a uniform stream. *Journal of fluid mechanics,* 581**,** 33.

CULBRETH, M., ALLANEAU, Y. & JAMESON, A. High-fidelity optimization of flapping airfoils and wings. 29th AIAA Applied Aerodynamics Conference, 2013. 3521.

DABIRI, J. O. 2009. Optimal vortex formation as a unifying principle in biological propulsion. *Annual review of fluid mechanics,* 41**,** 17-33.

DAVE, M., SPAULDING, A. & FRANCK, J. A. 2020. Variable thrust and high efficiency propulsion with oscillating foils at high Reynolds numbers. *Ocean Engineering,* 214**,** 107833.

DELAURIER, J. & HARRIS, J. 1982. Experimental study of oscillating-wing propulsion. *Journal of Aircraft,* 19**,** 368-373.

DENG, J., CAULFIELD, C. & SHAO, X. 2014. Effect of aspect ratio on the energy extraction efficiency of three-dimensional flapping foils. *Physics of Fluids,* 26**,** 043102.

DENG, J., SUN, L. & SHAO, X. 2015. Dynamical features of the wake behind a pitching foil. *Physical Review E,* 92**,** 063013.

DENG, J., SUN, L., TENG, L., PAN, D. & SHAO, X. 2016. The correlation between wake transition and propulsive efficiency of a flapping foil: A numerical study. *Physics of Fluids,* 28**,** 094101.

DEWEY, P. A., CARRIOU, A. & SMITS, A. J. 2012. On the relationship between efficiency and wake structure of a batoid-inspired oscillating fin. *Journal of fluid mechanics,* 691**,** 245.

DONG, H., MITTAL, R. & NAJJAR, F. 2006. Wake topology and hydrodynamic performance of low-aspect-ratio flapping foils. *Journal of Fluid Mechanics,* 566**,** 309.

DULLWEBER, A., LEIMKUHLER, B. & MCLACHLAN, R. 1997. Symplectic splitting methods for rigid body molecular dynamics. *The Journal of chemical physics,* 107**,** 5840-5851.

EHLERS, H., KONRATH, R., WOKOECK, R. & RADESPIEL, R. 2016. Three-dimensional flow field investigations of flapping wing aerodynamics. *AIAA Journal,* 54**,** 3434-3449.

ELDREDGE, J. D., TOOMEY, J. & MEDINA, A. 2010. On the roles of chord-wise flexibility in a flapping wing with hovering kinematics. *Journal of Fluid Mechanics,* 659**,** 94-115.

FEILICH, K. L. & LAUDER, G. V. 2015. Passive mechanical models of fish caudal fins: effects of shape and stiffness on self-propulsion. *Bioinspiration & biomimetics,* 10**,** 036002.

FERNANDEZ-PRATS, R. 2017. Effect of chordwise flexibility on pitching foil propulsion in a uniform current. *Ocean Engineering,* 145**,** 24-33.

FERZIGER, J. H., PERIĆ, M. & STREET, R. L. 2002. *Computational methods for fluid dynamics*, Springer.

FISH, F. & LAUDER, G. V. 2006. Passive and active flow control by swimming fishes and mammals. *Annu. Rev. Fluid Mech.,* 38**,** 193-224.

FLAMMANG, B. E., LAUDER, G. V., TROOLIN, D. R. & STRAND, T. 2011. Volumetric imaging of shark tail hydrodynamics reveals a three-dimensional dual-ring vortex wake structure. *Proceedings of the Royal Society B: Biological Sciences,* 278**,** 3670-3678.

FLOC'H, F., PHOEMSAPTHAWEE, S., LAURENS, J. M. & LEROUX, J. B. 2012. Porpoising foil as a propulsion system. *Ocean engineering,* 39**,** 53-61.

GARRICK, I. E. 1936. Propulsion of a Flapping and Oscillating Airfoil. *NACA Report,* 567.

GONZALO, A., ARRANZ, G., MORICHE, M., GARCíA-VILLALBA, M. & FLORES, O. 2018. From flapping to heaving: A numerical study of wings in forward flight. *Journal of Fluids and Structures,* 83**,** 293-309.

GRAY, J. 1936. Studies in animal locomotion: VI. The propulsive powers of the dolphin. *Journal of experimental biology,* 13**,** 192-199.

GREEN, M. A. & SMITS, A. J. 2008. Effects of three-dimensionality on thrust production by a pitching

panel. *Journal of fluid mechanics,* 615**,** 211.

GUERRERO, J. E. 2010. Wake signature and Strouhal number dependence of finite-span flapping wings. *Journal of Bionic Engineering,* 7**,** S109-S122.

GUGLIELMINI, L. & BLONDEAUX, P. 2004. Propulsive efficiency of oscillating foils. *European Journal of Mechanics-B/Fluids,* 23**,** 255-278.

GUGLIELMINI, L. & BLONDEAUX, P. 2009. Numerical experiments on the transient motions of a flapping foil. *European Journal of Mechanics-B/Fluids,* 28**,** 136-145.

HALL, K. C. & HALL, S. R. 1996. Minimum induced power requirements for flapping flight. *Journal of Fluid Mechanics,* 323**,** 285-315.

HAN, J., YUAN, Z. & CHEN, G. 2018. Effects of kinematic parameters on three-dimensional flapping wing at low Reynolds number. *Physics of Fluids,* 30**,** 081901.

HAN, J., ZHANG, Y. & CHEN, G. 2019. Effects of individual horizontal distance on the three-dimensional bionic flapping multi-wings in different schooling configurations. *Physics of Fluids,* 31**,** 041903.

HARPER, K. A., BERKEMEIER, M. D. & GRACE, S. 1998. Modeling the dynamics of spring-driven oscillating-foil propulsion. *IEEE Journal of Oceanic Engineering,* 23**,** 285-296.

HE, M., VEITCH, B., BOSE, N., COLBOURNE, B. & LIU, P. 2007. A three-dimensional wake impingement model and applications on tandem oscillating foils. *Ocean engineering,* 34**,** 1197-1210.

HEATHCOTE, S. & GURSUL, I. 2007. Flexible flapping airfoil propulsion at low Reynolds numbers. *AIAA journal,* 45**,** 1066-1079.

HEATHCOTE, S., MARTIN, D. & GURSUL, I. 2004. Flexible flapping airfoil propulsion at zero freestream velocity. *AIAA journal,* 42**,** 2196-2204.

HEATHCOTE, S., WANG, Z. & GURSUL, I. 2008. Effect of spanwise flexibility on flapping wing propulsion. *Journal of Fluids and Structures,* 24**,** 183-199.

HO, S., NASSEF, H., PORNSINSIRIRAK, N., TAI, Y.-C. & HO, C.-M. 2003. Unsteady aerodynamics and flow control for flapping wing flyers. *Progress in Aerospace Sciences,* 39**,** 635-681.

HOEIJMAKERS, H. W. & MULDER, J. Computational and experimental investigation into flapping wing propulsion. 54th AIAA aerospace sciences meeting, 2016. 0802.

HOKE, C., YOUNG, J. & LAI, J. 2015. Effects of time-varying camber deformation on flapping foil propulsion and power extraction. *Journal of Fluids and Structures,* 56**,** 152-176.

HOLLAND, J. H. 1992. *Adaptation in natural and artificial systems: an introductory analysis with*

applications to biology, control, and artificial intelligence, MIT press.

HOVER, F., HAUGSDAL, Ø. & TRIANTAFYLLOU, M. 2004. Effect of angle of attack profiles in flapping foil propulsion. *Journal of Fluids and Structures,* 19**,** 37-47.

HU, H., CLEMONS, L. & IGARASHI, H. 2011. An experimental study of the unsteady vortex structures in the wake of a root-fixed flapping wing. *Experiments in Fluids,* 51**,** 347-359.

HUA, R.-N., ZHU, L. & LU, X.-Y. 2013. Locomotion of a flapping flexible plate. *Physics of Fluids,* 25**,** 121901.

HUNT, J.C., WRAY, A.A. & MOIN, P. 1988. Eddies, streams, and convergence zones in turbulent flows. *Center For Turbulence Research,* Report CTR-S88.

ISHIHARA, D., HORIE, T. & NIHO, T. 2014. An experimental and three-dimensional computational study on the aerodynamic contribution to the passive pitching motion of flapping wings in hovering flies. *Bioinspiration & biomimetics,* 9**,** 046009.

ISOGAI, K., SHINMOTO, Y. & WATANABE, Y. 1999. Effects of dynamic stall on propulsive efficiency and thrust of flapping airfoil. *AIAA journal,* 37**,** 1145-1151.

IVERSON, D., RAHIMPOUR, M., LEE, W., KIWATA, T. & OSHKAI, P. 2019. Effect of chordwise flexibility on propulsive performance of high inertia oscillating-foils. *Journal of fluids and structures,* 91**,** 102750.

IZRAELEVITZ, J. S. & TRIANTAFYLLOU, M. S. 2014. Adding in-line motion and model-based optimization offers exceptional force control authority in flapping foils. *Journal of Fluid Mechanics,* 742**,** 5.

JONES, A. & BABINSKY, H. 2011. Reynolds number effects on leading edge vortex development on a waving wing. *Experiments in fluids,* 51**,** 197-210.

JONES, K., CASTRO, B., MAHMOUD, O. & PLATZER, M. A numerical and experimental investigation of flapping-wing propulsion in ground effect. 40th AIAA Aerospace Sciences Meeting & Exhibit, 2002a. 866.

JONES, K., CASTRO, B., MAHMOUD, O., POLLARD, S., PLATZER, M., NEEF, M., GONET, K. & HUMMEL, D. A collaborative numerical and experimental investigation of flapping-wing propulsion. 40th AIAA aerospace sciences meeting & exhibit, 2002b. 706.

JONES, K., DOHRING, C. & PLATZER, M. 1998. Experimental and computational investigation of the Knoller-Betz effect. *AIAA journal,* 36**,** 1240-1246.

JONES, K., DUGGAN, S. & PLATZER, M. Flapping-wing propulsion for a micro air vehicle. 39th Aerospace Sciences Meeting and Exhibit, 2001. 126.

JONES, K. & PLATZER, M. An experimental and numerical investigation of flapping-wing propulsion. 37th aerospace sciences meeting and exhibit, 1999. 995.

JONES, K., PLATZER, M., JONES, K. & PLATZER, M. Numerical computation of flapping-wing propulsion and power extraction. 35th Aerospace Sciences Meeting and Exhibit, 1997. 826.

JONES, K. D. & PLATZER, M. F. 2010. Design and development considerations for biologically inspired flapping-wing micro air vehicles. *Animal Locomotion.* Springer.

JONES, M. & YAMALEEV, N. K. 2015. Adjoint-based optimization of three-dimensional flapping-wing flows. *AIAA Journal,* 53**,** 934-947.

JONES, W. & LAUNDER, B. E. 1972. The prediction of laminarization with a two-equation model of turbulence. *International journal of heat and mass transfer,* 15**,** 301-314.

KANCHARALA, A. & PHILEN, M. 2014. Study of flexible fin and compliant joint stiffness on propulsive performance: theory and experiments. *Bioinspiration & biomimetics,* 9**,** 036011.

KANG, C.-K. & SHYY, W. Passive wing rotation in flexible flapping wing aerodynamics. 30th AIAA applied aerodynamics conference, 2012. 2763.

KATZ, J. & WEIHS, D. 1978. Hydrodynamic propulsion by large amplitude oscillation of an airfoil with chordwise flexibility. *Journal of Fluid Mechanics,* 88**,** 485-497.

KATZMAYR, R. 1922. Effect of periodic changes of angle of attack on behavior of airfoils.

KAYA, M. & TUNCER, I. H. 2007. Nonsinusoidal path optimization of a flapping airfoil. *AIAA journal,* 45**,** 2075-2082.

KERWIN, J. E. & HADLER, J. B. 2010. Principles of naval architecture series: Propulsion. *The Society of Naval Architects and Marine Engineers (SNAME)*.

KINSEY, T. & DUMAS, G. 2012a. Computational fluid dynamics analysis of a hydrokinetic turbine based on oscillating hydrofoils. *Journal of fluids engineering,* 134.

KINSEY, T. & DUMAS, G. 2012b. Optimal tandem configuration for oscillating-foils hydrokinetic turbine. *Journal of fluids engineering,* 134.

KINSEY, T. & DUMAS, G. 2012c. Three-dimensional effects on an oscillating-foil hydrokinetic turbine. *Journal of fluids engineering,* 134.

KNOLLER, R. 1909. Die Gesetze des Luftwiderstandes. *Flug- und Motortechnik (Wien),* 3 (21)**,** 1-7.

KOOCHESFAHANI, M. M. 1989. Vortical patterns in the wake of an oscillating airfoil. *AIAA journal,* 27**,** 1200-1205.

KüSSNER, H. 1935. Augenblicklicher Entwicklungsstand der Frage des Flugelflatterns.

Luftfahrtforschung, 12**,** 193.

LA MANTIA, M. & DABNICHKI, P. 2011. Effect of the wing shape on the thrust of flapping wing. *Applied Mathematical Modelling,* 35**,** 4979-4990.

LAI, J. & PLATZER, M. 1999. Jet characteristics of a plunging airfoil. *AIAA journal,* 37**,** 1529-1537.

LAI, J., YUE, J. & PLATZER, M. 2002. Control of backward-facing step flow using a flapping foil. *Experiments in Fluids,* 32**,** 44-54.

LI, C. & DONG, H. 2016. Three-dimensional wake topology and propulsive performance of low-aspect-ratio pitching-rolling plates. *Physics of Fluids,* 28**,** 071901.

LI, Y., PAN, D., MA, Z. & ZHAO, Q. 2019. Aspect ratio effect of a pair of flapping wings on the propulsion of a bionic autonomous underwater glider. *Journal of Bionic Engineering,* 16**,** 145-153.

LIAN, Y., BROERING, T., HORD, K. & PRATER, R. 2014. The characterization of tandem and corrugated wings. *Progress in Aerospace Sciences,* 65**,** 41-69.

LICHT, S., WIBAWA, M., HOVER, F. S. & TRIANTAFYLLOU, M. S. 2010. In-line motion causes high thrust and efficiency in flapping foils that use power downstroke. *Journal of Experimental Biology,* 213**,** 63-71.

LIGHTHILL, M. 1969. Hydromechanics of aquatic animal propulsion. *Annual review of fluid mechanics,* 1**,** 413-446.

LIGHTHILL, M. J. 1970. Aquatic animal propulsion of high hydromechanical efficiency. *Journal of Fluid Mechanics,* 44**,** 265-301.

LIGHTHILL, M. J. 1971. Large-amplitude elongated-body theory of fish locomotion. *Proceedings of the Royal Society of London. Series B. Biological Sciences,* 179**,** 125-138.

LIN, X., HE, G., HE, X. & WANG, Q. 2018. Dynamic response of a semi-free flexible filament in the wake of a flapping foil. *Journal of Fluids and Structures,* 83**,** 40-53.

LIU, N., PENG, Y., LIANG, Y. & LU, X. 2012. Flow over a traveling wavy foil with a passively flapping flat plate. *Physical Review E,* 85**,** 056316.

LIU, P. 1991. *Three dimensional oscillating foil propulsion.* Memorial University of Newfoundland.

LIU, P. 1996. *A time-domain panel method for oscillating propulsors with both chordwise and spanwise flexibility.* Memorial University of Newfoundland.

LIU, P. 2005a. Oscillating foil propulsion system. *US Patent,* 6877692.

LIU, P. 2005b. Propulsive performance of a twin-rectangular-foil propulsor in a counterphase oscillation.

Journal of ship research, 49**,** 207-215.

LIU, P. 2015. WIG (wing-in-ground) effect dual-foil turbine for high renewable energy performance. *Energy,* 83**,** 366-378.

LIU, P. & BOSE, N. 1993. Propulsive performance of three naturally occurring oscillating propeller planforms. *Ocean Engineering,* 20**,** 57-75.

LIU, P. & BOSE, N. 1997. Propulsive performance from oscillating propulsors with spanwise flexibility. *Proceedings of the Royal Society of London. Series A: Mathematical, Physical and Engineering Sciences,* 453**,** 1763-1770.

LIU, P., WANG, T., HUANG, G., VEITCH, B. & MILLAN, J. 2010. Propulsion characteristics of wing-in-ground effect dual-foil propulsors. *Applied Ocean Research,* 32**,** 103-112.

LIU, W. & XIAO, Q. Energy extraction by flexible flapping twin wing. International Conference on Offshore Mechanics and Arctic Engineering, 2013. American Society of Mechanical Engineers, V008T09A013.

LOH, T. 2020. *Fuzzy System Dynamics Risk Analysis (FuSDRA) of Autonomous Underwater Vehicle (AUV) deployment in the Antarctic.* University of Tasmania.

LU, Y. & SHEN, G. X. 2008. Three-dimensional flow structures and evolution of the leading-edge vortices on a flapping wing. *Journal of Experimental Biology,* 211**,** 1221-1230.

LUCAS, K. N., THORNYCROFT, P. J., GEMMELL, B. J., COLIN, S. P., COSTELLO, J. H. & LAUDER, G. V. 2015. Effects of non-uniform stiffness on the swimming performance of a passively-flexing, fish-like foil model. *Bioinspiration & biomimetics,* 10**,** 056019.

LUO, Y., XIAO, Q., SHI, G., WEN, L., CHEN, D. & PAN, G. 2020. A fluid–structure interaction solver for the study on a passively deformed fish fin with non-uniformly distributed stiffness. *Journal of Fluids and Structures,* 92**,** 102778.

MA, P., WANG, Y., XIE, Y. & ZHANG, J. 2018. Analysis of a hydraulic coupling system for dual oscillating foils with a parallel configuration. *Energy,* 143**,** 273-283.

MACKOWSKI, A. & WILLIAMSON, C. 2015. Direct measurement of thrust and efficiency of an airfoil undergoing pure pitching. *Journal of Fluid Mechanics,* 765**,** 524.

MANNAM, N. P. B. & KRISHNANKUTTY, P. 2018. Hydrodynamic study of flapping foil propulsion system fitted to surface and underwater vehicles. *Ships and Offshore Structures,* 13**,** 575-583.

MEDINA, A., ELDREDGE, J. D., KWEON, J. & CHOI, H. 2015. Illustration of wing deformation effects in three-dimensional flapping flight. *AIAA Journal,* 53**,** 2607-2620.

MENTER, F. R. 1994. Two-equation eddy-viscosity turbulence models for engineering applications.

AIAA journal, 32**,** 1598-1605.

MENTER, F. R., KUNTZ, M. & LANGTRY, R. 2003. Ten years of industrial experience with the SST turbulence model. *Turbulence, heat and mass transfer,* 4**,** 625-632.

MIAO, J.-M., SUN, W.-H. & TAI, C.-H. 2009. Numerical Analysis on Aerodynamic Force Generation of Biplane Counter-Flapping Flexible Airfoils. *Journal of aircraft,* 46**,** 1785-1794.

MICHELIN, S. & LLEWELLYN SMITH, S. G. 2009. Resonance and propulsion performance of a heaving flexible wing. *Physics of Fluids,* 21**,** 071902.

MILANO, M. & GHARIB, M. 2005. Uncovering the physics of flapping flat plates with artificial evolution. *Journal of Fluid Mechanics,* 534**,** 403-409.

MIVEHCHI, A., DAHL, J. & LICHT, S. 2016. Heaving and pitching oscillating foil propulsion in ground effect. *Journal of Fluids and Structures,* 63**,** 174-187.

MOLINA, J. & ZHANG, X. 2011. Aerodynamics of a heaving airfoil in ground effect. *AIAA journal,* 49**,** 1168-1179.

MOORE, N. 2014. Analytical results on the role of flexibility in flapping propulsion. *Journal of Fluid Mechanics*.

MOREIRA, D., MATHIAS, N. & MORAIS, T. 2020. Dual flapping foil system for propulsion and harnessing wave energy: A 2D parametric study for unaligned foil configurations. *Ocean Engineering,* 215**,** 107875.

MURRAY, M. & HOWLE, L. 2003. Spring stiffness influence on an oscillating propulsor. *Journal of Fluids and Structures,* 17**,** 915-926.

MYSA, R. C. & VENKATRAMAN, K. 2016. Intertwined vorticity and elastodynamics in flapping wing propulsion. *Journal of Fluid Mechanics,* 787**,** 175.

NEWMAN, J. 1973. The force on a slender fish-like body. *Journal of Fluid Mechanics,* 58**,** 689-702.

NEWMAN, J. & WU, T. 1973. A generalized slender-body theory for fish-like forms. *Journal of Fluid Mechanics,* 57**,** 673-693.

OLIVIER, M. & DUMAS, G. 2016. Effects of mass and chordwise flexibility on 2D self-propelled flapping wings. *Journal of Fluids and Structures,* 64**,** 46-66.

OYAMA, A., OKABE, Y., SHIMOYAMA, K. & FUJII, K. 2009. Aerodynamic multiobjective design exploration of a flapping airfoil using a navier-stokes solver. *Journal of Aerospace Computing, Information, and Communication,* 6**,** 256-270.

PARKER, K., VON ELLENRIEDER, K. & SORIA, J. 2007. Morphology of the forced oscillatory flow past a finite-span wing at low Reynolds number. *Journal of Fluid Mechanics,* 571**,** 327.

PERKINS, M., ELLES, D., BADLISSI, G., MIVEHCHI, A., DAHL, J. & LICHT, S. 2017. Rolling and pitching oscillating foil propulsion in ground effect. *Bioinspiration & biomimetics,* 13**,** 016003.

PESAVENTO, U. & WANG, Z. J. 2009. Flapping wing flight can save aerodynamic power compared to steady flight. *Physical review letters,* 103**,** 118102.

PICARD-DELAND, M., OLIVIER, M., DUMAS, G. & KINSEY, T. 2019. Oscillating-Foil Turbine Operating at Large Heaving Amplitudes. *AIAA Journal,* 57**,** 5104-5113.

PLATZER, M. F., JONES, K. D., YOUNG, J. & LAI, J. C. 2008. Flapping wing aerodynamics: progress and challenges. *AIAA journal,* 46**,** 2136-2149.

POLITIS, G. & TSARSITALIDIS, V. Biomimetic propulsion using twin oscillating wings. Proceedings of the Third International Symposium on Marine Propulsors (SMP'13), Launceston, Tasmania, Australia, 2013. 5-7.

POLITIS, G. K. & TSARSITALIDIS, V. T. 2014. Flapping wing propulsor design: An approach based on systematic 3D-BEM simulations. *Ocean engineering,* 84**,** 98-123.

QADRI, M. M., ZHAO, F. & TANG, H. 2020. Fluid-structure interaction of a fully passive flapping foil for flow energy extraction. *International Journal of Mechanical Sciences,* 177**,** 105587.

QUINN, D. B., MOORED, K. W., DEWEY, P. A. & SMITS, A. J. 2014. Unsteady propulsion near a solid boundary. *Journal of Fluid Mechanics,* 742**,** 152.

READ, D. A., HOVER, F. & TRIANTAFYLLOU, M. 2003. Forces on oscillating foils for propulsion and maneuvering. *Journal of Fluids and Structures,* 17**,** 163-183.

RICHARDS, A. J. & OSHKAI, P. 2015. Effect of the stiffness, inertia and oscillation kinematics on the thrust generation and efficiency of an oscillating-foil propulsion system. *Journal of Fluids and Structures,* 57**,** 357-374.

ROZHDESTVENSKY, K. V. & RYZHOV, V. A. 2003. Aerohydrodynamics of flapping-wing propulsors. *Progress in aerospace sciences,* 39**,** 585-633.

RYU, J., PARK, S. G., HUANG, W.-X. & SUNG, H. J. 2019. Hydrodynamics of a three-dimensional self-propelled flexible plate. *Physics of Fluids,* 31**,** 021902.

SANE, S. P. & DICKINSON, M. H. 2001. The control of flight force by a flapping wing: lift and drag production. *Journal of experimental biology,* 204**,** 2607-2626.

SCHERER, J. O. 1968. Experimental and theoretical investigation of large amplitude oscillation foil propulsion systems. HYDRONAUTICS INC LAUREL MD.

SCHNIPPER, T., ANDERSEN, A. & BOHR, T. 2009. Vortex wakes of a flapping foil. *Journal of Fluid Mechanics,* 633**,** 411.

SCHOUVEILER, L., HOVER, F. & TRIANTAFYLLOU, M. 2005. Performance of flapping foil propulsion. *Journal of fluids and structures,* 20**,** 949-959.

SHELLEY, M. J. & ZHANG, J. 2011. Flapping and bending bodies interacting with fluid flows. *Annual Review of Fluid Mechanics,* 43**,** 449-465.

SHYY, W., AONO, H., CHIMAKURTHI, S. K., TRIZILA, P., KANG, C.-K., CESNIK, C. E. & LIU, H. 2010. Recent progress in flapping wing aerodynamics and aeroelasticity. *Progress in Aerospace Sciences,* 46**,** 284-327.

SHYY, W., AONO, H., KANG, C.-K. & LIU, H. 2013. *An introduction to flapping wing aerodynamics*, Cambridge University Press.

SHYY, W., LIAN, Y., TANG, J., VIIERU, D. & LIU, H. 2007. *Aerodynamics of low Reynolds number flyers*, Cambridge University Press Cambridge.

SHYY, W., TRIZILA, P., KANG, C.-K. & AONO, H. 2009. Can tip vortices enhance lift of a flapping wing? *AIAA journal,* 47**,** 289-293.

SPAGNOLIE, S. E., MORET, L., SHELLEY, M. J. & ZHANG, J. 2010. Surprising behaviors in flapping locomotion with passive pitching. *Physics of Fluids,* 22**,** 041903.

SPALART, P. & ALLMARAS, S. A one-equation turbulence model for aerodynamic flows. 30th aerospace sciences meeting and exhibit, 1992. 439.

SPENTZOS, A., BARAKOS, G., BADCOCK, K., RICHARDS, B., WERNERT, P., SCHRECK, S. & RAFFEL, M. 2005. Investigation of three-dimensional dynamic stall using computational fluid dynamics. *AIAA journal,* 43**,** 1023-1033.

STERN, F., WILSON, R. & SHAO, J. 2006. Quantitative V&V of CFD simulations and certification of CFD codes. *International journal for numerical methods in fluids,* 50**,** 1335-1355.

STERN, F., WILSON, R. V., COLEMAN, H. W. & PATERSON, E. G. 2001. Comprehensive approach to verification and validation of CFD simulations—part 1: methodology and procedures. *J. Fluids Eng.,* 123**,** 793-802.

STOWERS, A. K. & LENTINK, D. 2015. Folding in and out: passive morphing in flapping wings. *Bioinspiration & biomimetics,* 10**,** 025001.

STREITLIEN, K., TRIANTAFYLLOU, G. S. & TRIANTAFYLLOU, M. S. 1996. Efficient foil propulsion through vortex control. *AIAA journal,* 34**,** 2315-2319.

STROUHAL, V. 1878. *Über eine besondere Art der Tonerregung*, Stahel.

TANG, J., VIIERU, D. & SHYY, W. 2008. Effects of Reynolds number and flapping kinematics on hovering aerodynamics. *AIAA journal,* 46**,** 967-976.

TAYLOR, G. I. 1952. Analysis of the swimming of long and narrow animals. *Proceedings of the Royal Society of London. Series A. Mathematical and Physical Sciences,* 214**,** 158-183.

TAYLOR, G. K., NUDDS, R. L. & THOMAS, A. L. 2003. Flying and swimming animals cruise at a Strouhal number tuned for high power efficiency. *Nature,* 425**,** 707-711.

THAWEEWAT, N., PHOEMSAPTHAWEE, S. & JUNTASARO, V. 2018. Semi-active flapping foil for marine propulsion. *Ocean Engineering,* 147**,** 556-564.

THEODORSEN, T. 1935. General Theory of Aerodynamic Instability and the Mechanism of Flutter. *NACA Report,* 496.

TIAN, F.-B., LUO, H., SONG, J. & LU, X.-Y. 2013. Force production and asymmetric deformation of a flexible flapping wing in forward flight. *Journal of Fluids and Structures,* 36**,** 149-161.

TOOMEY, J. & ELDREDGE, J. D. 2008. Numerical and experimental study of the fluid dynamics of a flapping wing with low order flexibility. *Physics of Fluids,* 20**,** 073603.

TRIANTAFYLLOU, M. S., TECHET, A. H. & HOVER, F. S. 2004. Review of experimental work in biomimetic foils. *IEEE Journal of Oceanic Engineering,* 29**,** 585-594.

TRIANTAFYLLOU, M. S., TRIANTAFYLLOU, G. & YUE, D. 2000. Hydrodynamics of fishlike swimming. *Annual review of fluid mechanics,* 32**,** 33-53.

TUNCER, I. H. & KAYA, M. 2003. Thrust generation caused by flapping airfoils in a biplane configuration. *Journal of Aircraft,* 40**,** 509-515.

TUNCER, I. H. & KAYA, M. 2005. Optimization of flapping airfoils for maximum thrust and propulsive efficiency. *AIAA journal,* 43**,** 2329-2336.

TUNCER, I. H. & PLATZER, M. F. 2000. Computational study of flapping airfoil aerodynamics. *Journal of aircraft,* 37**,** 514-520.

VAN TRUONG, T., BYUN, D., KIM, M. J., YOON, K. J. & PARK, H. C. 2013. Aerodynamic forces and flow structures of the leading edge vortex on a flapping wing considering ground effect. *Bioinspiration & biomimetics,* 8**,** 036007.

VEILLEUX, J.-C. & DUMAS, G. 2017. Numerical optimization of a fully-passive flapping-airfoil turbine. *Journal of Fluids and Structures,* 70**,** 102-130.

VERSTEEG, H. K. & MALALASEKERA, W. 2007. *An introduction to computational fluid dynamics: the finite volume method*, Pearson education.

VEST, M. S. & KATZ, J. 1996. Unsteady aerodynamic model of flapping wings. *AIAA journal,* 34**,** 1435-1440.

VON ELLENRIEDER, K. D., PARKER, K. & SORIA, J. 2003. Flow structures behind a heaving and

pitching finite-span wing. *Journal of Fluid Mechanics,* 490**,** 129.

VON ELLENRIEDER, K. D., PARKER, K. & SORIA, J. 2008. Fluid mechanics of flapping wings. *Experimental Thermal and Fluid Science,* 32**,** 1578-1589.

VON KÁRMÁN, T. & BURGERS, J. M. 1934. General Aerodynamic Theory - Perfect Fluids. *Aerodynamic Theory,* 2**,** 346-349.

WHITNEY, J. P. & WOOD, R. J. 2010. Aeromechanics of passive rotation in flapping flight. *Journal of fluid mechanics,* 660**,** 197.

WILCOX, D. C. 1988. Reassessment of the scale-determining equation for advanced turbulence models. *AIAA journal,* 26**,** 1299-1310.

WILLIS, D., ISRAELI, E., PERSSON, P.-O., DRELA, M., PERAIRE, J., SWARTZ, S. & BREUER, K. A computational framework for fluid structure interaction in biologically inspired flapping flight. 25th AIAA Applied Aerodynamics Conference, 2007. 3803.

WILLIS, D., PERSSON, P. O., ISRAELI, E., PERAIRE, J., SWARTZ, S. & BREUER, K. Multifidelity approaches for the computational analysis and design of effective flapping wing vehicles. 46th AIAA Aerospace Sciences Meeting and Exhibit, 2008. 518.

WILSON, R. V., STERN, F., COLEMAN, H. W. & PATERSON, E. G. 2001. Comprehensive approach to verification and validation of CFD simulations—Part 2: Application for RANS simulation of a cargo/container ship. *J. Fluids Eng.,* 123**,** 803-810.

WU, J., SHU, C., ZHAO, N. & YAN, W. 2014. Fluid dynamics of flapping insect wing in ground effect. *Journal of Bionic Engineering,* 11**,** 52-60.

WU, T. Y.-T. 1961. Swimming of a waving plate. *Journal of Fluid Mechanics,* 10**,** 321-344.

WU, T. Y.-T. 1971a. Hydromechanics of swimming propulsion. Part 1. Swimming of a two-dimensional flexible plate at variable forward speeds in an inviscid fluid. *Journal of Fluid Mechanics,* 46**,** 337-355.

WU, T. Y.-T. 1971b. Hydromechanics of swimming propulsion. Part 2. Some optimum shape problems. *Journal of Fluid Mechanics,* 46**,** 521-544.

WU, T. Y.-T. 1971c. Hydromechanics of swimming propulsion. Part 3. Swimming and optimum movements of slender fish with side fins. *Journal of fluid mechanics,* 46**,** 545-568.

WU, T. Y. 2011. Fish swimming and bird/insect flight. *Annual Review of Fluid Mechanics,* 43**,** 25-58.

XIAO, Q., HU, J. & LIU, H. 2014. Effect of torsional stiffness and inertia on the dynamics of low aspect ratio flapping wings. *Bioinspiration & Biomimetics,* 9**,** 016008.

XIAO, Q. & LIAO, W. 2010. Numerical investigation of angle of attack profile on propulsion

performance of an oscillating foil. *Computers & Fluids,* 39**,** 1366-1380.

XIAO, Q. & ZHU, Q. 2014. A review on flow energy harvesters based on flapping foils. *Journal of fluids and structures,* 46**,** 174-191.

XU, G., DUAN, W. & XU, W. 2017. The propulsion of two flapping foils with tandem configuration and vortex interactions. *Physics of Fluids,* 29**,** 097102.

XU, M. & WEI, M. 2016. Using adjoint-based optimization to study kinematics and deformation of flapping wings. *Journal of Fluid Mechanics,* 799**,** 56.

YANG, T., WEI, M. & ZHAO, H. 2010. Numerical study of flexible flapping wing propulsion. *AIAA journal,* 48**,** 2909-2915.

YANG, W., WANG, L. & SONG, B. 2018. Dove: A biomimetic flapping-wing micro air vehicle. *International Journal of Micro Air Vehicles,* 10**,** 70-84.

YILMAZ, T. O. & ROCKWELL, D. 2012. Flow structure on finite-span wings due to pitch-up motion. *Journal of Fluid Mechanics,* 691**,** 518.

YOUNG, J., ASHRAF, M. A., LAI, J. C. & PLATZER, M. F. 2013. Numerical simulation of fully passive flapping foil power generation. *AIAA journal,* 51**,** 2727-2739.

YOUNG, J. & LAI, J. C. 2007. Mechanisms influencing the efficiency of oscillating airfoil propulsion. *AIAA journal,* 45**,** 1695-1702.

YOUNG, J., LAI, J. C. & PLATZER, M. F. 2014. A review of progress and challenges in flapping foil power generation. *Progress in aerospace sciences,* 67**,** 2-28.

YU, M., WANG, Z. & HU, H. 2013. Formation of bifurcated wakes behind finite span flapping wings. *AIAA journal,* 51**,** 2040-2044.

ZDUNICH, P., BILYK, D., MACMASTER, M., LOEWEN, D., DELAURIER, J., KORNBLUH, R., LOW, T., STANFORD, S. & HOLEMAN, D. 2007. Development and testing of the mentor flapping-wing micro air vehicle. *Journal of Aircraft,* 44**,** 1701-1711.

ZEYGHAMI, S., ZHONG, Q., LIU, G. & DONG, H. 2019. Passive pitching of a flapping wing in turning flight. *AIAA Journal,* 57**,** 3744-3752.

ZHANG, J., LIU, N.-S. & LU, X.-Y. 2010. Locomotion of a passively flapping flat plate. *Journal of Fluid Mechanics,* 659**,** 43.

ZHANG, Y., HAN, J. & CHEN, G. 2019. Effects of the flapping frequency on the thrust performance for three-dimensional bionic multi-wings in a schooling. *Physics of Fluids,* 31**,** 117110.

ZHENG, H., XIE, F., ZHENG, Y., JI, T. & ZHU, Z. 2019. Propulsion performance of a two-dimensional flapping airfoil with wake map and dynamic mode decomposition analysis. *Physical Review E,*

99**,** 063109.

ZHENG, L., HEDRICK, T. L. & MITTAL, R. 2013. A multi-fidelity modelling approach for evaluation and optimization of wing stroke aerodynamics in flapping flight. *Journal of Fluid Mechanics,* 721**,** 118.

ZHU, Q. 2007. Numerical simulation of a flapping foil with chordwise or spanwise flexibility. *AIAA journal,* 45**,** 2448-2457.

ZHU, Q. 2011. Optimal frequency for flow energy harvesting of a flapping foil. *Journal of fluid mechanics,* 675**,** 495.

ZHU, Q. 2012. Energy harvesting by a purely passive flapping foil from shear flows. *Journal of fluids and structures,* 34**,** 157-169.

ZHU, Q., LIU, Y. & YUE, D. K. 2006. Dynamics of a three-dimensional oscillating foil near the free surface. *AIAA journal,* 44**,** 2997-3009.

ZHU, Q. & PENG, Z. 2009. Mode coupling and flow energy harvesting by a flapping foil. *Physics of Fluids,* 21**,** 033601.

Appendices

A Modified Motion Solver

A 6-DOF motion solver in *OpenFOAM* toolbox was modified to achieve a semi-active oscillating mode for biplane configuration. Taking the version of *OpenFOAM-v1912* as an example, the source code of 6-DOF motion solver can be found in the installation package with following path:

/src/sixDoFRigidBodyMotion/sixDoFSolvers/symplectic

The modified motion solver including two files is demonstrated as follows:

- ***H* File**

```
// ********************************************************************** //

#ifndef symplectic_H
#define symplectic_H

#include "sixDoFSolver.H"

namespace Foam
{
namespace sixDoFSolvers
{

class symplectic
:
    public sixDoFSolver
{
     const scalar amplitude_;

     const scalar omega_;

     const scalar heave0_;

public:

    TypeName("symplectic");

        symplectic
        (
            const dictionary& dict,
            sixDoFRigidBodyMotion& body
```

```
        );

        virtual autoPtr<sixDoFSolver> clone() const
        {
            return autoPtr<sixDoFSolver>::NewFrom<symplectic>(dict_, body_);
        }

    virtual ~symplectic();

        virtual void solve
        (
            bool firstIter,
            const vector& fGlobal,
            const vector& tauGlobal,
            scalar deltaT,
            scalar deltaT0
        );
};

}
}

#endif

// ************************************************************************* //
```

- ***C* File**

```
// ************************************************************************* //

#include "symplectic.H"
#include "addToRunTimeSelectionTable.H"

namespace Foam
{
namespace sixDoFSolvers
{
    defineTypeNameAndDebug(symplectic, 0);
    addToRunTimeSelectionTable(sixDoFSolver, symplectic, dictionary);
}
}

Foam::sixDoFSolvers::symplectic::symplectic
```

```
(
    const dictionary& dict,
    sixDoFRigidBodyMotion& body
)
:
    sixDoFSolver(dict, body),
    amplitude_(readScalar(dict.lookup("amplitude"))),
    omega_(readScalar(dict.lookup("omega"))),
    heave0_(readScalar(dict.lookup("heave0")))
{}

Foam::sixDoFSolvers::symplectic::~symplectic()
{}

double ts;
int    i;

void Foam::sixDoFSolvers::symplectic::solve
(
    bool firstIter,
    const vector& fGlobal,
    const vector& tauGlobal,
    scalar deltaT,
    scalar deltaT0
)
{
    ts += deltaT;
    i += 1;

    v() = tConstraints() & (v0() + aDamp()*0.5*deltaT0*a0());
    pi() = rConstraints() & (pi0() + aDamp()*0.5*deltaT0*tau0());

    centreOfRotation()[0] = centreOfRotation0()[0] + deltaT*v()[0];
    centreOfRotation()[1] = heave0_ + amplitude_*sin(omega_*ts);
    centreOfRotation()[2] = centreOfRotation0()[2] + deltaT*v()[2];

    if (i&1)
    {
        Info<< "Time in prescribed motion t1: " << ts << endl;
    }
    else
    {
        Info<< "Time in prescribed motion t2: " << ts << endl;
    }
```

```
    Info<< "centreOfRotation() by symplectic: " << centreOfRotation() << nl
        << "deltaT: " << deltaT
        << endl;

    if (i&1)
    {
        ts = ts - deltaT;
    }

    Tuple2<tensor, vector> Qpi = rotate(Q0(), pi(), deltaT);
    Q() = Qpi.first();
    pi() = rConstraints() & Qpi.second();

    updateAcceleration(fGlobal, tauGlobal);

    v() += tConstraints() & aDamp()*0.5*deltaT*a();
    pi() += rConstraints() & aDamp()*0.5*deltaT*tau();
}

// ************************************************************************* //
```

B Numerical Settings of Dynamic Mesh

A general case with the moving domain for APWIGs needs to input the motion characteristics and specify the scheme of dynamic mesh in the *OpenFOAM* directory. The numerical settings for a two-dimensional situation are defined by following two files, in which the corresponding boundary conditions can be changed to implement a three-dimensional simulation.

- ***pointDisplacement* File**

```
// ********************************************************************** //

dimensions      [0 1 0 0 0 0 0];

internalField   uniform (0 0 0);

boundaryField
{
    BODY1
    {
    type            sixDoFRigidBodyDisplacement;
    mass            1.579544;
    centreOfMass    (0.042 0.1 0);
    momentOfInertia  (0.002172 0.003032 0.000886);
    orientation
    (
        1 0 0
        0 1 0
        0 0 1
    );
    velocity        (0 0 0);
    acceleration    (0 0 0);
    angularMomentum (0 0 0);
    torque          (0 0 0);
    g               (0 0 0);
    rho             rhoInf;
    rhoInf          1000;
    report          on;

    solver
    {
        type         symplectic;
        amplitude    0.05;
        omega        25.132741;
        heave0       0.1;
```

```
}

constraints
{
    yLine
    {
        sixDoFRigidBodyMotionConstraint line;
        centreOfRotation    (0.025 0.1 0);
        direction           (0 1 0);
    }

    zAxis
    {
        sixDoFRigidBodyMotionConstraint axis;
        axis                (0 0 1);
    }
}

restraints
{
    axialSpring
    {
        sixDoFRigidBodyMotionRestraint linearAxialAngularSpring;

        axis            (0 0 1);
        stiffness       1;
        damping         0;
        referenceOrientation $orientation;
    }
}

    value           uniform (0 0 0);
}

BODY2
{
type            sixDoFRigidBodyDisplacement;
mass            1.579544;
centreOfMass    (0.042 -0.1 0);
momentOfInertia  (0.002172 0.003032 0.000886);
orientation
(
    1 0 0
    0 1 0
```

```
    0 0 1
);
velocity        (0 0 0);
acceleration    (0 0 0);
angularMomentum (0 0 0);
torque          (0 0 0);
g               (0 0 0);
rho             rhoInf;
rhoInf          1000;
report          on;

solver
{
    type         symplectic;
    amplitude    -0.05;
    omega        25.132741;
    heave0       -0.1;
}

constraints
{
    yLine
    {
        sixDoFRigidBodyMotionConstraint line;
        centreOfRotation    (0.025 -0.1 0);
        direction           (0 1 0);
    }

    zAxis
    {
        sixDoFRigidBodyMotionConstraint axis;
        axis                (0 0 1);
    }
}

restraints
{
    axialSpring
    {
        sixDoFRigidBodyMotionRestraint linearAxialAngularSpring;

        axis           (0 0 1);
        stiffness      1;
        damping        0;
```

```
            referenceOrientation $orientation;
        }
    }

        value           uniform (0 0 0);
    }

    frontAndBackPlanes
    {
        type            empty;
    }

    ".*"
    {
        type            fixedValue;
        value           uniform (0 0 0);
    }
}


// ************************************************************************* //
```

- ***dynamicMeshDict* File**

```
// ************************************************************************* //

dynamicFvMesh      dynamicMotionSolverFvMesh;

motionSolverLibs
(
  "libsixDoFRigidBodyMotion_modified.so"
  "libfvMotionSolvers.so"
);

solver                displacementSBRStress;

displacementSBRStressCoeffs
{
     diffusivity       inversePointDistance (BODY1 BODY2);
}

// ************************************************************************* //
```